FRUSTRATED LEWIS PAIRS EMBEDDED INTO MICROPOROUS POLYMER NETWORKS

VORGELEGT VON
MATTHIAS GEORG TRUNK
GEBOREN IN SPEYER

VON DER FAKULTÄT II – MATHEMATIK UND NATURWISSENSCHAFTEN
DER TECHNISCHEN UNIVERSITÄT BERLIN
ZUR ERLANGUNG DES AKADEMISCHEN GRADES

DOKTOR DER NATURWISSENSCHAFTEN
DR. RER. NAT.

GENEHMIGTE DISSERTATION

PROMOTIONSAUSSCHUSS:

VORSITZENDER: PROF. DR. RER. NAT. JOHANNES TEICHERT
1. GUTACHTER: PROF. DR. RER. NAT. ARNE THOMAS
2. GUTACHTER: PROF. DR. RER. NAT. MARCUS ROSE

TAG DER WISSENSCHAFTLICHEN AUSSPRACHE: 18.09.2017

BERLIN 2018

Danksagung

Ich möchte allen Menschen danken, die mir diese Arbeit ermöglicht und zu ihrem Gelingen beigetragen haben, wobei Worte eigentlich nicht in der Lage sind, auszudrücken, wie glücklich ich mich schätze, mit so vielen großartigen Menschen aufgewachsen zu sein, gelernt, studiert, gearbeitet, gelacht, geweint und getanzt zu haben.

Herrn Prof. Dr. Arne Thomas gilt mein besonderer Dank für das Vertrauen, welches er nahezu ohne Kenntnis meiner Person in mich gesetzt und mir ohne zu zögern die Möglichkeit gegeben hat, diese Arbeit in seiner Gruppe anzufertigen. Ich hätte mir kein spannenderes Thema aussuchen können und kann mir auch niemanden vorstellen, der mir das Ausmaß an akademischer Freiheit erlaubt hätte, das mir hier zuteil wurde.

Bei Herrn Prof. Dr. Marcus Rose bedanke ich mich für die Übernahme der Zweitkorrektur, speziell in dieser für ihn spannenden und turbulenten Zeit.

Mein herzlicher Dank gilt außerdem Herrn Prof. Dr. Johannes Teichert für die Übernahme des Prüfungsvorsitzes sowie die fruchtbare Zusammenarbeit.

Der gesamten Arbeitsgruppe Funktionsmaterialien sowie allen Ehemaligen der letzten vier Jahre gebührt mein Dank für eine fantastische Zeit. Allen voran danke ich meinen Bürokollegen, Thomas Langenhahn, Nicolas Chaoui, Michaela König, Dr. Ali Yassin, Dr. Jérôme Roeser, Dr. Hakan Bildirir und Dr. Robert Dawson für eine allzeit entspannte Arbeitsatmosphäre. Hervorheben möchte ich außerdem Dr. Johannes Schmidt, Dr. Jérôme Roeser, Dr. Ali Yassin, Dr. Daniel Becker, Dr. Pradip Pachfule und Nicolas Chaoui, die meine Leidenschaft für die Chemie teilen. Darüber hinaus hatte ich das große Glück mit einer Reihe hervorragender Studenten zusammenarbeiten zu dürfen: Thomas „Tommy" Langenhahn, Anna Herrmann, Michaela „Manuela" König, Caro Knittel, Mathias Primbs und Sarah „Hexe" Vogl, die meine Arbeit unendlich an Erfahrungen und Ergebnissen bereichert haben. Sophie Kücken, die zu meinem Glück fast komplett parallel mit mir promoviert hat, danke ich dafür, jeden noch so schweren Arbeitstag mit ihrem Gesang im Labor zu erleichtern. Miriam „Drillsergeant" Klapproth danke ich für das Teilen meiner Abneigung gegenüber Mensaessen. Nicht zu vergessen sind die vielen Stunden, die ich mit Daniel B., Daniel H., Jérôme und Tommy am Billardtisch verbringen durfte. Bei Anne Svilarov, Svetlana Barg und Maria Unterweger bedanke ich mich ganz herzlich für das Meistern organisatorischer Aufgaben aller Art. Christina Eichenauer gilt großer Dank dafür, dass sie mein ständiges Drängeln ausgehalten hat.

Viele Personen haben außerdem mein Studium an der Ludwig-Maximilians-Universität zu einer einzigartigen, vielseitigen und lehrreichen Erfahrung gemacht, von denen einige gesonderte Erwähnung verdienen. Meine Familie, Hermine und Werner Tautz sowie Regine und Ulrich Bockmair mit Veronika, Valentin und Katharina haben mir den Einstieg in diesen ungewissen Lebensabschnitt dankenswerterweise so leicht wie möglich gemacht. Meine Kommilitonen Tim Gatzenmeier und Arne Lünser haben mir immer wieder unerwartete Dimensionen von Hartnäckigkeit und Durchhaltevermögen aufgezeigt. Ohne sie wäre die Grundlange für diese Dissertation wohl nie gelegt worden. Tim und Arne sowie Franziska, Shushu und Tine bin ich für ihre bis heute andauernde Freundschaft dankbar.

Ich hatte das Privileg in einem riesigen Kreis von Freunden aufzuwachsen, von denen ich einige hervorheben möchte: Claus Teuber, Daniel Jalalpoor, Christian Kaller,

Sylvia Kaller, Kathrin Wagner, René Rundio und Alexander Frank, ihr seid mehr als Freunde. Ihr seid Familie.

Besonders möchte ich mich auch bei meiner Berliner Tanzfamilie, Evelin, Hauke, Anne S., Tina, Carlos, Anne K., Severin, Eva H., René, Joanna, Christian, Eva P., Anja, Evgenia und Tine für unvergessliche Stunden auf dem Parkett bedanken.

Der größte Dank gebührt meiner Familie, insbesondere meinen Eltern, die mir Bildung ermöglicht haben und ohne die mir all das verwehrt geblieben wäre.

Zuletzt bedanke ich mich bei Janina, die mir zuliebe während meiner Promotion auf vieles verzichtet hat und mir trotzdem seit fast sieben Jahren jeden Tag aufs Neue die Welt zu Füßen legt.

Acknowledgments

Greatest thanks go to my family, especially my parents, who enabled me to receive a thorough education and without whom I would have been barred from all this.

Finally I want to thank Janina, who has for my sake dispensed with many things during the time I spent working on this treatise and after nearly seven years continues to put the world at my feet every single day.

Kurzzusammenfassung

Aufgrund ihrer vielseitigen potentiellen Anwendungsmöglichkeiten in Gasspeicherung und –trennung, Sensorik und Katalyse haben mikroporöse organische Materialien innerhalb der letzten 20 Jahre eine rasante Entwicklung erfahren. Neben geordneten Materialien wie metall-organischen Gerüstmaterialien (MOFs) und kovalent organischen Gerüstmaterialien (COFs) haben sich mikroporöse Polymernetzwerke (MPNs) als amorphe, aber nicht weniger vielversprechende Materialien entwickelt. Obwohl die kristallinen Strukturen von MOFs und COFs eine größere Vielfalt analytischer Methoden und dadurch leichtere Charakterisierung erlauben, basieren ihre Synthesen auf dem Vorhandensein von Heteroatomen wie Stickstoff, Sauerstoff oder Metallen. Diese Anforderung entfällt bei MPNs, sodass diese theoretisch aus reinen Kohlenwasserstoffgerüsten bestehen können. Dies ermöglicht den direkten oder postsynthetischen Einbau sensibler funktioneller Gruppen, die andernfalls mit dem Gerüst des porösen Materials reagieren und dadurch inaktiviert oder es sogar zersetzen würden.

Obwohl MPNs seit über einem Jahrzehnt erforscht werden, besteht immer noch großer Optimierungsbedarf bei vielen der angewendeten Synthesemethoden. Das erste Kapitel dieser Arbeit beschäftigt sich daher mit der Synthese von MPNs durch die Sonogashira-Hagihara-Reaktion. Die Parameter dieser Synthesemethode wurden optimiert und ergaben eine simple, aus praktischer Sicht sehr attraktve Eintopf-Prozedur. Desweiteren kommt das neue Protokoll ohne die Verwendung von Kupfersalz als Co-Katalysator aus und benötigt nur ein Drittel des bisher verwendeten Palladium-Katalysators. Folglich erfolgt die Reaktion sehr viel langsamer, was dazu führt, dass Einschlüsse von Oligomeren durch vorzeitiges Ausfallen vermieden werden und nur minimale Mengen an unreagierten Endgruppen übrigbleiben. Gegenüber dem bisher verwendeten Protokoll, welches auf einem 50 % Überschuss von Alkingruppen beruht, welche sich nach Ausfallen des festen Produkts unter Bildung von Eninen noch quervernetzen können, basiert das neue Protokoll auf Verwendung stöchiometrischer Mengen funktioneller Gruppen. Dies führt zur Bildung von Poly(aryleneethynylenen) mit streng kontrollierten Strukturen und unerreichten BET-Oberflächen von bis zu 2552 $m^2 \cdot g^{-1}$. Diese Ergebnisse wurden in *Chemistry – A European Journal* unter dem Titel *Copper-Free Sonogashira Coupling for High-Surface-Area Conjugated Microporous Poly(aryleneethynylene) Networks* veröffentlicht und von den Gutachtern mit dem Prädikat *Hot Paper* versehen.

Das für die Synthese von hochoberflächigen MPNs erarbeitete Protokoll wurde bei der Ausarbeitung weiterer Projekte angewendet. Eines dieser Projekte behandelt Polymere auf Basis der Cyanovinyleinheit, die sich als interessante funktionelle Gruppe zur Synthese von polymeren mit hoher CO_2-Affinität und leichter Rezyklierbarkeit herausgestellt hat. Darüber hinaus wurde bei diesen Netzwerken eine Proportionalität zwischen dem eingebauten Massenanteil der Cyanovinylgruppe und der CO_2-Adsorptionsenthalpie festgestellt, die ein potentiell interessantes Werkzeug für das Design neuer Carbon Capture Materialien ist. Die Ergebnisse dieses Projekts wurden unter dem Titel *Structure–Thermodynamic-Property Relationships in Cyanovinyl-based*

Microporous Polymer Networks for the Future Design of Advanced Carbon Capture Materials im Journal *Advanced Functional Materials* veröffentlicht.

Frustrierte Lewis-Paare (FLPs) sind eine vergleichsweise junge Klasse von Organokatalysatoren. Ein FLP besteht aus einem Elektronendonor und einem –akzeptor, welche synergistisch zusammenwirken um kleine Moleküle wie H_2 und CO_2 zu aktivieren. Durch das Zusammenspiel von Säure und Base kann H_2 heterolytisch in ein Proton und ein Hydrid gespalten werden, welche an ihr respektives Gegenstück addieren und ein Salz bilden. Unter Regeneration des ursprünglichen FLPs kann der so aktivierte Wasserstoff in einer metallfreien Hydrierung auf ein Substrat übertragen werden. In Anbetracht des Interesses an porösen Materialien für die Wasserstoffspeicherung oder katalytische Anwendungen beschäftigt sich der letzte Teil dieser Dissertation mit dem Einbau eines funktionalen FLPs in ein mikroporöses Material sowie dessen Charakterisierung. Als Wirtsmaterialien wurden MPNs ausgewählt, da sie im Gegensatz zu MOFs und COFs ohne Heteroatome in der Zielstruktur synthetisiert werden können, die die beabsichtigte Funktionalität beeinflussen. Zwei Triphenylphosphin-Derivate mit von konventionellen, löslichen FLPs abgeleiteten Strukturmotiven wurden durch Yamamoto-Polymerisation zu MPNs mit BET-Oberflächen von ca. $1000 \ m^2{\cdot}g^{-1}$ und unterschiedlichem sterischen Anspruch polymerisiert. Durch Phosphor-Festkörper-NMR-Messungen konnte gezeigt werden, dass durch Imprägnierung der Polymere mit einer starken, kommerziell erhältlichen Lewis-Säure der Grad an Frustration in Abhängigkeit der sterischen Abschirmung des Phosphorzentrums manipuliert werden kann. Durch NMR-Analyse von Isotopenaustauschexperimenten wurde bewiesen, dass die erhaltenen FLPs in der Lage sind, Wasserstoff heterolytisch zu spalten. Diese Dissertation liefert damit die ersten Beweise für FLP-Chemie zwischen einem festen organischen Katalysator und einer gelösten Spezies. Diese Ergebnisse wurden unter dem Titel *Room-Temperature Activation of Hydrogen by Semi-immobilized Frustrated Lewis Pairs in Microporous Polymer Networks* im *Journal of the American Chemical Society* publiziert.

Short Summary

Over the last two decades, microporous organic materials have seen remarkable development due to their potential applications in gas storage and separation, sensing, and catalysis. Aside from ordered materials such as metal-organic frameworks (MOFs) and covalent organic frameworks (COFs), microporous polymer networks (MPNs) have emerged as a family of amorphous yet highly promising materials for a range of applications. Although the crystallinity of MOFs and COFs enables more analytic methods and thereby facilitates their characterization, heteroatoms are required to enable reversibility of the bond forming reaction. That demand is not posed on microporous polymers, therefore they can exist as a pure hydrocarbon skeleton. This in return offers the possibility to employ functional moieties which would otherwise react with the scaffold itself, rendering them inactive, or even destroying the scaffold of the porous material.

Despite MPNs being researched for over a decade, room for optimization of many of the employed bond forming reactions remains. The first chapter of this thesis therefore focuses on the formation of MPNs via Sonogashira-Hagihara reaction. The parameters for this method were optimized, yielding a facile one-pot procedure, which is advantageous from a practical point of view. Furthermore it does not necessitate a copper co-catalyst, and requires only a third of the molar amount of palladium catalyst used previously. Consequentially the reaction proceeds more slowly, precluding inclusion of oligomers by premature precipitation, yielding only minute amounts of unreacted end groups. As opposed to the hitherto employed protocol, which relies on a 50 % excess of alkyne groups, which are able to crosslink after precipitation under formation of enyne moieties, the new protocol is based on stoichiometric amounts of functional groups in the monomers, which leads to poly(aryleneethynylene) networks of rigorously controlled structures and unprecedented BET surface areas of up to 2552 $m^2 \cdot g^{-1}$. These results were published in *Chemistry – A European Journal* and the paper entitled *Copper-Free Sonogashira Coupling for High-Surface-Area Conjugated Microporous Poly(arylene-ethynylene) Networks* was rated *Hot Paper*.

The obtained protocol for the synthesis of high surface area MPNs was employed in a number of research topics. One of these focuses on polymers based on the cyanostilbene unit, which turned out to be highly interesting for the formation of polymers exhibiting high CO_2 affinity yet facile recyclability. Furthermore, a proportionality between the included weight percentage of the cyanostilbene moiety and the CO_2 adsorption enthalpy was established, which is a potentially powerful tool for the design of new carbon capture materials. The results of this work were published in an article entitled *Structure–Thermodynamic-Property Relationships in Cyanovinyl-based Microporous Polymer Networks for the Future Design of Advanced Carbon Capture Materials* in the journal *Advanced Functional Materials*.

Frustrated Lewis pairs (FLPs) are a relatively new class of organocatalysts. A FLP consists of an electron donor and an acceptor, which are synergistically capable of effecting the activation of small molecules such as H_2 or CO_2. Through the interplay of Lewis acid and base, H_2 for instance is heterolytically cleaved into a proton and a hydride

ion, which add to their respective counterparts to form a salt. This activated hydrogen can then be transferred onto a substrate in a metal-free catalytic hydrogenation under regeneration of the original FLP. In the light of the importance of porous materials for applications in hydrogen storage and catalysis, the goal of the last part of this treatise encompassed the synthesis and characterization of a functional FLP incorporated into a microporous material. MPNs were chosen as host materials since they could be, in contrast to MOFs and COFs, synthesized without having to include heteroatoms offering other functionalities than the desired ones. Utilizing Lewis basic building blocks mimicking motifs borrowed from conventional, solution-based FLP chemistry, offering varying degrees of steric encumbrance, two microporous polymer networks exhibiting BET surface areas around $1000\ m^2 \cdot g^{-1}$ were obtained by Yamamoto polymerization. By impregnation of the polymers with a commercially available, strong Lewis acid it was shown that the degree of frustration can be tuned according to the amount of steric hindrance around the basic site by phosphorus solid state NMR measurements. The obtained FLPs were able to split dihydrogen heterolytically as was shown by isotope scrambling experiments, yielding the first proof of concept for FLP chemistry combining a dissolved species and a fully organic solid catalyst. These findings were published under the title *Room-Temperature Activation of Hydrogen by Semi-immobilized Frustrated Lewis Pairs in Microporous Polymer Networks* in the *Journal of the American Chemical Society*.

List of Publications

Parts of this dissertation have been published:

[1] *"Copper-Free Sonogashira Coupling for High-Surface-Area Conjugated Microporous Poly(aryleneethynylene) Networks"*, Matthias Trunk, Anna Herrmann, Hakan Bildirir, Ali Yassin, Johannes Schmidt, Arne Thomas, *Chemistry – A European Journal* **2016**, *22*, 7179–7183. https://dx.doi.org/10.1002/chem.201600783

- ❖ All monomer and polymer syntheses. Most of the analytical work. Complete writing of the manuscript.

[2] *"Room-Temperature Activation of Hydrogen by Semi-Immobilized Frustrated Lewis Pairs in Microporous Polymer Networks"*, Matthias Trunk, Johannes F. Teichert, Arne Thomas, *Journal of the American Chemical Society* **2017**, 139, 3615–3618. https://dx.doi.org/10.1021/jacs.6b13147

- ❖ Design and synthesis of the target structures. All of the experiments and analytics. Complete writing of the manuscript.

[3] *"Structure-Thermodynamic Property-Relationships in Cyanovinyl-Based Microporous Polymer Networks for the Future Design of Advanced Carbon Capture Materials"*, Ali Yassin, Matthias Trunk, Frank Czerny, Pierre Fayon, Abbie Trewin, Johannes Schmidt, Arne Thomas, *Advanced Functional Materials* **2017**, 27, 1700233. https://dx.doi.org/10.1002/adfm.201700233

- ❖ Concept development and most of the polymer synthesis. Recording and critical evaluation of solid state nuclear magnetic resonance data. Some of the manuscript writing.
- ❖ Ali Yassin and Matthias Trunk share first authorship as acknowledged in the publication

Further scientific contributions of the author:

[4] *"Chemistry and Structures of Hexakis(halogenomethyl)-, Hexakis(azidomethyl)-, and Hexakis(nitratomethyl)disiloxanes"*, Laura Ascherl, Camilla Evangelisti, Thomas M. Klapötke, Burkhard Krumm, Julia Nafe, Anian Nieder, Sebastian Rest, Christian Schütz, Muhamed Suceska, Matthias Trunk, *Chemistry – A European Journal* **2013**, *19*, 9198–9210. https://dx.doi.org/10.1002/chem.201300226

- ❖ Some of the experimental work.

[5] *"Thermally Induced Crosslinking of Poly(N-Propargyl Glycine)"*, Christian Secker, Sarah M. Brosnan, Felix R. P. Limberg, Ulrike Braun, Matthias Trunk, Peter Strauch, Helmut Schlaad, *Macromolecular Chemistry and Physics* **2015**, *216*, 2080–2085. https://dx.doi.org/10.1002/macp.201500223

- ❖ Recording and critical evaluation of solid state nuclear magnetic resonance data on thermally crosslinked polymers.

[6] *"Trends and Challenges for Microporous Polymers"*, Nicolas Chaoui, Matthias Trunk, Robert Dawson, Johannes Schmidt, Arne Thomas, *Chemical Society Reviews* **2017**, 46, 3302–3321. https://dx.doi.org/10.1039/C7CS00071E

  ❖ Chapter on heteroatom-incorporating microporous polymer networks.

List of Abbreviations

Abbreviation	Designation
BCF	Tris(pentafluorophenyl)borane
BET	Brunauer-Emmett-Teller
CP/MAS	Cross-polarization magic angle spinning
DCM	Dichloromethane
DEB	1,4-Diethynylbenzene
DIB	1,4-Diiodobenzene
DIBP	4,4'-Diiodobiphenyl
DMF	Dimethylformamide
eq	Equivalent
FLP	Frustrated Lewis pair
HMTEBP	2,2',4,4',6,6'-Hexamethyl-3,3',5,5'-tetraethynylbiphenyl
LA	Lewis acid
LB	Lewis base
NMR	Nuclear magnetic resonance
PAF	Porous aromatic framework
PPN	Porous polymer network
PSD	Pore size distribution
PSM	Postsynthetic modification
QSDFT	Quenched state density functional theory
SA	Surface area
TGA	Thermogravimetric analysis
THF	Tetrahydrofuran
TEB	1,3,5-Triethynylbenzene
TEPM	Tetrakis(4-ethynylphenyl)methane
TIB	1,3,5-Triiodobenzene
TIPM	Tetrakis(4-iodophenyl)methane

Contents

1 Introduction

Continued global population growth and ever increasing standards of technology entail a growing energy and resource demand which will in the near future be satisfied mainly by fossil fuels, i.e. petroleum, natural gas, and coal.[1] While these carbon-based fuels will be sufficient to sustain the world energy requirements for the foreseeable future, calls for sustainable processes and technologies grow louder to reduce the ecological impact of current energy technologies, to preserve as much of earth's natural environment as possible, and to prevent the already changing climate from being altered further. One manifestation of these efforts is that, following the Fukushima disaster of 2011, the German government drastically accelerated its plans to achieve a low-carbon, non-nuclear but affordable energy supply. In the course of this *Energiewende* great sums of money are invested in the improvement and implementation of renewable energy technologies worldwide. In any case, the question is not if, but when the move away from fossil fuels will take place.

An important aspect in dealing with this transition is the fact that fossil fuels such as petroleum and natural gas are not only energy sources but also convenient energy carriers. The replacement of fossil energy sources by renewables, e.g. solar, wind, or hydroelectricity means that the produced energy either needs to be converted to synthetic hydrocarbon fuel by conventional methods such as the Fischer-Tropsch process[2], or that alternative energy carrier systems need to be implemented.

A potential candidate as energy carrier for the post-fossil fuel era is molecular hydrogen.[3] The buildup of a hydrogen economy has been scientifically envisioned[4] but also heavily criticized due to the high losses contained within a hydrogen economy.[5] Hydrogen gas displays a considerably higher energy density than electric batteries due to its high energy density per weight.[6] On the other hand its low energy density per volume necessitates the use of high pressures or extremely low temperatures to make it viable for transport. As an industrially widely used material it has the advantage of being

compatible with existing high-pressure facilities, but the energy requirements for pressurization or cryocooling are prohibitively high, as are the costs for durable tanks needed for safe storage and transport, and the extra weight added by heavy tanks further reduces its viability for automotive and other mobile applications. Materials with the ability to chemically bind and (catalytically) release hydrogen under consideration encompass main group hydrides[7,8], amine-boranes[8,9], and liquid organic hydrogen carriers (LOHCs)[10]. Only the latter offer a viable solution regarding economically feasible regeneration, however (see Fig. 1).[8]
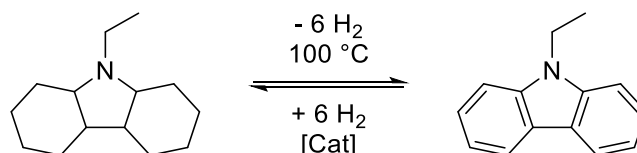
Fig. 1: Thermal dehydrogenation and catalytic hydrogenation of *N*-ethylcarbazol

Although the most abundant element on earth and in the universe, hydrogen in its elemental form makes up less than 1 % of all hydrogen atoms on earth.[3] Due to its inherently high energy density and reactivity, it is mostly found in combination with oxygen as water or in the form of hydrocarbons. To be utilized as an energy carrier, hydrogen needs to be produced artificially. This is currently realized predominantly via steam reforming, and the obtained hydrogen is used on-site or nearby to minimize safety issues during transportation. Although three to ten times as expensive as steam reforming of hydrocarbons[11], another method for the production of hydrogen is via proton exchange membrane electrolysis of water, which is deemed an economically feasible production method when coupled with wind or solar energy.[12] Recent developments in photocatalysis enable hydrogen production via photochemical water-splitting under concurrent consumption of a sacrificial agent, but after only a couple of years this research is still in its infancy and far from industrially relevant efficacy.[13–16] The safe storage and controlled release of hydrogen is the prime motivation for several of the topics discussed within this treatise.

While the production of energy is supposed to become cleaner and cheaper in the first place, the reduction of greenhouse gas emissions is aspired. To that end, tremendous efforts are being invested in finding less energy-intensive alternatives to large-scale industrial processes such as cryogenic distillation for the separation of air and the production of high purity gases, as well as the production of other basic and fine chemicals. Apart from the fact that fossil fuels are ultimately exhaustible and the transition to alternative energy sources is inevitable, already released amounts of greenhouse gases are heavily contributing to climate change and need to be dealt with immediately. Since CO_2 has been identified as the main source of global warming and ocean acidification, one approach deals first and foremost with its removal from the atmosphere and the oceans.[17] CO_2 is the main waste product released during fossil fuel and carbohydrate combustion for energy production, furthermore it constitutes up to 50 % of landfill gas emissions.[18] An attractive approach to reduce CO_2 emissions into the atmosphere in the first place is post-combustion CO_2 capture; implementation via retrofitting to existing facilities is possible.[19] Current industrially applied CO_2 capture

methods have been in use for several decades and are mostly based on liquid amine-scrubbing baths. Here, the underlying fixation of CO_2 is of chemisorptive nature and relies on the formation of a covalent bond between an amine function and the carbon atom of CO_2. Subsequent proton shift to a neighbouring amine moiety leads to the formation of a highly stable ammonium carbamate salt (see Fig. 2). The inherent drawback of this chemisorptive process is the high energy penalty incurred during regeneration of the sorbent, i.e. removal of the fixated CO_2.
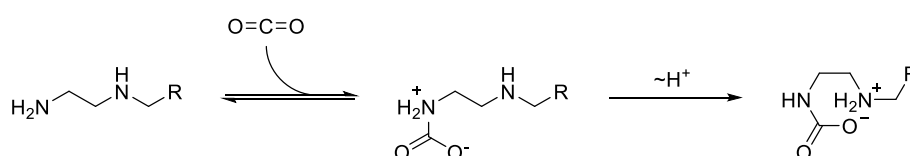
Fig. 2: Carbon dioxide capture by amine scrubbing via chemisorptive carbamate formation

In this context, solid amine-grafted sorbents are an avidly sought-after solution. Solids typically have lower heat capacities than liquids, consequently solid adsorbents suffer lower energy penalties upon regeneration and are therefore of particular interest. As of yet, their expensiveness and relatively low CO_2 adsorption capacity render these materials only academically interesting.[20] To be industrially viable, a CO_2 capture material ought to exhibit sufficiently strong affinity towards CO_2 to bestow a high selectivity for CO_2 over competing gases under realistic conditions, i.e. in wet mixed gas feeds at approximately 15 vol-% CO_2. On the other hand, the interaction must be weak enough for the sorbent to be regenerated under mild conditions. Features matching these requirements are typically displayed by materials offering strong physisorptive features. The boundaries between chemi- and physisorption are not clearly distinguishable but are conventionally accepted to lie between 45 and 55 kJ·mol^{-1}. Furthermore, the material would need to be producible via a low cost route with a high space-time yield. The ultimate goal for the treatment of CO_2 is its facile industrial transformation into useful feedstock materials to complete the carbon cycle and eventually obtain zero carbon fuel.

This work is a cumulative dissertation based on three articles published in peer-reviewed scientific journals. The articles are given in full length including supporting information in the final chapter. Following this introduction, Chapter 2 serves to explain some of the scientific foundations on which this treatise rests. Since the functional materials emanating herefrom are the results of the mergers of different concepts such as frustrated Lewis pair chemistry and microporous polymer chemistry, an overview of the recent literature in each respective field is given. In Chapter 3 specific goals and the motivation to target the projects treated in this work are formulated. Additional unpublished results are given in Chapter 4. Chapter 5 summarizes this work and makes some projections on potential future endeavors.

2 Theory

In this chapter, a basic knowledge of the principles underlying the projects elaborated within this dissertation is conveyed. Moreover, a literature overview is given, pointing out several landmark contributions to the respective fields.

2.1 Microporosity

In light of the aforementioned goals, microporous materials have garnered tremendous attention over the last two decades.[21] To understand the special properties of microporous materials and the mechanism of adsorption of gas molecules in micropores an analogy to an everyday material is appropriate. Similar to the way a sponge soaks up water into its interconnected channels and pores, microporous materials have pores smaller by several orders of magnitude, so small in fact that the interactions of pore walls with single gas molecules become significant. Depending on its polarity, every surface has the ability to interact with a potential adsorbate. The strength of this interaction is the isosteric heat of adsorption and expressed via the amount of energy that is released during the adsorption process per amount of adsorbed species, given in $kJ \cdot mol^{-1}$. For a large pore volume the volume occupied by single adsorbate molecule on the adsorbent surface is negligible relative to the whole pore. However, the smaller the pores become the more pores – and consequently pore walls – fit into a given amount of space (see Fig. 3). An increased amount of pore walls yields a very much increased accessible surface area which can adsorb a larger amount of gas molecules, given that the connectivity between pores is sufficiently high.
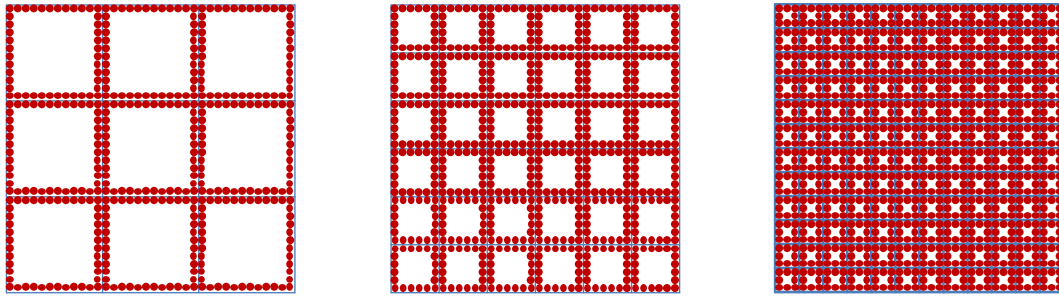
Fig. 3: Schematic representation of a 2D lattice (blue lines) with differently sized pores filled with a monolayer of guest molecules (red dots). Additional pore walls reduce the pore diameter but increase surface area and thus number of adsorption sites.

2.1.1 Brunauer-Emmett-Teller Theory

To gain knowledge of the size and nature of the accessible surface area the pores of a host material are filled with a probe species in a controlled fashion. Prior to analysis the pores need to be thoroughly emptied under reduced pressure and possibly elevated temperature to overcome any adhesive interaction between contingent adsorbates and the host material. Once in its activated form, the sample can subsequently be treated with the probe gas. The added amount of adsorbate and the corresponding pressure change inside the measuring cell are recorded and plotted against each other. Depending on the size and geometry of the pores, differently shaped adsorption curves are obtained and classified according to the International Union of Pure and Applied Chemistry, IUPAC (see Fig. 4, I-VI).[22,23]
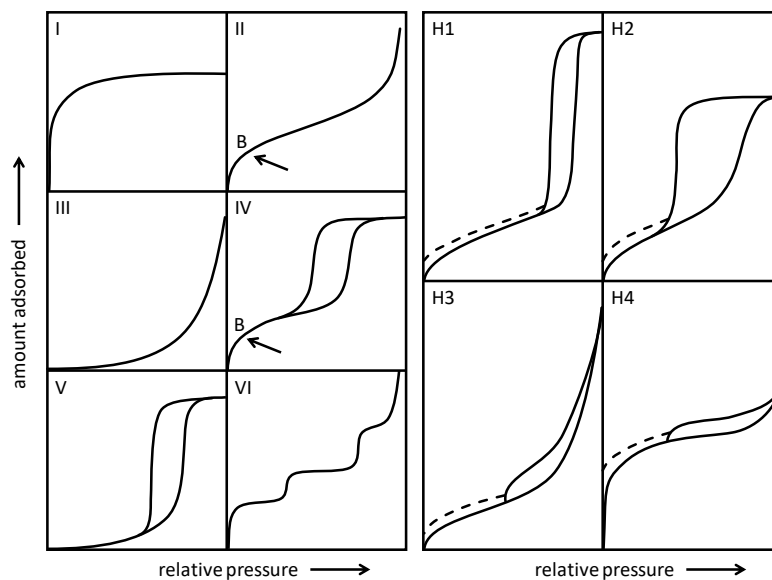
Fig. 4: Classificaton of isotherm and hysteresis types according to IUPAC[22,23]

From the recorded adsorption isotherms the accessible surface area is calculated via the method developed by Brunauer, Emmett, and Teller (BET method).[24] This method is a derivative of the Langmuir adsorption model, the theory behind which is based on the formation of a monolayer of adsorbate on a hypothetical infinite, even surface. The BET

method expands this theory to take into account multilayer adsorption as well and is based on three hypotheses: (1) gas molecules adsorb on solids in infinite layers; (2) there is no special interaction between the adsorbed layers; (3) the Langmuir theory can be applied to each layer. The BET equation can be formulated as

$$\frac{p}{n^a(p_0 - p)} = \frac{C-1}{n_m^a C} \cdot \frac{p}{p_0} + \frac{1}{n_m^a C}$$ (Eq. 1)

$$y \ = \ S \ \cdot \ x \ + \ I$$

where p_0 and p are the equilibrium and saturation pressure, n^a is the adsorbed molar amount of gas, and n_m^a is the adsorbed molar amount of gas in the first monolayer. The BET constant C is further defined by

$$C = exp\left(\frac{E_1 - E_L}{RT}\right)$$ (Eq. 2)

where E_1 and E_L are the heats of adsorption for the monolayer and all higher layers, respectively. Upon adsorption molecules or atoms forfeit their gaseous properties, i.e. their movement is strongly reduced and they occupy less space. The heat of adsorption E_1 is specific for the interaction between the first monolayer of adsorbate and adsorptive whereas according to the hypotheses outlined above, probe molecules in the next layers are not influenced by the surface texture and only experience interaction between molecules of their own kind. Thus the adsorbate is in a "quasi-liquid" state and E_L is equal to the heat of liquefaction. The BET constant C and the monolayer capacity n_m^a can be obtained via

$$C = 1 + \frac{S}{I} \quad and \quad n_m^a = \frac{1}{S+I}$$ (Eq. 3)

Using the Avogadro constant N_A and taking into account the area occupied by one single adsorbate molecule a_m, the total surface area SA_{total} contained within a given sample as well as the specific surface area SA, independent of sample mass m, can be calculated via

$$SA_{total} = n_m^a \cdot N_A \cdot a_m \quad and \quad SA = \frac{SA_{total}}{m}$$ (Eq. 4)

The applicability of the BET method to microporous materials has been called into question due to various concerns, e.g. that monolayer structures may differ on various surfaces and that, similar to capillary forces on the macroscopic scale, enhanced physical adsorption in small pores tends to lead to overestimated micropore surface areas.[25] Walton and Snurr simulated nitrogen adsorption isotherms in a series of microporous MOFs to determine whether the application of the BET method yields meaningful and comparable results. The authors found a surprisingly good congruence between surface areas calculated from crystal structure data and surface areas calculated from simulated isotherms.[26] The possibilities of the BET method do not end with the calculation of mere

surface areas. The deduction of further properties such as pore size distribution, pore geometry, micropore volume, total pore volume, and many others is possible.

A special feature, in particular of many porous organic materials, are deviations of the desorption curve from the corresponding adsorption curve, called hystereses (see Fig. 4, H1-H4). It has been theorized that the occurrence of hystereses is a result of an overly fast desorption process by which the equilibrium pressure is not reached over a broad pressure range but at a certain pressure results in the abrupt desorption of a significant amount of guest molecules.

In many MOFs one or several steps in the adsorption curve can be observed as the result of a phase change in the material upon adsorption of an adsorbate. This phenomenon is known as gate opening effect and it can be exploited for the selective adsorption and separation of hydrocarbons, which is an otherwise highly energy-demanding process.[27]

According to IUPAC classifications, microporous materials include pores with diameters of less than 2 nm. Larger pores are classified as mesopores, which range between 2 and 50 nm in diameter. Pores above this size are referred to as macropores and, as discussed previously, have little influence on the gas sorption properties of a material. Instead, they are of significant importance for mass diffusivity, regarding transport of substrates through a solid material, e.g. in heterogeneous catalysis.

Similarly to the macroscopically observed capillary forces, smaller pores get filled preferably over larger ones. Thus, microporous materials, which lie in the focus of this thesis, are characterized by type I isotherms which feature a strong ascent of the adsorption curve at very low relative pressures (< 0.1 $p \cdot p_0^{-1}$) and level out into a plateau beyond this pressure range (see Fig. 4, I). Additional mesoporosity is often observed in so-called "soft" microporous materials such as porous organic polymers, which are often observed to swell upon contact with guest molecules, i.e. gases or liquids. This can be misleading as their existence is not actually due to permanent porosity but a consequence of gradual pore filling at the given temperature, which is usually very low (77 K) and not representative of the conditions under which the material is expected to be applied. Mesopores are characterized by type II isotherms featuring a steady ascent (see Fig. 4, II) or sometimes even pronounced steps (see Fig. 4, VI) in the adsorption curve. Macropores are mainly observed in "hard" inorganic materials such as silicas or as interparticular void between particle agglomerates.

Research on high-surface-area materials has precipitated the inception of a highly counterintuitive concept. A hypothetical gas tank of an arbitrary volume can absorb a certain amount of gas at a given temperature and pressure. Depending on the type of gas to be stored, the tank is typically made of an alloy such as carbon steel, which offers little to no interaction with the gas it is filled with. Looking at the tank from a porosity point of view, the tank literally consists of one large pore with negligible surface area, i.e. a ratio of pore volume to surface area that approaches infinite. If the same tank were to be filled with a low-density scaffold (see Fig. 5) of a material which offers favorable interaction with the gas in question, the gas molecules would adsorb to the surface of the scaffold and subsequently occupy less space than they would in the empty tank. Achieving the correct balance between the degree of tank filling, total surface area, applied pressure

and temperature, it is conceivable to design a tank filled with scaffold which is able to host more gas than the empty tank would. Investigations into this concept have yielded MOF materials which are able to deliver up to three times the amount of methane the empty tank could hold.[28]
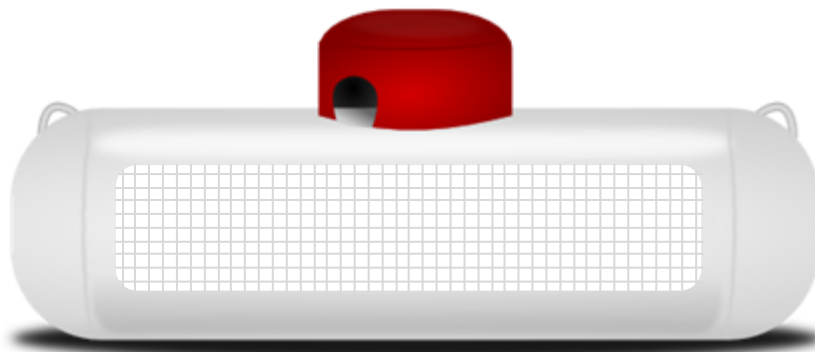
Fig. 5: Schematic of a tank equipped with scaffold providing additional sites for physisorption

Due to its simple availability and low price nitrogen gas has been established as standard probe adsorbate. It exhibits a quadrupolar moment, is hard to polarize, and therefore only undergoes physisorptive interactions with the sorbent. Nonetheless, for various reasons nitrogen is not the best choice as a probe gas and only suited for a rough estimate of the accessible surface area. Better alternatives are argon or krypton as these are single-atom probes for which no differentiation needs to be made between side-on or end-on interaction with the adsorbent, as is the case with the diatomic nitrogen molecule, the occupied area of which is dependent on the orientation of the molecule on the probed surface. The obvious drawback of the noble gases is that they are prohibitively more expensive. Carbon dioxide offers a smaller diameter than the aforementioned probe gases and therefore yields more detailed information on the existence and quality of ultramicropores, i.e. pores below 0.7 nm, which is the bilayer thickness of nitrogen.[29] Depending on diameter and polarizability, different gases may yield remarkably varying surface areas for one and the same material. All of the above mentioned gases only give information about the surface area that is accessible to themselves and no other substances, hence surface areas calculated from sorption isotherms using different probe gases are not comparable.

2.1.2   Ideal Absorbed Solution Theory

Differences in affinity and pore accessibility can be exploited. Considering carbon dioxide for example, due to the large difference in electronegativity between the two oxygen atoms and the central carbon atom it is much more easily polarizable than dinitrogen and as a result forms strong chemisorptive bonds with electron donors. This affinity offers the possibility to preferentially adsorb CO_2 over N_2 or CH_4, which are industrially important separations. The goldstandard for the determination of such selectivities is the Ideal Absorbed Solution Theory (IAST) by Myers and Prausnitz.[30] Assuming an ideal mixture of two gases, which is normally the case, adsorption equilibria of gas mixtures can

conveniently be calculated from the pure adsorption isotherms recorded at equal temperature on the same sorbent without any actual mixture data via

$$S_{ads} = \frac{q_1/q_2}{p_1/p_2}$$
(Eq. 5)

with dimensionless adsorption selectivity S_{ads}, gas phase pressure p_i, and q_i, the molar loading of species i given as

$$q_i = q_{i,sat} \frac{b_i p_i}{1 + b_i p_i}$$
(Eq. 6)

where b_i is the Langmuir constant and $q_{i,sat}$ is the saturation capacity of species i. Thus it is possible to calculate, for instance, the selectivity for CO_2 over N_2 at a partial pressure of CO_2 of 0.15, which is a typical value for flue gas streams. The IAST method was used in this treatise to determine the CO_2/N_2 selectivity of microporous polymer networks.

2.1.3 Microporous Materials

The first permanently microporous materials to be broadly explored were activated carbons. Such materials were obtained as early as the beginning of the 20th century by carbonization of mixtures of carbonaceous precursors and metal halides followed by partial oxidation with steam or carbon dioxide. In the 1970s continued efforts precipitated in activated carbons with impressive surface areas of more than 3000 $m^2 \cdot g^{-1}$ synthesized from aromatic precursors activated with potassium hydroxide by American Oil Company.[31] Today, activated carbons can be produced from industrial by-products from regenerative resources such as rice husk, coconut husk, or nutshells. Applications of activated carbons are in purification of gas, water, and metals as well as in sewage treatment, heterogeneous catalysis, and many others.

Another class of early researched microporous materials are the naturally occurring zeolites.[32] The simplest form of zeolites are aluminosilicates, consisting of alternating, corner-sharing clusters in the form of neutral silicate SiO_4 and negatively charged aluminate AlO_4 tetrahedra, the latter of which prompt the pores of the zeolite to be filled with loosely bound countercations such as sodium or potassium. Zeolites are also synthetically accessible and have long since found their way into everyday life as ion exchange materials, solid adsorbents, and catalysts.

In 1974, Davankov et al. obtained "macronet isoporous gels" by cross-linking polystyrene chains with para-substituted chloromethyl-phenyl and –biphenyl units.[33] The resulting materials differed from conventionally formed polystyrene-divinylbenzene copolymers by a "high inner surface area and porosity in the dry state" of up to 1000 $m^2 \cdot g^{-1}$. This permanent porosity is a result of a high degree of cross-linking which is reflected in the designation given this class of materials, namely hyper-crosslinked polymers (HCPs).

In 1990, Hoskins and Robson published a paper on a new type of hybrid organic-inorganic material based on the solid-state structures of $Zn(CN)_2$ and $Cd(CN)_2$.[34] From these the authors derived the first design patterns for "scaffolding-like materials comprising infinite polymeric frameworks of 3D-linked molecular rods", which were designated porous coordination polymers (PCPs) and inspired a handful of follow-up publications by others.[35–37] However, it was not until 1995, when Yaghi and his group invented a subclass of PCPs denoted metal-organic frameworks (MOFs), that research on this still relatively new type of materials tangibly gained momentum (see Fig. 6). Like the prevenient PCPs, MOFs can be viewed as metal-ligand complexes or clusters, frequently referred to as secondary building units (SBUs), which are connected by rigid, organic struts (linkers).[38] The underlying complex bond forming reaction is reversible, therefore the laws of thermodynamics allow for the formation of highly crystalline materials. In contrast to PCPs, MOFs exhibit permanent porosity upon removal of the reaction medium in which they are synthesized, which is their key feature and selling point. The notion of permanently porous host-guest systems quickly gained so much popularity that a whole branch of interdisciplinary research was spawned, encompassing inorganic, organic, metal-organic, complex, and physical chemistry, spreading into catalysis, chemical engineering, and large-scale production.[39,40]
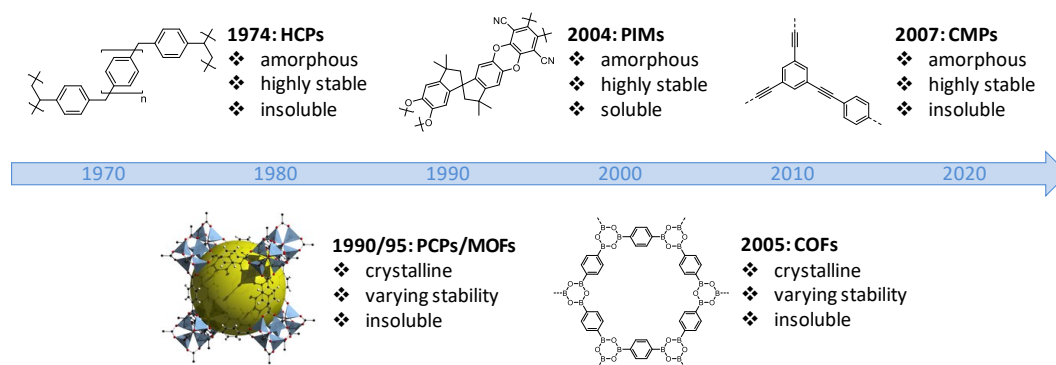
Fig. 6: Chronological appearances of the superclasses of microporous organic materials

It was shown that, similarly to zeolites, these organic-inorganic hybrid materials have well-defined pore sizes and structures. The applicability of the BET theory for the calculation of porosity properties, accessible surface area and pore sizes, has since been controversially discussed and verified.[26,29] Due to being mostly organic in nature, MOFs suffer from inferior chemical and thermal stabilities compared to zeolites. Their true value lies in the possibility of functionalization; the whole organic chemistry toolbox is at the designer's disposal. In fact the only limitation here is posed by functional groups which are incompatible with the complexation reaction forming the SBUs and which cannot be introduced by modification of the formed solid in a so-called postsynthetic modification.

Since their inception, PCPs/MOFs have attracted the attention of researchers the world over in a rarely paralleled fashion. Therefore it is hardly surprising that a decade after the first report on MOFs, fully organic but also crystalline materials were invented in the form of covalent organic frameworks (COFs). In these materials the metal nodes are replaced by organic molecules containing three or more bonding sites, offering the possibility to yield 2D as well as 3D porous structures. As is the case with MOFs, the bond

forming reactions yielding COFs are based on reversible reactions such as the trimerization of boronic acids or their condensation with catechol derivatives[41], and the condensation of aldehydes and primary amines to yield imines[42] (see Fig. 7).
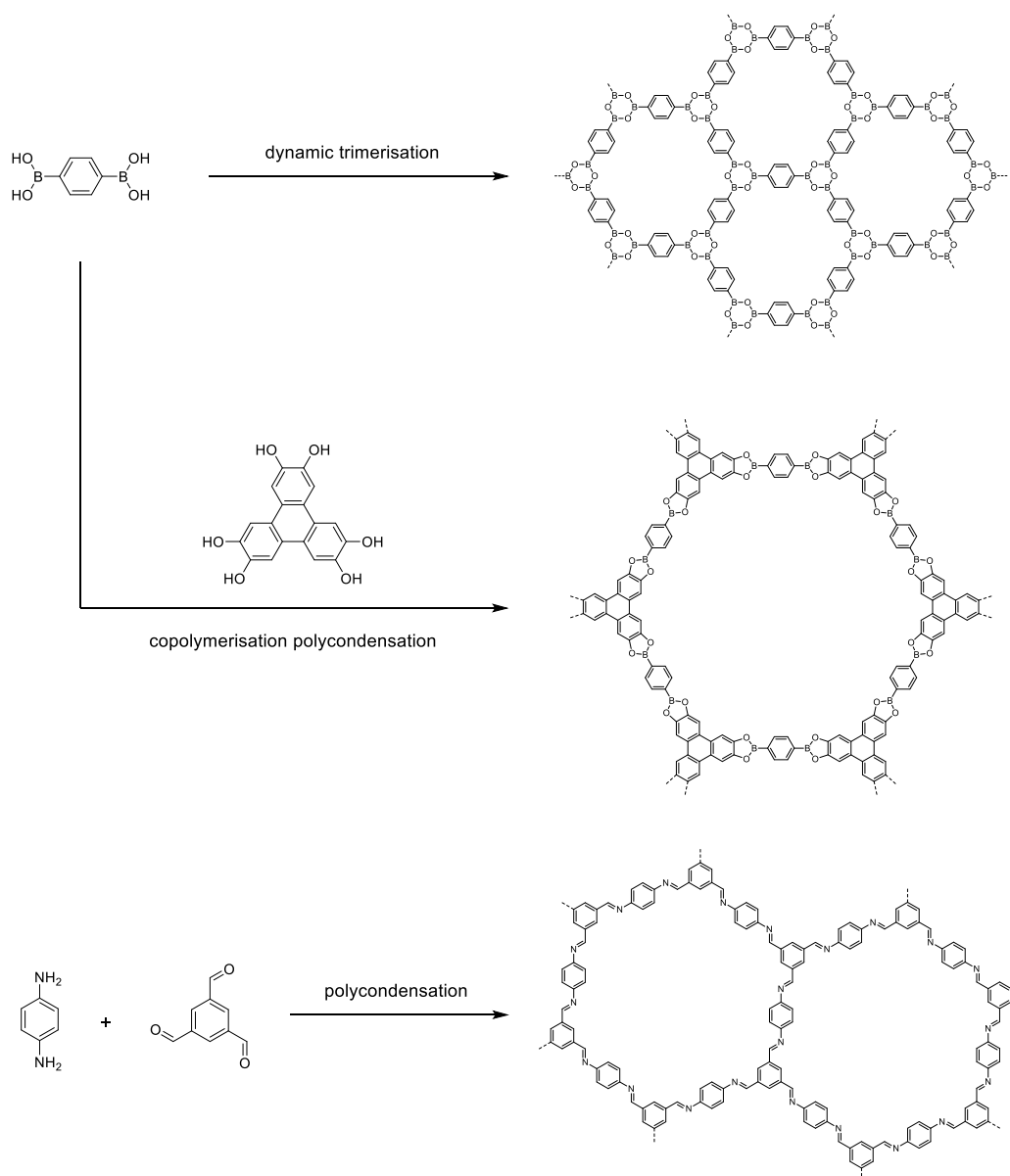
Fig. 7: First examples of COF formation reactions via dynamic trimerisation of diboronic acid compounds, boronate ester formation, and polyimine condensation[41,42]

The field of COF chemistry has since equally explosively proliferated, if as yet on a much smaller scale than MOFs (see Fig. 8). Recently, COFs based on main group elements beyond C, H, N, B, and O have been reported.[43,44] The first generations of MOFs and COFs were relatively labile to a multitude of conditions such as acidic, basic, or even simple aqueous conditions. However, over the last years reports of highly chemically stable structures of both classes have been reported.[45,46]

Even before COFs were known, in 2004 McKeown and coworkers invented a material with somewhat odd properties. By nucleophilic subsitution of the fluorine atoms at an extremely electron-deficient aromat by a spirocyclic monomer containing two
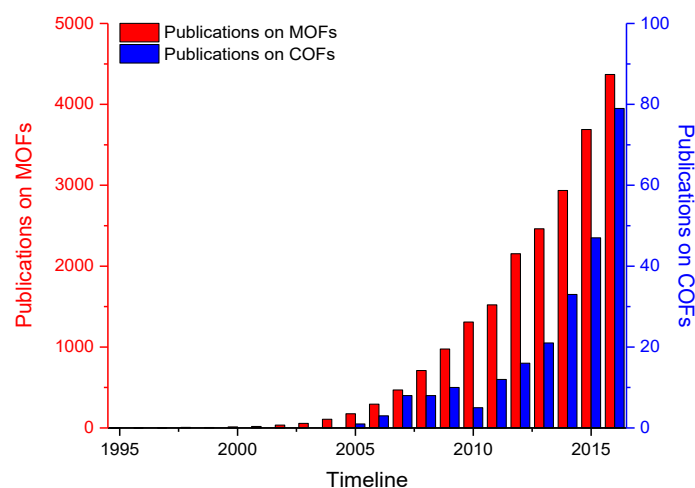
Fig. 8: Results of SciFinder keyword searches for "metal organic framework" (1995-2016) and "covalent organic framework" (2005-2016) as of February 2017

perpendicularly oriented *ortho*-dihydroxybenzene rings a linear, ladder-like polymer with multiple kinks in its backbone is formed (see Fig. 9). These kinks preclude space-efficient packing of the polymer chains, thereby merging the concept of microporosity into a soluble polymer, and the ensuing class of materials is aptly named polymers of intrinsic microporosity (PIMs).[47] These materials represent the *only* type of soluble and therefore viably processable polymeric microporous materials. Employing bent monomers is a facile way to impart microporosity on formally linear polymers. PIMs have been used to form membranes directly or mixed with other polymers or fillers to obtain multi-component membranes with increased gas separation properties.[48–50] Other functionalities that have been successfully incorporated in PIMs include spirobifluorene[51] and triptycene[52] as alternative porogenic units, Tröger's base for preferential CO_2 adsorption[53], and photo-switches to enable porosity manipulation by an external stimulus[54]. Introducing further contortion eventually leads to self-contained molecular compounds enclosing a single cavity, denoted microporous cage compounds or molecular crystals.[55–60]
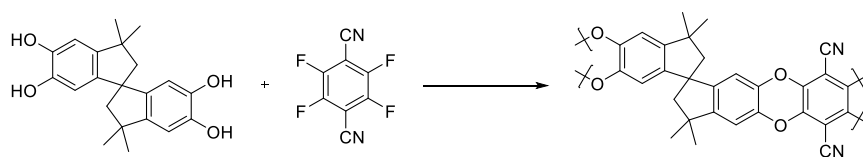
Fig. 9: Synthesis of PIM-1 by nucleophilic aromatic subsitution

Shortly after the inception of PIMs and COFs, microporous polymer networks (MPNs) emerged.[61] These materials are conceptually similar to the well-known superabsorbers[62], which are amorphous, 3D-crosslinked polymeric materials with the capacity to swell and take up large amounts of solvents. If that solvent is water the swollen materials are referred to as hydrogels, and as such have for decades experienced everyday uses, e.g. in disposable diapers or soft contact lenses. Among others, more novel applications of hydrogels are in tissue engineering[63] and drug delivery[64]. The younger MPNs however are largely hydrophobic and water-repellant, but can absorb significant

amounts of organic solvents. The swelling capability and solvent uptake capacity are limited by the degree of crosslinking. If rigid, linear struts (similar to linkers in MOF chemistry) are used, the host material is not able to collapse and pack space-efficiently upon removal of the guest molecules, i.e. the solvent, yielding a material with permanent porosity. Often employed structural motifs in MPN chemistry are linear moieties such as *para*-substituted benzene rings or acetylene groups, trigonal-planar structures such as 1,3,5-trisubstituted benzenes, and tetrahedral building blocks such as adamantane or tetraphenylmethane derivatives.

In great contrast to MOFs and COFs, MPNs are formed via irreversible C–C bond formation reactions, resulting in non-crystalline, i.e. amorphous structures. Thus they feature largely undefined pore structures and the analytical results are based on average values. A pointed difference between amorphous and ordered materials is the frequent appearance of a steady incline in the adsorption isotherms of amorphous materials, which has been falsely attributed to mesoporosity but is in fact a result of swelling of the material caused by adsorption of the probe gas.[23] Another typical feature of porous organic materials is the fact that even after presumably complete desorption of the adsorbate, the desorption curve does not form a closed loop with the origin of the adsorption curve. Much as the sometimes very pronounced hystereses, the origin of this non-closure is not entirely understood. However, it is often ascribed to the softness of the materials and their ability to undergo minor structural changes during the course of the measurement. Despite these inaccuracies, for lack of alternatives, the BET theory is applied for analysis of this class of materials as well.

Since their first appearance a plethora of MPNs have been created by various reaction types and their naming scheme has become arbitrary at best. Names such as covalent organic polymers (COPs), various types of porous organic polymers (xPOPs), porous polymer networks (PPNs), porous aromatic frameworks (PAFs), element-organic frameworks (EOFs), and others are essentially describing the same class of materials depending on the preference of the respective principal investigator and/or the type of polymerization reaction. Sometimes even the same theoretical (idealized) network can result from different reactions but have differing properties (e.g. PAF-1[65]/PPN-6[66]; PPN-4[67]/EOF-2[68]). The materials herein are commonly designated MPNs.
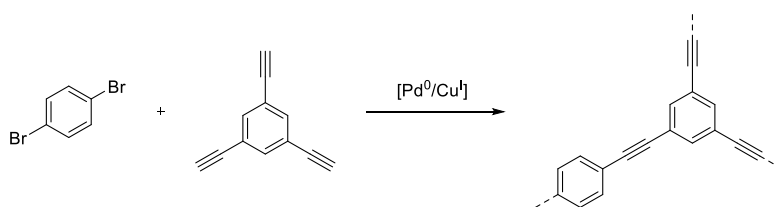
Fig. 10: Synthesis of conjugated microporous poly(aryleneethynylene) networks[61]

Probably the two most established methods to produce highly crosslinked MPNs are a variant of the Sonogashira coupling[61] and the Yamamoto-type Ullmann coupling[69] (henceforth referred to as *Sonogashira polymerization* and *Yamamoto polymerization* for reasons of simplicity). The first amorphous MPNs were reported by the group of Cooper in 2007, showing that crystallinity is not a prerequisite for highly porous materials. These first MPNs were the product of Sonogashira polymerizations, yielding porous

poly(aryleneethynylene) (PAE) networks featuring surface areas between 500 and 1000 $m^2 \cdot g^{-1}$ (see Fig. 10).[61]

Firstly introduced into the field of porous polymers by the group of Thomas in 2009[69], the nickel-mediated Yamamoto polymerization was used later that year by another group for the polymerization of a brominated tetraphenylmethane building block, yielding one of the archetypal microporous polymer networks, denoted porous aromatic framework PAF-1, with an ultrahigh BET surface area exceeding 5600 $m^2 \cdot g^{-1}$ (see Fig. 11).[65] Whereas the synthesis of PAF-1 was carried out in DMF without cosolvent at 80 °C (henceforth referred to as *PAF route*), yet another group showed that the principally same porous polymer network, this time denoted PPN-6, could be obtained in a room temperature synthesis using a solvent mixture of DMF and THF (henceforth referred to as *PPN route*). With a slightly larger, silicon-based monomer, a material of exceptionally high BET surface area of more than 6400 $m^2 \cdot g^{-1}$, namely PPN-4, was obtained with this method in 2011.[67] Other MPNs synthesized via Pd-catalyzed cross-coupling reactions such as Suzuki[70–72] and recently Hartwig-Buchwald[73] couplings have been reported. Other reaction types employed for polymerization include Eglinton homocoupling[74], Friedel-Crafts alkylation[75], Bergmann cyclization of ene-diyne systems[76], Click-chemistry[77], electropolymerization[78], nucleophilic substitution reactions[68,79,80], alkyne metathesis[81], oxidative polymerization[82], direct C–H arylation of fluorinated arenes[83], mechano-chemical synthesis[84], thermal polymerization[85,86], and more.
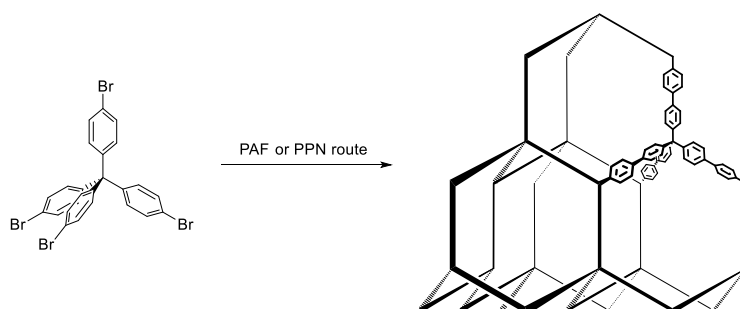
Fig. 11: Idealized excerpt of the diamandoid target structure resulting from the Yamamoto polymerization of tetrakis(4-bromophenyl)methane[65,67]

Owing to the irreversible bond forming reactions, MPNs in general have high chemical and thermal stability, which the majority of MOFs and COFs lack. The true merit of MPNs though lies in their highly simple makeup. While COF chemistry is based on main group heteroatoms and MOFs furthermore on metal ions, MPNs can in many cases forgo the use of heteroatoms entirely and hence be considered pure hydrocarbon skeletons. Notwithstanding in this assessment are unreacted end groups, residual catalyst, or other residues originating from the coupling reaction. This unique homogeneity is especially advantageous when designing microporous catalyst materials with sensitive active sites as it allows for the exclusion of functional groups with reactivity which is non-orthogonal to that of the intended catalytic sites. Based on the existence of reversible C–C bond forming reactions, a pure hydrocarbon COF is theoretically possible, but such a structure has yet to be synthesized. Alkyne metathesis offers such a reversible bond forming

reaction and has been successfully applied for the synthesis of MPNs[81], yielding the highest surface area PAE networks until this work.[87]

Interestingly, when it comes to application, unfunctionalized networks are quite useless as they offer no specific interaction with guest molecules. Designing a material with a certain purpose in mind, the incorporation of at least one functional group is indispensable.[88] Endowing porous polymers with functional groups has significant impact on their affinity towards certain gases and these values can be rationally tuned to some extent.[89] As a consequence of such functionalization uptake capacities of materials with comparable surface areas with and without varying functionalities can differ strongly.[90] Thus the overall sorption behaviour of a material can be manipulated, for example to specifically absorb one gas over another to achieve special gas separation properties.

The selective adsorption of hydrogen for the purpose of increased uptake capacities is of particular interest. Theoretical studies have shown that an accumulation of alkyne groups in a hypothetical ordered porous organic polymer should significantly raise the amount of stored hydrogen at high pressures.[91] In fact the amount of stored hydrogen in otherwise unfunctionalized MPNs could be increased by improving the chemical structure of conjugated microporous PAE networks as part of this work.[87]

As mentioned previously, finding the right balance between adsorption strength and ease of regeneration for the selective adsorption of carbon dioxide is of paramount importance. Possibilities for tuning the CO_2 adsorption strength based on Lewis acidic and basic moieties as well as combinations thereof will be discussed later within the introduction and further elaborated as part of this thesis.

Beyond gas separation and storage, another prospective field for insoluble porous materials is catalysis. The immobilization of catalytically active species known from homogeneous catalysis yields a heterogeneous catalyst. Despite their crosslinkage porous organic materials often retain a high degree of flexibility so that solvent-induced swelling may enable the diffusion of species which are significantly larger than the pore diameter calculated from an adsorption isotherm. Especially due to this phenomenon it is obvious that in respect to heterogeneous catalysis, permanent porosity offers no advantage at all, as long as the catalyst is swellable in the respective solvent and diffusion of the substrate(s) is possible. However, in a gas phase reaction such as the direct reduction of CO_2 with H_2 for example, this would be a different matter. Intriguingly, no such reaction has been published yet.

The strategies employed for the immobilization of metal-based catalytically active structures are manifold. In the case of MOFs, catalytically active transition metals may already be part of the SBUs.[92] However, if the material is supposed to act as a catalyst this is only possible if the catalytic cycle is not reliant on extensive changes in geometry around the node which might cause the porous structure to collapse, or if the SBUs contain open metal sites readily available for substrate interactions. On the other hand, it is possible to incorporate ligands into the organic backbone and fixate metal ions in MOFs[92,93], COFs[92], or porous polymers[94], which can then be utilized as heterogeneous catalysts. Moreover, catalytically active hybrid materials can be obtained by immobilization of inorganic nanoparticles in the pores of any of the mentioned materials, sometimes using the aforementioned coordination sites as seed points.[94–97]

Recently, the transition from coordinative metal-support interactions to electrostatic interaction has been made by introducing catalytically active moieties into the pores of microporous polymer networks by incorporating weakly coordinating anions into their scaffold.[98] Building on this foundation, single-ion conducting solid electrolytes[99] as well as materials with extra-framework adsorption sites for iodine capture[100] have been synthesized. But not only catalysts based on immobilized (transition) metals have been reported; there exists even a handful of examples of immobilized organocatalysts which have been introduced into microporous polymer networks[101–103], and to which this work contributes another example to be discussed further along the line.[104]

2.2 Frustrated Lewis Pairs

An interesting new class of organocatalysts are so-called *frustrated Lewis pairs* (FLPs).[105] The catalytic activity of this relatively young class of molecular materials is based on the very peculiar interplay between Lewis acidic and Lewis basic moieties. Very high steric encumbrance around both of these reactive centers precludes covalent bond formation, thereby maintaining their individual reactivity. This unquenched state is referred to as „frustrated" and offers the possibility to exploit the remaining reactivity for the activation of small molecules, namely H_2, CO_2, CH_4, N_2O, and others (Fig. 12).[106] It is this affinity towards small molecules which renders this type of catalyst particularly attractive for incorporation in a solid material.
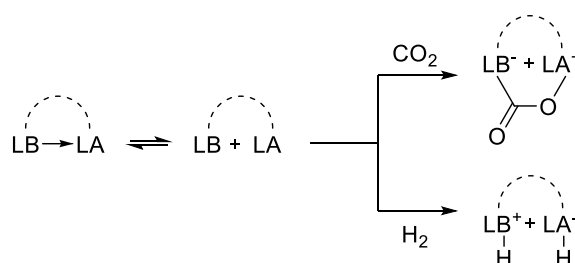
Fig. 12: Lewis acid (LA) and Lewis base (LB), linked by dashed half-circle line to indicate possibility of both being in one molecule and H_2 and CO_2 activation products

The earliest reports of a FLP dates back as far as 1942 when Brown and coworkers found that 2,6-lutidine and BMe_3 do not react, whereas 2,6-lutidine and the smaller BF_3 form a stable adduct (see Fig. 13).[107]

Interestingly, in the decades following the initial reports by Brown and coworkers, similar observations were made around sterically encumbered triphenylboron and "tritylnatrium", which were unreactive towards each other but afforded reactivity *in presence of a third component*, which was not reactive to either the proffered Lewis acid or the base alone.[108] Thus, small molecule activation by a FLP was already reported but the concept disregarded for 40 years in favor of sole Lewis acid or base chemistry.[109–111]
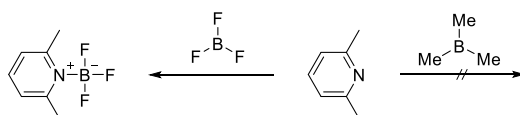
Fig. 13: Earliest report of a FLP[107]

Today, the special merit of these materials lies in the fact that they can be tuned to very specific catalytic applications without the need for a (transition) metal. Some scattered reports of metal-containing FLPs exist[112–115], rendering this advantage moot and leading highly interesting concepts such as metal-free hydrogen activation ad absurdum. For the sake of simplicity, the FLPs treated herein are entirely based on main group elements such as boron, phosphorus, nitrogen, and oxygen.

The first example of a FLP was published in 2006 by the group of Stephan[105] when the behaviour of sterically encumbered phosphines in the presence of tris(pentafluoro-phenyl)borane (hereafter abbreviated as BCF) was probed. Since the reactivity of the Lewis acidic and basic centers could not be quenched otherwise, an unexpected nucleophilic aromatic substitution reaction of dimesitylphosphine with BCF led to an asymmetric phosphine-borane (see Fig. **14**). Immediate addition of the substituted fluoride ion to the acidic boron center formally afforded the HF adduct of the phosphine-borane (**a**). This HF adduct could be converted into the dihydrogen adduct by fluoride-to-hydride exchange using Me_2SiHCl (**b**) under elimination of Me_2SiClF. Treating this dihydrogen adduct in vacuo readily yields the free phosphine-borane under liberation of hydrogen gas (**c**). Interestingly, removal of HF with a Grignard reagent directly gives the free phosphine-borane (**d**), which is able to cleave H_2 under mild conditions. Exposing the free phosphine-borane to hydrogen at ambient temperature yields the hydrogen activation product again (**e**).
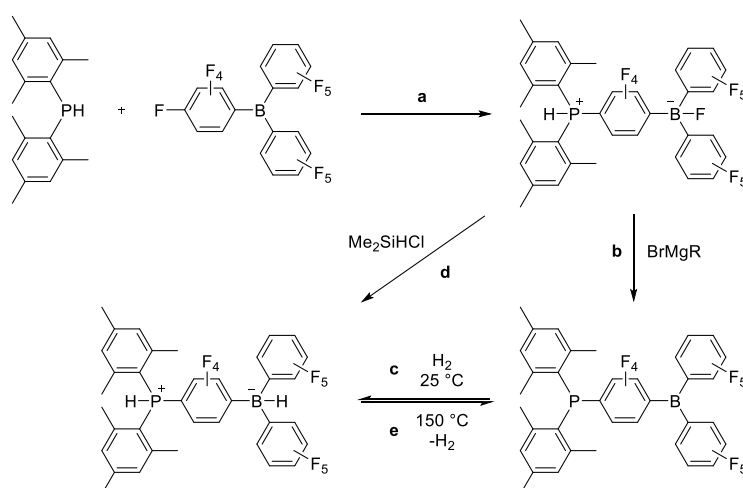
Fig. 14: Archetypal FLP by Stephan *et al.* [105]

A decent amount of FLPs has been reported, ranging from unimolecular materials[105,116–120] to systems comprising two[121–124] and even three components[125,126] determining the reactivity of the FLP. The aforementioned intramolecular phosphine-borane was obtained in an unexpected asymmetrization of BCF by nucleophilic attack of

a secondary phosphine. This nucleophilic substitution can be entirely precluded by substitution of all *para*-positioned fluorine atoms of BCF, yielding a Lewis acid similar to BCF in sterical demand and Lewis acidity. Combining this molecule (aka Stephan's borane) with a sterically encumbered tertiary phosphine gives rise to a FLP capable of activating dihydrogen without further reaction (see Fig. 15).[127]
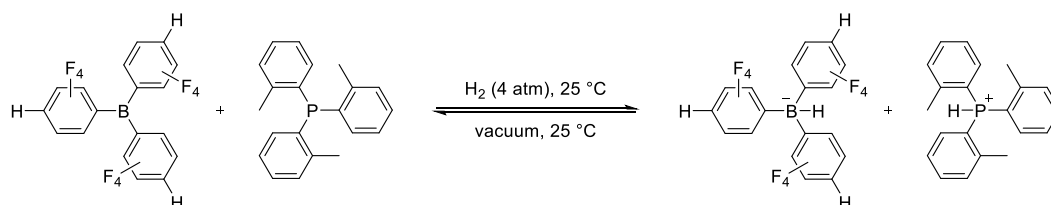
Fig. 15: Reversible dihydrogen activation by a FLP at ambient temperature[127]

The mechanism of dihydrogen activation by intramolecular Lewis pairs is subject of an ongoing discussion.[116,128–131] In any case it is deemed necessary that in the equilibrium state at a given temperature at least a certain percentage of Lewis acid and base are not bound covalently, i.e. they do not exist as a Lewis adduct. When these free species react with a substrate, they are removed from the equilibrium, which is shifted, and further free acid and base molecules are made available, and so forth. Prior to the dihydrogen activation itself the formation of an encounter complex is assumed, in which Lewis acid, dihydrogen, and Lewis base usually align in a more or less linear fashion.[116,128,130] The lone pair of the Lewis base donates electron density into the antibinding orbital of the hydrogen molecule, destabilizing the covalent bond between the protons and causing the electron pair to shift towards the Lewis acid. When this double polarization is sufficiently strong, the covalent bond is broken, dihydrogen split heterolytically, and the nascent proton and hydride adsorbed onto their respective counterparts. The product is either a zwitterion or an ion pair depending on whether the underlying FLP is of intra- or intermolecular nature, i.e. whether the active centers are contained within the same molecule or not.[132] It is important to note that in cases of both moieties existing within one molecule, the activation mechanism need not necessarily be directly discernible, and may even seem deceptively simple. Intramolecular dihydrogen activation can easily be confused with intermolecular activation. Although seeming entirely possible on paper, the geometry of a given unimolecular FLP may not permit the formation of an intramolecular encounter complex. In such cases theoretical studies can be helpful to elucidate the activation mechanism.[116,129]

For instance, the ethylene-bridged intramolecular FLP by Erker *et al.* based on bridged dimesitylphosphine and bis(pentafluorophenyl)borane units was found to coexist in a *closed* and an *open* state in solution (see Fig. 16), both of which could conceivably facilitate dihydrogen cleavage. Originally, activation of H_2 was assumed to proceed via intramolecular fashion, whereas quantum chemical calculations on this and structurally related systems give conclusive evidence of energetically favorable stacking of two bifunctional molecules via a twofold head-to-tail interaction (*dimer*). This dimer is capable of activating two equivalents of dihydrogen in two consecutive bimolecular activation processes (*dimer-H2* and *dimer-2H2*).
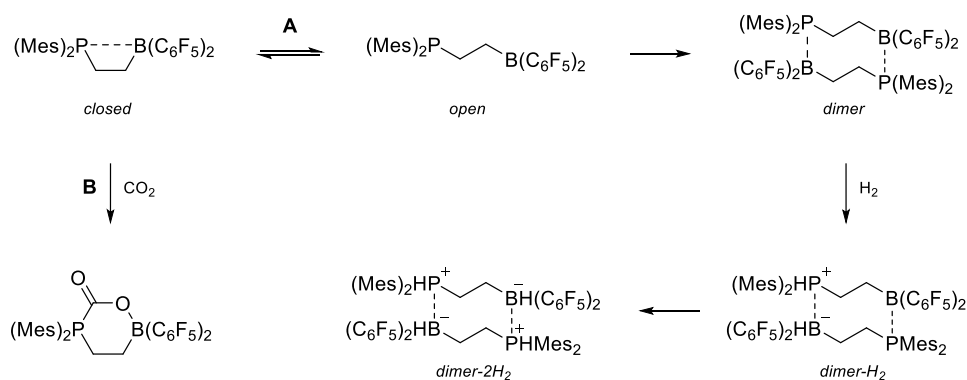
Fig. 16: Proposed intermolecular activation mechanism of two equivalents of H$_2$ by ethylene-bridged intra-molecular FLP (pathway A)[129] and proposed direct activation of CO$_2$ by closed form (pathway B)[134]

Although hydrogen is the most widely studied substrate, FLPs have been shown to be capable of activating other small molecules. In the wake of the discussion about carbon capture and sequestration, studies toward activation and transformation of carbon dioxide into valuable feedstock materials are of particular interest. To that end the carbon dioxide adduct of the aforementioned intramolecular ethylene-bridged FLP was synthesized by pressurizing a pentane solution of the intramolecular FLP with 2 bar of carbon dioxide (see Fig. 16). The adduct precipitated in near-quantitative yield and was isolated, studied by X-ray crystallography, and the assumed structure of the cyclic adduct confirmed.[133] This particular activation process was studied in detail by Pu and Privalov.[134] Interestingly, according to this gas phase study, carbon dioxide can be activated directly from the *closed* isomer without significant stretching of the P–B bond. The question arising logically from this point on is whether this activated form of carbon dioxide can be reduced to form methanol, which would be one such valuable feedstock material. The answer is positive but reserved; there exist several reports of carbon dioxide being activated by FLPs and its subsequent reduction with hydrogen.[135,136] However, yields of these reactions are very low (typically below 30 %) and not based on catalytic but stoichiometric reactions, so this chemistry is obviously still in its early stages. Theoretical calculations have been undertaken to develop rules for the rational design of FLPs for this process.[137]

An interesting approach would be to combine two differently reactive FLPs, one of which selectively activates dihydrogen and the other one carbon dioxide, with the combination of these activation processes affording catalytic reduction of carbon dioxide to formic acid. In one case the authors of a combined experimental and computational study report the simultaneous activations of CO$_2$ and an unspecified hydroborane as reducing agent within an intramolecular FLP, affording the hydroboration of CO$_2$. The product of the catalytic cycle is eliminated in the form of a methoxy-boron species which can be hydrolyzed to methanol. However, this study is of mainly mechanistic nature and no catalytic results are reported.[138]
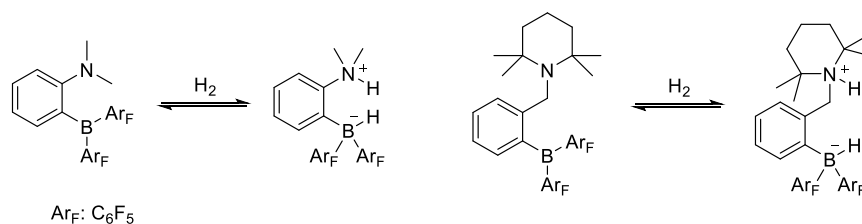
Fig. 17: Reversible hydrogen activation by intramolecular FLPs based on aminoboranes

In any case, the use of FLPs as hydrogenation catalysts for metal-free hydrogenation reactions of organic molecules is well established by now. Several series of intramolecular FLPs are based on the *ortho*-substituted *ansa*-aminoborane or the related *ortho*-borylaniline core (see Fig. 17).[116–119]

Subsequent to the activation of hydrogen, these and other hydrogen-activating FLPs have been applied for the hydrogenation of various substrate families, among others C=O[139], C=N[120], and various types of C=C[140,141] double bonds. Further applications are dehydrosilylation of alcohols and silanes to silanolethers[126] and the dehydrogenation of amine-boranes, which prove to be interesting candidates as novel H_2 storage materials.[142]

To date, the greatest challenge in further developing FLP chemistry is posed by their tedious handling. The uniting feature of most "conventional" FLPs is the highly sensitive super acid BCF or a closely related moiety (see Fig. 18).
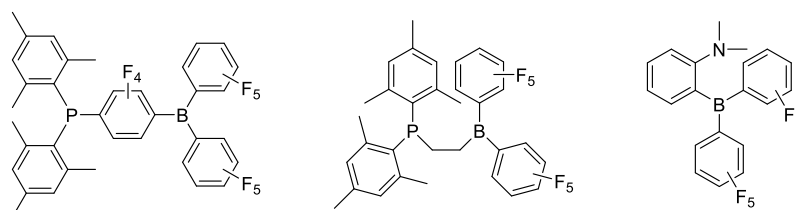
Fig. 18: Examples of FLPs incorporating moieties structurally related to $B(C_6F_5)_3$

The presence of these superacidic boron centers causes the materials to be highly susceptible towards humidity[143]. Upon contact of BCF with water molecules an extremely hard to cleave Lewis adduct is formed which is even prone to slow protodeborylation, i.e. hydrolysis under loss of one of the perfluorinated phenyl rings. In the case of FLPs, this circumstance is aggravated since proton transfer from H_2O to the basic component can occur, rendering the whole FLP inactive. Next to triarylboron species, examples of other possible sources of Lewis acidity for FLPs capable of activating both H_2 and CO_2 in presence of phosphines are silylium ions[125] and fluorophosphonium ions, all of which bring the same susceptibility towards humidity with them.[144]

To judge the acid strength of a molecule the method developed by Gutmann and Beckett[145] as well as Childs'[146] method are frequently used. These methods rely on changes in the chemical shifts upon addition of specific probe molecules to the acidic substances. The Gutmann-Beckett method is based on the chemical shift of triethylphosphine oxide as judged by $^{31}P\{^1H\}$ NMR whereas the Childs' method relies on the aldehyde proton of crotonaldehyde and the Lewis acid strength is determined by

^{1}H NMR spectroscopy. For both methods, the acidity of a given acid is then evaluated by referencing the extent of the respective shift to the shift of the probe in combination with BCF (see Table 1). In the example given below, the Lewis acidity of the aforementioned Stephan's borane[127] (see Fig. 15) is determined. Exchange of the *para*-fluorine atom on each perfluorophenyl ring of BCF results in slightly lower Lewis acidity than the reference.

Table 1: Example of the Gutmann-Beckett method to determine the Lewis acidity of B(p-C$_6$F$_4$H)$_3$ relative to B(C$_6$F$_5$)$_3$ in CD$_2$Cl$_2$[127]

	Et$_3$PO–B(C$_6$F$_5$)$_3$	Et$_3$PO	Et$_3$PO–B(p-C$_6$F$_4$H)$_3$
δ(^{31}P{^{1}H})	78.1	51.5	77.3
Δ_δ($\delta_{adduct} - \delta_{Et_3PO}$)	26.6		25.8
Δ_δ(Et$_3$PO–B(p-C$_6$F$_4$H)$_3$) / Δ_δ(Et$_3$PO–B(C$_6$F$_5$)$_3$)	0.97		

Instead of relying on a superacid and relatively weak base, Mummadi *et al.* recently opted to switch functionalities and were able to afford dihydrogen activation with so-called "inverse" FLPs based on organosuperbases and relatively weak Lewis acids.[147] While conceptually intriguing, the superbases bring with them the same caveats as super acids.

To facilitate the handling and to broaden the scope of application for FLPs, advances in respect to the stability of Lewis acids were made. Recently, Soós and coworkers[148], following up on preliminary work by Ashley et al.[149], developed an electronically fine-tuned triarylborane by exchanging one pentafluorophenyl unit of BCF with a 2,6-dichlorophenyl unit. The increased steric bulk around the boron atom renders the molecule less electrophilic and thus moisture-resistant without diminishing its Lewis acidity. Consequentially this acid can be manipulated under open-bench conditions, no glovebox or Schlenk technique required. This Lewis acid forms FLPs with ethereal solvents such as diethyl ether and can be applied for the reduction of ketones and aldehydes under relatively mild conditions (usually 20 bar H$_2$, 55 °C).
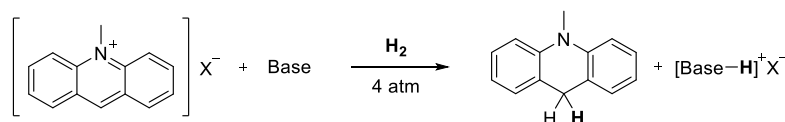
Fig. 19: Orbital-selective hydrogen activation by FLPs based on *N*-methylacridinium salts[126]

Another report of air- and moisture-stable FLPs is based on *N*-methylacridinium as acidic component, circumventing the sensitivity of boron-based Lewis acids entirely.[126] The authors base this exclusive reactivity on a high hydride ion affinity and low oxophilicity at the C9 position of the *N*-methylacridinium moiety (see Fig. 19). Depending on the anion accompanying the acridinium salt, the hydrogen activation product is able to catalyze the reductive transfer hydrogenation and hydrosilylation of aldimines using amine-boranes

and silanes, respectively, as well as the dehydrosilylation of aliphatic and aromatic alcohols by silanes.
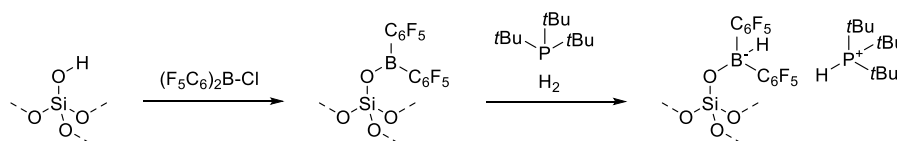
Fig. 20: Reaction of bis(pentafluorophenyl)boryl chloride with silica and subsequent H₂ activation with tris(*tert*-butyl)phosphine[150]

Great advances in the field of FLP chemistry have obviously been made within the last decade. But, for all the efforts invested into their development, incorporation into porous organic materials has until the time of this dissertation not been reported. The sole instance of solid FLP chemistry has been published only recently and stems from the field of silica-supported materials.[150] This report focuses on the immobilization of a bis(pentafluorophenyl)boryl species by reaction of bis(pentafluorophenyl)borane with a porous silica matrix to effect Si–O–B formation, the product of which is in combination with tris(*tert*-butyl)phosphine able to cleave H₂ (see Fig. 20).

2.3 Lewis Acids and Bases in Microporous Polymer Networks

Prior to this thesis, the incorporation of FLPs into purely organic porous materials had yet to be reported. The number of reports on purely basic materials however is vast since these are of enormous interest for the purpose of carbon capture, and therefore widely explored.[151,152] In many cases the affinity towards CO_2 is bestowed upon the material by the presence of heteroatoms offering a lone pair for electrostatic interaction (see Fig. 21).
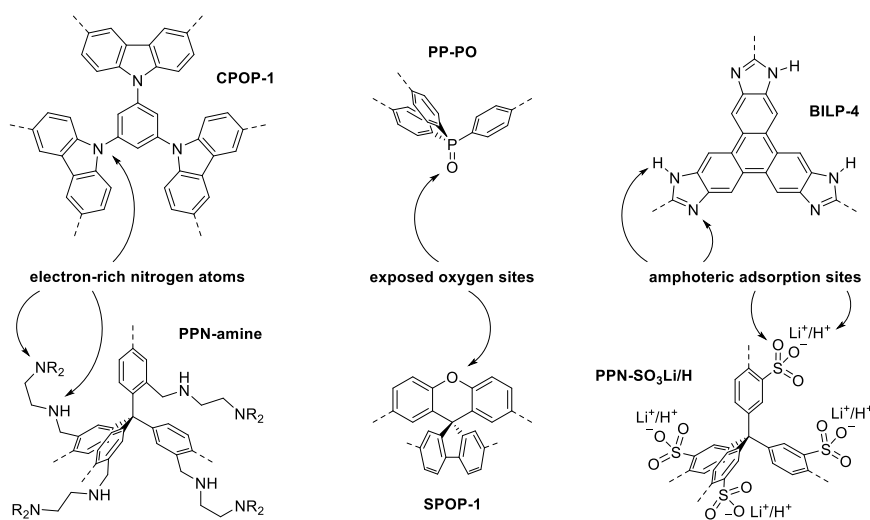
Fig. 21: Examples of Lewis basic and amphoteric MPNs for preferential CO_2 adsorption

While an integral part of imine COFs, a large number of amorphous networks based on nitrogen atoms are known. These networks can either be formed by

polycondensation reactions involving amine moieties, by C–C coupling reactions of nitrogen-containing building blocks, or by postsynthetic introduction of alkylamines. Especially the latter technique has been explored in MOF chemistry since nucleophilic amine groups are often strong ligands and would therefore interfere with the MOF formation.[153,154]

Some scattered reports on purely Lewis acidic materials exist, some of these focusing on materials with metal ions as Lewis acidic sites. In most cases these ions are countercations to and accompanied by non-weakly coordinating anions, i.e. conjugated bases to organic acids such as phenylsulfonates.[66] These materials are actually Lewis amphoteric and the CO_2 affinity is a function of both Lewis acidity and basicity, whereby the direct interaction between the two needs to be overcome beforehand. Exceptions are networks in which metal ions are counterions to weakly coordinating anions, such as polyborate networks, where the cations are only coordinated by solvent molecules and only the Lewis acid strength of the metal ion determines the guest binding strength.[98,99] After activation free coordination sites can be generated and are accessible to adsorbates such as H_2 and CO_2.

Table 2: Examples of MPNs for preferential CO_2 adsorption

Designation[a]	Functional moiety[b]	SA_{BET} [m²·g⁻¹][c]	P [bar][d]	T [K][e]	Q_{st,CO_2} [kJ·mol⁻¹][f]	CO_2 uptake[g] [mmol·g⁻¹]	[wt%]
PAF-1[65]	Biphenyl	5640	40	298	n.d.	29.5	130
PPN-4[67]	Biphenyl	6461	50	295	n.d.	38.9	171
PPN-6[66]	Biphenyl	4023	1	295	17	1.3	5.7[†]
PPN-6-SO₃H[66]	Sulfonic acid	1254	1	295	30.4	3.6	15.8[†]
PPN-6-SO₃Li[66]	Lithium sulfonate	1186	1	295	35.7	3.7	16.2[†]
PPN-6-CH₂-DETA[155]	Alkylamine	555	1	295	56	4.3	18.9[†]
P4[87]	Alkyne	2552	1	273	24.3	3.4	14.8
BILP-4[156]	Benzimidazole	708	1	273	28.7	5.3	23.5
CPOP-1[157]	Carbazole	2220	1	273	27	4.8	21.2
SPOP-3[158]	Xanthene	965	1	273	n.d.	2.6	11.6
PP-PO[159]	Phosphine oxide	1353	1	273	n.d.	3.8	16.9
P6	Cyanovinyl	112	1	273	40.3	2.0	9.0

[a]Designation given in the original publication; [b]moiety predominantly responsible for host-guest interaction; [c]BET surface area; experimental [d]pressure and [e]temperature; [f]isosteric heat of adsorption; [g]carbon dioxide uptake at 273 K and 1 bar; [†]the conversion to wt% in the original publication was found to be incorrect and the values are given here in corrected form

Purely Lewis acidic, charge-neutral MPNs on the other hand are not widely studied. At the time of writing only two instances of boron as the sole heteroatom in the network are found in literature. In both cases these polymers are based on the sterically very demanding and synthetically well accessible tris(tetramethyl)borane building block. Due to the absence of fluorine atoms or other electron-deficient substituents[160] this tecton is only moderately Lewis acidic but highly resistant to water complexation due to the strong steric overcharge. The group of Mu prepared a MPN containing tris(tetra-methylphenyl)borane via alkyne homocoupling with a surface area of 815 m²·g⁻¹.[161] Despite the incorporation of boron sites, the uptake of CO_2 is on par with but not superior to reported boron-containing COFs at the time, which can be attributed to the low

electrophilicity due to strong steric repulsion. Suresh *et al.* coupled the same structural motif via Sonogashira coupling with a biphenyl unit to obtain a sensor for the detection of fluoride ions, thereby proving sufficient Lewis acidity and electrophilicity to react with the very small fluoride anion.[162] The material exhibits a comparatively low BET surface area of 390 $m^2 \cdot g^{-1}$ and is, due to a lack of strong Lewis acidity, not suitable for any reported FLP chemistry with triarylphosphines.
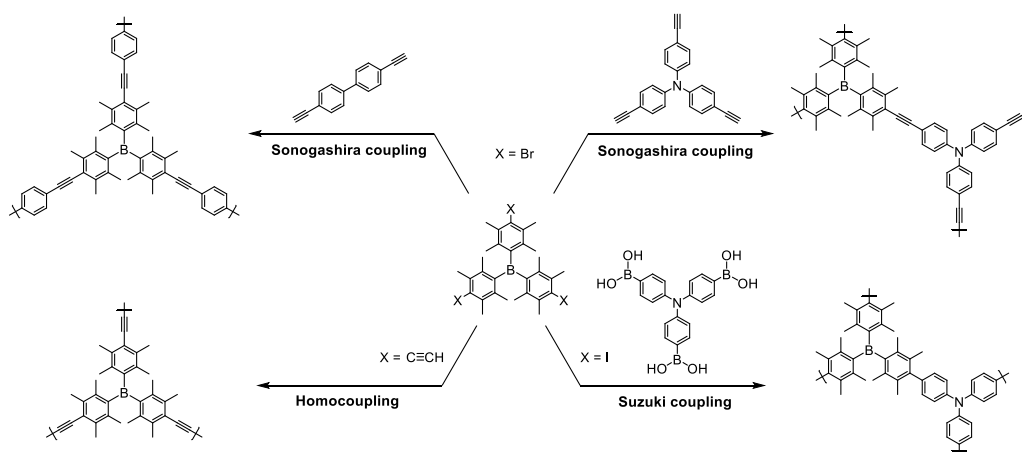
Fig. 22: Examples of boron-containing MPNs[161–163]

The phenylene-bridged FLP systems by Stephan and coworkers[105] as well as Repo and coworkers[116,119] are not only bifunctional acid and base molecules but, due to their conjugated π-electron system, donor-acceptor systems as well, which is often reflected in very deep coloring of these systems. The combination of such moieties in this manner is not only interesting for FLP chemistry but also known from the field of optoelectronics.[21]

A handful of porous organic materials including donor as well as acceptor moieties are known. Mu and coworkers[161] as well as Feng and coworkers[163] were the first to couple the aforementioned tris(tetramethylphenyl)borane to tritopic nitrogen-based monomers to form porous π-conjugated donor-acceptor polymers via Sonogashira coupling and Suzuki coupling, respectively. The resulting materials featured BET surface areas between 600 and 1300 $m^2 \cdot g^{-1}$ and interesting luminescence properties, but no cooperative effects on H_2 and CO_2 sorption properties, which turned out to be largely in line with the respective N_2 surface areas. Two years later the less sterically demanding tris(2,6-dimethylphenyl)borane building block was coupled via Suzuki coupling to a triphenylamine building block, again by Mu and coworkers.[164] The reaction yielded a material which could selectively sense and scavenge fluoride over other common anions. It exhibited a BET surface area of 950 $m^2 \cdot g^{-1}$ and was easily recyclable by stirring in ethereal solution of a sacrificial fluoride scavenger such as BF_3–OEt_2.

The electronic interplay between Lewis acid and base has also been exploited by electropolymerization of a structure featuring the aforementioned tris(tetramethyl-phenyl)borane motif coupled to three *N*-phenylcarbazole units. The resulting polymer films could be formed on various supports and, after ligation of the boron center with fluoride ions, exhibited interesting electronic features such as tunability to be either electron- or hole-selective electrodes depending on the oxidation state of the system.[165]

No highly Lewis acidic MPNs have as yet been reported. Hence, this thesis and the derived publications give the first results of organic FLP-type microporous materials.

3 Goal and Motivation

In view of the importance of microporous materials with applications as hydrogen or carbon dioxide storage materials as well as catalysts, it seems promising to extend the scope of immobilized systems to FLPs. Employed for the purpose of catalysis, this immobilization enables recyclability by simple filtration, washing, and drying of the catalyst. In respect to gas storage, the presence of opposing polarities in close proximity but precluded from mutual quenching has been proven to have a great impact on small molecules, thus strong host-guest interactions for solid materials containing FLPs are to be expected. In fact, in this way chemisorption and physisorption of hydrogen as well as carbon dioxide could theoretically be achieved in one single material offering multiple types of adsorption sites. It has to be noted that altough conceptually of high interest, the absolute uptake would presumably be too low to be of immediate practical relevance. To achieve sufficient gravimetric uptakes a high degree of functionalization is necessary. This condition is aggravated by the fact that, next to a sterically encumbered Lewis basic moiety, many simple and well characterized FLPs contain derivatives of BCF comprising perfluorinated benzene rings and therefore high molecular masses, which in turn raise the overall weight of the material and reduce the gravimetric uptake.

Since most simple FLPs rely on highly Lewis acidic BCF, which is quite challenging to handle due to its extreme susceptibility towards nucleophiles, it seems wise to focus on a bimolecular system in which the basic component can be immobilized and the solid material impregnated with BCF under inert conditions. Using a simple two-component boron/phosphorus FLP system as a model[122], the remaining question is what type of matrix can be utilized to incorporate a FLP. Microporous polymer networks lend themselves as host materials since they can be designed without inclusion of heteroatoms in the target structures, thereby offering no competing functionalities beyond the desired ones. This opens the possibility to employ BCF without rendering it inactive, or destroying the backbone of the porous material by coordination of or even reaction with the boron

center. Moreover, shielding by a hydrophobic environment is expected to protect BCF against ubiquitous air humidity, which is sufficient to deactivate many FLPs after a short time. The degree of hydrophobicity is known to be enhancable by incorporation of alkyl chains to stabilize otherwise sensitive materials.[166,167]

To achieve a high degree of functionalization it is expedient to employ a homopolymerization technique since these methods allow the direct coupling of functional units to one another without the necessity of a co-monomer, avoiding nonfunctional domains in the polymer. Due to the ability of triphenylphosphine species to oxidize to triphenylphosphine oxide it is unsuitable to employ polymerization methods such as Friedel-Crafts alkylations or oxidative polymerizations requiring the use of oxidants such as $FeCl_3$. The Yamamoto polymerization on the other hand is intriguing since the polymerization of a triphenylphosphine-based monomer via this method is reported.[159] Conveniently, triarylphosphines are easy to handle and not very reactive on their own except for slow oxidation in air, hence facile handling of the monomers and straightforward polymer synthesis is to be expected.

Given these prerequisites, the first goal is to partially embed the chemically robust Lewis basic component of the model FLP into a MPN followed by addition of the much more sensitive Lewis acid under inert conditions. After proving the functionality of this semi-immobilized FLP it is possible to progress in several directions. The ultimate goal should be the immobilization of a full FLP.

The semi-immobilization approach also can be extended to other polymerization methods such as the highly versatile Sonogashira coupling. However, several of the synthetic aspects of this method were unclear at the time of conception of this project. Therefore a critical examination of the Sonogashira polymerization conditions seemed purposive.

The working mechanism of traditional amine-scrubbing facilities relies on the formation of highly stable carbamate salts. Since the main disadvantage of these facilities is their high energy demand for regeneration, the development of carbon capture materials with sorption enthalpies on the verge between physi- and chemisorption seems promising. The high stability of the formed carbamate salt stems from the ability of the carbon-binding amine group to release a proton to an adjacent amine under formation of a stabilized, zwitterionic structure. An as yet unexplored class of materials for carbon capture are MPNs bearing nitrile moieties. This class of materials is well known for its luminescence properties and is easily accessible via Knoevenagel polycondensation reaction. Potential tectons for porous materials formed via this reaction are commercially available or can be readily synthesized from inexpensive precursors. The highly polar nitrile group exhibits an exposed nitrogen-centered lone electron pair and small steric hindrance but no nitrogen-bound hydrogen atoms to abstract, hence stabilization via proton shift cannot occur. Thus, resulting materials might offer a good balance between sorption strength and regenerability. On the other hand the nitrile group is only weakly basic and should therefore not interfere with the majority of established polymerization processes.

4 Extension of Copper-free Sonogashira Coupling for High-Surface-Area Conjugated Microporous Poly(aryleneethynylene) Networks

Following the 1990's surge of publications in the field of microporous materials, the first systematic study of insoluble 3D amorphous networks was reported in 2007 by the group of Cooper in the form of conjugated microporous poly(aryleneethynylene) networks, formed by a variant of the Sonogashira-Hagihara coupling.[61] Due to their cost-effectiveness, robustness and ease of synthesis, these materials have since been the focus of hundreds of publications.

4.1 CMPs, MPNs and PAEs

These networks are commonly referred to as conjugated microporous polymers and abbreviated CMPs. However, this designation is somewhat equivocal since very often the actually conjugated sections are rather short and not longer than two *para*-substituted benzene rings connected by an alkyne group. Beyond this length the conjugation is usually broken by a tetrahedral, sp^3-hybridized carbon atom or a *meta*-substituted benzene ring. Hence this designation is more accurately used for truly conjugated materials such as polyphenylenes.[168] Sometimes the abbreviation CMP is even used interchangeably with MPN. Independent of their origin, amorphous microporous polymers in general are herein referred to as microporous polymer networks (MPNs), and polymers resulting from Sonogashira-type coupling reactions are designated poly(aryleneethynylene) (PAE) networks.

4.2 Structural Analysis

Given that the reported procedure was simple and consistently produced microporous materials, the focus of the overwhelming majority of publications was set on the immediate properties of the products. In an early publication, DMF was identified as the ideal reaction medium in respect to surface area maximization (see Fig. 23).[169] After that, only very few publications expressed explicit interest in the formation mechanism of the networks and their structure beyond the incorporated functional units.[170–172] Since the formed networks are utterly insoluble and amorphous, accurate structural analysis is no easy feat due to spectral analysis suffering from severe peak broadening.
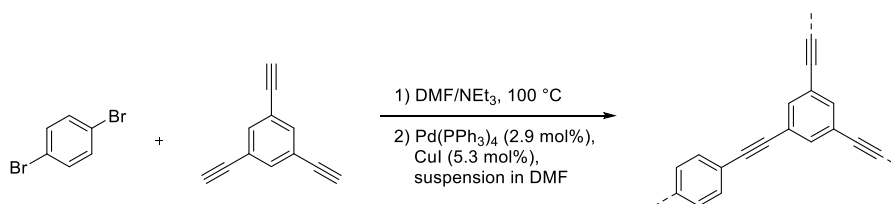
Fig. 23: Optimized PAE network synthesis conditions from 2010 involving catalyst hot-injection[169]

Seven years after their first appearance the group of Cooper put forth a discussion of the mechanism of PAE formation with strong emphasis on end group analysis.[170] This report conclusively demonstrates that with reaction times extended to 18 hours, BET surface area and total pore volume of the model network CMP-1 are maximized while the amount of unreacted alkyne end groups approaches only trace level. This is particularly noteworthy because the original protocol uses a 1:1 ratio of the depicted monomers, resulting in a 50 % excess of alkynes (see Fig. 23).[61,77,167,169,173,174] This approach dispenses with chemical intuition but empirically yielded the highest surface area materials, hence many citing works have followed this procedure.[94] The mechanistic study reasons that although crosslinking should be higher when using the correct stoichiometry[170], premature precipitation of the oligomers bearing halides instead of alkynes may hinder the reactivity so that efficient crosslinking is kinetically precluded. Providing a large excess of alkynes guarantees smaller, alkyne-capped particles which crosslink over elongated reaction times, allegedly forming diynes in alkyne-alkyne homocoupling reactions.

Shortly after the group of Bunz made advances in this area as well.[172] The authors created a homocoupled alkyne network using a Pd^0/Cu^I-based co-catalyst system and a tetrahedral tin-based monomer comprising acid-labile C–Sn bonds. The network was digested with acid and the short, soluble fragments analyzed by liquid NMR, showing that under conventional polymerization conditions not only alkyne homocoupling occurs, but that up to four alkyne groups can react, yielding a whole family of enyne configurations.

After initial experiments towards optimization based on structural analysis by Bildirir[175] this stoichiometry conundrum was treated further in the course of this work. The necessity of the employed hot-injection of catalyst and the relatively high catalyst loading were also examined. **Article I** reports on the optimization of the synthesis parameters.[87] As a result, a facile one-pot procedure yielding unprecedentedly pure structures and high surface areas was obtained, which was applied to further systems.

4.3 Coupling Efficiency

Apart from the aforementioned end group analysis[170], an often neglected way to judge the coupling efficiency of metal-catalyzed polymerization reactions is the yield in which a polymer is obtained. If every monomer reacts perfectly with all its reactive sites to form an agglomerate that is large enough to precipitate and be collected, the practical yield should be 100 %. Since all the previously discussed C–C coupling reactions (with exception of alkyne methathesis, to a certain degree) as well as many other MPN forming reactions afford kinetic products, the emergence of structural defects, which cannot be corrected due to the irreversibility of the reactions, is highly probable. Thus, not all reactive sites will react, leading to open ends within or on the edges of the network. Many C–C coupling reactions involve halide atoms. Of these, especially iodine, often favored by merit of its high reactivity, is very heavy compared to carbon and hydrogen. Therefore unreacted iodine atoms markedly increase the weight of the product. If all but a few reactive sites have found a corresponding partner it is possible for the reaction to result in yields exceeding the theoretical 100 %.

Interestingly, this is not entirely disadvantageous. If the yield of a polymer lies far below 100 %, e.g. 70 %, it is highly probable that one of the reactants is unreactive under the given conditions and that a large amount of monomer is not included in the product. Furthermore, since reactivity was too low to include all monomers, it can be surmised that significant amounts of unreacted end groups are included as well. Thus, the actual yield in terms of functional units would be even lower than the 70 % determined by weight. On the other hand, if the yield exceeds 100 % it is highly probable that the actual yield in terms of functional units is near or at 100 % with the unreacted halide atoms adding extra weight. A yield far above 100 % is an indication that precipitation occured prematurely and that the reaction should be repeated at lower concentration or using different catalyst amounts to obtain a higher degree of cross-linking.

It is important to note that the assessment of polymerization efficacy based on yield is of qualitative nature only and needs to be corroborated by complementary methods such as solid state NMR or IR spectroscopy.

It must also be noted that this method is in no way applicable to materials obtained by Yamamoto polymerization. This method is not metal-catalyzed but metal-mediated, which means that it requires the use of stochiometric amounts of metal species to afford a coupling event at every reactive site. The nickel species undergoes transformation from Ni^0 to Ni^{II} during the reaction and cannot be reduced in situ to be re-used. This circumstance renders it a very expensive method. At the same time it simplifies assessment by yield because unreacted end groups will still insert Ni^0, form a carbanion, and be quenched during acidic aqueous workup, affording the C–H species which hardly influences the weight of the sample. Thus, a quantitative yield is the optimal outcome of a Yamamoto polymerization.

4.4 Application of the Improved PAE Synthesis Protocol

If all reaction partners display only two reactive sites, polymerization leads to the formation of chain strands instead of a network. With the exception of PIMs, the minimum structural requirement posed on monomers for the formation of microporous polymer networks is that at least one of the monomers is tripodal. Ideally the reacting positions of a building block are symmetrically distributed over the whole molecule to span the largest possible surface area. In case of bipodal, tripodal and tetrapodal monomers, the reacting sites are ideally located in linear, trigonal-planar, and tetrahedral alignment, respectively, resulting in D_{2h}, D_{3h}, and T_d symmetry. Breaking of the symmetry can still result in suitable building blocks, for instance with various C_2, C_3, and C_4 symmetry types. All monomers used in this work adhere to one of these three symmetry types.

Given equal reactivity of the functional group positions an increase in dimensionality of the starting material should theoretically result in an increase in surface area. For widening the scope of the developed synthesis protocol it is expedient to establish a library of building blocks. These were purchased from commercial sources or prepared after reported procedures. In analogy to CMP-1, the herein obtained reaction product of 1,4-diiodobenzene with 1,3,5-triethynylbenzene is denoted **PAE-1**.

4.4.1 Unfunctionalized Model Compounds

By merit of their ideal structures and commercial as well as synthetic availability, 1,4-diethynylbenzene (**DEB**, C_2) and 1,3,5-triethynylbenzene (**TEB**, C_3) are highly suited alkyne monomers. However, both materials are self-reactive at ambient temperature and arrive in varying states of decomposition after purchase. The as-purchased yellow to brown powders were therefore sublimated under high vacuum, in the case of **TEB** at elevated temperatures, yielding white crystals of **DEB** and **TEB**, which were stored in the freezer to avoid degradation. Tetrakis(4-ethynylphenyl)methane (**TEPM**, C_4) was synthesized as tetrahedral alkyne compound after a reported three-step procedure starting from tetraphenylmethane via bromination, cross-coupling with ethynyltrimethylsilane, and subsequent removal of the trimethylsilyl group.[176] Notably, **TEPM** does not exhibit the same self-reactive behavior as **DEB** and **TEB** and can be stored at ambient temperature indefinitely.

Since the polymer synthesis conditions were optimized for the reactions of **TEB** with 1,4-diiodobenzene (**DIB**, C_2) and tetrakis(4-iodophenyl)methane (**TIPM**, C_4), all other given results are unoptimized. Since test reactions indicated that the elaborated conditions were unsuitable for reactions involving 1,4-dibromobenzene, mostly iodinated building blocks were used. Whereas **DIB** and the extended 4,4'-diiodobiphenyl (**DIBP**) are commercial, 1,3,5-triiodobenzene (**TIB**, C_3,) was prepared from 1,3,5-tribromobenzene after a reported two-step procedure[177] via one-pot magnesiation/silylation reaction and subsequent trimethylsilyl-iodine exchange using iodine monochloride. **TIPM** was obtained by iodination of tetraphenylmethane according to literature.[178]

Table 3: List of experiments with unfunctionalized halides and alkynes

	Halide	Alkyne	Product structure (excerpt)	SA_{BET} [m²·g⁻¹]
1				914
2				2552
3				873
4				1720
5				1121
6				1811
7				1606
8				1969
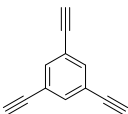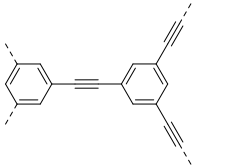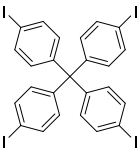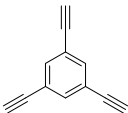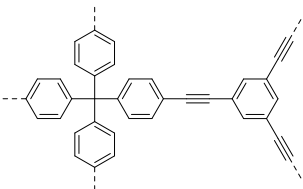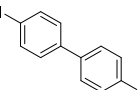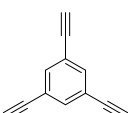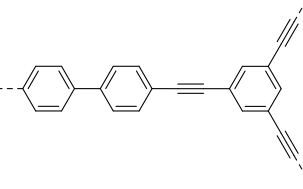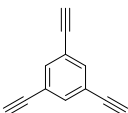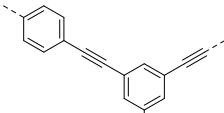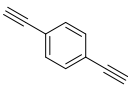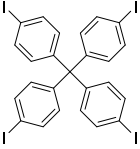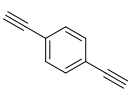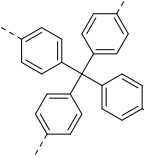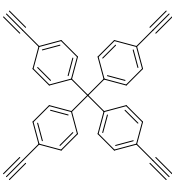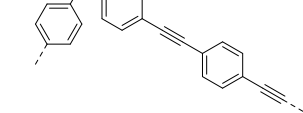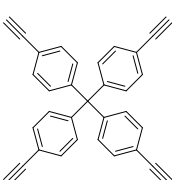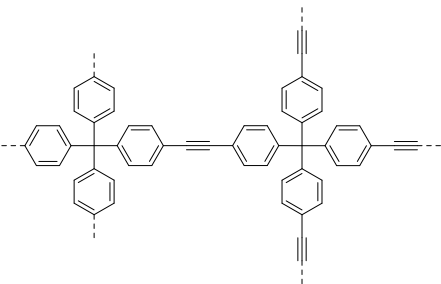
The best results obtained by reaction of the enumerated alkynes and organohalides are summarized (see Table 1). Surprisingly, the highest surface area of 2552 $m^2 \cdot g^{-1}$ was found for the combination ($C_4 + C_3$), i.e. **TIPM** + **TEB** instead of the polymer comprising two tetrahedral monomers, **TIPM** + **TEPM**. This material exhibited a maximum surface area of 1969 $m^2 \cdot g^{-1}$, which is close to the value of 1917 $m^2 \cdot g^{-1}$ obtained by the earlier protocol[77], the highest reported surface area of a Sonogashira polymer until the appearance of **Article I**.[87] Whereas the reactions of tetrahedral **TIPM** with linear **DEB** and trigonal-planer **TEB** gave the expected yellow and off-white, voluminous materials, the product of the reaction of **TIPM** and **TEPM** yielded brown, condensed crumbs instead of the expected colorless, voluminous material (see Fig. 24). According to the results obtained previously, color and texture of the products are indicative of the degree of cross-linking and hence the surface area. Thus the lower than expected surface area of the ($C_4 + C_4$) reaction product is in agreement with its poor texture quality.

Fig. 24: From left to right: products of TIPM + DEB ($C_4 + C_2$), TIPM + TEB, ($C_4 + C_3$) and TIPM + TEPM ($C_4 + C_4$).

The optimized protocol affords materials with large amounts of internal alkyne groups which have been shown to exhibit a high affinity towards H_2 and CO_2. **TIPM** + **TEB** yields a material exhibiting isosteric heats of adsorption of 6.5 and 24.3 $kJ \cdot mol^{-1}$ for H_2 and CO_2, respectively, both showing small loading dependency. These values are significantly higher than those of reference high-surface-area materials PPN-4[67] (4 $kJ \cdot mol^{-1}$ for H_2) and PPN-6[66] (17 $kJ \cdot mol^{-1}$ for CO_2). In combination with the high BET surface area these isosteric heats of adsorption lead to uptake capacitites of 1.55 wt% hydrogen and 14.7 wt% CO_2 (3.36 $mmol \cdot g^{-1}$) as reported in **Article I**.[87]

In some cases, reversing the functionalities of the starting materials can lead to the same networks (see Table 3, entries 4 and 5 as well as entries 6 and 7). In those cases, two surface areas for the product structure are given. These experiments are useful to determine how the functional group positions influence the reactivity of the building block as a whole under a given set of conditions. Since the experiments of **TIPM** with **DEB** and **TEB** yielded reasonable results, but the $C_4 + C_4$ reaction gives a material of lower than expected surface area and poor texture quality it is expedient to assume that the use of **TEPM** gives rise to lower quality coupling reactions. To test this hypothesis the reaction **TEPM** + **DIB** was carried out, which should theoretically yield the same network as the successful reaction of **TIPM** with **DEB** (see Fig. 25, entries 6 and 7). As expected, the texture of the resulting material is similar to the that of the reaction **TIPM** + **TEPM**, thus the hypothesis holds true. With 1606 $m^2 \cdot g^{-1}$, the BET surface area of the **TEPM**-derived control polymer is lower than that of the **TIPM**-derived product of 1811 $m^2 \cdot g^{-1}$.
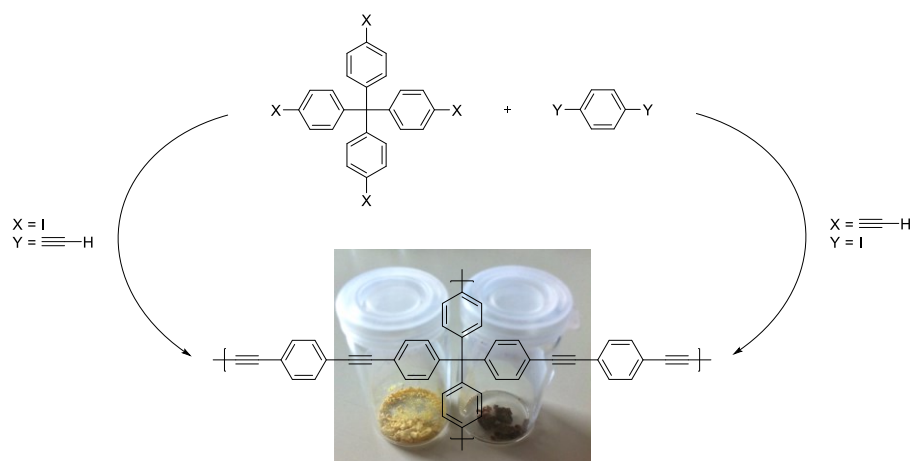
Fig. 25: Control experiment showing higher reactivity of 1,4-diethynylbenzene over tetrakis(4-ethynyl-phenyl)benzene. Left sample: TIPM + DEB; right sample: DIB + TEPM.

A possible explanation is that the reaction conditions were optimized for **TEB**, which is structurally more similar to **DEB** than to **TEPM**. In both molecules, **DEB** and **TEB**, multiple alkyne groups are connected to the same aromatic ring. Being oxidized forms of alkanes, alkynes are electron-deficient and remove electron density from the central aromatic system. In the case of **TEB**, the three *meta*-substituted alkyne groups are not electronically conjugated but nevertheless draw electron density from the same system whereas the alkyne groups in **DEB** are in *para*-position and can directly influence one another. The Brønsted acidity of alkynes is known to increase upon removal of electron density. In **TEPM** only one alkyne group is connected to an aromatic ring, which apparently results in insufficiently high acidity to achieve the required deprotonation rate of the alkyne proton under the given conditions. Another hint towards the trueness of this supposition is the apparent stability of **TEPM**. While **DEB** and **TEB** quickly decompose at ambient temperature even when stored under inert gas, **TEPM** is stable. This decomposition may be the result of the same high reactivity which enables their use under the elaborated conditions.

Zhou and coworkers realized the same dependency of coupling efficiency on alkyne acidity.[74] The authors developed a series of substituted biphenyls with varying steric demands especially on the 2,2' and 6,6' positions (see Fig. 26). The biphenyl system is increasingly distorted due to increasingly bulky substituents. Introduction of methoxy groups leads to an angle between the benzene rings of almost 90 ° in the crystal structure, resulting in a distorted tetrahedral C_4 geometry.
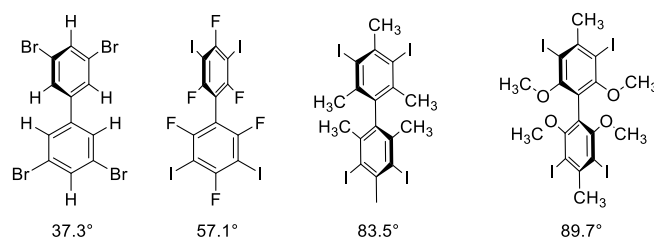
Fig. 26: Structures and torsion angles of substituted biphenyl building blocks

Cross-coupling of the depicted structures with ethynyltrimethylsilane and subsequent deprotection gives compounds in which two alkyne moieties are present on one aromatic ring, two of which are coupled together. In the study by the group of Zhou the resulting tetraalkyne compounds were homocoupled via Cu^{II}-mediated alkyne homocoupling reaction (see Fig. 27). Although the tetramethoxybiphenyl species has a torsion angle close to 90 ° the product does not display the highest BET surface area. This is in fact obtained by the bimesityl structure with slightly less torsion (83.5 ° vs. 89.7 °). The authors reason that the extremely high electron density on the aromatic rings induced by the methoxy groups dampens the alkyne acidity and that therefore the hexamethyl derivative offers the best balance of contortion and electron density hence alkyne acidity. Even this material with its remarkable SA_{BET} of 3420 $m^2 \cdot g^{-1}$ does not reach its theoretical surface area of 5703 $m^2 \cdot g^{-1}$ by a long shot.
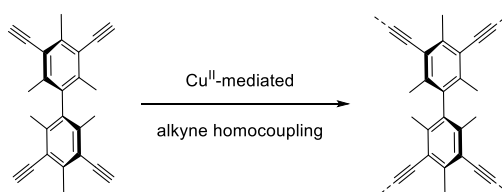
Fig. 27: Cu^{II}-mediated alkyne homocoupling of 2,2',4,4',6,6'-hexamethyl-3,3',5,5'-tetraethynylbiphenyl

Inspired by these experiments the monomer 2,2',4,4',6,6'-hexamethyl-3,3',5,5'-tetraethynylbiphenyl (**HMTEBP**) was synthesized according to the reported route to have a tetrahedral alkyne compound in hand with which the previously obtained surface area might still be surpassed. **HMTEBP** was reacted with linear DIB and tetrahedral TIPM under the developed conditions. However, the appearances of the materials indicate poorly cross-linked networks. Both materials display an inhomogeneous color and texture with partly bright and lighter particles but also partly brown and condensed crumbs. The assumption of poor cross-linking is further supported by the comparatively low SA_{BET} values of 1115 $m^2 \cdot g^{-1}$ (**HMTEBP + DIB**) and 1534 $m^2 \cdot g^{-1}$ (**HMTEBP + TIPM**). Possible reasons for the inefficient coupling reactions are that the alkyne groups are only *meta*-conjugated and therefore not influencing one another strongly enough to effect sufficient acidity. Moreover, the methyl groups induce a higher electron density into the biphenyl system which also reduces the alkyne acidity, albeit not as much as methoxy groups. It is also conceivable that the methyl groups pose steric hindrance. On the one hand the system is proven to undergo efficient homocoupling under the influence of overstoichiometric amounts of Cu^{II} salt as coupling reagent, on the other hand the palladium complex might be bulkier than the Cu^{II} reagent and require more space to function efficiently.

4.4.2 Electron-Rich Heterocycles

Due to the high H_2 and CO_2 uptake capacities of PAEs published earlier[87], polymerization of an electron-rich heterocycle seems advisable. Commercial 2,5-diiodothiophene and **TEB** were polymerized to yield an ochre, strongly fluorescing powder in 98 % yield. The

voluminous powder exhibits a SA_{BET} of 787 m$^2 \cdot$g^{-1} and almost exclusively pores with a diameter of 0.61 nm (see Fig. 28 and Fig. 29). The BET surface area and ^{13}C solid state NMR spectrum are comparable to literature materials synthesized under strongly differing conditions.[171,179]
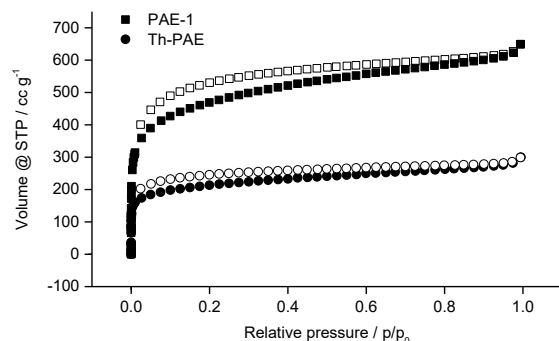
Fig. 28: N$_2$ sorption isotherms of PAE-1 and Th-PAE; solid symbols: adsorption branch; empty symbols: desorption branch
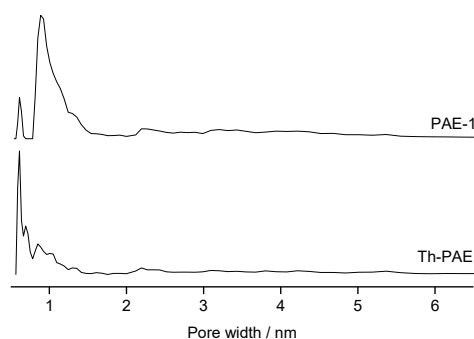
Fig. 29: Pore size distribution of Th-PAE and PAE-1

4.4.3 Perfluorinated Monomers

Since the ultimate goal of this thesis is the incorporation of FLPs into porous polymer networks the polymerization of building blocks common to these systems was investigated. Many known FLPs rely on tris(pentafluorophenyl)borane or structurally related compounds as Lewis acidic species. Therefore the incorporation of perfluorinated building blocks as model systems into PAEs via the improved Sonogashira polymerization method was investigated. To that end two polymers, **F-PAE-1** and **F-PAE-2**, of the type (C$_2$ + C$_3$) were synthesized from commercially available iodinated and perfluorinated monomers, 2,3,5,6-tetrafluoro-1,4-diiodobenzene (**F-DIB**) and 2,4,6-trifluoro-1,3,5-triiodobenzene (**F-TIB**), and their respective counterparts, **TEB** and **DEB** (see Fig. 30).
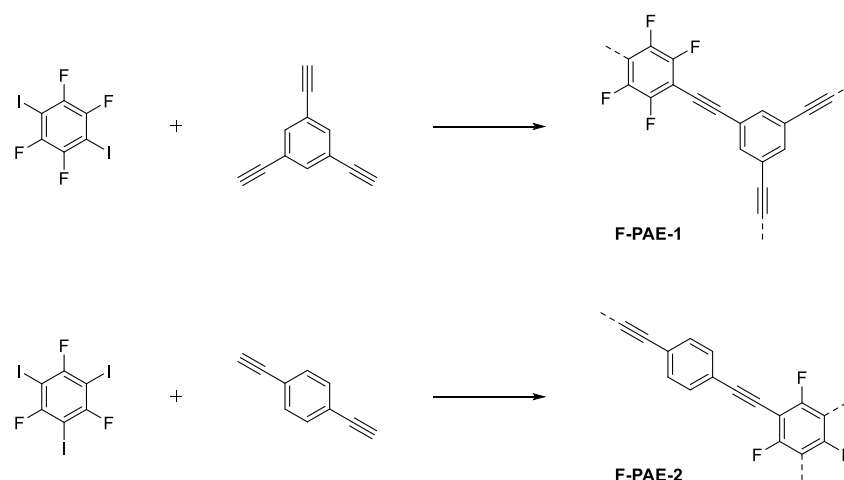
Fig. 30: Synthesis of F-PAEs from perfluorinated building blocks

In the case of **F-PAE-1** the formation of a solid took unusually long. While **PAE-1** and similar networks precipitate within a matter of minutes, the bright yellow reaction mixture of **F-PAE-1** took 40 minutes at 100 °C to solidify into a dark yellow block, which is an unusually long time until precipitation.

Conventional workup yields **F-PAE-1** as a black, light powder exhibiting a SA_{BET} of 890 $m^2 \cdot g^{-1}$ (see Fig. 31). A hysteresis can be observed between a relative pressure of 0.5 and 1. The relative pore size distribution is similar to that of **PAE-1** with the largest and second largest populations of micropores around 0.6 and 1.0 nm, respectively, albeit with a different ratio. A flat and broad range of mesopores is found between 2 and 12 nm (see Fig. 32). Surface area, pore size distribution, and texture indicate an appreciable degree of cross-linking, keeping in mind that the perfluorinated tetrafluorobenzene is considerably heavier than its unfluorinated equivalent, which vindicates a reduced specific surface area. However, the reaction proceeds with a yield of only 61 % which indicates an incomplete reaction.
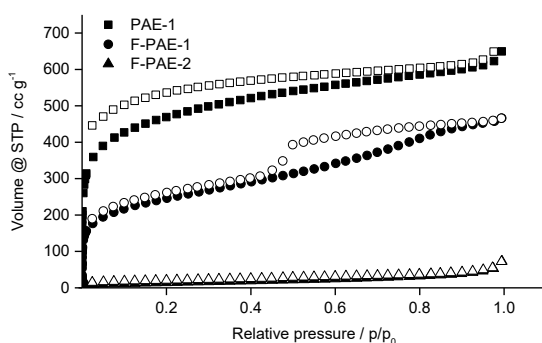
Fig. 31: N₂ sorption isotherms of F-PAEs and PAE-1 for comparison; solid symbols: adsorption branch; empty symbols: desorption branch
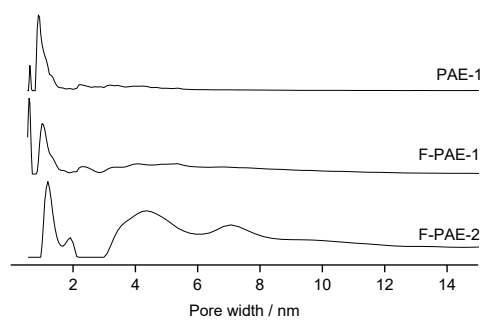
Fig. 32: Normalized pore size distributions of F-PAEs and PAE-1 for comparison

The yield is even lower in the case of **F-PAE-2**, which is obtained in only 48 % yield as a brown powder. Its SA_{BET} is merely 54 $m^2 \cdot g^{-1}$ (see Fig. 31) with micropores being virtually non-existent (see Fig. 32). In this case, precipitation took place within a matter of minutes. Upon filtration and washing of the as-synthesized material, several fractions of yellow and brown color were washed out with various solvents which indicates the formation of oligomers instead of a cross-linked network, hence an incomplete reaction.

It is obvious that the presence of fluorine atoms in either of the iodinated building blocks is kinetically unfavorable for the PAE formation, critically so in the case of **F-PAE-2**. In the case of **F-PAE-1**, where **F-DIB** is used and chain growth can only occur when both iodine atoms have reacted, precipitation takes unusually long, indicating a slow chain growth. For **F-PAE-2**, this kinetic hindrance has a different effect. Reaction of two out of three iodine atoms on one benzene ring causes the polymer chains to to grow linearly until solidification occurs. For cross-linking, however, the third iodine atom has to react as well, which is highly improbable after solidification of the bulk of the material. Hence, a high percentage of the starting material cannot form a network and is washed out as oligomers. The polymer remaining after filtration is poorly cross-linked and exhibits no micropores as well as a very small surface area.

In analogy to the synthesis of the unfluorinated but otherwise isostructural **PAE-1** the reactions were carried out in concentrated fashion as this was shown to maximize surface area and conversion. It seems likely that higher dilution would lead to improved results when using fluorinated organohalides. On the one hand the limits of solubility would most probably be reached at a later point in the polymer formation. On the other hand, continued stirring after precipitation would increase the probability of particles finding further suitable reaction partners and enhance cross-linking drastically.

The formation of **F-PAE-1** shows that the formation of highly fluorinated high-surface-area polymers can be accomplished by the improved PAE synthesis protocol but offers room for further optimization.

4.4.4 Phosphine Monomers

As outlined in **Article III**, to create a functional FLP the incorporation of highly Lewis acidic moieties via Sonogashira or Yamamoto polymerization is unfeasible due to their high reactivity and potential interactions with catalyst, solvent or reaction intermediates.[104] Therefore, polymers based on Lewis basic structures known from simple FLPs were targeted. Triphenylphosphine derivatives are regularly employed as basic species in FLPs and it has been shown that a triphenylphosphine derivative can be used for the formation of a high-surface-area MPN via Yamamoto homopolymerization.[159] Two sterically encumbered triphenylphosphine monomers (**M1** and **M2**) were synthesized from simple, commercially available building blocks via standard metalation-nucleophilic substitution procedures with each monomer containing one functional unit of phosphine (see Fig. 33).
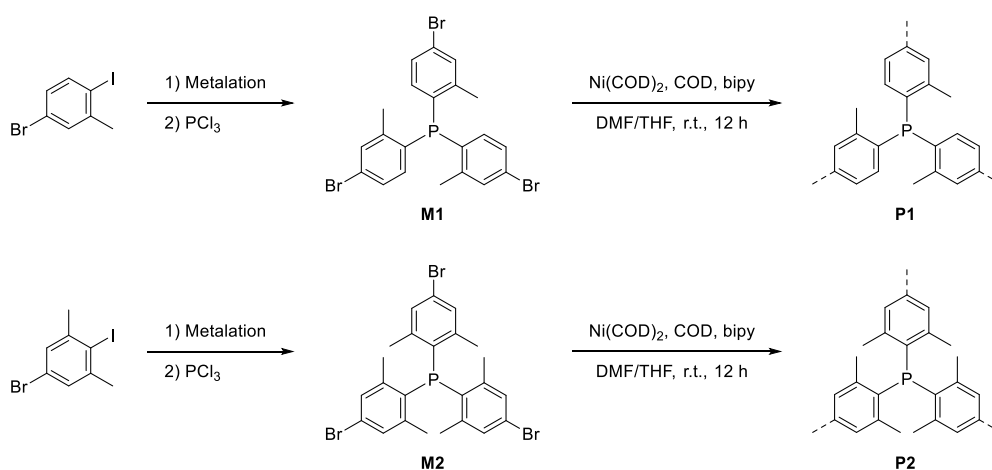
Fig. 33: Syntheses of phosphine monomers and polymers[104]

The two obtained monomers **M1** and **M2** differ in the degree of methylation around their phosphine core, yielding Lewis bases which are able to form gradually weaker bonds with Lewis acids such as BCF. The crystal structure of **M2**, tris(4-bromo-2,6-dimethylphenyl)phosphine, was obtained by slow evaporation of a diethyl ether solution, unambiguosly revealing its propeller-like, pyramidal structure (see Fig. 34).
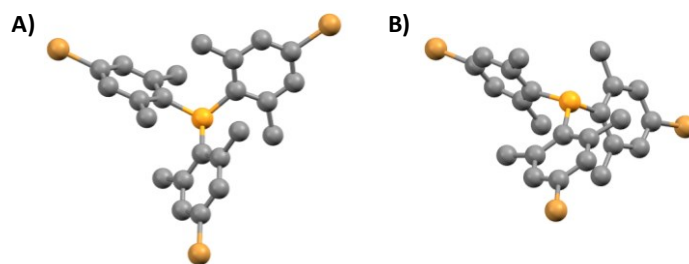
Fig. 34: Crystal structure of tris(4-bromo-2,6-dimethylphenyl)phosphine revealing its propeller-like (A) and pyramidal (B) structure. Gray: carbon, yellow: phosphorus, brown: bromine atoms. Hydrogen omitted for clarity.

To obtain polymers of the highest possible functional group density, both monomers were polymerized via Yamamoto polymerization, yielding the materials reported in **Article III**.[104] To combine the benefits of phosphine-containing polymers with PAEs and to explore further routes to potential insoluble Lewis basic FLP components, **M2** was additionally polymerized via Sonogashira polymerization using a slight variation of the improved copper-free protocol (see Fig. 35). The amount of Pd catalyst was doubled to 1.3 % per alkyne/halide to compensate for the lower reactivity of aryl bromides compared to aryl iodides. Three reactions with co-monomers **DEB**, **TEB** and **TEPM** yielded microporous polymers **P-PAE-1**, **-2**, and **-3** in yields of 104, 98, and 109 %, respectively. The yields indicate high degrees of turnover and cross-linking with small amounts of unreacted end groups.
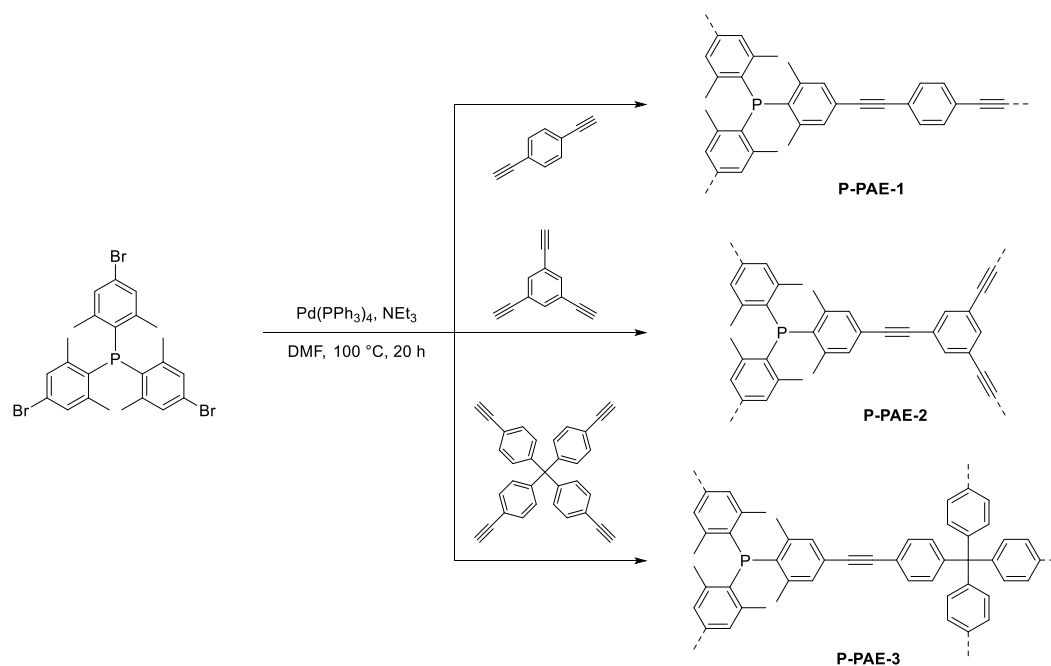
Fig. 35: Synthesis of P-PAEs

After standard workup **P-PAE-1** and **-2** were obtained as light and voluminous powders immediately whereas **P-PAE-3** yielded rather condensed, but nevertheless bright yellow nuggets which could be ground to light powder as well. All materials show hues of yellow according to the length and geometry of their conjugated π-electron systems. **P-PAE-1** possesses the longest conjugated segment and exhibits an intense yellow color.

P-PAE-2 and **-3** are less brilliant but are of a very similar pale yellow with **P-PAE-2** being slightly more intense. These observations are in agreement with the colors of previously obtained, unfunctionalized PAE networks. Here the system with the longest conjugation (biphenyl-linked **TEB**) is the most deeply colored as well, whereas 1,3,5-trisubstituted benzene and tetraphenylmethane-linked materials are beige and slightly off-white, respectively. The beige color is the result of very weak *meta*-conjugation whereas in tetraphenylmethane there is no conjugation beyond the sp^3-hybridized carbon at all. Analogously, the color of **P-PAE-2** comprising **TEB** is slightly more intense than that of **P-PAE-3** comprising tetraphenylmethane nodes.
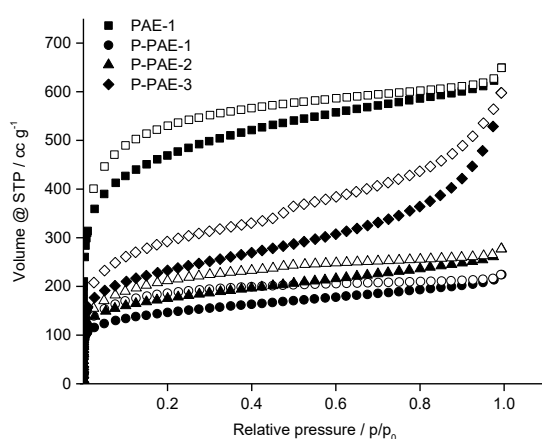
Fig. 36: N$_2$ adsorption isotherms of P-PAEs and PAE-1 for comparison; solid symbols: adsorption branch; empty symbols: desorption branch
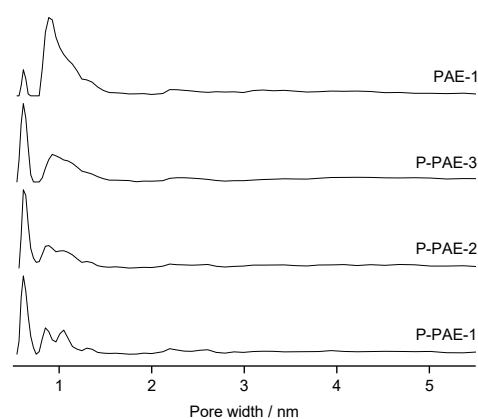
Fig. 37: Pore size distributions of P-PAEs and PAE-1 for comparison

The SA_{BET} of **P-PAE-1** through **-3** were determined to be 535, 639, and 847 m$^2 \cdot$g^{-1} (see Fig. 36). All three **P-PAEs** exhibit a main pore size population at a diameter of 0.61 nm accompanied by minor populations between 0.85 and 1.05 nm (see Fig. 37). The further this ratio changes to higher values the larger the SA_{BET} becomes. These trends are in accord with the dimensionalities of the alkyne monomers: **DEB** (C$_2$) < **TEB** (C$_3$) < **TEPM** (C$_4$).

The ^{13}C solid state NMR spectra of **P-PAEs** are clear of unreacted alkyne functions (see Fig. 38). Surprisingly, even for **P-PAE-3**, which is synthesized from the usually sluggishly reacting **TEPM**, complete consumption of alkyne functions is observed. This observation is in agreement with the color and highest surface area of the material. All peaks belonging to the phosphine subunit can be identified by comparison with the phosphine homopolymer (see Fig. 38). All other peaks can be assigned to the alkyne moieties by comparison with the results obtained previously.[87] In all copolymer ^{31}P spectra the position of the phosphine peak is virtually unchanged compared to the homopolymer (see Fig. 39).
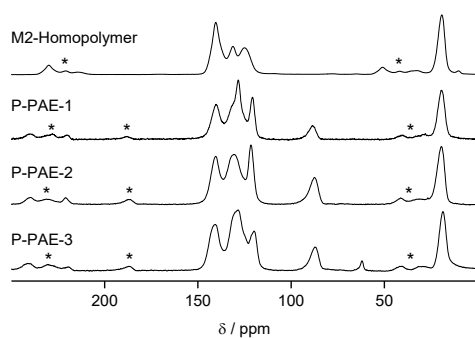
Fig. 38: ^{13}C solid state NMR spectra of P-PAEs and homopolymer of M2 for comparison. Asterisks denote spinning sidebands.
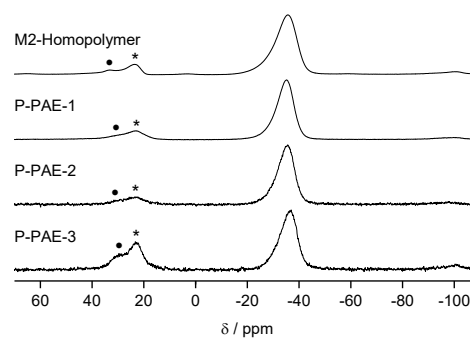
Fig. 39: ^{31}P solid state NMR spectra of P-PAEs and homopolymer of M2 for comparison. Asterisks denote spinning sidebands. Solid dots denote phosphine oxide impurities.

It is conceivable that one or several of the deviations present in these syntheses are responsible for changes in the PAE formation mechanism. Variables differentiating this series of materials from unfunctionalized polymers are the presence of 0.33 equivalents of a weakly coordinating phosphine, which is present in the form of **M2** itself in addition to triphenylphosphine in the catalyst, the use of a brominated but highly electron-rich monomer, and the increased amount of catalyst. Therefore it is complex to identify which factor(s) may contribute to the changed mechanism and account for the here improved reactivity of **TEPM** relative to **DEB** and **TEB**.

4.5 Conclusions on the Polymerization Mechanism

The mechanism of the copper-free Sonogashira reaction is not fully elucidated.[180] Removal of the Cu^I salt reduces the mechanism to a single catalytic cycle. Still, several rate-determining steps are possible.

The coupling reaction starts with an oxidative addition, i.e. the Pd^0 insertion into a C–X bond, effectively forming a carbanion of the form C–Pd^{II}(L)$_2$–X (see Fig. 40). This is followed by the exchange of halide X with an acetylide anion. In the presence of Cu^I, this is when transmetalation of the acetylide from Cu^I to Pd^{II} takes place after Cu^I serves to acidify and displace the alkyne proton. During the halide-to-acetylide exchange, an adduct of the form base–HX is eliminated, H being the former alkyne proton and X the displaced halide. After isomerisation of the square-planar Pd^{II} complex reductive elimination of the product occurs under formation of a new C–alkyne bond.

In this treatise, copper-free coupling reactions were used exclusively for the synthesis of MPNs. When the alkyne component is not activated by Cu^I, the Pd^{II}-inserted species serves to activate this as well as the halide.[180] The mechanism further depends on the combination of alkyne, amine base, and phosphine ligand used in the coupling.[180]

The feasibility of four different alkynes with varying degrees of conjugation and reactivity under the optimized reaction conditions was examined and their reactivity determined to be in the order **TEB ≈ DEB > TEPM ≈ HMTEBP**.
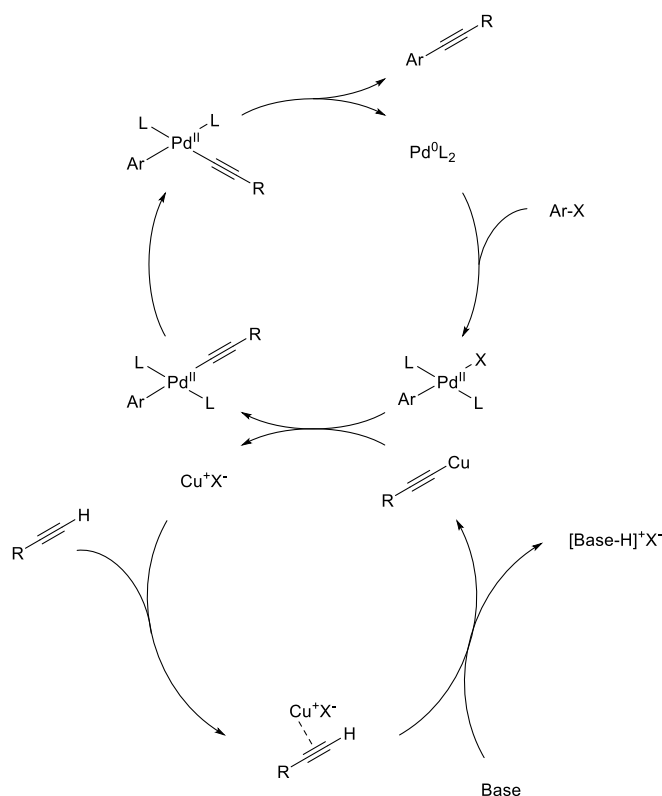
Fig. 40: Catalytic cycles of the Cu^I and Pd^0-cocatalyzed Sonogashira-Hagihara cross-coupling reaction

Next to different alkyne compounds, several types of aryl halides were used. When electron-deficient aromates are used as halide components the inserted metal can be accommodated more easily by stabilization of the formed carbanion, leading to a faster Pd insertion. On the other hand, if the aryl species is too electron-deficient, reductive elimination is effectively hindered and the subsequent reaction slowed. In the case of the strongly electron-deficient perfluorinated aryl iodides the resulting PAE networks were obtained in low yield and/or low surface area. Additionally, precipitation took far longer than usual which hints towards a slugghish reaction.

Employing electron-rich thiophene and triphenylphosphine derivatives as monomers afforded highly cross-linked PAE networks in excellent yields and comparatively high surface area materials without further optimization, even starting from the brominated material in the case of the triphenylphosphine derivative.

According to these results it can be concluded that, on the aryl halide side, a sufficiently fast reductive elimination is crucial for achieving high conversion efficiency and highly cross-linked PAE networks. It must be pointed out though that in the case of the triphenylphosphine derivative several factors come into play, which may on their own or in combination be decisive. On the alkyne side it is obvious that the electronic structure of the alkyne is crucial to whether it is a feasible cross-linking agent or not. Further investigations using alkyne as well as halide monomers of different electron-densities may provide deeper mechanistic insight.

5 Summary

Article I delivers an optimizated procedure for the synthesis of conjugated microporous poly(aryleneethynylene) networks via Sonogashira polymerization. The result of this optimization study is a copper-free one-pot protocol employing very low palladium loadings and the intuitive ratio of 1:1 of alkyne to iodide functions. The resulting materials exhibit superior structural homogeneity over reported materials as well as extremely low amounts of unreacted end groups and side products in the form of enyne moieties. Furthermore they feature very high BET surface areas of up to 2552 $m^2 \cdot g^{-1}$.

  Article II gives an account of five cyanovinylene-based polymers for enhanced CO_2 sorption. These polymers were obtained by direct Knoevenagel condensation of readily available monomers as well as Yamamoto and Sonogashira polymerizations of a monomer obtained by Knoevenagel condensation. The BET surface areas of the resulting polymers range between 60 and 520 $m^2 \cdot g^{-1}$. This series displays a distinct proportionality between the included weight percentage of cyanovinylene groups and the isosteric heat of adsorption for CO_2, utterly independent of surface area and pore size. The total surface area does influence uptake capacities, however. The adsorption enthalpy could be tailored to a strong physisorption value of 40 $kJ \cdot mol^{-1}$ by inclusion of up to 50.5 wt% cyanovinylene content. The unprecedented interaction between CO_2 and immobilized, electron-enriched nitrile groups is described for the first time and substantiated by extensive computational studies performed by P. Fayon and A. Trewin at the University of Lancaster. These studies reveal the formation of pockets which can easily accommodate CO_2 molecules. The low nitrogen-accessible BET surface area and high isosteric heat of adsorption for CO_2 of **P6** give rise to an exceptional CO_2/N_2 selectivity close to 100. The introduction of such materials into membranes for the purpose of gas separation is currently underway at Bundesanstalt für Materialprüfung (BAM), Berlin. The remarkable correlation found herein represents an important tool for the future design of carbon capture materials with optimal ratios of working capacity to regeneration effort.

Article III reports on the immobilization of Lewis basic moieties into microporous polymer networks via Yamamoto polymerization, mimicking components of solution-based FLPs. The networks exhibit permanent microporosity with BET surface areas around 1000 $m^2 \cdot g^{-1}$. Tunability of the interaction strength between boron and phosphorus atoms of strongly Lewis acidic tris(pentafluorophenyl)borane and the immobilized triphenylphosphine derivatives according to their steric encumbrance was proven by ^{31}P solid state NMR. The composite materials obtained by impregnation of the polymeric Lewis basic materials with stoichiometric amounts of BCF were capable of splitting dihydrogen far more efficiently than either of the individual components under the same conditions. The success of the dihydrogen splitting was proven by isotope scrambling experiments. Thus the first proof of principle for the applicability of semi-immobilized FLPs in a fully organic polymer is given.

Application of the optimized Sonogashira polymerization procedure to various systems such as electron-rich and electron-deficient aryl iodides yielded functionalized materials with high BET surface areas and possible applications as porous supports and components in FLP chemistry. The protocol was applied to phosphine monomer **M2**, the crystal structure of which was obtained and which was also used to synthesize the most active hydrogen-splitting network. The resulting networks **P-PAE-1** to **-3** offer hierarchical surface areas ranging between 535 and 847 $m^2 \cdot g^{-1}$ according to the dimensionality of the applied co-monomer. The materials are ready for borane impregnation and subsequent hydrogen splitting experiments.

It is desirable that further investigations yield a fully immobilized FLP manageable under open-bench conditions. Similarly to solution-based FLP chemistry, the synthesis of bifunctional Lewis acidic and basic monomers is tedious and the subsequent polymerization bound to pose an even greater challenge. Therefore postsynthetc modification of a Lewis basic material with a Lewis acidic precursor has been identified as a viable option and should be considered for further syntheses.

Most FLPs entail the problem of water lability. One possible approach to this obstacle is to increase the hydrophobicity of the host material by introduction of perfluorinated moieties or alkyl chains to be able to handle the material without the aid of glovebox or Schlenk technique. Highly moisture-resistant MOFs were accessible via incorporation of perfluorinated moieties in this manner[181,182] and via postsynthetic modification of originally moisture-sensitive MOFs[166]. Thus not only FLPs but other sensitive catalysts could be incorporated into water-resistant MPNs as well, e.g. BCF-derived Lewis acidic polymers, yielding a highly sought-after "solid BCF".

6 Bibliography

[1]   IEA (International Energy Agency), *World Energy Outlook 2013*, London, **2013**.
[2]   R. W. Dorner, D. R. Hardy, F. W. Williams, H. D. Willauer, *Energy Environ. Sci.* **2010**, *3*, 884–890.
[3]   L. Schlapbach, A. Züttel, *Nature* **2001**, *414*, 353–358.
[4]   J. O. M. Bockris, *Int. J. Hydrogen Energy* **2013**, *38*, 2579–2588.
[5]   U. Bossel, *Proc. IEEE* **2006**, *94*, 1826–1837.
[6]   A. Züttel, *Naturwissenschaften* **2004**, *91*, 157–172.
[7]   C. Li, P. Peng, D. W. Zhou, L. Wan, *Int. J. Hydrogen Energy* **2011**, *36*, 14512–14526.
[8]   G. Moussa, R. Moury, U. B. Demirci, T. Şener, P. Miele, *Int. J. Energy Res.* **2013**, *37*, 825–842.
[9]   T. B. Marder, *Angew. Chem. Int. Ed.* **2007**, *46*, 8116–8118.
[10]   D. Teichmann, W. Arlt, P. Wasserscheid, R. Freymann, *Energy Environ. Sci.* **2011**, *4*, 2767–2773.
[11]   "Hydrogen Production - Florida Solar Energy Center," can be found under http://www.fsec.ucf.edu/en/consumer/hydrogen/basics/production.htm, **2017**.
[12]   M. Carmo, D. L. Fritz, J. Mergel, D. Stolten, *Int. J. Hydrogen Energy* **2013**, *38*, 4901–4934.
[13]   M. Schröder, K. Kailasam, J. Borgmeyer, M. Neumann, A. Thomas, R. Schomäcker, M. Schwarze, *Energy Technol.* **2015**, *3*, 1014–1017.
[14]   K. Kailasam, M. B. Mesch, L. Möhlmann, M. Baar, S. Blechert, M. Schwarze, M. Schröder, R. Schomäcker, J. Senker, A. Thomas, *Energy Technol.* **2016**, *4*, 744–750.
[15]   R. S. Sprick, B. Bonillo, R. Clowes, P. Guiglion, N. J. Brownbill, B. J. Slater, F. Blanc, M. A. Zwijnenburg, D. J. Adams, A. I. Cooper, *Angew. Chem. Int. Ed.* **2016**, *55*, 1792–1796.
[16]   R. S. Sprick, B. Bonillo, M. Sachs, R. Clowes, J. R. Durrant, D. J. Adams, A. I. Cooper, *Chem. Commun.* **2016**, *52*, 10008–10011.
[17]   National Research Council, N. A. Press, *Ocean Acidification*, National Academies Press, Washington, D.C., **2010**.
[18]   United States Environmental Protection Agency, "Basic Information about Landfill Gas," can be found under https://www.epa.gov/lmop/basic-information-about-

landfill-gas, **2017**.

[19]   J. D. Figueroa, T. Fout, S. Plasynski, H. McIlvried, R. D. Srivastava, *Int. J. Greenh. Gas Control* **2008**, *2*, 9–20.

[20]   C.-H. Yu, *Aerosol Air Qual. Res.* **2012**, *12*, 745–769.

[21]   A. Thomas, *Angew. Chem. Int. Ed.* **2010**, *49*, 8328–8344.

[22]   K. S. W. Sing, D. H. Everett, R. A. W. Haul, L. Moscou, R. A. Pierotti, J. Rouquérol, T. Siemieniewska, *Pure Appl. Chem.* **1985**, *57*, 2201–2218.

[23]   M. Thommes, K. Kaneko, A. V. Neimark, J. P. Olivier, F. Rodriguez-Reinoso, J. Rouquerol, K. S. W. Sing, *Pure Appl. Chem.* **2015**, *87*, 1051–1069.

[24]   S. Brunauer, P. H. Emmett, E. Teller, *J. Am. Chem. Soc.* **1938**, *60*, 309–319.

[25]   K. Sing, *Colloids Surfaces A Physicochem. Eng. Asp.* **2001**, *187–188*, 3–9.

[26]   K. S. Walton, R. Q. Snurr, *J. Am. Chem. Soc.* **2007**, *129*, 8552–8556.

[27]   N. Nijem, H. Wu, P. Canepa, A. Marti, K. J. Balkus, T. Thonhauser, J. Li, Y. J. Chabal, *J. Am. Chem. Soc.* **2012**, *134*, 15201–15204.

[28]   F. Gándara, H. Furukawa, S. Lee, O. M. Yaghi, *J. Am. Chem. Soc.* **2014**, *136*, 5271–5274.

[29]   Y.-S. Bae, a. O. Yazaydın, R. Q. Snurr, *Langmuir* **2010**, *26*, 5475–5483.

[30]   A. L. Myers, J. M. Prausnitz, *AIChE J.* **1965**, *11*, 121–127.

[31]   F. Schüth, K. Sing, J. Weitkamp, *Handbook of Porous Solids*, Wiley-VCH Verlag GmbH, Weinheim, Germany, **2008**.

[32]   R. M. Barrer, *Proc. R. Soc. A Math. Phys. Eng. Sci.* **1938**, *167*, 392–420.

[33]   V. A. Davankov, S. V Rogoshin, M. P. Tsyurupa, *J. Polym. Sci. Polym. Symp.* **1974**, *47*, 95–101.

[34]   B. F. Hoskins, R. Robson, *J. Am. Chem. Soc.* **1990**, *112*, 1546–1554.

[35]   M. Fujita, Y. J. Kwon, S. Washizu, K. Ogura, *J. Am. Chem. Soc.* **1994**, *116*, 1151–1152.

[36]   B. F. Abrahams, B. F. Hoskins, D. M. Michail, R. Robson, *Nature* **1994**, *369*, 727–729.

[37]   D. Venkataraman, G. B. Gardner, S. Lee, J. S. Moore, *J. Am. Chem. Soc.* **1995**, *117*, 11600–11601.

[38]   O. M. Yaghi, G. Li, H. Li, *Nature* **1995**, *378*, 703–706.

[39]   S. Karak, S. Kandambeth, B. P. Biswal, H. S. Sasmal, S. Kumar, P. Pachfule, R. Banerjee, *J. Am. Chem. Soc.* **2017**, *139*, 1856–1862.

[40]   N. Trukhan, U. Mueller, *Process for Preparing a Porous Metal-organic Framework Composed of Zinc Methylimidazolate*, **2013**, US20130012717.

[41]   A. P. Cote, A. Benin, N. Ockwig, M. O'Keeffe, A. Matzger, O. M. Yaghi, *Science* **2005**, *310*, 1166–1170.

[42]   F. J. Uribe-Romo, J. R. Hunt, H. Furukawa, C. Klöck, M. O'Keeffe, O. M. Yaghi, *J. Am. Chem. Soc.* **2009**, *131*, 4570–4571.

[43]   Y. Du, H. Yang, J. M. Whiteley, S. Wan, Y. Jin, S.-H. H. Lee, W. Zhang, *Angew. Chem. Int. Ed.* **2016**, *55*, 1737–1741.

[44]   J. Roeser, D. Prill, M. J. Bojdys, P. Fayon, A. Trewin, A. N. Fitch, M. U. Schmidt, A. Thomas, *Nat. Chem.* **2017**, 1–6.

[45]   S. Kandambeth, A. Mallick, B. Lukose, M. V. Mane, T. Heine, R. Banerjee, *J. Am. Chem. Soc.* **2012**, *134*, 19524–19527.

[46]   B. Wang, X.-L. Lv, D. Feng, L.-H. Xie, J. Zhang, M. Li, Y. Xie, J.-R. Li, H.-C. Zhou, *J. Am. Chem. Soc.* **2016**, *138*, 6204–6216.

[47]   P. M. Budd, B. S. Ghanem, S. Makhseed, N. B. McKeown, K. J. Msayib, C. E. Tattershall, *Chem. Commun.* **2004**, 230–231.

[48]   P. M. Budd, E. S. Elabas, B. S. Ghanem, S. Makhseed, N. B. McKeown, K. J. Msayib, C. E. Tattershall, D. Wang, *Adv. Mater.* **2004**, *16*, 456–459.

[49]   P. Budd, K. Msayib, C. Tattershall, B. Ghanem, K. Reynolds, N. McKeown, D. Fritsch, *J. Memb. Sci.* **2005**, *251*, 263–269.

[50]   T. Mitra, R. S. Bhavsar, D. J. Adams, P. M. Budd, A. I. Cooper, *Chem. Commun.* **2016**, *52*, 5581–5584.

[51]   J. Weber, Q. Su, M. Antonietti, A. Thomas, *Macromol. Rapid Commun.* **2007**, *28*, 1871–1876.

[52]   M. Carta, M. Croad, R. Malpass-Evans, J. C. Jansen, P. Bernardo, G. Clarizia, K. Friess, M. Lanč, N. B. McKeown, *Adv. Mater.* **2014**, *26*, 3526–3531.

[53]   A. Del Regno, A. Gonciaruk, L. Leay, M. Carta, M. Croad, R. Malpass-Evans, N. B. McKeown, F. R. Siperstein, *Ind. Eng. Chem. Res.* **2013**, *52*, 16939–16950.

[54]   D. Becker, N. Konnertz, M. Böhning, J. Schmidt, A. Thomas, *Chem. Mater.* **2016**, *28*, 8523–8529.

[55]   T. Tozawa, J. T. A. Jones, S. I. Swamy, S. Jiang, D. J. Adams, S. Shakespeare, R. Clowes, D. Bradshaw, T. Hasell, S. Y. Chong, et al., *Nat. Mater.* **2009**, *8*, 973–978.

[56]   J. R. Holst, A. Trewin, A. I. Cooper, *Nat. Chem.* **2010**, *2*, 915–920.

[57]   N. B. McKeown, *J. Mater. Chem.* **2010**, *20*, 10588–10597.

[58]   M. Mastalerz, M. W. Schneider, I. M. Oppel, O. Presly, *Angew. Chem. Int. Ed.* **2011**, *50*, 1046–1051.

[59]   M. Mastalerz, I. M. Oppel, *Angew. Chem. Int. Ed.* **2012**, *51*, 5252–5255.

[60]   G. Zhang, O. Presly, F. White, I. M. Oppel, M. Mastalerz, *Angew. Chem. Int. Ed.* **2014**, *53*, 1516–1520.

[61]   J.-X. Jiang, F. Su, A. Trewin, C. D. Wood, N. L. Campbell, H. Niu, C. Dickinson, A. Y. Ganin, M. J. Rosseinsky, Y. Z. Khimyak, et al., *Angew. Chem. Int. Ed.* **2007**, *46*, 8574–8578.

[62]   F. L. Buchholz, A. T. Graham, *Modern Superabsorbent Polymer Technology*, New York, USA, **1998**.

[63]   B. D. MacArthur, R. O. C. Oreffo, *Nature* **2005**, *433*, 19–19.

[64]   Y. Brudno, D. J. Mooney, *J. Control. Release* **2015**, *219*, 8–17.

[65]   T. Ben, H. Ren, S. Ma, D. Cao, J. Lan, X. Jing, W. Wang, J. Xu, F. Deng, J. M. Simmons, et al., *Angew. Chem. Int. Ed.* **2009**, *48*, 9457–9460.

[66]   W. Lu, D. Yuan, J. P. Sculley, D. Zhao, R. Krishna, H.-C. Zhou, *J. Am. Chem. Soc.* **2011**, *133*, 18126–18129.

[67]   D. Yuan, W. Lu, D. Zhao, H.-C. Zhou, *Adv. Mater.* **2011**, *23*, 3723–3725.

[68]   M. Rose, W. Böhlmann, M. Sabo, S. Kaskel, *Chem. Commun.* **2008**, *1*, 2462–2464.

[69]   J. Schmidt, M. Werner, A. Thomas, *Macromolecules* **2009**, *42*, 4426–4429.

[70]   J. Brandt, J. Schmidt, A. Thomas, J. D. Epping, J. Weber, *Polym. Chem.* **2011**, *2*, 1950–1952.

[71]   D. Xiao, Y. Li, L. Liu, B. Wen, Z. Gu, C. Zhang, Y. S. Zhao, *Chem. Commun.* **2012**, *48*, 9519–9521.

[72]   B. Bonillo, R. S. Sprick, A. I. Cooper, *Chem. Mater.* **2016**, *28*, 3469–3480.

[73]   Y. Liao, J. Weber, B. M. Mills, Z. Ren, C. F. J. Faul, *Macromolecules* **2016**, *49*, 6322–6333.

[74]   W. Lu, Z. Wei, D. Yuan, J. Tian, S. Fordham, H.-C. Zhou, *Chem. Mater.* **2014**, *26*, 4589–4597.

[75]   R. Dawson, T. Ratvijitvech, M. Corker, A. Laybourn, Y. Z. Khimyak, A. I. Cooper, D. J. Adams, *Polym. Chem.* **2012**, *3*, 2034–2038.

[76]   X.-M. Zhang, X. Ding, A. Hu, B.-H. Han, *Polym. Chem.* **2015**, *6*, 4734–4741.

[77]   J. R. Holst, E. Stöckel, D. J. Adams, A. I. Cooper, *Macromolecules* **2010**, *43*, 8531–8538.

[78]   A. Palma-Cando, G. Brunklaus, U. Scherf, *Macromolecules* **2015**, *48*, 6816–6824.

[79]   J. Fritsch, M. Rose, P. Wollmann, W. Böhlmann, S. Kaskel, *Materials* **2010**, *3*, 2447–

2462.

[80] J. Fritsch, F. Drache, G. Nickerl, W. Böhlmann, S. Kaskel, *Microporous Mesoporous Mater.* **2013**, *172*, 167–173.

[81] Y. Zhu, H. Yang, Y. Jin, W. Zhang, *Chem. Mater.* **2013**, *25*, 3718–3723.

[82] J. Schmidt, J. Weber, J. D. Epping, M. Antonietti, A. Thomas, *Adv. Mater.* **2009**, *21*, 702–705.

[83] D. Liu, Q. Chen, Y. Zhao, L. Zhang, A. Qi, B. Han, *ACS Macro Lett.* **2013**, *2*, 522–526.

[84] E. Troschke, S. Grätz, T. Lübken, L. Borchardt, *Angew. Chem. Int. Ed.* **2017**, *56*, 6859–6863.

[85] C. Widling, M. Forster, V. M. Suresh, U. Scherf, *Sci. China Chem.* **2017**, 8–11.

[86] W. Liu, X. Luo, Y. Bao, Y. P. Liu, G.-H. Ning, I. Abdelwahab, L. Li, C. T. Nai, Z. G. Hu, D. Zhao, et al., *Nat. Chem.* **2017**, *9*, 563–570.

[87] M. Trunk, A. Herrmann, H. Bildirir, A. Yassin, J. Schmidt, A. Thomas, *Chem. Eur. J.* **2016**, *22*, 7179–7183.

[88] N. Chaoui, M. Trunk, R. Dawson, J. Schmidt, A. Thomas, *Chem. Soc. Rev.* **2017**, *46*, 3302–3321.

[89] R. Dawson, A. I. Cooper, D. J. Adams, *Prog. Polym. Sci.* **2012**, *37*, 530–563.

[90] R. Dawson, D. J. Adams, A. I. Cooper, *Chem. Sci.* **2011**, *2*, 1173–1177.

[91] X. Wu, R. Wang, H. Yang, W. Wang, W. Cai, Q. Li, *J. Mater. Chem. A* **2015**, *3*, 10724–10729.

[92] S. M. J. Rogge, A. Bavykina, J. Hajek, H. Garcia, A. I. Olivos-Suarez, A. Sepúlveda-Escribano, A. Vimont, G. Clet, P. Bazin, F. Kapteijn, et al., *Chem. Soc. Rev.* **2017**, *46*, 3134–3184.

[93] C. R. Kim, T. Uemura, S. Kitagawa, *Chem. Soc. Rev.* **2016**, *45*, 3828–3845.

[94] U. H. F. Bunz, K. Seehafer, F. L. Geyer, M. Bender, I. Braun, E. Smarsly, J. Freudenberg, *Macromol. Rapid Commun.* **2014**, *35*, 1466–1496.

[95] M. Meilikhov, K. Yusenko, D. Esken, S. Turner, G. Van Tendeloo, R. A. Fischer, *Eur. J. Inorg. Chem.* **2010**, *2010*, 3701–3714.

[96] Q.-L. Zhu, Q. Xu, *Chem. Soc. Rev.* **2014**, *43*, 5468–5512.

[97] P. Pachfule, M. K. Panda, S. Kandambeth, S. M. Shivaprasad, D. D. Díaz, R. Banerjee, *J. Mater. Chem. A* **2014**, *2*, 7944–7952.

[98] S. Fischer, J. Schmidt, P. Strauch, A. Thomas, *Angew. Chem. Int. Ed.* **2013**, *52*, 12174–12178.

[99] J. F. Van Humbeck, M. L. Aubrey, A. Alsbaiee, R. Ameloot, G. W. Coates, W. R. Dichtel, J. R. Long, *Chem. Sci.* **2015**, *6*, 5499–5505.

[100] Z. Yan, Y. Yuan, Y. Tian, D. Zhang, G. Zhu, *Angew. Chem. Int. Ed.* **2015**, *54*, 12733–12737.

[101] D. S. Kundu, J. Schmidt, C. Bleschke, A. Thomas, S. Blechert, *Angew. Chem. Int. Ed.* **2012**, *51*, 5456–5459.

[102] J.-X. Jiang, Y. Li, X. Wu, J. Xiao, D. J. Adams, A. I. Cooper, *Macromolecules* **2013**, *46*, 8779–8783.

[103] J. Luo, X. Zhang, J. Zhang, *ACS Catal.* **2015**, *5*, 2250–2254.

[104] M. Trunk, J. F. Teichert, A. Thomas, *J. Am. Chem. Soc.* **2017**, *139*, 3615–3618.

[105] G. C. Welch, R. R. S. Juan, J. D. Masuda, D. W. Stephan, *Science* **2006**, *314*, 1124–1126.

[106] G. Ménard, J. A. Hatnean, H. J. Cowley, A. J. Lough, J. M. Rawson, D. W. Stephan, *J. Am. Chem. Soc.* **2013**, *135*, 6446–6449.

[107] H. C. Brown, H. I. Schlesinger, S. Z. Cardon, *J. Am. Chem. Soc.* **1942**, *64*, 325–329.

[108] G. Wittig, L. Gonsior, H. Vogel, *Justus Liebigs Ann. Chem.* **1965**, *688*, 1–13.

[109] G. Wittig, A. Rückert, *Justus Liebigs Ann. Chem.* **1950**, *566*, 101–113.

[110] G. Wittig, H. Schloeder, *Justus Liebigs Ann. Chem.* **1955**, *592*, 38–53.

[111]   W. Tochtermann, *Angew. Chem. Int. Ed.* **1966**, *5*, 351–371.

[112]   A. M. Chapman, D. F. Wass, *Dalt. Trans.* **2012**, *41*, 9067–9072.

[113]   B. Pan, M. W. Bezpalko, B. M. Foxman, C. M. Thomas, *Dalt. Trans.* **2012**, *41*, 9083–9090.

[114]   A. T. Normand, C. G. Daniliuc, B. Wibbeling, G. Kehr, P. Le Gendre, G. Erker, *J. Am. Chem. Soc.* **2015**, *137*, 10796–10808.

[115]   M. P. Boone, D. W. Stephan, *Organometallics* **2014**, *33*, 387–393.

[116]   K. Chernichenko, B. Kótai, I. Pápai, V. Zhivonitko, M. Nieger, M. Leskelä, T. Repo, *Angew. Chem. Int. Ed.* **2015**, *54*, 1749–1753.

[117]   V. Sumerin, F. Schulz, M. Atsumi, C. Wang, M. Nieger, M. Leskelä, T. Repo, P. Pyykkö, B. Rieger, *J. Am. Chem. Soc.* **2008**, *130*, 1–24.

[118]   V. Sumerin, K. Chernichenko, M. Nieger, M. Leskelä, B. Rieger, T. Repo, *Adv. Synth. Catal.* **2011**, *353*, 2093–2110.

[119]   K. Chernichenko, M. Nieger, M. Leskelä, T. Repo, *Dalt. Trans.* **2012**, *41*, 9029–9032.

[120]   P. Spies, S. Schwendemann, S. Lange, G. Kehr, R. Fröhlich, G. Erker, *Angew. Chem. Int. Ed.* **2008**, *47*, 7543–7546.

[121]   D. W. Stephan, G. Erker, *Angew. Chem. Int. Ed.* **2010**, *49*, 46–76.

[122]   G. C. Welch, D. W. Stephan, *J. Am. Chem. Soc.* **2007**, *129*, 1880–1881.

[123]   T. J. Herrington, A. J. W. Thom, A. J. P. White, A. E. Ashley, *Dalt. Trans.* **2012**, *41*, 9019–9022.

[124]   S. C. Binding, H. Zaher, F. Mark Chadwick, D. O'Hare, *Dalt. Trans.* **2012**, *41*, 9061–9066.

[125]   M. Reißmann, A. Schäfer, S. Jung, T. Müller, *Organometallics* **2013**, *32*, 6736–6744.

[126]   E. R. Clark, M. J. Ingleson, *Angew. Chem. Int. Ed.* **2014**, *53*, 11306–11309.

[127]   M. Ullrich, A. J. Lough, D. W. Stephan, *J. Am. Chem. Soc.* **2009**, *131*, 52–53.

[128]   L. L. Zeonjuk, N. Vankova, A. Mavrandonakis, T. Heine, G.-V. Röschenthaler, J. Eicher, *Chem. Eur. J.* **2013**, *19*, 17413–17424.

[129]   L. Liu Zeonjuk, P. St. Petkov, T. Heine, G.-V. Röschenthaler, J. Eicher, N. Vankova, *Phys. Chem. Chem. Phys.* **2015**, *17*, 10687–10698.

[130]   V. Sumerin, F. Schulz, M. Nieger, M. Atsumi, C. Wang, M. Leskelä, P. Pyykkö, T. Repo, B. Rieger, *J. Organomet. Chem.* **2009**, *694*, 2654–2660.

[131]   D. J. Scott, M. J. Fuchter, A. E. Ashley, *Chem. Soc. Rev.* **2017**, *Advance Article*.

[132]   P. Spies, G. Erker, G. Kehr, K. Bergander, R. Fröhlich, S. Grimme, D. W. Stephan, *Chem. Commun.* **2007**, *2*, 5072–5074.

[133]   C. M. Mömming, E. Otten, G. Kehr, R. Fröhlich, S. Grimme, D. W. Stephan, G. Erker, *Angew. Chem. Int. Ed.* **2009**, *48*, 6643–6646.

[134]   M. Pu, T. Privalov, *Chem. Eur. J.* **2013**, *19*, 16512–16517.

[135]   A. E. Ashley, A. Thompson, D. O'Hare, *Angew. Chem. Int. Ed.* **2009**, *48*, 9839–9843.

[136]   S. D. Tran, T. A. Tronic, W. Kaminsky, D. Michael Heinekey, J. M. Mayer, *Inorganica Chim. Acta* **2011**, *369*, 126–132.

[137]   L. Liu, N. Vankova, T. Heine, *Phys. Chem. Chem. Phys.* **2016**, *18*, 3567–3574.

[138]   M.-A. Courtemanche, M.-A. Légaré, L. Maron, F.-G. Fontaine, *J. Am. Chem. Soc.* **2014**, *136*, 10708–10717.

[139]   T. Mahdi, D. W. Stephan, *J. Am. Chem. Soc.* **2014**, *136*, 15809–15812.

[140]   L. Greb, P. Oña-Burgos, B. Schirmer, S. Grimme, D. W. Stephan, J. Paradies, *Angew. Chem. Int. Ed.* **2012**, *51*, 10164–10168.

[141]   H. Wang, R. Fröhlich, G. Kehr, G. Erker, *Chem. Commun.* **2008**, 5966–5968.

[142]   A. J. M. Miller, J. E. Bercaw, *Chem. Commun.* **2010**, *46*, 1709–1711.

[143]   T. Beringhelli, D. Maggioni, G. D'Alfonso, *Organometallics* **2001**, *20*, 4927–4938.

[144]   T. vom Stein, M. Peréz, R. Dobrovetsky, D. Winkelhaus, C. B. Caputo, D. W. Stephan, *Angew. Chem. Int. Ed.* **2015**, *54*, 10178–10182.

[145] M. A. Beckett, G. C. Strickland, J. R. Holland, K. S. Varma, K. Sukumar Varma, *Polymer* **1996**, *37*, 4629–4631.

[146] R. F. Childs, D. L. Mulholland, A. Nixon, *Can. J. Chem.* **1982**, *60*, 809–812.

[147] S. Mummadi, D. K. Unruh, J. Zhao, S. Li, C. Krempner, *J. Am. Chem. Soc.* **2016**, *138*, 3286–3289.

[148] Á. Gyömöre, M. Bakos, T. Földes, I. Pápai, A. Domján, T. Soós, *ACS Catal.* **2015**, *5*, 5366–5372.

[149] A. E. Ashley, T. J. Herrington, G. G. Wildgoose, H. Zaher, A. L. Thompson, N. H. Rees, T. Krämer, D. O'Hare, *J. Am. Chem. Soc.* **2011**, *133*, 14727–14740.

[150] J. Xing, J. Buffet, N. H. Rees, P. Nørby, D. O'Hare, *Chem. Commun.* **2016**, *52*, 10478–10481.

[151] P. Li, Y. Zhao, *Chem. Asian J.* **2013**, *8*, 1680–1691.

[152] K. Sakaushi, M. Antonietti, *Bull. Chem. Soc. Jpn.* **2015**, *88*, 386–398.

[153] A. Demessence, D. M. D'Alessandro, M. L. Foo, J. R. Long, *J. Am. Chem. Soc.* **2009**, *131*, 8784–8786.

[154] T. M. McDonald, J. A. Mason, X. Kong, E. D. Bloch, D. Gygi, A. Dani, V. Crocellà, F. Giordanino, S. O. Odoh, W. S. Drisdell, et al., *Nature* **2015**, *519*, 303–308.

[155] W. Lu, J. P. Sculley, D. Yuan, R. Krishna, Z. Wei, H.-C. Zhou, *Angew. Chem. Int. Ed.* **2012**, *51*, 7480–7484.

[156] M. G. Rabbani, H. M. El-Kaderi, *Chem. Mater.* **2011**, *23*, 1650–1653.

[157] Q. Chen, M. Luo, P. Hammershøj, D. Zhou, Y. Han, B. W. Laursen, C. Yan, B.-H. Han, *J. Am. Chem. Soc.* **2012**, *134*, 6084–6087.

[158] Q. Chen, J.-X. Wang, Q. Wang, N. Bian, Z.-H. Li, C.-G. Yan, B.-H. Han, *Macromolecules* **2011**, *44*, 7987–7993.

[159] Q. Zhang, Y. Yang, S. Zhang, *Chem. Eur. J.* **2013**, *19*, 10024–10029.

[160] I. B. Sivaev, V. I. Bregadze, *Coord. Chem. Rev.* **2014**, *270–271*, 75–88.

[161] X. Liu, Y. Zhang, H. Li, S A, H. Xia, Y. Mu, *RSC Adv.* **2013**, *3*, 21267–21270.

[162] V. M. Suresh, A. Bandyopadhyay, S. Roy, S. K. Pati, T. K. Maji, *Chem. Eur. J.* **2015**, *21*, 10799–10804.

[163] W. Zhao, X. Zhuang, D. Wu, F. Zhang, D. Gehrig, F. Laquai, X. Feng, *J. Mater. Chem. A* **2013**, *1*, 13878–13884.

[164] Z. Li, H. Li, H. Xia, X. Ding, X. Luo, X. Liu, Y. Mu, *Chem. Eur. J.* **2015**, *21*, 17355–17362.

[165] C. Gu, N. Huang, Y. Chen, H. Zhang, S. Zhang, F. Li, Y. Ma, D. Jiang, *Angew. Chem. Int. Ed.* **2016**, *55*, 3049–3053.

[166] J. G. Nguyen, S. M. Cohen, *J. Am. Chem. Soc.* **2010**, *132*, 4560–4561.

[167] R. Dawson, A. Laybourn, R. Clowes, Y. Z. Khimyak, D. J. Adams, A. I. Cooper, *Macromolecules* **2009**, *42*, 8809–8816.

[168] L. Chen, Y. Honsho, S. Seki, D. Jiang, *J. Am. Chem. Soc.* **2010**, *132*, 6742–6748.

[169] R. Dawson, A. Laybourn, Y. Z. Khimyak, D. J. Adams, A. I. Cooper, *Macromolecules* **2010**, *43*, 8524–8530.

[170] A. Laybourn, R. Dawson, R. Clowes, T. Hasell, A. I. Cooper, Y. Z. Khimyak, D. J. Adams, *Polym. Chem.* **2014**, *5*, 6325–6333.

[171] B. Kim, N. Park, S. M. Lee, H. J. Kim, S. U. Son, *Polym. Chem.* **2015**, *6*, 7363–7367.

[172] A. C. Uptmoor, J. Freudenberg, S. T. Schwäbel, F. Paulus, F. Rominger, F. Hinkel, U. H. F. Bunz, *Angew. Chem. Int. Ed.* **2015**, *54*, 14673–14676.

[173] J. Jiang, F. Su, A. Trewin, C. D. Wood, H. Niu, J. T. A. Jones, Y. Z. Khimyak, A. I. Cooper, *J. Am. Chem. Soc.* **2008**, *130*, 7710–7720.

[174] E. Stöckel, X. Wu, A. Trewin, C. D. Wood, R. Clowes, N. L. Campbell, J. T. A. Jones, Y. Z. Khimyak, D. J. Adams, A. I. Cooper, *Chem. Commun.* **2009**, 212–214.

[175] H. Bildirir, Synthesis of Functional Microporous Polymers for Catalytic and Electronic Applications, Doctoral Dissertation, Technische Universität Berlin, **2015**.

[176] P.-Z. Li, X.-J. Wang, J. Liu, J. S. Lim, R. Zou, Y. Zhao, *J. Am. Chem. Soc.* **2016**, *138*, 2142–2145.

[177] M. Banno, T. Yamaguchi, K. Nagai, C. Kaiser, S. Hecht, E. Yashima, *J. Am. Chem. Soc.* **2012**, *134*, 8718–8728.

[178] I. Aujard, J. Baltaze, J. Baudin, E. Cogné, F. Ferrage, L. Jullien, É. Perez, V. Prévost, L. M. Qian, O. Ruel, *J. Am. Chem. Soc.* **2001**, *123*, 8177–8188.

[179] X. Zhuang, F. Zhang, D. Wu, N. Forler, H. Liang, M. Wagner, D. Gehrig, M. R. Hansen, F. Laquai, X. Feng, *Angew. Chem. Int. Ed.* **2013**, *52*, 9668–9672.

[180] A. Tougerti, S. Negri, A. Jutand, *Chem. Eur. J.* **2007**, *13*, 666–676.

[181] C. Yang, U. Kaipa, Q. Z. Mather, X. Wang, V. Nesterov, A. F. Venero, M. A. Omary, *J. Am. Chem. Soc.* **2011**, *133*, 18094–18097.

[182] T.-H. Chen, I. Popov, O. Zenasni, O. Daugulis, O. Š. Miljanić, *Chem. Commun.* **2013**, *49*, 6846–6848.

7 Experimental Part

7.1 Materials and Methods

7.1.1 Analytics

Inert reactions were carried out in an MBraun glovebox type MB 120 BG. All glassware and stir bars were flame-dried before being channelled into the glovebox.

^{1}H NMR, ^{13}C NMR and ^{31}P NMR spectra were recorded on a Bruker Avance II 200 spectrometer in the given solvent.

^{13}C{^{1}H} CP/MAS and ^{31}P MAS measurements were carried out using a Bruker Avance 400 MHz Solid State spectrometer operating at 100.6 MHz for ^{13}C, 168 MHz for ^{31}P and a Bruker 4 mm double resonance probe-head operating at a spinning rate of 9 or 10 kHz. Data evaluation was performed via software TopSpin 3.5 pl 7.

Nitrogen sorption analyses were conducted at 77 K using an Autosorb-iQ-MP from Quantachrome. The pore size distributions were calculated from the adsorption isotherms by quenched solid density functional theory (QSDFT) using the slit/cylindrical pore model for carbon adsorbents. Before analysis, all samples were degassed at 80 °C for 12 h. BET surface areas were determined over a 0.05-0.1 or 0.05-0.15 p/p_0 range. Data evaluation was performed via software AsiQwin (v. 3.01).

7.1.2   Chemicals

Chemical	Acronym/Formula	Purity	Supplier
Acetic acid (conc.)	AcOH	100 %	Carl Roth
Bis(triphenylphosphino)palladium(II) chloride	$Pd(PPh_3)_2Cl_2$	99.99+ %	Sigma-Aldrich
Bromine	Br_2	99.8 %	Alfa Aesar
Copper(I) iodide	CuI	>98 %	Sigma-Aldrich
Cyclohexane	-	99.9 %	Carl Roth
1,2-Dibromoethane	-	99 %	Sigma-Aldrich
Dichloromethane	DCM	99.5 %	Carl Roth
Diethylether	Et_2O	99 % (BHT-stab.)	Sigma-Aldrich
1,4-Diethynylbenzene	DEB	96 %	Sigma-Aldrich
1,4-Diiodobenzene	DIB	99 %	Sigma-Aldrich
1,4-diiodotetrafluorobenzene	F-DIB	98 %	Manchester Organics
2,5-Diiodothiophene	-	99 %	ABCR
Diisopropylamine	DIPA	99.95 %, anhydrous	Sigma-Aldrich
Dimethylformamide	DMF	99.8 %, anhydrous	Alfa Aesar
Ethanol	EtOH	99.5 %	Carl Roth
Hexane	-	95 %	Carl Roth
Hydrogen chloride (aqueous solution)	HCl	37 %	Carl Roth
Iodine	I_2	99.5 %	Alfa Aesar
Iron(III) chloride	$FeCl_3$	98 %, anhydrous	Acros Organics
Magnesium	Mg	99.98 %	Sigma-Aldrich
Methanol	MeOH	99.8 %	Carl Roth
Methyl iodide	MeI	>99 %	Sigma-Aldrich
Periodic acid	HIO_4	99 %	Sigma-Aldrich
Potassium carbonte	K_2CO_3	99+ %	Sigma-Aldrich
Sulfuric acid (conc.)	H_2SO_4	96 %	Carl Roth
Tetraphenylmethane	TPM	96 %	Alfa Aesar
1,3,5-trifluoro-2,4,6-triiodobenzene	F-TIB	97 %	Manchester Organics
Tetrahydrofuran	THF	99.9 %, anhydrous	Sigma-Aldrich
Tetrakis(triphenylphosphine)palladium(0)	$Pd(PPh_3)_4$	99 %	Sigma-Aldrich
Triethylamine	NEt_3	99 %, anhydrous	Sigma-Aldrich
Trimethylsilylacetylene	-	98 %	ABCR
Triphenylphosphine	PPh_3	99 %	Sigma-Aldrich

1,4-diethynylbenzene and 1,3,5-triethynylbenzene were sublimated before use (10^{-3} mbar, 25 °C and 40 °C, respectively). The synthetic procedures to obtain 1,3,5-tri-iodobenzene and tetrakis(4-iodophenyl)methane[87] as well as tris(4-bromo-2,6-dimethyl-phenyl)phosphine[104], which were used herein, are reported elsewhere.

7.2 Experimental Procedures

7.2.1 Monomer Syntheses

All monomer syntheses not described in **Articles I-III** are given here.

7.2.1.1 Tetrakis(4-bromophenyl)methane

$C_{25}H_{16}Br_4$
636.02 g·mol^{-1}
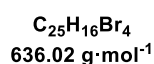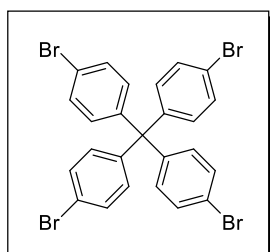
A 100 mL two-necked roundbottom flask equipped with a reflux condenser and a septum was charged with tetraphenylmethane (4.00 g, 12.5 mmol, 1.00 eq). Through the septum, bromine (8 mL, 156 mmol, 12.5 eq) was added dropwise while stirring under strong steam evolution. After complete addition the mixture was stirred for 45 minutes at ambient temperature and then cooled to 0 °C with an ice bath. Ethanol (50 mL) was added upon which an orange suspension formed. This was allowed to warm to ambient temperature overnight. Sodium hydrogen sulfite (saturated aqueous solution, 50 mL) was added until the solid decolorized. The solid was filtered off and washed with more sodium hydrogen sulfite solution, water, and ethanol. The solid was absorbed onto silica gel and purified via column chromatography (hexane) to yield a colorless, crystalline solid. Yield, 4.93 g (7.75 mmol, 62 %).

^{1}H NMR (CDCl$_3$, 200 MHz): δ [ppm] = 7.39 (d, 8 H, J = 8.8 Hz, C$_{Ar}$–H), 7.01 (d, 8 H, J = 8.8 Hz, C$_{Ar}$–H).

^{13}C{^{1}H} NMR (CDCl$_3$, 50 MHz): δ [ppm] = 144.4 (C$_{Ar}$–C$_{quart}$), 132.3 (C$_{Ar}$–H), 131.1 (C$_{Ar}$–H), 120.8 (C–Br), 63.6 (C$_{quart}$).

7.2.1.2 Tetrakis(4-(trimethylsilylethynyl)phenyl)methane

$C_{45}H_{52}Si_4$
705.25 g·mol^{-1}
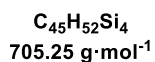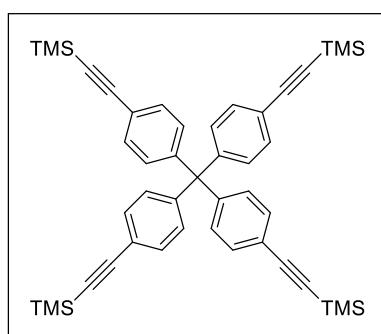
Inside the glovebox, a 250 mL Schlenk flask was charged with tetrakis(4-bromophenyl)methane (2.50 g, 3.93 mmol, 1.00 eq), triphenylphosphine (103 mg, 0.39 mmol, 0.10 eq), bis(triphenylphosphine)palladium(II) chloride (138 mg, 0.20 mmol, 0.05 eq) and copper(I) iodide (51.0 mg, 0.27 mmol, 0.07 eq). The solids were suspeded in THF (25 mL) and diisopropylamine (25 mL), the flask sealed with a septum, and removed from the glovebox. Trimethylsilylacetylene (3.30 mL, 23.6 mmol, 6.00 eq) was added dropwise via syringe through the septum to yield an orange solution. The mixture was heated to 60 °C for 24 hours upon which the solution turned green and a solid precipitated. After cooling to ambient temperature the mixture was filtered off and the white filter cake washed with DCM. The brown filtrate was washed with water twice (150 and 100 mL) and the aqueous phases washed with DCM (2 x 50 mL each). The combined organic phases were dried over magnesium sulfate, absorbed onto silica gel

and purified via column chromatography (starting from 100 % hexane using a low gradient to hexane/DCM 8:2) to yield tetrakis(4-(trimethylsilylethynyl)phenyl)methane as a light yellow solid. Yield, 2.77 g (0.39 mmol, 99 %).

^{1}H NMR (CDCl$_3$, 200 MHz): δ [ppm] = 7.34 (d, 8 H, J = 8.6 Hz, C$_{Ar}$–H), 7.05 (d, 8 H, J = 8.6 Hz, C$_{Ar}$–H), 7.05 (s, 36 H, CH$_3$).

^{13}C{^{1}H} NMR (CDCl$_3$, 50 MHz): δ [ppm] = 146.0 (*C*$_{Ar}$–C$_{quart}$), 131.4 (*C*$_{Ar}$–H), 130.7 (*C*$_{Ar}$–H), 121.2 (*C*$_{Ar}$–C≡C), 104.6 (C$_{Ar}$–*C*≡C), 94.8 (C$_{Ar}$–C≡*C*), 64.7 (C$_{quart}$), -0.07 (CH$_3$).

7.2.1.3   Tetrakis(4-ethynylphenyl)methane
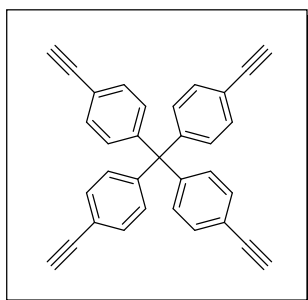
C$_{33}$H$_{20}$
416.52 g·mol^{-1}

Tetrakis(4-(trimethylsilylethynyl)phenyl)methane (2.17 g, 3.07 mmol, 1.00 eq) was dissolved in a mixture of DCM (50 mL) and methanol (50 mL) and potassium carbonate (2.50 g, 18.09 mmol, 5.90 eq) added. The mixture was stirred at ambient temperature for 18 hours, washed with water (80 mL), and the aqueous phase washed with DCM (2 x 50 mL). The combined organic phases were dried over magnesium sulfate, absorbed onto silica gel and purified via column chromatography (starting from 100 % hexane using a low gradient to hexane/DCM 75:25) to yield tetrakis(4-ethynylphenyl)methane as a light yellow solid. Yield, 1.05 g (2.52 mmol, 82 %).

^{1}H NMR (CDCl$_3$, 200 MHz): δ [ppm] = 7.39 (d, 8 H, J = 8.6 Hz, C$_{Ar}$–H), 7.12 (d, 8 H, J = 8.6 Hz, C$_{Ar}$–H), 3.07 (s, 4 H, C≡C–H).

^{13}C{^{1}H} NMR (CDCl$_3$, 50 MHz): δ [ppm] = 146.2 (*C*$_{Ar}$–C$_{quart}$), 131.7 (*C*$_{Ar}$–H), 130.8 (*C*$_{Ar}$–H), 120.3 (*C*$_{Ar}$–C≡C), 83.2 (C$_{Ar}$–*C*≡C), 77.6 (C$_{Ar}$–C≡*C*), 64.8 (C$_{quart}$).

7.2.1.4   2,2',4,4',6,6'-Hexamethylbiphenyl
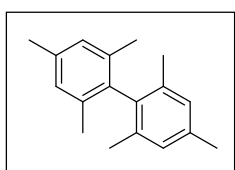
C$_{18}$H$_{22}$
238.37 g·mol^{-1}

A 500 mL three-necked flask equipped with reflux condenser was charged with magnesium turnings (1.44 g, 59.0 mmol, 1.28 eq), a pinch of iodine and THF (anhydrous, 250 mL). The solution was heated to 80 °C and 2-bromomesitylene (7.00 mL, 46.0 mmol, 1.00 eq) added dropwise. After heating to reflux for 3 hours, methyl iodide (2 drops) was added and heating continued for 20 hours. More methyl iodide was added and the mixture heated to 80 °C for 24 hours during which a black solution formed under total consumption of magnesium. The mixture was allowed to cool to ambient temperature and transferred to another 500 mL flask containing a mixture of anhydrous FeCl$_3$ (0.22 g, 1.36 mmol, 0.03 eq), 1,2-dibromoethane (2.4 mL) and THF (anhydrous, 3 mL) and stirred at ambient temperature under inert atmosphere. After 1 hour the reaction was terminated by addition of HCl solution (1 N, 5.0 mL). The solvents were evaporated under reduced pressure and the residue extracted with DCM to yield a deep brown solution. DCM was strongly reduced at the rotary evaporator and colorless crystals precipitated by addition of methanol. Yield, 0.83 g (3.50 mmol, 15 %).

1H NMR (CDCl$_3$, 200 MHz): δ [ppm] = 6.93 (s, 4 H, C$_{Ar}$–H), 2.33 (s, 6 H, *p*-CH$_3$), 1.86 (s, 12 H, *o*-CH$_3$).

13C{1H} NMR (CDCl$_3$, 50 MHz): δ [ppm] = 137.0 (*C*$_{Ar}$–*C*$_{Ar}$), 136.0 (*p*-*C*$_{Ar}$–CH$_3$), 135.5 (*o*-*C*$_{Ar}$–CH$_3$), 128.2 (*C*$_{Ar}$–H), 21.1 (*p*-*C*$_{Ar}$–CH$_3$), 19.8 (*o*-*C*$_{Ar}$–CH$_3$).

7.2.1.5 3,3',5,5'-Tetraiodo-2,2',4,4',6,6'-hexamethylbiphenyl
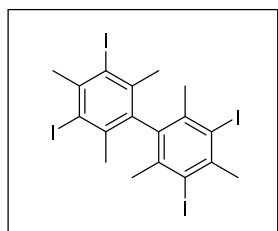
C$_{18}$H$_{18}$I$_4$
741.96 g·mol^{-1}

Bimesityl (0.64 g, 2.68 mmol, 1.00 eq), iodine (1.13 g, 4.45 mmol, 1.66 eq) and periodic acid (0.50 g, 2.20 mmol, 0.82 eq) were suspended in a mixture of acetic acid/concentrated sulfuric acid/deionized water (40:8:1) and heated to 90 °C overnight. Water (50 mL) was added and the resulting suspension stirred for 15 minutes, filtered off, and the yellow solid washed with ethanol until it was colorless. The colorless solid was dried in air. Yield, 1.43 g (1.93 mmol, 72 %).

1H NMR (CDCl$_3$, 200 MHz): δ [ppm] = 3.03 (s, 12 H, *o*-CH$_3$), 2.05 (s, 6 H, *p*-CH$_3$).

7.2.1.6 3,3',5,5'-Tetraethynyl-2,2',4,4',6,6'-hexamethylbiphenyl
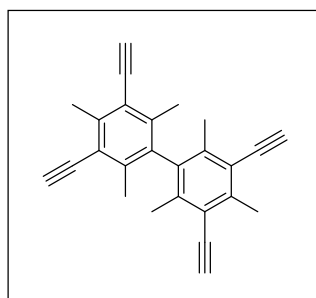
C$_{26}$H$_{22}$
334.46 g·mol^{-1}

In a flame-dried Schlenk flask, 3,3',5,5'-tetraiodobimesityl (660 mg, 0.89 mmol, 1.00 eq), Pd(PPh$_3$)$_4$ (116.0 mg, 0.10 mmol, 0.03 eq), and copper(I) iodide (38.1 mg, 0.20 mmol, 0.06 eq) were dissolved in a mixture of THF/NEt$_3$ (30 mL, 1:1 v/v). Trimethylsilylacetylene (0.58 mL, 4.07 mmol, 1.14 eq) was added and the mixture heated to 90 °C for 5 hours and allowed to cool to ambient temperature overnight. HCl solution (10 %, 50 mL) was added, the phases separated, the organic phase washed with brine, and dried over sodium sulfate. The solvent was removed under reduced pressure, the brown residue suspended in diethyl ether, and absorbed onto silica gel. After column chromatography (cyclohexane) a yellow solid was obtained. This was dissolved in DCM/methanol (20 mL, 1:1 v/v), K$_2$CO$_3$ (984 mg, 7.12 mmol, 2.00 eq) added, and the mixture stirred at ambient temperature overnight. Magnesium sulfate was added, the suspension filtered off, and the filtrate reduced at the rotary evaporator. The brownish residue was dissolved in diethyl ether and absorbed onto silica gel. Purification via column chromatography (cyclohexane) yielded the product as a yellow, foamy substance which was repeatedly dissolved in diethyl ether and the solvent removed again until a yellow, crystalline solid formed. Yield, 109 mg (0.33 mmol, 37 % after two steps).

1H NMR (CDCl$_3$, 200 MHz): δ [ppm] = 3.52 (s, 4 H, C≡C–H), 2.66 (s, 6 H, *p*-CH$_3$), 2.01 (s, 12 H, *o*-CH$_3$).

13C{1H} NMR (CDCl$_3$, 50 MHz): δ [ppm] = 143.0, 139.0, 137.0, 120.9, 85.3, 81.3, 20.0, 18.6.

7.2.2 Polymer Syntheses

All polymer syntheses not described in **Articles I-III** are given here.

7.2.2.1 1,3,5-Triiodobenzene + 1,4-Diethynylbenzene (inverse PAE-1 Synthesis)
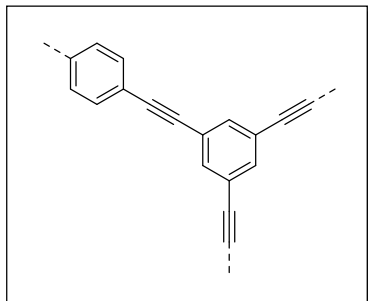
A 5 ml sample vial was charged with 1,3,5-triiodobenzene (199.8 mg, 0.44 mmol, 1.00 eq), 1,4-diethynylbenzene (84.0 mg, 0.66 mmol, 1.50 eq), Pd(PPh$_3$)$_4$ (10.0 mg, 8.7 μmol, 0.65 % per halide/alkyne) DMF (2 mL) and NEt$_3$ (1 mL), and the mixture stirred for 10 minutes at ambient temperature inside the glovebox. A septum was applied, the sealed vial removed from the glovebox, and put into a pre-heated oil bath at 100 °C. The mixture solidified after 3.5 minutes and was kept at 100 °C for 20 hours, removed from the oil bath, and allowed to cool to ambient temperature. The formed solid was suspended in methanol, filtered off, purified by Soxhlet extraction with methanol overnight and dried under reduced pressure for 8 hours to afford a bright yellow, voluminous powder. Yield, 129.3 mg (112 %).

^{13}C CP/MAS NMR (100 MHz): δ [ppm] = 134, 128, 125, 121, 86.

SA_{BET} [m^2·g^{-1}] = 1121.

7.2.2.2 Tetrakis(4-iodophenyl)methane + 1,4-Diethynylbenzene
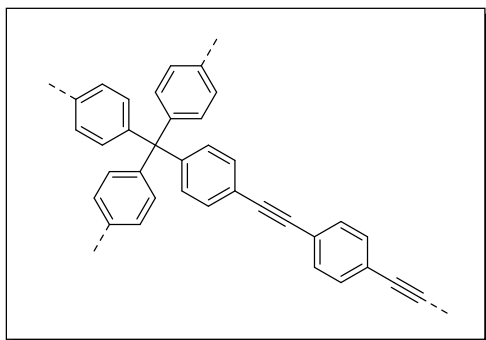
A 50 ml sample vial was charged with tetrakis(4-iodophenyl)methane (70.5 mg, 0.086 mmol, 1.00 eq), 1,4-diethynylbenzene (21.6 mg, 0.17 mmol, 2.00 eq), Pd(PPh$_3$)$_4$ (2.5 mg, 2.2 μmol, 0.65 % per halide/alkyne), DMF (20 mL) and NEt$_3$ (10 mL), and the mixture stirred for 10 minutes at ambient temperature inside the glovebox. A septum was applied, the sealed vial removed from the glovebox, and put into a pre-heated oil bath at 100 °C. The mixture solidified after 7 minutes and was kept at 100 °C for 6 hours, removed from the oil bath, and allowed to cool to ambient temperature. The formed solid was suspended in methanol, filtered off, purified by Soxhlet extraction with methanol overnight and dried under reduced pressure overnight to afford a yellow, voluminous powder. Yield, 55.1 mg 113 %).

^{13}C CP/MAS NMR (100 MHz): δ [ppm] = 143, 134, 128, 125, 121, 120, 88, 80, 62.

SA_{BET} [m^2·g^{-1}] = 1811.

7.2.2.3   1,4-Diiodobenzene + Tetrakis(4-ethynylphenyl)methane
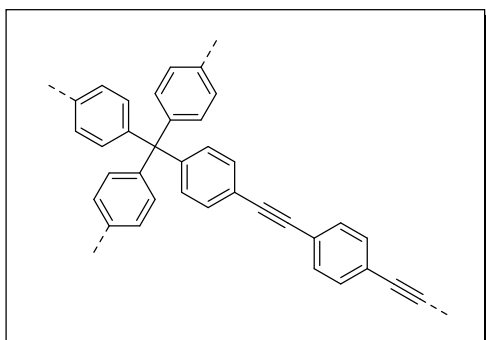
A 50 ml sample vial was charged with 1,4-diiodobenzene (56.4 mg, 0.17 mmol, 1.00 eq), tetrakis(4-ethynylphenyl)methane (35.6 mg, 0.085 mmol, 0.50 eq), Pd(PPh$_3$)$_4$ (2.5 mg, 2.2 µmol, 0.65 % per halide/alkyne), DMF (20 mL) and NEt$_3$ (10 mL), and the mixture stirred for 10 minutes at ambient temperature inside the glovebox. A septum was applied, the sealed vial removed from the glovebox, and put into a pre-heated oil bath at 100 °C. The mixture solidified after several minutes and was kept at 100 °C for 20 hours, removed from the oil bath, and allowed to cool to ambient temperature. The formed solid was suspended in methanol, filtered off, purified by Soxhlet extraction with methanol overnight and dried under reduced pressure overnight to afford a brown, condensed solid. Yield, 51.9 mg (108 %).

^{13}C CP/MAS NMR (100 MHz): δ [ppm] = 143, 134, 128, 125, 121, 120, 88, 80, 62.

SA_{BET} [m$^2 \cdot$g^{-1}] = 1606.

7.2.2.4   Tetrakis(4-iodophenyl)methane + Tetrakis(4-ethynylphenyl)methane
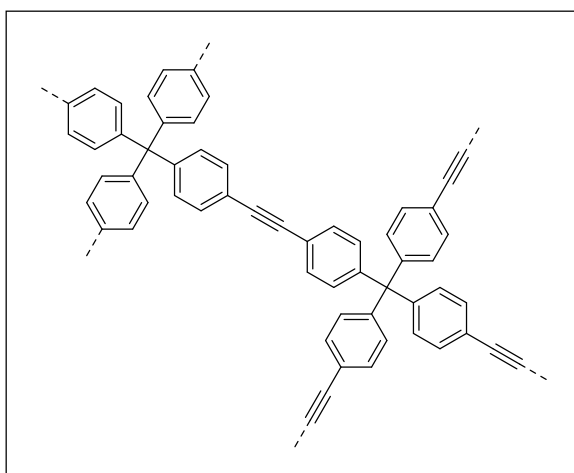
A 50 ml sample vial was charged with tetrakis(4-iodophenyl)methane (73.5 mg, 0.89 mmol, 1.00 eq), tetrakis(4-ethynylphenyl)methane (37.1 mg, 0.89 mmol, 1.00 eq), Pd(PPh$_3$)$_4$ (2.6 mg, 2.2 µmol, 0.65 % per halide/alkyne), DMF (10 mL) and NEt$_3$ (5 mL), and the mixture stirred for 10 minutes at ambient temperature inside the glovebox. A septum was applied, the sealed vial removed from the glovebox, and put into a pre-heated oil bath at 100 °C. Before all monomer was dissolved, a colorless precipitate started to form after 5 minutes and was kept at 100 °C for 20 hours, removed from the oil bath, and allowed to cool to ambient temperature. The formed solid was suspended in methanol, filtered off, purified by Soxhlet extraction with methanol overnight and dried under reduced pressure overnight to afford a condensed, brown powder. Yield, 74.9 mg (115 %).

^{13}C CP/MAS NMR (100 MHz): δ [ppm] = 143, 134, 128, 125, 120, 88, 80, 62.

SA_{BET} [m$^2 \cdot$g^{-1}] = 1969.

7.2.2.5   1,4-Diiodobenzene + 3,3',5,5'-tetraethynyl-2,2',4,4',6,6'-hexamethylbiphenyl
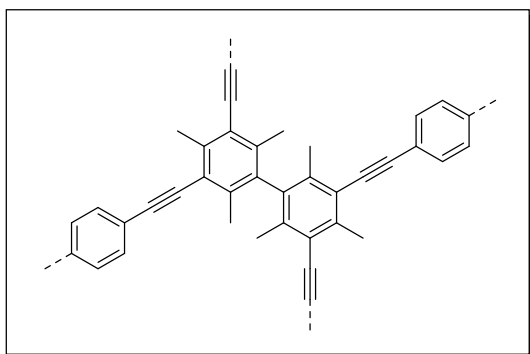
A 50 ml sample vial was charged with 1,4-diiodobenzene (66.0 mg, 0.20 mmol, 1.00 eq), 3,3',5,5'-tetraethynyl-2,2',4,4',-6,6'-hexamethylbiphenyl (33.4 mg, 0.10 mmol, 2.00 eq), Pd(PPh$_3$)$_4$ (3.0 mg, 2.6 µmol, 0.65 % per halide/alkyne), DMF (24 mL) and NEt$_3$ (12 mL), and the mixture stirred for 10 minutes at ambient temperature inside the glovebox. A septum was applied, the sealed vial removed from the glovebox, and put into a pre-heated oil bath at 100 °C. The mixture turned pale yellow over time and a yellow precipitate formed after a few minutes. The mixture was kept at 100 °C for 20 hours, removed from the oil bath, and allowed to cool to ambient temperature. The formed solid was suspended in methanol, filtered off, purified by Soxhlet extraction with methanol overnight and dried in the vacuum oven at 80 °C for 6 hours to afford an inhomogeneous brown and beige, condensed solid. Yield, 51.5 mg (107 %).

^{13}C CP/MAS NMR (100 MHz): δ [ppm] = 134, 128, 120, 95, 87, 15.

SA_{BET} [m$^2 \cdot$g^{-1}] = 1115.

7.2.2.6   Tetrakis(4-iodophenyl)methane + 3,3',5,5'-tetraethynyl-2,2',4,4',6,6'-hexamethylbiphenyl
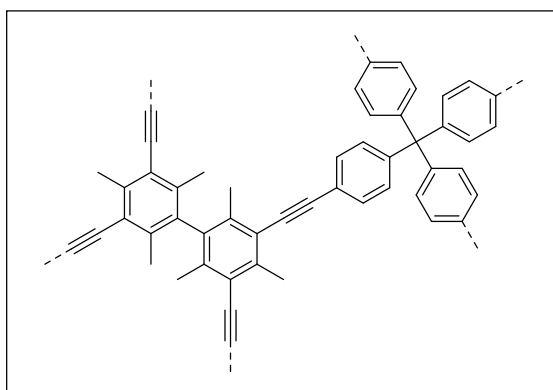
A 50 ml sample vial was charged with tetrakis(4-iodophenyl)methane (83.5 mg, 0.10 mmol, 1.00 eq), 3,3',5,5'-tetraethynyl-2,2',4,4',6,6'-hexamethylbiphenyl (33.8 mg, 0.10 mmol, 1.00 eq), Pd(PPh$_3$)$_4$ (3.1 mg, 2.7 µmol, 0.65 % per halide/alkyne), DMF (24 mL) and NEt$_3$ (12 mL), and the mixture stirred for 10 minutes at ambient temperature inside the glovebox. A septum was applied, the sealed vial removed from the glovebox, and put into a pre-heated oil bath at 100 °C. The mixture turned yellow over time and a colorless solid precipitated after a few minutes. The mixture was kept at 100 °C for 20 hours, removed from the oil bath, and allowed to cool to ambient temperature. The formed solid was suspended in methanol, filtered off, purified by Soxhlet extraction with methanol overnight and dried under reduced pressure for 5 hours to afford an inhomogeneous, brown and off-white solid. Yield, 68.8 mg (105 %).

^{13}C CP/MAS NMR (100 MHz): δ [ppm] = 142, 134, 128, 119, 95, 88, 84, 62, 14.

SA_{BET} [m$^2 \cdot$g^{-1}] = 1534.

7.2.2.7   2,3,5,6-Tetrafluoro-1,4-diiodobenzene + 1,3,5-Triethynylbenzene (F-PAE-1)
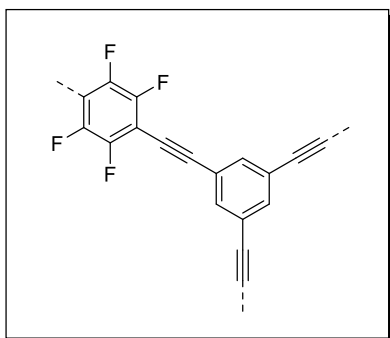
A 5 ml sample vial was charged with 2,3,5,6-tetrafluoro-1,4-diiodobenzene (401.9 mg, 1.00 mmol, 1.00 eq), 1,3,5-triethynylbenzene (100.1 mg, 0.67 mmol, 0.67 eq), Pd(PPh$_3$)$_4$ (15.0 mg, 13 µmol, 0.65 % per halide/alkyne), DMF (3 mL) and NEt$_3$ (1.5 mL), and the mixture stirred for 10 minutes at ambient temperature inside the glovebox. A septum was applied, the sealed vessel removed from the glovebox, and put into an oil bath pre-heated to 100 °C. The intensely bright yellow mixture turned pale yellow after a few seconds, then increasingly darker and more intensely yellow and solidified after ca. 40 minutes at 100 °C to a dark yellow block. The mixture was kept at 100 °C for 20 hours, removed from the oil bath, and the reaction quenched by addition of methanol. The dark brown solid was stirred in methanol for 2 hours, filtered off, washed with acetone, THF, and methanol, purified *via* Soxhlet extraction with methanol overnight and dried in the vacuum oven at 80 °C for 4 hours. afford a black, voluminous powder. Yield, 150.5 mg (61 %).

^{13}C CP/MAS NMR (100 MHz): δ [ppm] = 144, 142, 132, 120, 102, 96, 78, 73.

SA_{BET} [m$^2 \cdot$g^{-1}] = 890.

7.2.2.8   1,3,5-Triiodo-2,4,6-trifluorobenzene + 1,4-Diethynylbenzene (F-PAE-2)
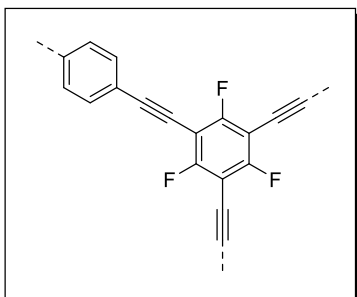
A 5 ml sample vial was charged with 1,3,5-triiodotrifluorobenzene (339.8 mg, 0.67 mmol, 1.00 eq), 1,4-diethynylbenzene (126.2 mg, 1.00 mmol, 1.00 eq), Pd(PPh$_3$)$_4$ (15 mg, 13 µmol, 0.65 % per halide/alkyne), DMF (3 mL) and NEt$_3$ (1.5 mL), and the mixture stirred for 10 minutes at ambient temperature inside the glovebox. A septum was applied, the sealed vial removed from the glovebox, and put into a pre-heated oil bath at 100 °C. A yellow solid precipitated from the dark yellow mixture after a few minutes of heating. The mixture was kept at 100 °C for 20 hours, removed from the oil bath, and allowed to cool to ambient temperature. The formed solid was suspended in methanol and stirred for 2 hours, filtered off, washed with acetone, THF, and methanol. While washing with acetone and THF parts of the solid dissolved and the filtrates were yellow and brown, respectively. The remaining solid was purified *via* Soxhlet extraction with methanol overnight and dried in the vacuum oven at 80 °C for 4 hours to yield a brown powder. Yield, 101.5 mg (48 %).

^{13}C CP/MAS NMR (100 MHz): δ [ppm] = 158, 130, 118, 97, 80, 75.

SA_{BET} [m$^2 \cdot$g^{-1}] = 54.

7.2.2.9 2,5-Diiodothiophene and 1,3,5-Triethynylbenzene (Th-PAE)
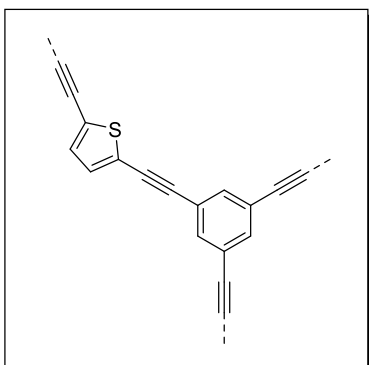
A 5 ml sample vial was charged with 2,5-diiodothiophene (111.5 mg, 0.33 mmol, 1.00 eq), 1,3,5-triethynylbenzene (33.5 mg, 0.22 mmol, 0.67 eq), Pd(PPh$_3$)$_4$ (5.0 mg, 4.3 µmol, 0.65 % per halide/alkyne), DMF (2 mL) and NEt$_3$ (1 mL), and the mixture stirred for 10 minutes at ambient temperature inside the glovebox. A septum was applied, the sealed vial removed from the glovebox, and put into a pre-heated oil bath at 100 °C. The solution turned from light yellow to red and started to solidify after 9 minutesIt was kept at 100 °C for 20 hours, removed from the oil bath, and allowed to cool to ambient temperature. The formed reddish solid was suspended in methanol, filtered off, purified by Soxhlet extraction with methanol overnight and dried under reduced pressure for at 80 °C for 6 hours to afford a voluminous, ochre powder. Yield, 59 mg (98 %).

^{13}C CP/MAS NMR (100 MHz): δ [ppm] = 129, 121, 90, 81.

SA$_{BET}$ [m^2·g^{-1}] = 787.

7.2.2.10 Tris(4-bromo-2,6-dimethylphenyl)phosphine + 1,4-Diethynylbenzene (P-PAE-1)
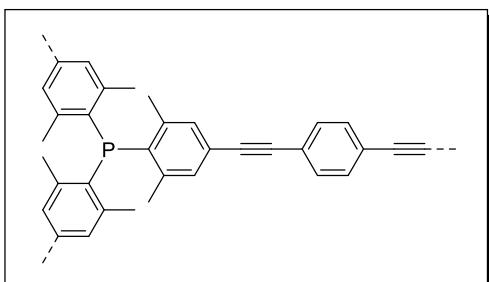
A 25 ml sample vial was charged with tris(4-bromo-2,6-dimethylphenyl)phosphine (200 mg, 0.34 mmol, 1.00 eq), 1,4-diethynyl-benzene (65.0 mg, 0.52 mmol, 1.50 eq), Pd(PPh$_3$)$_4$ (15.5 mg, 13 µmol, 1.30 % per halide/alkyne), DMF (6 mL) and NEt$_3$ (3 mL), and the mixture stirred for 10 minutes at ambient temperature inside the glovebox. A septum was applied, the sealed vial removed from the glovebox, and put into a pre-heated oil bath at 100 °C. The mixture solidified after a few minutes and was kept at 100 °C for 20 hours, removed from the oil bath, and allowed to cool to ambient temperature. The formed solid was suspended in methanol, filtered off, purified by Soxhlet extraction with methanol overnight and dried under reduced pressure for 5 hours to afford an intensely yellow powder. Yield, 188.6 mg (104 %).

^{13}C CP/MAS NMR (100 MHz): δ [ppm] = 140, 132, 129, 126, 121, 89, 19.

^{31}P CP/MAS NMR (128 MHz): δ [ppm] = -35.

SA$_{BET}$ [m^2·g^{-1}] = 535.

7.2.2.11 Tris(4-bromo-2,6-dimethylphenyl)phosphine + 1,3,5-Triethynylbenzene (P-PAE-2)
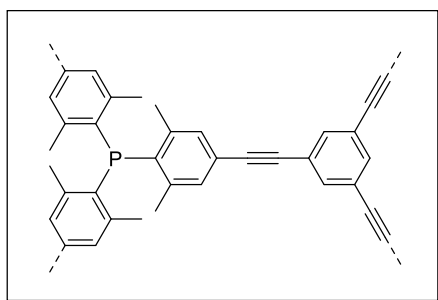
A 25 ml sample vial was charged with tris(4-bromo-2,6-dimethylphenyl)phosphine (194.3 mg, 0.33 mmol, 1.00 eq), 1,3,5-triethynylbenzene (50.0 mg, 0.33 mmol, 1.00 eq), Pd(PPh$_3$)$_4$ (15.5 mg, 13 µmol, 1.30 % per halide/alkyne), DMF (6 mL) and NEt$_3$ (3 mL), and the mixture stirred for 10 minutes at ambient temperature inside the glovebox. A septum was applied, the sealed vial removed from the glovebox, and put into a pre-heated oil bath at 100 °C. The yellow mixture solidified after a few minutes and was kept at 100 °C for 20 hours, removed from the oil bath, and allowed to cool to ambient temperature. The formed solid was suspended in methanol, filtered off, purified by Soxhlet extraction with methanol overnight and dried under reduced pressure for 5 hours to afford a bright yellow powder. Yield, 160.2 mg (98 %).

^{13}C CP/MAS NMR (100 MHz): δ [ppm] = 140, 130, 125, 121, 89, 19.

^{31}P CP/MAS NMR (128 MHz): δ [ppm] = -35.

SA$_{BET}$ [m$^2\cdot$g^{-1}] = 639.

7.2.2.12 Tris(4-bromo-2,6-dimethylphenyl)phosphine + Tetrakis(4-ethynylphenyl)-methane (P-PAE-3)
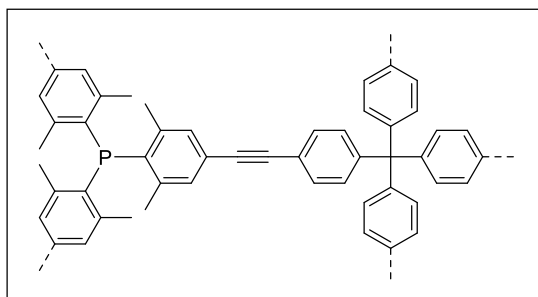
A 25 ml sample vial was charged with tris(4-bromo-2,6-dimethylphenyl)phosphine (200 mg, 0.34 mmol, 1.00 eq), tetrakis(4-ethynylphenyl)phosphine (104.1 mg, 0.25 mmol, 0.75 eq), Pd(PPh$_3$)$_4$ (15.5 mg, 13 µmol, 1.30 % per halide/alkyne), DMF (6 mL) and NEt$_3$ (3 mL), and the mixture stirred for 10 minutes at ambient temperature inside the glovebox. A septum was applied, the sealed vial removed from the glovebox, and put into a pre-heated oil bath at 100 °C. The mixture solidified after a few minutes and was kept at 100 °C for 20 hours, removed from the oil bath, and allowed to cool to ambient temperature. The formed solid was suspended in methanol, filtered off, purified by Soxhlet extraction with methanol overnight and dried under reduced pressure for 5 hours to afford a bright yellow powder. Yield, 237.5 mg (109 %).

^{13}C CP/MAS NMR (100 MHz): δ [ppm] = 143, 130, 128, 125, 121, 120, 89, 19.

^{31}P CP/MAS NMR (128 MHz): δ [ppm] = -35.

SA$_{BET}$ [m$^2\cdot$g^{-1}] = 847.

7.3 Crystallographic Data

Table 4: Crystallographic data for tris(4-bromo-2,6-dimethylphenyl)phosphine

Compound	Tris(4-bromo-2,6-dimethylphenyl)phosphine
Empirical formula	$C_{24}H_{24}PBr_3$
Formula weight	583.13
Temperature/K	298
Crystal system	orthorhombic
Space group	P21212
a/Å	24.4850(4)
b/Å	23.2736(5)
c/Å	8.12323(15)
α/°	90.00
β/°	90.00
γ/°	90.00
Volume/Å^3	4629.05(15)
Z	9
ρcalcg/cm^3	1.883
μ/mm^{-1}	8.060
F(000)	2592.0
Crystal size/mm^3	0.4 × 0.4 × 0.2
Radiation	CuKα (λ = 1.54184)
2Θ range for data collection/°	5.24 to 147.26
Index ranges	30 $\leq$ h $\leq$ 28, 27 $\leq$ k $\leq$ 28, 6 $\leq$ l $\leq$ 9
Reflections collected	18611
Independent reflections	8042 [R_{int} = 0.1104, R_{sigma} = 0.1288]
Data/restraints/parameters	8042/0/517
Goodness of fit on F2	1.030
Final R indexes [I>=2σ (I)]	R1 = 0.0712, wR2 = 0.1643
Final R indexes [all data]	R1 = 0.0945, wR2 = 0.1946
Largest diff. peak/hole / e Å^3	1.01/1.40
Flack parameter	0.08(5)

8 Publications

Article I

"Copper-Free Sonogashira Coupling for High-Surface-Area Conjugated Microporous Poly(Aryleneethynylene) Networks"

▌ **Microporous Materials** |*Hot Paper*|

Copper-Free Sonogashira Coupling for High-Surface-Area Conjugated Microporous Poly(aryleneethynylene) Networks

Matthias Trunk,* Anna Herrmann, Hakan Bildirir, Ali Yassin, Johannes Schmidt, and Arne Thomas*[a]

Abstract: A modified one-pot Sonogashira cross-coupling reaction based on a copper-free methodology has been applied for the synthesis of conjugated microporous poly(aryleneethynylene) networks (CMPs) from readily available iodoarylenes and 1,3,5-triethynylbenzene. The polymerization reactions were carried out by using equimolar amounts of halogen and terminal alkyne moieties with extremely small loadings of palladium catalyst as low as 0.65 mol%. For the first time, CMPs with rigorously controlled structures were obtained without any indications of side reactions, as proven by FTIR and solid-state NMR spectroscopy, while showing Brunauer–Emmett–Teller (BET) surface areas higher than any poly(aryleneethynylene) network reported before, reaching up to 2552 $m^2 g^{-1}$.

Introduction

Over the last two decades, microporous organic materials have seen remarkable development due to their potential applications in gas storage, separation, sensing, and catalysis.[1,2] This development has been accelerated by the general trend towards sustainability and a call for less energy-intensive alternatives for industrial procedures, such as cryogenic distillation. Aside from ordered materials, such as metal–organic frameworks (MOFs)[3] and covalent organic frameworks (COFs),[4,5] microporous polymer networks (MPNs) have emerged as a family of amorphous yet highly promising materials for a range of applications.[6–10] Apart from polymeric materials, porous organic molecules have gained an increasing amount of attention recently.[11–16] Extensive studies have produced unique combinations of high accessible surface areas and chemical robustness, as well as thermal stability, often surpassing MOFs and COFs in those respects, although in exchange for ordered structures.[1,2,17] A plethora of porous polymers has been obtained through a variety of polymerization methods. Especially the palladium-catalyzed procedure following the Sonogashira-type protocol published by Cooper et al.[6] to produce conjugated microporous poly(aryleneethynylene) networks (CMPs) is a commonly employed method to incorporate functional groups into porous polymer backbones.[18] Further functional groups can be grafted onto the polymer backbones postsynthetical-

ly.[19–21] The importance of these materials is emphasized by the recent commercialization of CMP-1 by Sigma–Aldrich.[22]

Since 2007, different protocols for CMP syntheses with varying solvents, temperature, starting materials, and stoichiometry have been reported.[23–26] Initially, ethynyl-functionalized aromatic compounds were reacted with aryl iodides, which were later often succeeded by more readily available bromides, whereby lower degrees of condensation accompanied by slightly lower surface areas were observed.[18,27] Surprisingly and solely based on empirical findings, the highest surface area for a given CMP was obtained by use of a 50% excess of alkyne functions, which should actually give unreacted alkyne end groups within the resulting network structures,[23] and be detrimental for reaching high surface areas in a MPN. A recent article addresses the issue of this counterintuitive stoichiometry in depth, focusing on the network formation with special attention paid to open end groups within the network.[28] Herein, the empirically found necessity for an excess of ethynyl groups for the formation of high-surface-area materials is rationalized by an ongoing reaction of ethynyl end groups, which are trapped within the precipitated material. These ethynyl groups cross-link during elongated reaction times, whereas halide end groups would remain unreactive after gelation, giving dead ends within the polymer. The steady decrease in terminal ethynyl functions was shown to be accompanied by a rise in nitrogen-accessible surface area. Nevertheless, the use of equimolar monomer ratios can also be found in the literature.[10,24,29,30] Recently, Son and co-workers used the correct stoichiometry to create impressive surface areas of almost 1800 $m^2 g^{-1}$ by systematic variation of the phosphine ligand accompanying the palladium catalyst.[26]

To elucidate the exact formation mechanism and the nature of the homocoupling product, Bunz and co-workers created a homocoupled CMP from a tetrahedral tin-based monomer, which was digested after polymerization. The fragments were

[a] M. Trunk, A. Herrmann, Dr. H. Bildirir, Dr. A. Yassin, Dr. J. Schmidt, Prof. Dr. A. Thomas
Department of Chemistry, Functional Materials
Technische Universität Berlin
Hardenbergstrasse 40, 10623 Berlin (Germany)
E-mail: arne.thomas@tu-berlin.de
matthias.trunk@tu-berlin.de

analyzed to shed light on the structure of the struts linking the former nodes, and thereby on the mechanism of internal cross-linking. The struts were found to consist of isomeric enynes originating from dimers, trimers, and tetramers of alkyne groups.[31]

To make the conventional homogeneous Sonogashira coupling less susceptible to oxygen and to prevent the formation of side-products, copper-free variants have been developed, although the copper-free mechanism is yet unknown.[32,33] Motivated by these routes and to avoid the aforementioned side-reactions during CMP formation, we developed a copper-free polymerization method employing the exact stoichiometry of alkyne and halide functions.

From a practical point of view, the addition of the catalyst into the hot reaction mixture in the form of a slurry, as it was reported before, seemed to us unfeasible.[6] Residues of insoluble catalyst remaining inside the syringe, cannula, or the vessel used for the preparation of the slurry can prove detrimental to reproducibility and rinsing aforementioned vessel with solvent makes the reaction prone to oxygen contamination. Thus, the herein presented route was originally developed to provide a facile and robust one-pot procedure, using equimolar amounts of ethynyl and halide groups, thus avoiding side-reactions while keeping the conversion efficiency of functional groups as high as possible.

Results and Discussion

To understand and perhaps eliminate the empirically found necessity for a large excess of alkyne functionalities, the reaction parameters were optimized for commercial starting materials, 1,4-diiodobenzene and 1,3,5-triethynylbenzene (TEB). However, the first problem for a controlled polymer synthesis was posed by the varying states in which TEB arrives after purchase (Figure 1 a). Purification of the as-purchased monomer by column chromatography gave a yellow, crystalline powder (Figure 1 b). Further investigation showed that the monomer can be purified by a simple sublimation procedure ($40\,°C\,10^{-3}$ mbar) to give pristine, colorless crystals, which correspond to the expected appearance (Figure 1 c).

Storage of the alkyne at $8\,°C$ showed no evidence of decomposition over several months, whereas elongated exposure to ambient temperature caused the material to turn brown, even when stored under inert conditions. We attribute this behavior to a high inherent reactivity of multi-alkyne compounds, which could in part account for the need of an excess of these compounds when non-purified monomers are applied, because parts of the ethynyl groups have already reacted and thus are not available for further polymerization.

It is a known fact that the use of aryl iodides over bromides facilitates a smoother reaction, which lowers the probability of unreacted end groups. Therefore, iodoarylenes were exclusively used in this study. Upon testing different conditions, it was found
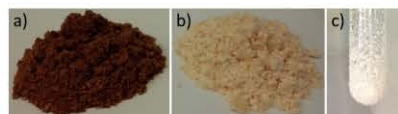
Figure 1. Varying states of 1,3,5-triethynylbenzene: a) as-purchased; b) after column chromatography from dichloromethane; and c) after sublimation.

that for aryl iodides and polyalkynes, high surface areas could be obtained when the amount of palladium catalyst [Pd(PPh$_3$)$_4$] was reduced to 0.65 mol% per iodide/alkyne moiety, whereas the co-catalyst, copper(I) iodide, was omitted completely.[34] Reaction of TEB with 1,3,5-triiodobenzene, 1,4-diiodobenzene, 4,4'-diiodobiphenyl, and tetrakis(4-iodophenyl)-methane in a mixture of DMF/NEt$_3$ (2:1) gave highly electrostatic, spongy materials **P1–P4** (Scheme 1). The resultant powders range from off-white to yellow, according to the length and geometry of the conjugated system. Materials **P1** and **P4**, consisting only of weakly electronically conjugated 1,3-connected aromatics, were obtained as beige and off-white, respectively. In contrast, polymers emerging from 1,4-functionalised arylenes form longer conjugated aromatic systems, giving rise to different hues of yellow (**P2** and **P3**). It should be noted that materials with structures similar to these materials are described in literature—**P1** corresponds to CMP-X,[24] **P2** and **P3** correspond to CMP-1 and -2,[6] respectively, and a structure similar to **P4** was also reported.[35]

However, not only are the materials reported herein much closer to their ideal structures, but they also exhibit significantly enhanced BET surface areas. Furthermore, **P1–P4** are fluorescent under UV light ($\lambda = 254$ nm, light fluorescence; 366 nm,
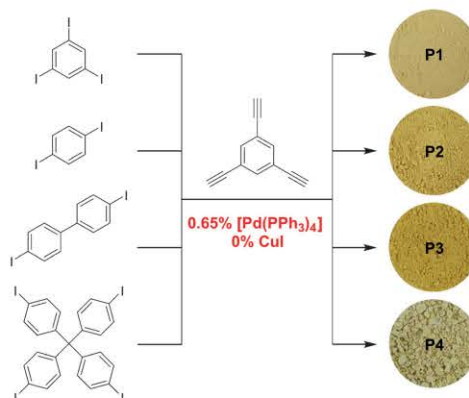
Scheme 1. Copper-free synthetic procedure towards CMPs based on 1,3,5-triethynylbenzene. All reactions were carried out in a mixture of dimethylformamide/triethylamine (2:1) at 100 °C for 20 h.

strong fluorescence), whereas reproduced CMP-1 was found to be non-fluorescent.

Compound **P1** was synthesized by reaction of TEB with 1,3,5-triiodobenzene. According to its highly symmetrical (ideal) structure, **P1** exhibits three major peaks at $\delta = 131$, 121, and 86 ppm in the ^{13}C CP/MAS NMR spectrum (Figure 2).
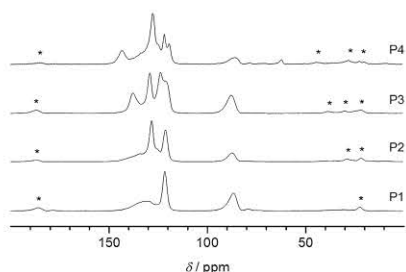
Figure 2. ^{13}C NMR spectra of **P1**–**P4**; asterisks (*) denote spinning sidebands.

These peaks can be unambiguously assigned to C_{Ar}—H (130–133 ppm, very broad), the quaternary carbon atom C_{Ar}—C≡C (121 ppm), and the acetylenic carbon atoms C≡C (86 ppm). Compounds **P2**, **P3**, and **P4** were synthesized by reaction of TEB with 1,4-diiodobenzene, 4,4′-diiodobiphenyl, and tetra-kis(4-iodophenyl)methane, respectively. As can be seen, the peak positions of the triethynylbenzene motif in **P2**, **P3**, and **P4** are largely unchanged from that in **P1** (Figure 2, dashed lines). All remaining peaks of **P2**, **P3**, and **P4** can be assigned accordingly (see the Supporting Information). Additionally, for **P1** and **P4**, small amounts of unreacted alkyne groups were found at $\delta = 78$ ppm.

The high conversion efficiency of this method was confirmed by FTIR measurements (Figure 3). Comparison of the
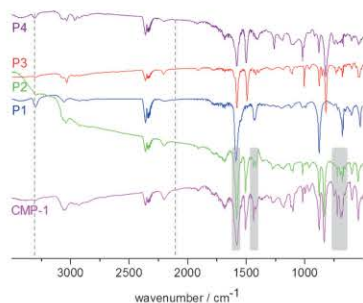
Figure 3. FTIR spectra of **P1** (blue), **P2** (green), **P3** (red), and **P4** (purple) exhibiting very low concentrations of terminal alkyne moieties (2100 and 3300 cm^{-1}, dashed lines), and conventional CMP-1 (pink). Structural differences between CMP-1 and **P2** are highlighted (shaded insets).

peak intensities for internal alkynes (2200 cm^{-1}) and terminal alkynes (2100 and 3300 cm^{-1}, dashed lines) showed low concentrations of terminal alkyne moieties for **P1** and **P4**, and traces for **P2** and **P3**, which is in good agreement with the NMR data. Furthermore, structural differences between **P2** and CMP-1, prepared by the conventional method by hot injection under excess of TEB, can be observed (Figure 3, shaded insets). The occurrence of a shoulder at 1600 cm^{-1} and the additional band at 1440 cm^{-1} in the CMP-1 spectrum resulted from the formation of enyne moieties, which is in agreement with IR data reported before[36] and the NMR data acquired by Bunz and co-workers.[31]

These enyne groups are the product of coupling of the remaining terminal alkyne groups, which can therefore no longer be observed for CMP-1, despite the huge excess of TEB employed in the synthesis. Further differences can be observed in the fingerprint region around 700 cm^{-1}.

As was pointed out previously, the same network structure as **P1** has been reported before.[24] However, the previous solid-state ^{13}C NMR spectrum exhibited an additional sharp peak at $\delta = 131$ ppm, which we attribute to only partially consumed starting material due to non-optimal reaction conditions and less reactive 1,3,5-tribromobenzene. Consequently, the resulting network would exhibit a lower degree of conversion. Testament to this assumption are the comparatively low reported surface areas, which lie in the range of 370 to 400 m^2 g^{-1}, whereas for **P1** a surface area of 914 m^2 g^{-1} was detected. For **P2** and **P3**, 1720 and 873 m^2 g^{-1} were obtained (Figure 4). These values surpass the surface areas of structurally
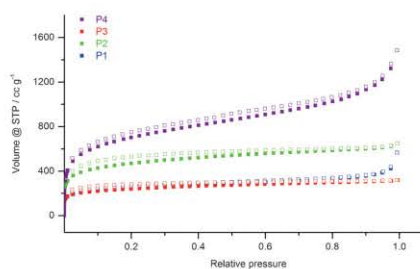
Figure 4. N$_2$ uptake at 77 K for **P1** (blue), **P2** (green), **P3** (red), and **P4** (purple).

related materials obtained by the conventional method of 834 m^2 g^{-1} for CMP-1 and 634 m^2 g^{-1} for CMP-2 (Table 1). The most significant surface-area enhancement was found for **P4**, which exhibited an impressive surface area of 2552 m^2 g^{-1}. This equals more than five times the accessible surface area of the structurally related material published previously,[35] and is the highest BET surface area of any poly(aryleneethynylene) network reported to date, surpassing even those formed by dynamic alkyne metathesis.[10]

Table 1. Surface-area comparison of **P1–P4** and structurally related materials, as well as CO_2 and H_2 uptake capacities of the materials reported herein.

	S_{BET} (reported) [m²g⁻¹]	S_{BET} (this work) [m²g⁻¹]	CO_2 uptake [mmol g⁻¹][a]	H_2 uptake [wt%][b]
P1/CMP-X[24]	397	914	3.01	1.32
P2/CMP-1[6]	834	1720	2.53	1.36
P3/CMP-2[6]	634	873	2.12	1.00
P4/E2[35]	488	2552	3.36	1.59

[a] CO_2 sorption experiments were performed at 273 K and 1 bar. [b] H_2 sorption experiments were carried out at 77 K and 1 bar.

The high accessible surface area of **P4** also gives rise to considerable sorption capacity towards other gases; the total uptake values for H_2 at 77 K and 1 bar, as well as for CO_2 at 273 K and 1 bar are among the highest reported for as-synthesized MPNs.[2,37] Especially the almost linear shape of the CO_2 adsorption curve suggests remarkable uptake under high pressure (see the Supporting Information).

In compounds **P1–P3**, two dominant pore sizes around 0.6 and 0.9 nm were found according to non-local (NL) DFT calculations derived from the nitrogen-sorption measurements (Figure 5). A decrease in the relative intensity of the smaller pores is accompanied by an increase in surface area. The same tendency was reported previously[26] and culminates in **P4** for which pores at 1.10 nm were observed exclusively, and which has the highest BET surface area.
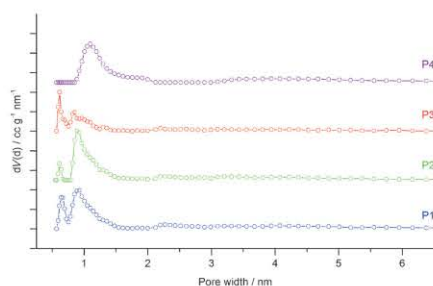
Figure 5. Pore-size distributions of **P1** (blue), **P2** (green), **P3** (red), and **P4** (purple).

Conclusion

We herein present an improved protocol for the synthesis of conjugated microporous polymers based on the Sonogashira cross-coupling reaction. Experiments were carried out in a facile one-pot procedure, and the amounts of halide and alkyne groups were adjusted to 1:1. By reduction of the amount of palladium catalyst to 0.65 mol% and removal of the co-catalyst, copper(I) iodide, for the first time, CMPs with rigorously controlled chemical structure and high BET surface areas of up to 2552 m²g⁻¹ were obtained. We will continue to gain

further mechanistic insights into the polymerization reaction and widen the applicability of this facile and highly efficient synthesis protocol.

Experimental Section

Materials: All chemicals were used as received unless otherwise noted. Tetrakis(4-iodophenyl)methane and 1,3,5-triiodobenzene were synthesized according to a literature procedure with slight modifications (see the Supporting Information). 1,3,5-Triethynylbenzene was purchased from TCI and sublimated before use (40 °C 10⁻³ mbar). Tetrakis(triphenylphosphine)palladium(0) (99.9%), 1,4-diiodobenzene (99%), 1,3,5-tribromobenzene (98%), anhydrous tetrachloromethane (≥99.5%), anhydrous dimethylformamide (99.8%), and triethylamine (≥99.5%) were purchased from Sigma–Aldrich. 4,4′-Diiodobiphenyl (99%) was purchased from Alfa Aesar. Bis(trifluoroacetoxy)iodobenzene (98%) and iodine (99.5%) were purchased from Acros Organics. Tetraphenylmethane (96%) was purchased from Manchester Organics.

Synthetic procedure for P1: Inside the glovebox, a 50 mL glass vial was charged with 1,3,5-triethynylbenzene (100.6 mg, 670 µmol), 1,3,5-triiodobenzene (305.4 mg, 670 µmol), [Pd(PPh₃)₄] (15.1 mg, 13 µmol), dimethylformamide (12 mL), and triethylamine (6 mL). The vessel was closed with a silicone septum, extracted from the glovebox, and immersed in an oil bath preheated to 100 °C. The colorless solution turned increasingly yellow, and a voluminous pale yellow precipitate formed after several minutes. The mixture was kept at 100 °C for 20 h, quenched by addition of methanol, and filtered. The resulting beige solid was purified by Soxhlet extraction from methanol overnight and dried in the vacuum oven at 80 °C overnight.

Synthetic procedure for P2: Inside the glovebox, a 5 mL glass vial was charged with 1,3,5-triethynylbenzene (100.1 mg, 667 µmol), 1,4-diiodobenzene (329.9 mg, 1.00 mmol), [Pd(PPh₃)₄] (7.5 mg, 6.5 µmol), dimethylformamide (3 mL), and triethylamine (1.5 mL). The vessel was closed with a silicone septum, extracted from the glovebox, and immersed in an oil bath preheated to 100 °C. The colorless solution turned increasingly yellow, and a voluminous yellow precipitate formed after several minutes. The mixture was kept at 100 °C for 20 h, quenched by addition of methanol, and filtered. The resulting yellow solid was purified by Soxhlet extraction from methanol overnight and dried in the vacuum oven at 80 °C overnight.

Synthetic procedure for P3: Inside the glovebox, a 50 mL glass vial was charged with 1,3,5-triethynylbenzene (100.3 mg, 668 µmol), 4,4′-diiodobiphenyl (406.7 mg, 1.00 mmol), [Pd(PPh₃)₄] (15.1 mg, 13 µmol), dimethylformamide (12 mL), and triethylamine (6 mL). The vessel was closed with a silicone septum, extracted from the glovebox, and immersed in an oil bath preheated to 100 °C. The colorless solution turned increasingly yellow, and a voluminous yellow precipitate formed after several minutes. The mixture was kept at 100 °C for 20 h, quenched by addition of methanol, and filtered. The resulting yellow solid was purified by Soxhlet extraction from methanol overnight and dried in the vacuum oven at 80 °C overnight.

Synthetic procedure for P4: Inside the glovebox, a 50 mL glass vial was charged with 1,3,5-triethynylbenzene (20.1 mg, 134 µmol), tetrakis(4-iodophenyl)methane (82.8 mg, 101 µmol), [Pd(PPh₃)₄] (3.1 mg, 2.7 µmol), dimethylformamide (24 mL), and triethylamine (12 mL). The vessel was closed with a silicone septum, extracted from the glovebox, and immersed in an oil bath preheated to 100 °C. The colorless solution turned increasingly yellow, and a volu-

CHEMISTRY
A European Journal
Full Paper

ChemPubSoc
Europe

minous pale yellow precipitate formed after several minutes. The mixture was kept at 100 °C for 20 h, quenched by addition of methanol, and filtered off. The resulting off-white solid was purified by Soxhlet extraction from methanol overnight and dried in the vacuum oven at 80 °C overnight.

Synthetic procedure for reproduced CMP-1: Inside the glovebox, [Pd(PPh$_3$)$_4$] (50.1 mg, 43 µmol) and CuI (15.0 mg, 79 µmol) were suspended in dimethylformamide (1.5 mL) and taken up into a syringe. A 5 mL glass vial was charged with 1,3,5-triethynylbenzene (150.2 mg, 1.00 mmol), 1,4-diiodobenzene (330.0 mg, 1.00 mmol), dimethylformamide (1.5 mL), and triethylamine (1.5 mL). The vessel was equipped with a silicone septum and a balloon, the vial and syringe were extracted from the glovebox, and the vial was immersed in an oil bath preheated to 100 °C. After 5 min, the catalyst mixture was added into to the vial through the septum. The colorless solution turned yellow instantly, and a brown precipitate formed after a few seconds. The mixture was kept at 100 °C for 20 h, quenched by addition of methanol, and filtered. The resulting brown solid was purified by Soxhlet extraction from methanol overnight and dried in the vacuum oven at 80 °C overnight.

Further experimental and analytical data are given in the Supporting Information.

Acknowledgements

[1] A. Thomas, *Angew. Chem. Int. Ed.* **2010**, *49*, 8328–8344; *Angew. Chem.* **2010**, *122*, 8506–8523.
[2] R. Dawson, A. I. Cooper, D. J. Adams, *Prog. Polym. Sci.* **2012**, *37*, 530–563.
[3] O. M. Yaghi, G. Li, H. Li, *Nature* **1995**, *378*, 703–706.
[4] A. P. Côté, A. I. Benin, N. W. Ockwig, M. O'Keeffe, A. J. Matzger, O. M. Yaghi, *Science* **2005**, *310*, 1166–1170.
[5] P. Kuhn, M. Antonietti, A. Thomas, *Angew. Chem. Int. Ed.* **2008**, *47*, 3450–3453; *Angew. Chem.* **2008**, *120*, 3499–3502.
[6] J.-X. Jiang, F. Su, A. Trewin, C. D. Wood, N. L. Campbell, H. Niu, C. Dickinson, A. Y. Ganin, M. J. Rosseinsky, Y. Z. Khimyak, A. I. Cooper, *Angew. Chem. Int. Ed.* **2007**, *46*, 8574–8578; *Angew. Chem.* **2007**, *119*, 8728–8732.
[7] T. Ben, H. Ren, S. Ma, D. Cao, J. Lan, X. Jing, W. Wang, J. Xu, F. Deng, J. M. Simmons, *Angew. Chem. Int. Ed.* **2009**, *48*, 9457–9460; *Angew. Chem.* **2009**, *121*, 9621–9624.
[8] J. Schmidt, M. Werner, A. Thomas, *Macromolecules* **2009**, *42*, 4426–4429.
[9] S. Fischer, J. Schmidt, P. Strauch, A. Thomas, *Angew. Chem. Int. Ed.* **2013**, *52*, 12174–12178; *Angew. Chem.* **2013**, *125*, 12396–12400.
[10] Y. Zhu, H. Yang, Y. Jin, W. Zhang, *Chem. Mater.* **2013**, *25*, 3718–3723.
[11] T. Tozawa, J. T. Jones, S. I. Swamy, S. Jiang, D. J. Adams, S. Shakespeare, R. Clowes, D. Bradshaw, T. Hasell, S. Y. Chong, *Nat. Mater.* **2009**, *8*, 973–978.
[12] T. Hasell, S. Y. Chong, K. E. Jelfs, D. J. Adams, A. I. Cooper, *J. Am. Chem. Soc.* **2012**, *134*, 588–598.
[13] G. Zhang, O. Presly, F. White, I. M. Oppel, M. Mastalerz, *Angew. Chem. Int. Ed.* **2014**, *53*, 1516–1520; *Angew. Chem.* **2014**, *126*, 1542–1546.
[14] S. M. Elbert, F. Rominger, M. Mastalerz, *Chemistry* **2014**, *20*, 16707–16720.
[15] T. Mitra, K. E. Jelfs, M. Schmidtmann, A. Ahmed, S. Y. Chong, D. J. Adams, A. I. Cooper, *Nat. Chem.* **2013**, *5*, 276–281.
[16] N. Giri, M. G. Del Pópolo, G. Melaugh, R. L. Greenaway, K. Rätzke, T. Koschine, L. Pison, M. F. C. Gomes, A. I. Cooper, S. L. James, *Nature* **2015**, *527*, 216–220.
[17] U. H. F. Bunz, K. Seehafer, F. L. Geyer, M. Bender, I. Braun, E. Smarsly, J. Freudenberg, *Macromol. Rapid Commun.* **2014**, *35*, 1466–1496.
[18] R. Dawson, A. Laybourn, R. Clowes, Y. Z. Khimyak, D. J. Adams, A. I. Cooper, *Macromolecules* **2009**, *42*, 8809–8816.
[19] W. Lu, D. Yuan, J. Sculley, D. Zhao, R. Krishna, H.-C. Zhou, *J. Am. Chem. Soc.* **2011**, *133*, 18126–18129.
[20] Z. Xiang, D. Cao, W. Wang, W. Yang, B. Han, J. Lu, *J. Phys. Chem. C* **2012**, *116*, 5974–5980.
[21] B. Kiskan, J. Weber, *ACS Macro Lett.* **2012**, *1*, 37–40.
[22] Commercial CMP-1 from Sigma Aldrich," can be found under http://www.sigmaaldrich.com/catalog/product/aldrich/799491?lang = de&region = DE.
[23] R. Dawson, A. Laybourn, Y. Z. Khimyak, D. J. Adams, A. I. Cooper, *Macromolecules* **2010**, *43*, 8524–8530.
[24] D. Tan, W. Fan, W. Xiong, H. Sun, Y. Cheng, X. Liu, C. Meng, A. Li, W.-Q. Deng, *Macromol. Chem. Phys.* **2012**, *213*, 1435–1440.
[25] R. Dawson, D. J. Adams, A. I. Cooper, *Chem. Sci.* **2011**, *2*, 1173–1177.
[26] B. Kim, N. Park, S. M. Lee, H. J. Kim, S. U. Son, *Polym. Chem.* **2015**, *6*, 7363–7367.
[27] J. Jiang, F. Su, A. Trewin, C. D. Wood, H. Niu, J. T. A. Jones, Y. Z. Khimyak, A. I. Cooper, *J. Am. Chem. Soc.* **2008**, *130*, 7710–7720.
[28] A. Laybourn, R. Dawson, R. Clowes, T. Hasell, A. I. Cooper, Y. Z. Khimyak, D. J. Adams, *Polym. Chem.* **2014**, *5*, 6325–6333.
[29] D. Tan, W. Xiong, H. Sun, Z. Zhang, W. Ma, C. Meng, W. Fan, A. Li, *Microporous Mesoporous Mater.* **2013**, *176*, 25–30.
[30] H. Bildirir, J. P. Paraknowitsch, A. Thomas, *Chem. Eur. J.* **2014**, *20*, 9543–9548.
[31] A. C. Uptmoor, J. Freudenberg, S. T. Schwäbel, F. Paulus, F. Rominger, F. Hinkel, U. H. F. Bunz, *Angew. Chem. Int. Ed.* **2015**, *54*, 14673–14676.
[32] U. H. F. Bunz, *Chem. Rev.* **2000**, *100*, 1605–1644.
[33] R. Chinchilla, C. Nájera, *Chem. Soc. Rev.* **2011**, *40*, 5084.
[34] J. N. Wilson, S. M. Waybright, K. McAlpine, U. H. F. Bunz, *Macromolecules* **2002**, *35*, 3799–3800.
[35] E. Stöckel, X. Wu, A. Trewin, C. D. Wood, R. Clowes, N. L. Campbell, J. T. Jones, Y. Z. Khimyak, D. J. Adams, A. I. Cooper, *Chem. Commun.* **2009**, 212–214.
[36] N. Kakusawa, K. Yamaguchi, J. Kurita, *J. Organomet. Chem.* **2005**, *690*, 2956–2966.
[37] R. Dawson, A. I. Cooper, D. J. Adams, *Polym. Int.* **2013**, *62*, 345–352.

CHEMISTRY
A European Journal

Supporting Information

Copper-Free Sonogashira Coupling for High-Surface-Area Conjugated Microporous Poly(aryleneethynylene) Networks

Matthias Trunk,* Anna Herrmann, Hakan Bildirir, Ali Yassin, Johannes Schmidt, and Arne Thomas*[a]

chem_201600783_sm_miscellaneous_information.pdf

76

Table of Contents

Materials and methods

Inert reactions were carried out in an MBraun glovebox type MB 120 BG. All glassware and stir bars were flame-dried before being channelled into the glovebox.

^{1}H NMR and ^{13}C NMR were recorded on a Bruker Avance II 400 MHz spectrometer in the given solvent. Elemental analysis was performed on a Thermo FlashEA 1112 Organic Elemental Analyser at 1020 °C employing Dynamic Flash Combustion method. Nitrogen, hydrogen and carbon dioxide sorption analyses were conducted at 77 and 273 K as indicated using an Autosorb-iQ-MP from Quantachrome equipped with a Quantachrome CryoCooler for temperature regulation. The pore size distributions were calculated from the adsorption isotherms by quenched solid density functional theory (QSDFT) using the slit/cylindrical pore model for carbon adsorbents. Before analysis, samples were degassed at 80 °C for 12 h. BET surface areas were determined over a 0.1-1.5 p/p_0 range. X-ray powder diffraction (XRD) patterns were measured in reflection mode (Cu K$_\alpha$ radiation) on a Bruker D8 diffractometer equipped with scintillation counter. ^{13}C{^{1}H} CP/MAS measurements were carried out using a Bruker Avance 400 spectrometer operating at 100.6 MHz for ^{13}C and a Bruker 4 mm double resonance probe-head operating at a spinning rate of 10 kHz. TGA measurements were carried out under air and nitrogen on a Mettler Toledo TGA 1 Star^e thermal instrument with a heating rate of 10 K min^{-1}. FTIR spectra were obtained as KBr pellets on a Varian 640-IR spectrometer. Transmission electron microscopy experiments were performed on a FEI Tecnai G2 20 S-TWIN transmission electron microscope (FEI company, Eindhoven, Netherlands) equipped with a LaB6 source at 200 kV acceleration voltage. Images were recorded with a GATAN MS794 P CCD camera. EDX analyses were carried out with an EDAX r-TEM SUTW detector.

All chemicals were used as received unless otherwise noted. Tetrakis(4-iodophenyl)methane and 1,3,5-triiodobenzene were synthesised according to literature with slight modifications (see below).[1,2] 1,3,5-Triethynylbenzene was purchased from TCI and purified before use (see below). Tetrakis(triphenylphosphine)palladium(0) (99.9 %), 1,4-diiodobenzene (99 %), 1,3,5-tribromobenzene (98 %), anhydrous tetrachloromethane (≥99.5 %), anhydrous dimethylformamide (99.8 %) and triethylamine (≥99.5 %) were purchased from Sigma Aldrich. 4,4'-Diiodobiphenyl (99 %) was purchased from Alfa Aesar. Bis(trifluoroacetoxy)iodobenzene (98 %) and iodine (99.5 %) were purchased from Acros Organics. Tetraphenylmethane (96 %) was purchased from Manchester Organics.

Experimental details

1,3,5-Triethynylbenzene was purchased from TCI. Colors of as-purchased compound ranged from yellowish-red to dark brown, which could not be attributed to the molecular structure of TEB but which could conceivably be caused by impurities from the synthesis or decay of the monomer. Purification of the as-purchased monomer by column chromatography with dichloromethane as eluent yielded a yellow, crystalline powder (see main article, Fig. 1b). Further investigation showed that the monomer can be purified by sublimation (40 °C/10^{-3} mbar) to yield pristine, colorless crystals (Fig. 1c), which turn brown upon elongated exposure to ambient temperature.

1,3,5-Triiodobenzene was synthesised in a two-step procedure according to literature. To a suspension of magnesium (3.24 g, 133.31 mmol) and trimethylsilyl chloride (19.5 mL, 153.65 mmol) in dry tetrahydrofuran (20 mL) a solution of 1,3,5-tribromobenzene (11.27 g, 35.80 mmol) in dry tetrahydrofuran (20 mL) was added dropwise over 45 minutes under argon atmosphere. The suspension was stirred at ambient temperature overnight, then heated to reflux overnight, and poured into ice water. The resulting solid was collected by filtration and extracted with diethyl ether (2 x 25 mL). The collected organic phases were washed with NH_4Cl (20 mL) and water (20 mL), and dried over $MgSO_4$. The solvent was removed and the crude product purified by distillation under reduced pressure (90 °C, 10^{-3} mbar) to yield tris(trimethylsilyl)benzene as a colorless oil. Yield, 5.58 g (18.94 mmol, 53 %).

^{1}H NMR (200 MHz, $CDCl_3$): δ = 7.72 (s, 3 H), 0.30 (s, 27 H) ppm

Tris(trimethylsilyl)benzene (889 mg, 3.02 mmol) was dissolved in dry dichloromethane (15 mL) and cooled to 0 °C. Iodine monochloride solution (10 mL, 1.0 M in dichloromethane, 10 mmol) was added within 1 hour *via* syringe pump upon which the solution turned pink. After stirring overnight at ambient temperature, $NaHSO_3$ solution (40 %) was added upon which the red solution turned yellow and a solid precipitated. Dichloromethane was added until all precipitated solid was dissolved. The organic phase was separated, washed with aqueous HCl (10 %) and brine, and dried over anhydrous $MgSO_4$. The solvent was removed at the rotary evaporator to yield a yellow crude product. This was washed several times with acetone to yield a colorless, crystalline solid. Yield, 1.25 g (2.75 mmol, 91 %).

^{1}H NMR (200 MHz, THF-*d8*): δ = 8.06 ppm

^{13}C NMR (50 MHz, THF-*d8*): δ = 143.6, 94.4 ppm

Tetrakis(4-iodophenyl)methane. Tetraphenylmethane (1.00 g, 3.12 mmol), iodine (1.90 g, 7.49 mmol) and bis(trifluoroacetoxy)iodobenzene (3.22 g, 7.49 mmol) were suspended in tetrachloromethane and heated to reflux for 3 days. After cooling to ambient temperature the suspension was filtered off, the filter cake washed with copious amounts of ethanol and a small amount of dichloromethane. The off-white solid was recrystallized from tetrahydrofuran to yield a white, crystalline solid. Yield, 897 mg (1.09 mmol, 35 %).

^{1}H NMR (500 MHz, $CDCl_3$): δ = 7.58 (d, *J* = 8.7 Hz, 2 H), 6.88 (d, *J* = 8.7 Hz, 2 H) ppm

^{13}C NMR (125 MHz, CDCl$_3$): δ = 137.1, 132.6 ppm. Quaternary carbon atoms could not be detected due to the low solubility of the compound.

*Synthetic procedure for **P1**:* Inside the glovebox, a 50 mL glass vial was charged with 1,3,5-triethynylbenzene (100.6 mg, 670 µmol), 1,3,5-triiodobenzene (305.4 mg, 670 mmol), Pd(PPh$_3$)$_4$ (15.1 mg, 13 µmol), dimethylformamide (12 mL), and triethylamine (6 mL). A silicone septum was applied, the vessel extracted from the glovebox, and immersed in an oil bath preheated to 100 °C. The colorless solution turned increasingly yellow and a voluminous pale yellow precipitate formed after several minutes. The mixture was kept at 100 °C for 20 hours, quenched by addition of methanol, and filtered off. The resulting beige solid was purified by Soxhlet extraction from methanol overnight and dried in the vacuum oven at 80 °C overnight.

*Synthetic procedure for **P2**:* Inside the glovebox, a 5 mL glass vial was charged with 1,3,5-triethynylbenzene (100.1 mg, 667 µmol), 1,4-diiodobenzene (329.9 mg, 1.00 mmol), Pd(PPh$_3$)$_4$ (7.5 mg, 6.5 µmol), dimethylformamide (3 mL), and triethylamine (1.5 mL). A silicone septum was applied, the vessel extracted from the glovebox, and immersed in an oil bath preheated to 100 °C. The colorless solution turned increasingly yellow and a voluminous yellow precipitate formed after several minutes. The mixture was kept at 100 °C for 20 hours, quenched by addition of methanol, and filtered off. The resulting yellow solid was purified by Soxhlet extraction from methanol overnight and dried in the vacuum oven at 80 °C overnight.

*Synthetic procedure for **P3**:* Inside the glovebox, a 50 mL glass vial was charged with 1,3,5-triethynylbenzene (100.3 mg, 668 µmol), 4,4'-diiodobiphenyl (406.7 mg, 1002 µmol), Pd(PPh$_3$)$_4$ (15.1 mg, 13 µmol), dimethylformamide (12 mL), and triethylamine (6 mL). A silicone septum was applied, the vessel extracted from the glovebox, and immersed in an oil bath preheated to 100 °C. The colorless solution turned increasingly yellow and a voluminous yellow precipitate formed after several minutes. The mixture was kept at 100 °C for 20 hours, quenched by addition of methanol, and filtered off. The resulting yellow solid was purified by Soxhlet extraction from methanol overnight and dried in the vacuum oven at 80 °C overnight.

*Synthetic procedure for **P4**:* Inside the glovebox, a 50 mL glass vial was charged with 1,3,5-triethynylbenzene (20.1 mg, 134 µmol), tetrakis(4-iodophenyl)methane (82.8 mg, 101 µmol), Pd(PPh$_3$)$_4$ (3.1 mg, 2.7 µmol), dimethylformamide (24 mL), and triethylamine (12 mL). A silicone septum was applied, the vessel extracted from the glovebox, and immersed in an oil bath preheated to 100 °C. The colorless solution turned increasingly yellow and a voluminous pale yellow precipitate formed after several minutes. The mixture was kept at 100 °C for 20 hours, quenched by addition of methanol, and filtered off. The resulting off-white solid was purified by Soxhlet extraction from methanol overnight and dried in the vacuum oven at 80 °C overnight.

Synthetic procedure for reproduced CMP-1: Inside the glovebox, Pd(PPh$_3$)$_4$ (50.1 mg, 43 µmol) and CuI (15.0 mg, 79 µmol) were suspended in dimethylformamide (1.5 mL) and taken up into a syringe. A 5 mL glass vial was charged with 1,3,5-triethynylbenzene (150.2 mg, 1.00 mmol), 1,4-diiodobenzene (330.0 mg, 1.00 mmol), dimethylformamide (1.5 mL), and triethylamine (1.5 mL). A silicone septum equipped with a balloon was applied, the vial and syringe extracted from the glovebox, and the vial immersed in an oil bath preheated to 100 °C. After 5 minutes the catalyst mixture was added into to the vial through the septum. The colorless solution turned yellow instantly and a brown precipitate

80

formed after a few seconds. The mixture was kept at 100 °C for 20 hours, quenched by addition of methanol, and filtered off. The resulting brown solid was purified by Soxhlet extraction from methanol overnight and dried in the vacuum oven at 80 °C overnight.

Solid state nuclear magnetic resonance

The solid state ^{13}C CP/MAS NMR spectra reported here (Fig. S 1) are somewhat more detailed than the spectra reported previously.[3–5] Starting from the highly symmetrical structure of **P1**, all other carbon atoms can be assigned systematically. In the spectrum of **P2**, two carbon atoms *C1* and *C3* are visible as shoulders, which have never been distinguishable before, and have thus never been included in the peak assignment. Of special noteworthiness are the similarities between the structures of **P2** (*C1-C4*) and **P4** (*C2-C5*), where all peaks corresponding to a large, similar structural unit can be found in the same positions. In the spectrum of **P3**, which has the same structural unit, carbon atom *C2* coincides with the valley between *C1* and *C3* and can therefore only be surmised, whereas it is clearly visible in the same position in the spectra of **P2** and **P4**, and slightly shifted in **P1**, as a broad and flat peak.
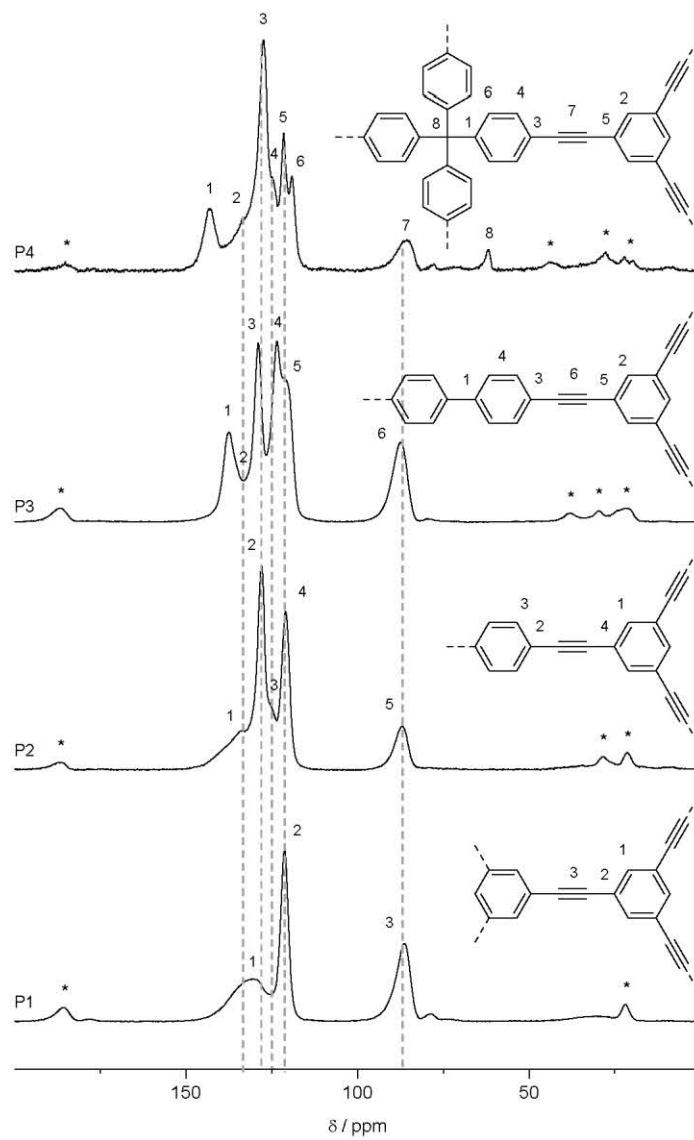
Figure S 1: Solid state ^{13}C NMR spectra of **P1-P4** and peak assignments

H₂ and CO₂ sorption experiments
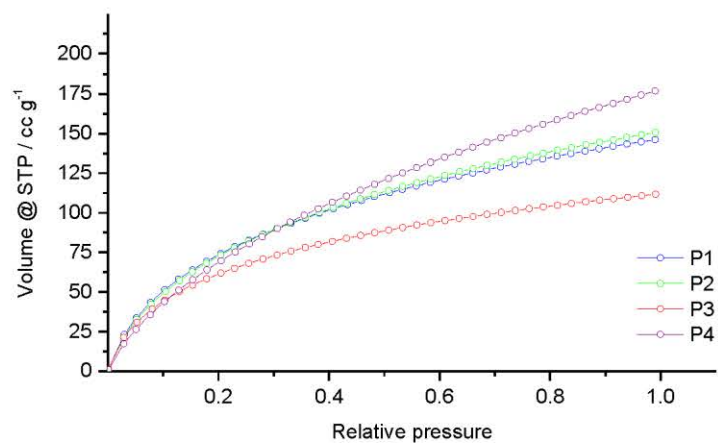
Figure S 2: H$_2$ sorption isotherms measured at 77 K, 1 bar
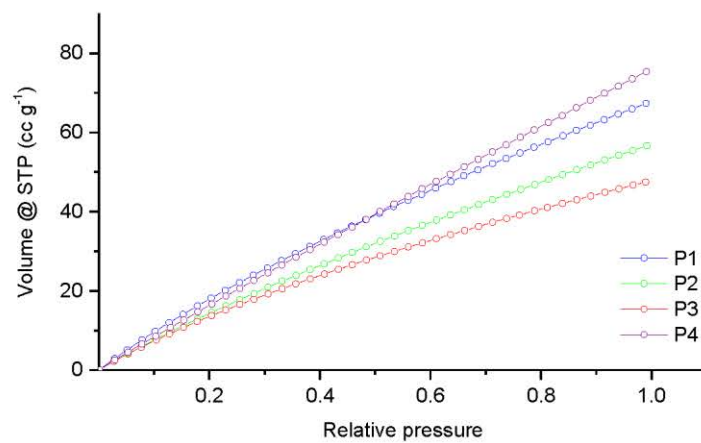
Figure S 3: CO$_2$ sorption isotherms measured at 273 K, 1 bar

Thermogravimetric measurements

All materials are stable until at least 200 °C in air, above which temperature they slowly start to gain mass of 8, 6, 6, and 4 wt%, respectively, which could be the result of oxidation or hydroxylation of triple bonds; decomposition of the materials in air begins around 400 °C. **P1-P3** are stable up to 400 °C in nitrogen, showing signs of slow degradation at temperatures beyond this point, whereas **P4** exhibits remarkable stability even beyond 400 °C, retaining more than 82 % of its mass at 1000 °C.
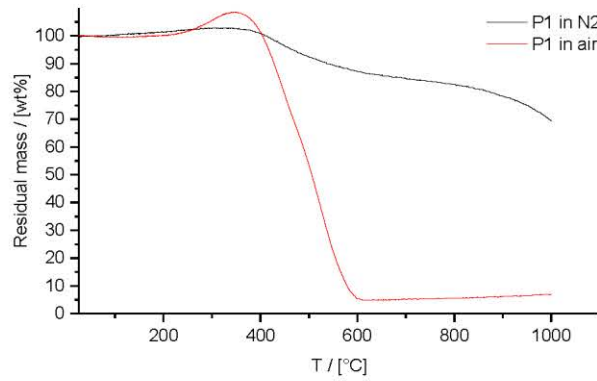
Figure S 4: TGA measurement of **P1** in N_2 and air
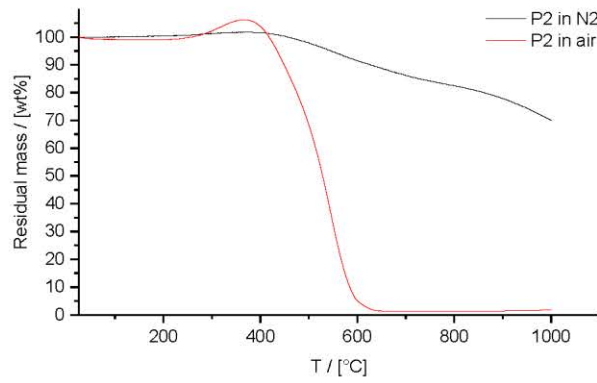
Figure S 5: TGA measurement of **P2** in N_2 and air
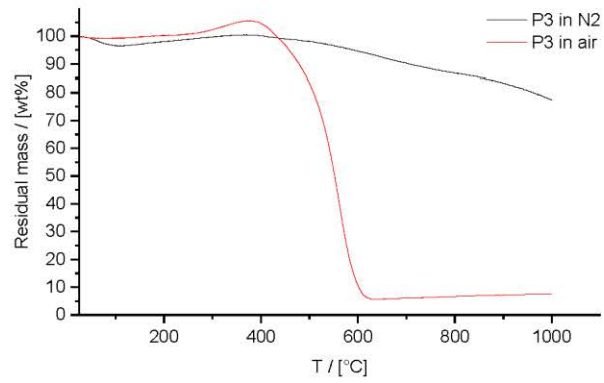
Figure S 6: TGA measurement of **P3** in N_2 and air
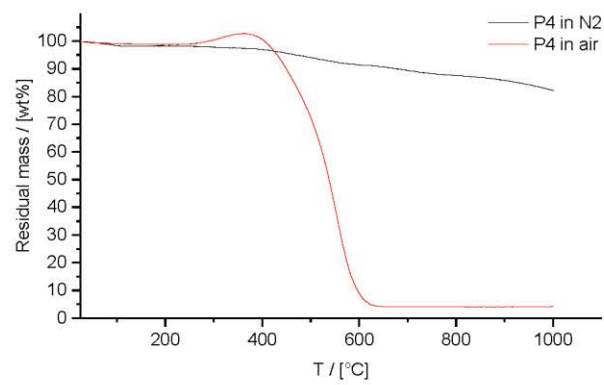
Figure S 7: TGA measurement of **P4** in N_2 and air

X-Ray Diffraction

XRD measurements gave no further insights due to the amorphous nature of these materials.
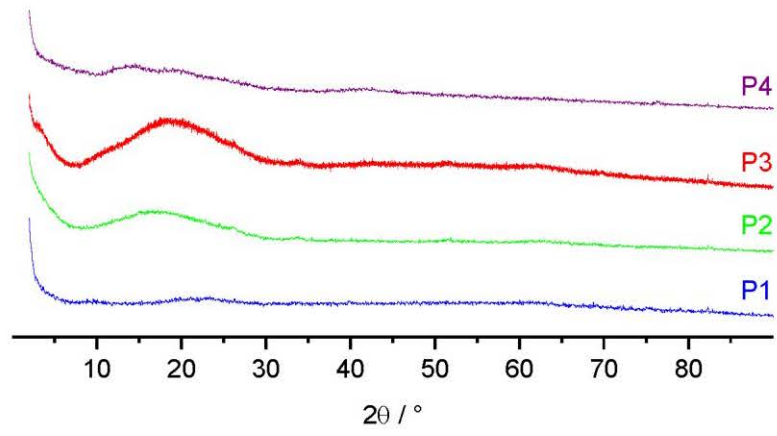
Figure S 8: Powder XRD patterns of P1-P4

Yields and end group analysis

The yields of some of the polymers in this work exceed 100 %. If this excess weight is considered as iodine-hydrogen pairs resulting from dead ends trapped within the network, the amount of unreacted groups divided by the total amount of iodine atoms in the monomer equals the percentage of conversion (Table 1). The results corroborate the solid state NMR and FTIR measurements. The yields of the resulting polymers were calculated based on the masses of the starting materials and the resulting polymers with accuracy to 0.1 mg.

Table S 1: End group analysis of **P1-P4**

	Yield [mg]	Yield [%]	Open end groups [%]	Conversion [%]
P1	191.1	128	16.4	83.6
P2	163.0	94	0	100
P3	268.7	107	7.1	92.9
P4	59.7	116	16.1	83.9

Elemental analysis

Table S 2: Elemental analysis of **P1-P4** (averaged over two independent measurements). For all compounds, understated carbon values are observed.

	C [%] calc./found	H [%] calc./found	N [%] calc./found
P1	97.28/78.77	2.72/2.71	0.00/0.00
P2	96.53/88.28	3.47/3.69	0.00/0.00
P3	96.30/89.60	3.70/4.01	0.00/0.00
P4	96.07/85.66	3.93/4.26	0.00/0.16

Transmission electron microscopy
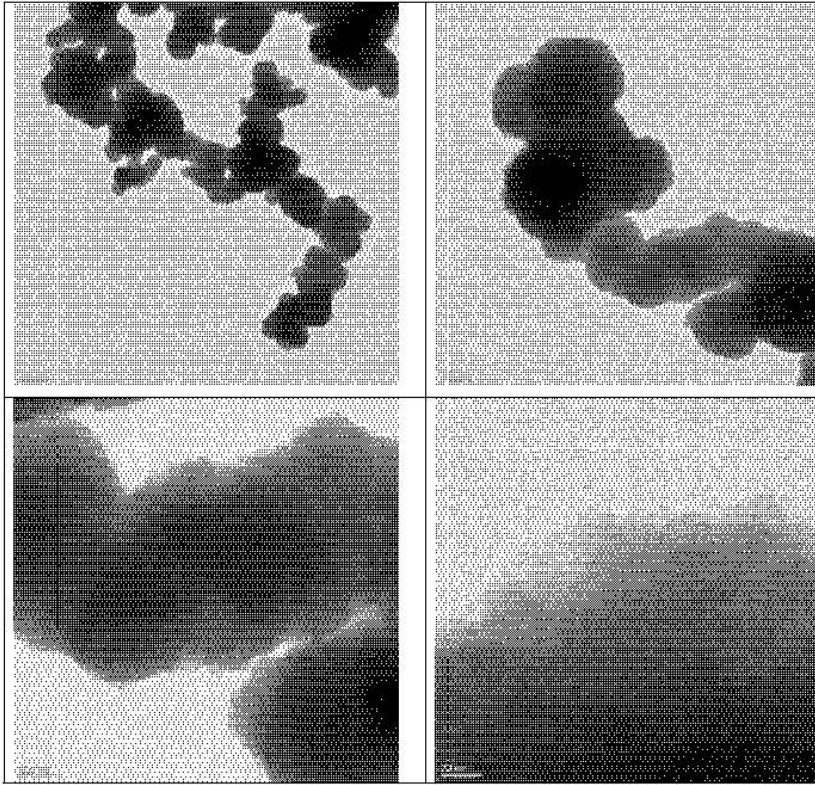
Figure S 9: TEM images of **P2**

Energy dispersive X-ray spectroscopy
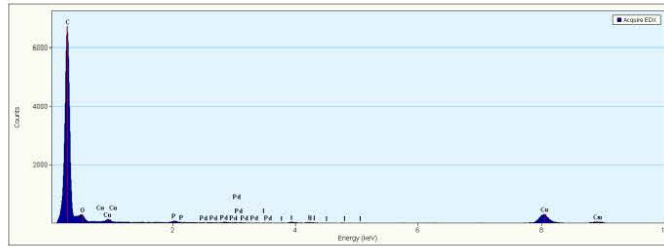
Figure S 10: EDX measurement of **P2**

References

[1]   I. Aujard, J. Baltaze, J. Baudin, E. Cogné, F. Ferrage, L. Jullien, É. Perez, V. Prévost, L. M. Qian, O. Ruel, *J. Am. Chem. Soc.* **2001**, *123*, 8177–8188.

[2]   M. Banno, T. Yamaguchi, K. Nagai, C. Kaiser, S. Hecht, E. Yashima, *J. Am. Chem. Soc.* **2012**, *134*, 8718–8728.

[3]   J.-X. Jiang, F. Su, A. Trewin, C. D. Wood, N. L. Campbell, H. Niu, C. Dickinson, A. Y. Ganin, M. J. Rosseinsky, Y. Z. Khimyak, *Angew. Chemie Int. Ed.* **2007**, *46*, 8574–8578.

[4]   D. Tan, W. Fan, W. Xiong, H. Sun, Y. Cheng, X. Liu, C. Meng, A. Li, W.-Q. Deng, *Macromol. Chem. Phys.* **2012**, *213*, 1435–1440.

[5]   J. R. Holst, E. Stöckel, D. J. Adams, A. I. Cooper, *Macromolecules* **2010**, *43*, 8531–8538.

Article II

FULL PAPER

Carbon Capture

ADVANCED FUNCTIONAL MATERIALS

www.afm-journal.de

Structure–Thermodynamic-Property Relationships in Cyanovinyl-Based Microporous Polymer Networks for the Future Design of Advanced Carbon Capture Materials

Ali Yassin,* Matthias Trunk, Frank Czerny, Pierre Fayon, Abbie Trewin, Johannes Schmidt, and Arne Thomas*

Nitrogen-rich solid absorbents, which have been immensely tested for carbon dioxide capture, seem until this date to be without decisive molecular engineering or design rules. Here, a family of cyanovinylene-based microporous polymers synthesized under metal-catalyzed conditions is reported as a promising candidate for advanced carbon capture materials. These networks reveal that isosteric heats of CO_2 adsorption are directly proportional to the amount of their functional group. Motivated by this finding, polymers produced under base-catalyzed conditions with tailored quantities of cyanovinyl content confirm the systematical tuning of their sorption enthalpies to reach 40 kJ mol^{-1}. This value is among the highest reported to date in carbonaceous networks undergoing physisorption. A six-point-plot reveals that the structure–thermodynamic-property relationship is linearly proportional and can thus be perfectly fitted to tailor-made values prior to experimental measurements. Dynamic simulations show a bowl-shaped region within which CO_2 is able to sit and interact with its conjugated surrounding, while theoretical calculations confirm the increase of binding sites with the increase of Ph−C=C(CN)−Ph functionality in a network. This concept presents a distinct method for the future design of carbon dioxide capturing materials.

1. Introduction

As concluded from the recent scenarios developed by British Petroleum and the International Energy Agency, fossil fuel demands will continue to grow in the near future.[1] This is further driven by the discovery of new and emerging unconventional sources, such as tight oil and shale gas, which are becoming more technically accessible.[2] Meanwhile, continued CO_2 emissions have been associated with rising sea levels,

ocean acidification, increased droughts, reductions in crop productivity, and deaths due to infectious diseases.[3] Still, it is predicted in addressing the problem of global climate change, that a cigarette-like addiction for fossil fuel usage may generate a long period of time in which people express sincere desire to convert to clean energy resources but accomplish little to achieve it.[4] Until a zero carbon footprint could be reached, it seems of urgent priority now to bring foreword new materials that would serve under the technical processes developed for CO_2 capture.

One such process is the postcombustion capture from flue gas, a predominantly CO_2/N_2 gas separation at relatively low pressures, which has been the most explored strategy to date since it could be readily retrofitted to existing power plants.[5] However, due to stability and selectivity concerns in addition to the large amounts of energy required for their regeneration, through different swing adsorption techniques, even the best carbon-capture materials nowadays are unfeasible for large-scale deployment.[6] Originally, contributions in the field were meant to overcome the sequestration energy penalty of wet scrubbing methods, involving alkanolamines, and lead to the introduction of solid adsorbents, in particular porous ones, as potential solution to the problem. Zeolites, silica, activated carbons, metal-organic frameworks,[7] and lately tailor made covalent organic frameworks for carbon dioxide capture[8] had become under intensive consideration, while microporous polymer networks (MPNs) were much recently introduced as well.

MPNs attracted much attention due to their unique feature of combining high accessible surface areas with a wide range of functional groups while preserving chemical robustness and thermal stability, albeit in exchange of superior crystallinity.[9] Cooper and co-workers undertook sincere effort in investigating different MPNs for CO_2 capture and studied the effects of surface area,[10] water coadsorption,[11] and chemical functionality[12] in several conjugated networks (CMPs). Zhou and co-workers presented breakthrough uptakes of CO_2 by postfunctionalizing PPN-6 based materials with polyamines and sulfonates.[13] Yavuz and co-workers also showed much

Dr. A. Yassin, M. Trunk, F. Czerny, Dr. J. Schmidt,
Prof. A. Thomas
Department of Chemistry
Division of Functional Materials
Technische Universität Berlin
Hardenbergstr. 40, 10623 Berlin, Germany
E-mail: aliyassin_lb@hotmail.com; arne.thomas@tu-berlin.de
Dr. P. Fayon, Prof. A. Trewin
Department of Chemistry
Lancaster University
LA1 4YB Lancaster, UK

1700233 (1 of 9)

attention for carbon capture and introduced different novel MPNs with attractive properties and tuned enthalpies.[14] While considerable work is being conducted to investigate more advanced polymers for such applications, recognized by the escalation of reports in the literature,[15] the engineering rules for their molecular design seem without solid bases. It has been stated that tuning the thermodynamics of interaction between CO_2 and the adsorbent is one of the most crucial considerations in improving the energy efficiency of CO_2 capture.[16] Isosteric heats of adsorption were certainly modified, for example by changing the nature of incorporated functional group,[12,17] but the term "fine tuning" has been mistakenly, or probably too optimistically, used in literature only to describe diverse experimental values and qualitative changes in heats of adsorptions. To the best of our knowledge indisputable tuning of enthalpy to precise tailor-made quantities was heretofore out of reach.

2. Experimental Results and Discussion

Here, we describe the synthesis, characterization, and experimental gas sorption properties of a series of engineered MPNs produced under both metal-catalyzed and metal-free reaction conditions and demonstrate a prime example in which CO_2 enthalpies can be well tailored to definite values

via manipulating the corresponding content of cyanovinylene bridges. Theoretical models of the amorphous polymers were generated and their structures and porosities were assessed, while binding sites of carbon dioxide in these networks and their diffusion in the different cyanovinyl-based polymers were sampled by performing molecular dynamics simulations.

Although nitrogen-rich materials were immensely tested due to their high selectivities, still, the cyanovinyl linkage has not yet been investigated for carbon capture. Beyond such reason, our interest stems from the fact that this moiety could be generated via a green synthetic route through simple condensation reactions, in which water is the sole by-product.[18]

2.1. Networks P1–P4 Based on (Benzene-1,3,5-Triyl)Tris(2-Phenylacrylonitrile)

2.1.1. Synthesis of the Metal-Catalyzed Polymers under Optimized Conditions for Efficient Coupling

Since at first we wanted to investigate metal-catalyzed polymer networks, the tris-iodinated derivative of (benzene-1,3,5-triyl)-tris(2-phenylacrylonitrile), monomer 1 (**Figure 1**), was prepared in near-quantitative yields from commercially available compounds (Section S1, Supporting Information). Obtained single
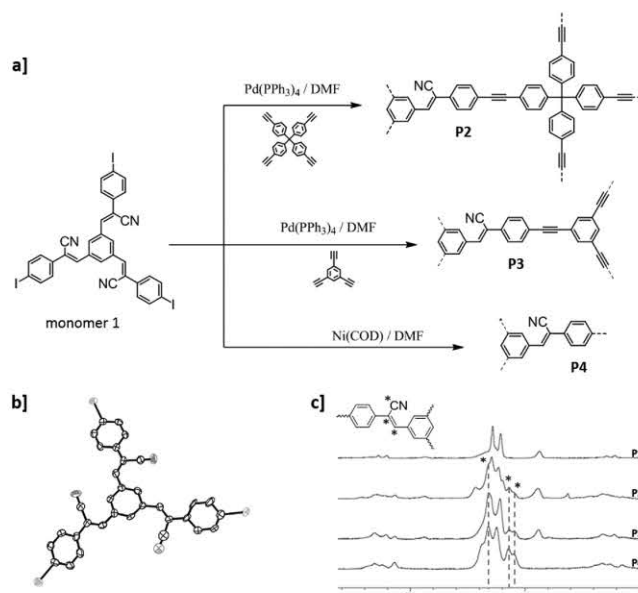
Figure 1. a) Metal-catalyzed reactions of monomer 1 under different conditions for MPNs **P2**, **P3**, and **P4**. b) Single crystal X-ray resolved structure of the monomer. c) ^{13}C solid state NMR of the MPNs showing the chemical shifts corresponding to the cyanovinyl moiety, and their absence in **P1**.

**ADVANCED
SCIENCE NEWS**
www.advancedsciencenews.com

**ADVANCED
FUNCTIONAL
MATERIALS**
www.afm-journal.de
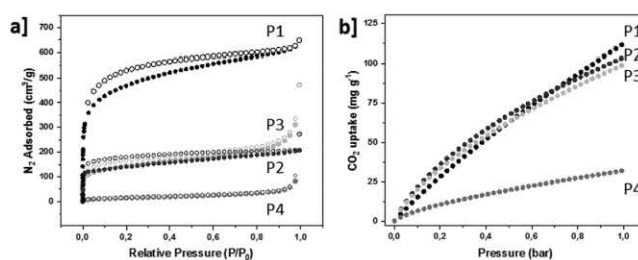
Figure 2. a) N_2 adsorption (solid) and desorption (hollow) isotherms of the metal-catalyzed networks at 77 K; b) CO_2 uptakes at 273 K.

crystals reveal through X-ray diffraction that phenyl rings adopt a *trans* confirmation relative to one another in a monoclinic crystal system (Figure 1b, and Section S11 and crystallographic data, Supporting Information). The monomer was later used as tecton to generate three different metal-catalyzed MPNs under optimized conditions; by coupling with tetrakis(4-ethynylphenyl) methane or 1,3,5-triethynylbenzene in a Sonogashira–Hagihara reaction, with Pd, to produce **P2** and **P3**, respectively and by direct polymerization via Yamamoto coupling,[19] with Ni, to produce **P4** (Figure 1a and Section S1, Supporting Information). As follows, the obtained networks have different weight percentages (wt%) of cyanovinylene content (precised in Section S2, Supporting Information). Poly(aryleneethynylene) network **P1** was prepared as unfunctionalized reference polymer free of cyanovinylene bridges. Under optimized synthetic conditions recently developed by our group,[20] triple bonds in **P1** are completely coupled excluding any homo-polymerization seen in previous reports.[21]

The obtained polymers, amorphous as concluded from powder (X-ray diffraction) XRD analysis (Section S3, Supporting Information), were initially characterized with solid-state ^{13}C NMR confirming the three corresponding cyanovinyl chemical shifts at 108, 114, and 132 ppm in the functionalized polymers; **P2**, **P3**, and **P4** (Figure 1c and Section S4, Supporting Information). Further investigations by Fourier transform infrared (FT-IR) spectroscopy also showed the characteristic –CN stretching at ≈2220 cm^{-1} (Section S5, Supporting Information). In both techniques these signals were absent for **P1** as eventually expected.

*2.1.2. Nitrogen Sorption Properties of the MPNs **P1–P4** and their Carbon Uptake*

The porosity of networks was analyzed by collecting nitrogen sorption measurements on activated samples at 77 K revealing type I isotherms (**Figure 2a**) with Brunauer–Emmett–Teller (BET) surface areas exceeding 500 $m^2\ g^{-1}$ for **P2** and **P3**. The largest quantities of N_2 uptake were observed at low relative-pressures indicative of adsorption into micro pores which is reflected in the pore size distribution calculated from their isotherms (Section S7, Supporting Information). While CMP-1 is already known to be a very porous material, **P1** consistently reaches a BET surface area of 1700 $m^2\ g^{-1}$ explaining its high

carbon dioxide uptake at 273 K (Figure 2b). Measurements were also recorded at 298 K to calculate the isosteric heats of adsorption (Q_{st}) from dual-site Langmuir fits of the CO_2 isotherms. Likewise they were performed with N_2 to determine the networks' selectivities under flue-gas conditions (85:15/N_2:CO_2) with single-gas isotherms (Section S8, Supporting Information) using the ideal adsorbed solution theory model.[22]

Table 1 depicts a table summarizing the gas sorption properties of the networks under different experimental conditions. **P1**, **P2**, and **P3** show impressive CO_2 capture values exceeding 100 mg g^{-1} at 273 K and decreasing by around 40% at higher temperature. A nitrile containing polymer structurally similar to **P2** was reported by Thirion et al. with BET surface area of 650 $m^2\ g^{-1}$ and interestingly similar CO_2 uptake near 100 mg g^{-1}.[23] The capture of carbon in **P1** comes mostly from its high porosity, which clearly relates the uptake in the other networks to their cyanovinyl content, making the latter a very interesting building block for carbon capture. Even for **P4**, which consists only of cyanostilbene units that are not entirely linear but rather more flexible and could relax into a nonporous condensed state,[24] the functional group maintains the polymer with an uptake of 32 mg of CO_2 per 1 g of material. It is noted however that selectivities of these networks over N_2 were relatively poor. In analyzing the measured isosteric heats of adsorption we discovered a close-to-perfect linear correlation with reference to the corresponding percentages of functional group (Table 1, bold values and Section S9, Supporting Information). This was inspired by similar well-studied relationships in π-conjugated systems which show strong dependence between structure and

Table 1. Gas sorption properties of the metal-catalyzed polymers.

Network	S_{BET} [$m^2\ g^{-1}$]	Pore width [nm]	CO_2 uptake[a] [mg g^{-1}]		Selectivity[b] CO_2/N_2	Q_{st} [kJ mol^{-1}]	Functional group [wt%]
			273 K	298 K			
P1	1700	1.35	111	59	Ref. [14]	**20.9**	**0**
P2	520	0.85	103	58	15	**28.2**	**19.7**
P3	510	1.45	99	53	11	**30.2**	**25.4**
P4	60	1.47	32	19	19	**32.5**	**33.5**

[a]Uptakes at 1 bar; [b]Selectivities at flue gas conditions (85:15/N_2:CO_2). wt% represents the percentage of C_3H_1N per repeating unit of polymer (see Section S2 in the Supporting Information).

**ADVANCED
SCIENCE NEWS**
www.advancedsciencenews.com

**ADVANCED
FUNCTIONAL
MATERIALS**
www.afm-journal.de

the corresponding electronic property for example.[25] The relation obtained, $Q_{st} = 21.07 + 0.37(wt\%)$, predicts for instance, that a 45 wt% of incorporated functionality will result in a sorption enthalpy of 38 kJ mol^{-1}. This could be even tuned to values as high as 40 kJ mol^{-1} if the weight content is increased to 50%.

2.2. Networks P5 and P6 Based on (Benzene-1,3,5-Triyl) Triacetonitrile

2.2.1. Synthesis of the Base-Catalyzed Polymers under Metal-Free Reaction Conditions and their Gas Sorption Properties

To further investigate this unprecedented structure– thermodynamic-property relationship we designed another set of MPNs under metal-free conditions this time, where monomer 2 (benzene-1,3,5-triyl)triacetonitrile (Section S1, Supporting Information) was condensed with commercially available terephthalaldehyde or benzene-1,3,5-tricarbaldehyde, in presence of a base, to produce **P5** and **P6**, respectively. The only by-product of such polymerization is water (**Figure** 3a). The percentage of cyanovinylene bridges in these polymers are engineered to the definite values previously discussed, while solid state ^{13}C NMR and FT-IR confirmed the corresponding structures (Sections S3 and S4, Supporting Information).

Gas sorption measurements for **P5** and **P6** were collected under the same conditions of the previous networks (Table 2). Nitrogen isotherms show BET surface areas around 100 m^2 g^{-1} (Section S7, Supporting Information) which is expected in such relatively flexible systems, but captured CO$_2$ quantities still reach values of 90 mg g^{-1}. Indeed it has already been observed that BET surface areas do not directly dominate the carbon capture in polymer networks at low pressures.[10] The uptake was accompanied by a huge seven- to ninefold increase of selectivities over nitrogen gas reaching values close to 100 for **P6** (Section S10, Supporting Information). Figure S9 (Supporting Information) shows the measured isosteric heats of adsorption from the CO$_2$ isotherms collected at 273 and 298 K. The important contribution of the obtained data (Table 2, bold values) confirms the discussed relation earlier. Indeed sorption enthalpies of **P5** (with 44.7 wt% functional group) and **P6** (with 50.5 wt%) show the predicted values at ≈38 and 40 kJ mol^{-1}, respectively, as expected. **P6** has one of the highest enthalpies reported to date in carbonaceous physisorbents for CO$_2$; the next upper values in literature being related to direct chemisorption.[26] Plotting the enthalpy values of all the different networks (**P1–P6**) as function of the cyanovinyl content reveals an excellent matching with the best-fitting line in Figure 3c. Noteworthy this relation holds true for polymers prepared under several reaction conditions that are entirely different, as illustrated earlier (Section S9, Supporting Information).

2.2.2. Vacuum Swing Adsorption (VSA) and Temperature-Programmed Desorption Analysis (TPD) of the Polymers *P1–P6*

The energy penalty suffered during the regeneration step of materials used for carbon capture is usually associated with their high affinity to CO$_2$ as the adsorption process is mostly of chemical nature and involves bond formations that are hard
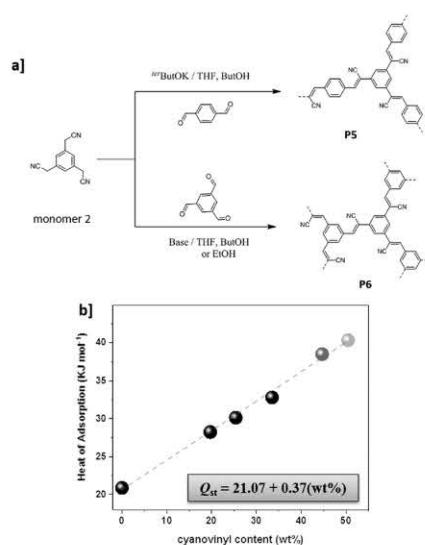
Figure 3. a) Metal-free condensation under basic conditions for **P5** (dark grey) and **P6** (light grey). b) The linear relationship between Q_{st} and the wt% of cyanovinyl content in the networks. The best fitting line is dashed. **P5** (pink) and **P6** (dark yellow).

to break. We were able, through the presented concept, to generate networks with their highest enthalpy values tuned just below the chemisorption barrier (45–55 kJ mol^{-1}) at which the regeneration is expected to require minimal energy. To test this, network **P6** (40 kJ mol^{-1}) was cycled under conditions similar to VSA with an autosorb iQ2 automated analyzer. In every cycle the material was saturated with CO$_2$ up to 1 bar at room temperature. Desorption was followed by applying under pressure, without any thermal heating, for an automated period of time during which the analyzer relaxes to some stable pressure. In average 4 min at 1 mbar and ambient temperature were enough for the complete desorption and regeneration of the material (**Figure** 4a, starting point of every isotherm). In addition, after 10 cycles there was not any apparent loss in uptake capacity, thus indicating the high stability and cyclability of this network (Figure 4a, end point of every isotherm).

Table 2. Gas sorption properties of the base-catalyzed polymers.

Network	S_{BET} [m^2 g^{-1}]	CO$_2$ uptake [mg g^{-1}]	Selectivity CO$_2$/N$_2$	Q_{st} [kJ mol^{-1}]	Functional group [wt%]
P5	80	59	74	**38.5**	44.7
P6	112	90	96	**40.3**	50.5
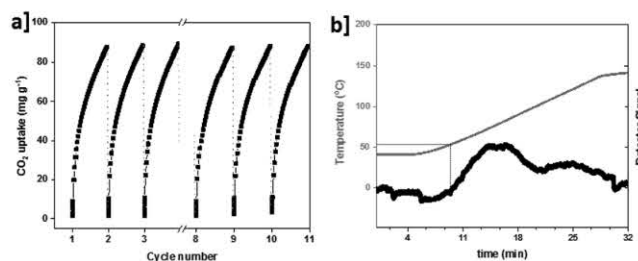
Figure 4. a) CO_2 isotherms for **P6** at 273 K and 1 bar, the material being cycled 10 times. Each regeneration step takes an average of 4 min at 1 mbar. b) TPD plot for **P6**. In grey is denoted the temperature ramp profile used for desorption. The signal for CO_2 is given by the black curve.

To further investigate the physisorptive nature of CO_2, TPD was performed on saturated samples with CO_2 at 1 bar.[27] Helium was used as carrier gas and the material was heated to elevated temperatures for the full evacuation of the host. TPD shows that gas release starts slightly above 50 °C while most of the CO_2 is already desorbed before 80 °C (Figure 4b). The enthalpy values of the networks, in addition to their straightforward regeneration under simple conditions, as demonstrated by the techniques, prove the physisorption character of CO_2 and contribute to their interest as being a cornerstone for designing new materials of higher surface areas with enhanced carbon uptakes while keeping this easy regeneration feature.

3. Dynamic Simulations and the Generation of Network Models

Generation of amorphous networks is challenging due to the lack of experimental data to aid the construction of a representative model. Furthermore, the generation process is often limited to small cells that do not allow for modeling of the nanoscale structure of the porous polymers which could have an influence on the final properties.

3.1. Construction of P1–P6 Network Models

Here, we use an automated structure generation methodology for the cyanovinyl-based extended network materials that exploits GPU hardware for increased speed and size of simulation. This methodology is implemented in the *Ambuild* code that integrates with HOOMD-blue and DL_POLY molecular dynamic simulation codes.[28] For each polymer we seed an initial simulation cell with stoichiometric quantities of the respective building blocks and solvent molecules. We designate end group atoms and cap atoms, together with a number of structural and geometric rules that build the network in a chemically realistic manner (**Figure 5**, Structures C1–D3).

For **P1**, we define the building blocks as 1,4,-diiodobenzene C1 and 1,3,5-triethynylbenzene D1 monomers with the cap atoms, respectively, phenyl-I and ethynyl-H, being removed

once a bond is formed between the respective phenyl-C and ethynyl-C end group atoms. Similarly, for **P2–P4** the common building block is defined as C2 (monomer 1), with the cap atom defined as the phenyl-I and the bonded phenyl-C as the end group. **P2** is constructed from C2 and D2, **P3** is constructed from C2 and D1, and **P4** is constructed from C2 alone. For **P5** and **P6** the monomer units are not used as the chemistry is challenging to mimic the building procedure, rather we define two further building units based on the resulting frameworks and monomer units; C3 based upon monomer 2, and D3 (1,3,5-triiodophenyl) based upon benzene-1,3,5-tricarbaldehyde. Thus, **P5** is constructed from C3 and C1 and **P6** is constructed
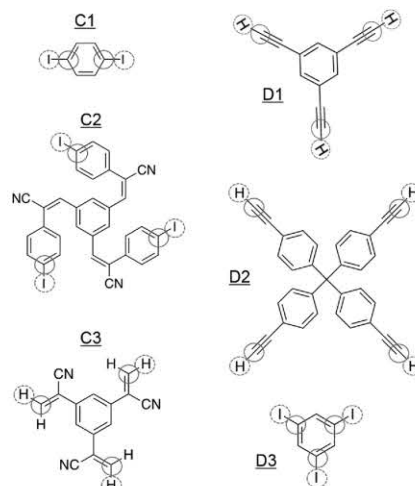
Figure 5. Structures optimized using DFT as building blocks for the construction of the network models. Atoms with a hashed circle are the designated cap atoms, and those with a solid circle are the end groups.

**ADVANCED
SCIENCE NEWS**
www.advancedsciencenews.com

**ADVANCED
FUNCTIONAL
MATERIALS**
www.afm-journal.de

Table 3. The building block ratios for the respective polymer model systems.

Polymer	Building block 1	Building block 2	Ratio	Solvent
P1	C1	D1	3:2	DMF
P2	C2	D2	4:3	DMF
P3	C2	D1	1:1	DMF
P4	C2	–	–	DMF
P5	C3	C1	2:3	THF/BuOH (1:1)
P6	C3	D3	1:1	THF/BuOH (1:1)

from C3 and D3 (Table 3; Figure 5). In all cases bonding is tested between the respective cap atoms which are removed once a new bond is formed at the end groups based upon the geometrical and structural rules. For **P5** and **P6**, any cap atom or functionality that remains at the end of the network's generation procedure is replaced with the respective terminal group expected for the synthetic procedure.

A number of molecular dynamic (MD) simulation loops are undertaken with structural sampling for potential bond formation. Upon bond formation, the structure undergoes a full, rigid-body geometry optimization before returning to the MD loops. The full building procedure is reported (Section S12 and Table S2, Supporting Information).

3.2. Structure and Porosity Assessment of the Cyanovinyl-Based MPN Models

Here, we target network densities of 0.7–1.1 g cm^{-3} as this range is commonly determined for similar CMP materials with similar porosity data. CMP materials with high surface areas tend to have low densities. The networks are generated in presence of solvent to get the target density then "de-solvated" by removal of the solvent and further molecular dynamic and geometry optimization steps are undertaken to obtain the final network structures. **P1–P3** have densities between 0.76 and 0.81 g cm^{-3} obtained (Section S14, Supporting Information), consistent with other CMP materials with similar surface area and porosity uptake properties where the experimental density has been determined.[29] **P4** has a density of 0.76 g cm^{-3}, lower than expected given the relatively low surface area obtained experimentally. **P5** and **P6** have densities of 1.02 and 1.4 g cm^{-3}, respectively, consistent with the low surface areas obtained experimentally. We believe that the increased density reflects the increased flexibility of the network formed and its ability to pack efficiently.

Comparison of elemental analysis of the generated network materials to the experimental data shows the same trend of the weight percentage of carbon decreasing and a weight percentage of nitrogen increasing going from **P1** to **P6** (Table S3, Supporting Information).

Geometric surface areas were calculated for each model and are shown in Table S4 in the Supporting Information. The trend is in broad agreement with that obtained experimentally with surface areas decreasing from **P1** to **P6**. Calculated pore size distributions are shown in Section S15 in the Supporting

Information. For **P1–P4** they range between 5 and 18 Å, broadly centered around 10–12 Å, in agreement with the ranges observed experimentally. **P5** and **P6** have pore sizes ranging between 5 and 10 Å, reflecting the increased density and efficient packing of the network. The experimental pore size distribution for all polymers shows the presence of mesopores with pore widths greater than 30 Å. It is not possible to take account of these larger pores as the unit cell size artificially restricts the pore width to the microporous region (Figure S13, Supporting Information).

3.3. Carbon Dioxide Binding Sites in Cyanovinyl-Based MPNs Models

The binding energy of CO$_2$ to functional groups within the polymer network was assessed through density functional theory calculations with basis set superposition error (BSSE) correction. A fragment of the **P5** and **P6** polymer was generated as a representative structure for the CN rich functionality of each polymer. The binding energy of the CO$_2$ molecule was calculated for a number of positions. A similar high energy binding site for **P5** and **P6** was found where the CO$_2$ is able to interact with a CN, C=C, and a phenyl ring with a binding energy of 23.35 and 21.13 kJ mol^{-1}, respectively. Interestingly, the binding site forms a bowl shaped region within which the CO$_2$ is able to sit and interact with the conjugated functionality surrounding it. Adding a further fragment of the respective polymer results in a high energy-binding site surrounded by an additional bowl shaped region and the CO$_2$ is therefore able to interact with further conjugated functionality. This leads to an increased binding energy of 34.14 and 35.44 kJ mol^{-1} for **P5** and **P6**, respectively. A further fragment of the respective polymer is added to the existing binding site leading to binding energies of 45.86 and 42.97 kJ mol^{-1} (Section S16 and Tables S5–S10, Supporting Information). In conclusion, as the concentration of CN and associated C=C functionality increases so does the number of available high energy binding sites. This is in excellent agreement with the trend in isosteric heat of adsorption obtained experimentally for **P1** through to **P6**.

Assessment of the high energy binding sites with three polymer fragments reveals that the N atoms of the CN functionality are located between 3 and 9 Å apart with most being at ≈7.5 Å distance apart.

To assess the distribution of nitrile groups within the generated networks we performed a radial distribution analysis on the nitrogen atoms of the nitrile groups. **Figure** 6a shows the comparison of this distribution in the different polymer systems. All polymers show a peak at N−N distance of 3–5 Å reflecting the nitrogen–nitrogen distance of the nitrile groups within the respective C2 and C3 repeating units. Another peak at 8.5 Å is common to all the polymers representing the N−N distance between nearest neighbor C2 or C3 groups. **P2** has the sharp peaks in the radial distribution reflecting the relatively rigid nature of the network resulting in well-defined distances between neighboring nitrile groups. The peaks become progressively broader going from **P3** to **P6** reflecting the range of distances available due to the flexibility of the network. For **P4**, **P5**, and **P6**, the peak is shifted to lower values with **P5**
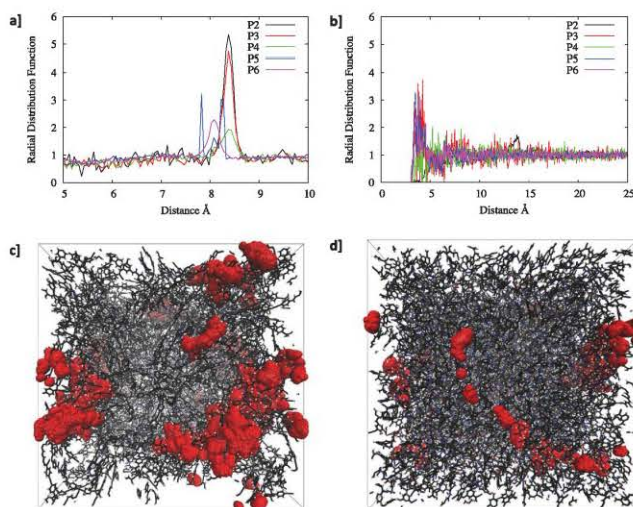
Figure 6. a) Comparison of the radial distribution of N in the polymers; b) comparison of the radial distribution of the C atom, in CO_2, to the N of the polymers; c) overlay of CO_2 diffusion in **P2**; and d) CO_2 diffusion in **P6**.

having an additional peak at 7.8 Å (Section S17, Supporting Information). This reflects the increasing concentration of CN functionality and the formation of additional high-energy CO_2 binding sites as described above.

3.4. Carbon Dioxide Binding

CO_2 can occupy a number of different sites within the pore structure and may be able to interact with multiple nitrile groups. To sample the sorption sites and their respective proximity to network nitrile groups we seed 10 CO_2 molecules within each network, we then perform molecular dynamics simulations and optimization sampling the radial distribution function of the central carbon atom of the CO_2 molecules to the nitrogen atom of the network nitrile groups. The resulting radial distribution plots are shown in Section S18 (Supporting Information).

The plots show that the CO_2 molecule for all systems is able to sample sites with a distance of 3.5 Å to the nitrile group (Figure 6b), the distance expected for the higher binding energy sites. For **P3**, **P4**, **P5**, and **P6** the CO_2 molecule is able to sample sites with a distance of 3.1 Å distance to a nitrile group. Furthermore, the number of times that sites of distance of 5 Å or less to a nitrile site, is greatly increased compared to **P2**.

To further assess the diffusion of CO_2, we perform molecular dynamic simulation of the diffusion of a molecule of CO_2 diffusing through **P6**. We describe the **P6** polymer as fully flexible with all bonds and angles being described fully

meaning that the **P6** polymer is able to be flexible and dynamic. As a comparison we also perform the same diffusion experiment with **P2** (Figure 6c,d).

The CO_2 molecule is able to freely diffuse through **P2** as the pore structure is large and connected. The diffusion of the CO_2 molecule is more restricted in **P6** but the molecule is still able to diffuse through a large volume and sample multiple binding sites. The diffusion coefficients were calculated for each polymer. In **P2**, diffusion coefficients of 5.2 and 12.15 nm² ns⁻¹ were calculated reflecting diffusion in a small pore and larger pore regions of the model, respectively (Figure S32, Supporting Information). In **P6**, a diffusion coefficient of 3.08 nm² ns⁻¹ was calculated (Figure S33, Supporting Information). The diffusion of the CO_2 in **P6** is slower as the system has only small pore regions with pore diameters less than 10 Å. Closer inspection of the CO_2 diffusion trajectory in **P6** shows that the molecule pathway is through pores that are surrounded by the conjugated functionality and we would hence expect that these pathways will have high energy binding sites.

4. Conclusion

In conclusion, we have successfully tuned the sorption enthalpies of carbon dioxide in amorphous polymer networks for tailor-made values by controlling the weight percentage of cyanovinylene content. Accordingly, we designed and synthesized microporous polymers under different polymerization methods with engineered percentages of

functional groups as interesting materials for carbon capture. While the networks achieved CO_2 uptakes higher than 100 mg g^{-1}, an unprecedented structure–thermodynamic-property relationship was revealed as the isosteric heats of adsorption proved to be linearly proportional to the content of the cyanovinyl group. In consequence, enthalpies were adjusted to tailor-made values by designing new polymers with the required amount of cyanovinyl bridges. An environmentally friendly metal-free condensation reaction from cheap starting materials, and only water as by-product, generated porous polymers with CO_2 sorption enthalpies as high as 40 kJ mol^{-1}, among the highest reported to date for physisorption in MPNs and exhibiting exceptional selectivities close to 100. TPD measurements and VSA technique confirmed the physisorptive nature of the interaction while regeneration of the polymer was achieved at slight under pressure and ambient temperature, or at 80 °C and under normal pressure. Thorough theoretical calculations and dynamic simulations of the amorphous polymers showed that the binding sites form a bowl shaped region for CO_2 adsorption and that these sites increase with the concentration of CN and associated C=C functionality in the networks.

Although these materials are not meant to be directly used for commercial application, the explored structure–property relationships in this study could draw the attention for new design rules of future polymers with advanced CO_2 capture properties. Moreover, their precisely controlled structures might give them high advantages as additives in mixed membranes for gas separation applications,[30] the issue we are currently developing with our materials.

5. Experimental Section

Experimental details including crystallography data, full synthetic procedures, FT-IR, elemental analysis and NMR spectra, powder XRD measurements, gas sorption properties, theoretical calculations, and dynamic simulations are available in the Supporting Information.

CCDC 1440645 contains the supplementary crystallographic data for this paper. These data can be obtained free of charge from The Cambridge Crystallographic Data Centre via www.ccdc.cam.ac.uk/data_request/cif.

Supporting Information

Supporting Information is available from the Wiley Online Library or from the author.

Conflict of Interest

The authors declare no conflict of interest.

[1] IEA: World Energy Outlook, BP Energy Outlook 2035, January 2014, Technical Report, **2015**.

[2] S. H. Mohr, J. Wang, G. Ellem, J. Ward, D. Giurco, *Fuel* **2015**, *141*, 120.

[3] Fourth Assessment Report of the Intergovernmental Panel on Climate Change, Summary for Policymakers, **2007**.

[4] S. Suranovic, *Global Environ. Change* **2013**, *23*, 598.

[5] M. Kanniche, R. Gros-Bonnivard, P. Jaud, J. Valle-Marcos, J.-M. Amann, C. Bouallou, *Appl. Therm. Eng.* **2010**, *30*, 53.

[6] C.-H. Yu, C.-H. Huang, C.-S. Tan, *Aerosol Air Qual. Res.* **2012**, *12*, 745.

[7] A. H. Lu, G. P. Hao, *Annu. Rep. Prog. Chem., Sect. A: Inorg. Chem.* **2013**, *109*, 484.

[8] a) N. Huang, X. Chen, R. Krishna, D. Jiang, *Angew. Chem. Int. Ed.* **2015**, *54*, 2986; b) N. Huang, R. Krishna, D. Jiang, *J. Am. Chem. Soc.* **2015**, *137*, 7079.

[9] a) A. Thomas, *Angew. Chem. Int. Ed.* **2010**, *49*, 8328; b) A. I. Cooper, *Adv. Mater.* **2009**, *21*, 1291; c) Y. Xu, S. Jin, H. Xu, A. Nagai, D. Jiang, *Chem. Soc. Rev.* **2013**, *42*, 8012.

[10] R. Dawson, E. Stockel, J. R. Holst, D. J. Adams, A. I. Cooper, *Energy Environ. Sci.* **2011**, *4*, 4239.

[11] R. Dawson, L. Stevens, T. Drage, C. Snape, M. Smith, D. J. Adams, A. I. Cooper, *J. Am. Chem. Soc.* **2012**, *134*, 10741.

[12] R. Dawson, D. J. Adams, A. I. Cooper, *Chem. Sci.* **2011**, *2*, 1173.

[13] a) W. Lu, J. Sculley, D. Yuan, R. Krishna, Z. Wei, H. C. Zhou, *Angew. Chem. Int. Ed.* **2012**, *51*, 7480; b) W. Lu, W. Verdegaal, J. Yu, P. Balbuena, H. K. Jeong, H. C. Zhou, *Energy Environ. Sci.* **2013**, *6*, 3559.

[14] a) H. Patel, F. Karadas, J. Byun, J. Park, E. Deniz, A. Canlier, Y. Jung, M. Atilhan, C. T. Yavuz, *Adv. Funct. Mater.* **2013**, *23*, 2270; b) D. Ko, H. Patela, C. T. Yavuz, *Chem. Commun.* **2015**, *51*, 2915; c) D. Thirion, V. Rozyyev, J. Park, J. Byun, Y. Jung, M. Atilhan, C. T. Yavuz, *Phys. Chem. Chem. Phys.* **2016**, *18*, 14177.

[15] R. Dawson, A. I. Cooper, D. J. Adams, *Polym. Int.* **2013**, *62*, 345.

[16] K. Sumida, D. Rogow, J. A. Mason, T. M. McDonald, E. D. Bloch, Z. R. Herm, T. H. Bae, J. R. Long, *Chem. Rev.* **2012**, *112*, 724.

[17] A. Torrisi, R. G. Bell, C. Mellot-Draznieks, *Cryst. Growth Des.* **2010**, *10*, 2839.

[18] Q. Bricaud, A. Cravino, P. Leriche, J. Roncali, *Synth. Met.* **2009**, *159*, 2534.

[19] a) J. Schmidt, M. Werner, A. Thomas, *Macromolecules* **2009**, *42*, 4426; b) W. Lu, D. Yuan, J. Sculley, D. Zhao, R. Krishna, H.C Zhou, *J. Am. Chem. Soc.* **2011**, *133*, 18126.

[20] M. Trunk, A. Herrmann, H. Bildirir, A. Yassin, J. Schmidt, A. Thomas, *Chem. Eur. J.* **2016**, *22*, 7179.

[21] A. Uptmoor, J. Freudenberg, T. Schwäbel, F. Paulus, F. Rominger, F. Hinkel, U. Bunz, *Angew. Chem. Int. Ed.* **2015**, *54*, 14673.

[22] A. L. Myers, J. M. Prausnitz, *AIChE J.* **1965**, *11*, 121.

[23] D. Thirion, J. S. Lee, E. Özdemir, C. T. Yavuz, Beilstein, *J. Org. Chem.* **2016**, *12*, 2274.

[24] Y. Lim, I. Choi, H. Lee, I. W. Kim, J. Y. Chang, *J. Mater. Chem. C* **2014**, *2*, 5963.

[25] a) A. Yassin, P. Leriche, J. Roncali, *Macromol. Rapid Commun.* **2010**, *31*, 1467; b) A. Yassin, R. Mallet, P. Leriche, J. Roncali,

ChemElectroChem **2014**, *1*, 1219; c) A. Yassin, D. Demeter, J. Roncali, *Tetrahedron Lett.* **2016**, *57*, 3945.

[26] Y. Zhao, X. Liu, Y. Han, *RSC Adv.* **2015**, *5*, 30310.

[27] A. Kumar, D. G. Madden, M. Lusi, K. J. Chen, E. Daniels, T. Curtin, J. Perry, M. Zaworotko, *Angew. Chem. Int. Ed.* **2015**, *54*, 14372.

[28] a) HOOMD-Blue Web page, http://codeblue.umich.edu/hoomd-blue (accessed April 2016); b) T. D. Nguyen, C. L. Phillips, J. A. Anderson, S. C. Glotzer, *Comput. Phys. Commun.* **2011**, *182*,

2307; c) I. T. Todorov, W. Smith, K. Trachenko, M. T. Dove, *J. Mater. Chem.* **2006**, *16*, 1911.

[29] a) J. X. Jiang, F. Su, A. Trewin, C. D. Wood, H. Niu, J. T. A. Jones, Y. Z. Khimyak, A. I. Cooper, *J. Am. Chem. Soc.* **2008**, *130*, 7710; b) J. Jiang, F. Su, A. Trewin, C. D. Wood, N. L. Campbell, H. Niu, C. Dickinson, A. Y. Ganin, M. J. Rosseinsky, Y. Z. Khimyak, A. I. Cooper, *Angew. Chem. Int. Ed.* **2007**, *46*, 1; c) A. Trewin, D. J. Willock, A. I. Cooper, *J. Phys. Chem. C* **2008**, *112*, 20549.

[30] C. Xu, N. Hedin, *Mater. Today* **2014**, *17*, 397.

1700233 (9 of 9)

**ADVANCED
FUNCTIONAL
MATERIALS**

Supporting Information

Structure–Thermodynamic-Property Relationships in Cyanovinyl-Based Microporous Polymer Networks for the Future Design of Advanced Carbon Capture Materials

Ali Yassin,* Matthias Trunk, Frank Czerny, Pierre Fayon, Abbie Trewin, Johannes Schmidt, and Arne Thomas*

WILEY-VCH

Supporting Information

Structure – Thermodynamic-property Relationships in Cyanovinyl-based Microporous Polymer Networks for the Future Design of Advanced Carbon Capture Materials

Ali Yassin,* Matthias Trunk, Frank Czerny, Pierre Fayon, Abbie Trewin, Johannes Schmidt and Arne Thomas*

Inert reactions were carried out using standard schlenk technique or in an MBraun glovebox type MB 120 BG. ^{1}H-NMR and ^{13}C-NMR were recorded on a Bruker Avance II 400 MHz spectrometer in the given solvent. Data are reported in the following order: chemical shift (δ) in ppm; multiplicities (s for singlet, d for doublet); coupling constants (J) in Hertz (Hz); number of protons. Elemental analyses were obtained on a Thermo FlashEA 1112 elemental analyzer. High Resolution mass spectra were recorded using a Thermo Fisher Scientific LTQ Orbitrap XL instrument with APCI ionisation. 4-iodophenylacetonitrile, 1,3,5-tris(bromomethyl)benzene, terephthalaldehyde and benzene-1,3,5-tricarbaldehyde were obtained and used as purchased from Sigma-Aldrich, ABCR and Manchester Organics Limited. Anhydrous grade solvents were used throughout (Sigma-Aldrich and Acros).

S1: Synthetic procedures for the preparation of the starting monomer, the metal-catalyzed and metal-free condensation polymers.
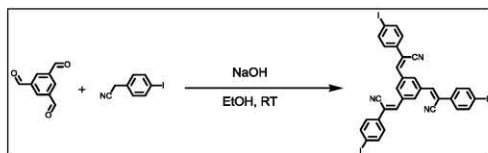
Monomer 1. Similar procedure reported for the bromo derivative,[1] to a solution of benzene-1,3,5-tricarbaldehyde (0.12 g, 0.75 mmol) and 4-bromophenylacetonitrile (0.605 g, 2.5 mmol) in ethanol (40 mL) was added sodium hydroxide (0.09 g) in ethanol (30 mL). After stirring for 2 days at room temperature, the precipitate was filtered and washed with ethanol. The product was obtained as crystalline pale yellow solid. Yield: 92%. ^{1}H NMR (200 MHz, CDCl$_3$, ppm): δ 8.39 (s, 3H), 7.82 (d, [3]J = 8.6 Hz, 6H), 7.62 (s, 3H), 7.45 (d, [3]J = 8.6 Hz, 6H). HRMS calc [M+H]$^+$ 837.87075 found [M+H]$^+$ 837.87106. IR ν 2220 cm^{-1} (C≡N).

1
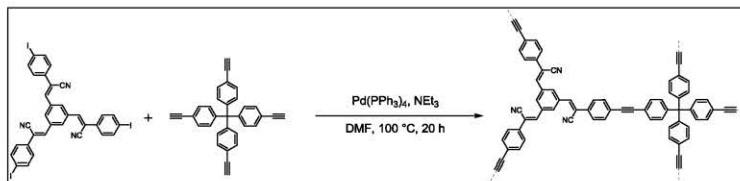
Synthesis of **P2**. Tetrakis(4-ethynylphenyl)methane (31.2 mg, 0.075 mmol) and monomer 1 (83.6 mg, 0.1 mmol) were added to triethylamine and DMF in a reaction vessel. After addition of the catalyst (2.4 mg) a septum was applied and the sealed vessel removed from the glovebox, and put into an oil bath pre-heated to 100 °C. The mixture turned from a yellow suspension to a yellow solution, which turned deeper yellow over time. After a few minutes an intensely yellow solid started to form. The suspension was kept at 100 °C for 20 hours. The reaction was quenched by addition of methanol, the yellow solid purified *via* Soxhlet extraction from methanol for 24 hours, and the resulting solid dried in the vacuum oven at 70 °C for 5 hours to produce P2 as brownish yellow network (85 mg, 108 %).
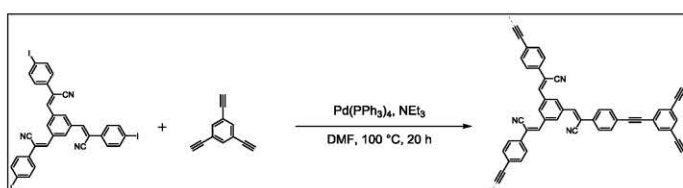
Synthesis of **P3**. 1,3,5-triethynylbenzene (15.3 mg, 0.10 mmol) and monomer 1 (83.6 mg, 0.10 mmol) were added to triethylamine and DMF in a reaction vessel. After addition of the catalyst (2.4 mg) a septum was applied and the sealed vessel removed from the glovebox, and put into an oil bath pre-heated to 100 °C. The mixture turned from a yellow suspension to a yellow solution, which turned deeper yellow over time. After a few minutes an intensely yellow solid started to form. The suspension was kept at 100 °C for 20 hours. The reaction was quenched by addition of methanol, the yellow solid purified *via* Soxhlet extraction from DCM for 3 hours, and dried in the vacuum oven at 60 °C for 4 hours to produce a bright yellow network (64 mg, 106 %).
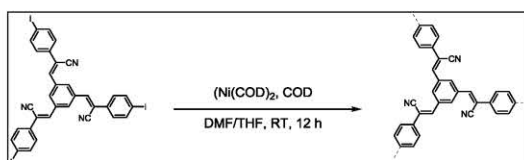
Synthesis of **P4**. To a solution of 2,2'-bipyridyl (90.1 mg, 0.58 mmol), bis(1,5-cyclooctadiene)nickel(0) (Ni(COD)$_2$, 158.7 mg, 0.58 mmol) and 1,5-cyclooctadiene (COD, 62.4 mg, 0.58 mmol) in anhydrous DMF/THF (15 mL/15 mL) was added monomer 1 (140.0 mg, 0.17 mmol), and the mixture was stirred at room temperature under argon atmosphere overnight. Then, the mixture was cooled in ice bath, HCl solution (20 %, 10 mL) was added and the resulting mixture was stirred for another hour. The precipitate was collected, then washed with THF and DCM, purified by Soxhlet extraction from THF and methanol and dried in vacuo to produce **P4** as yellow powder (47 mg, 103 %).

2
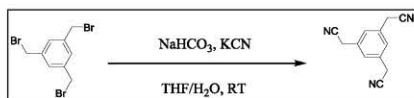
Monomer 2. Prepared as reported,[2] to a solution of 1,3,5-tris(bromomethyl)benzene (3.02 g, 8.50 mmol) in THF (25 mL) was added sodium bicarbonate (saturated solution, 30 ml) and sodium cyanide (4.17 g, 85.0 mmol) followed by 30 mL water. The solution was left to stir for 3 days after which it is was acidified with 1 M HCl. THF was removed via rotary evaporation to leave behind 1.53 g (92%) of an off-white solid. ^{1}H NMR (200 MHz, CDCl$_3$) δ 7.31 (s, 3H), 3.81 (s, 6H), IR: ν 2253 cm^{-1} (C≡N).
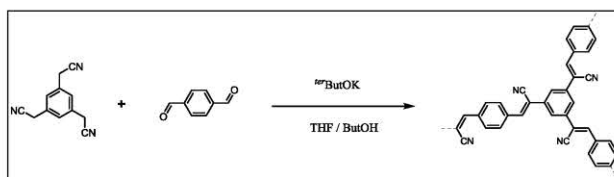
Synthesis of **P5**. Terephthalaldehyde (68 mg, 0.51 mmol) in 8 ml THF was added to a suspension of monomer 2 (66 mg, 0.34 mmol) in 8 ml of t-butanol. After complete dissolution, potassium tert-butoxide (114 mg, 1.02 mmol) was added and the mixture was heated and kept at 50°C overnight, then cooled and poured into methanol. Filtration and successive Soxhlet extractions with methanol and THF left a bright yellow solid (123 mg) with 106% yield.
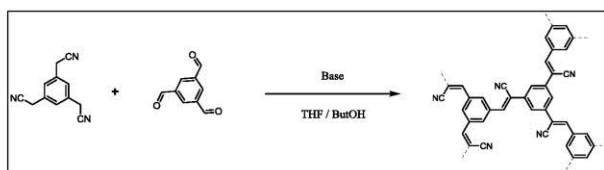
Synthesis of **P6**. Under Argon atmosphere, benzene-1,3,5-tricarbaldehyde (68 mg, 0.42 mmol) in 10 ml dry THF was added to a suspension of monomer 2 (82 mg, 0.42 mmol) in 10 ml of dry t-butanol. After complete dissolution, potassium tert-butoxide (155 mg, 1.38 mmol) was added and the mixture was heated and kept at 70°C overnight, then cooled and poured into methanol. Filtration and successive Soxhlet extractions with methanol and THF left a yellowish white solid (140 mg) with 110% yield.

3

WILEY-VCH

S2: Exact repeating units of the polymers.

Weight percentages of the cyanovinylene functional groups are calculated from the repeating units.
$wt\% = n*$(mass of $C_3H_1N_1$) / mass (repeating unit)

P1:

Cyanovinyl wt% = 0

P2:

Cyanovinyl wt% = 19.7

P3:

Cyanovinyl wt% = 25.4

P4:

Cyanovinyl wt% = 33.5

4

WILEY-VCH

P5:
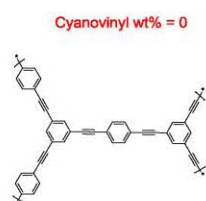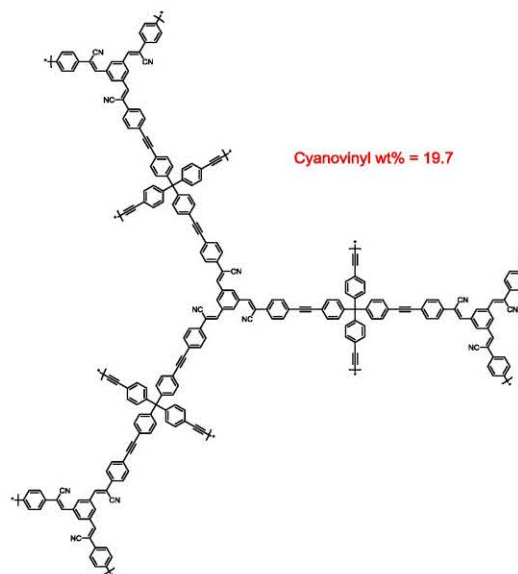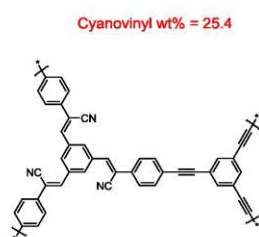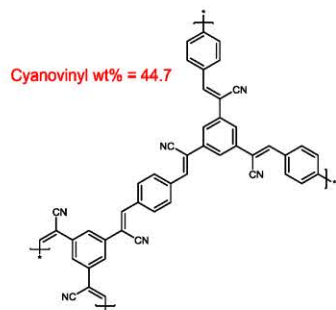
Cyanovinyl wt% = 44.7

P6:

Cyanovinyl wt% = 50.5
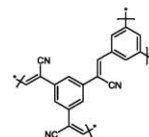
S3: <u>Powder X-ray diffraction patterns PXRD</u>.

Analysis was performed using a Bruker D8 Advance DaVinci X-ray diffractometer with a CuKα radiation and LynxEye™ SuperSpeed Detector. Samples were measured for 2θ between 2° and 90° with an increment of 0.05°.

5
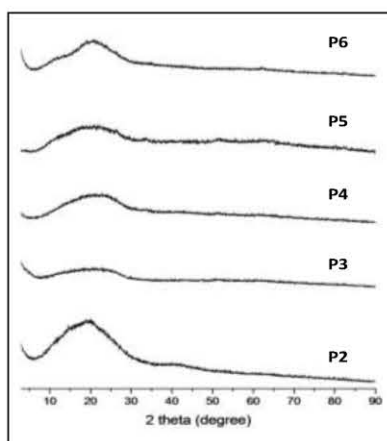
S4: solid state ^{13}CNMR of the Networks.

^{13}C{^{1}H} CP/MAS measurements were carried out using a Bruker Avance 400 spectrometer operating at 100.6 MHz for ^{13}C using a Bruker 4 mm double resonance probe-head operating at a spinning rate of 10 kHz.

6

WILEY-VCH

7
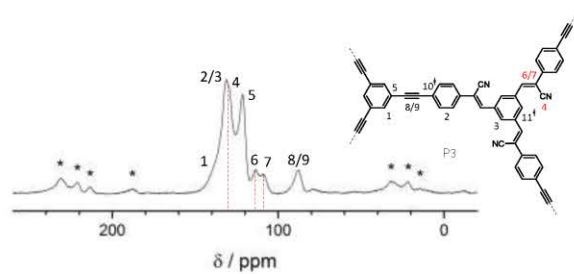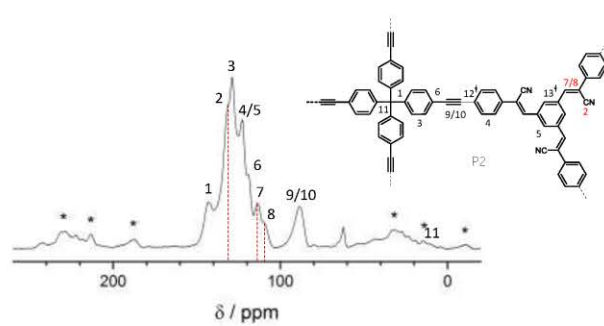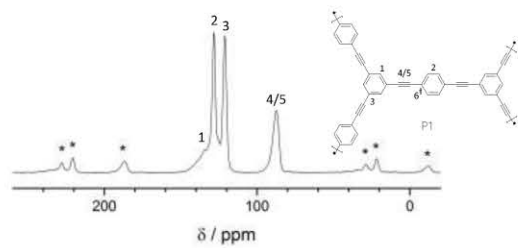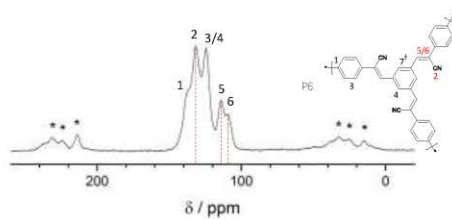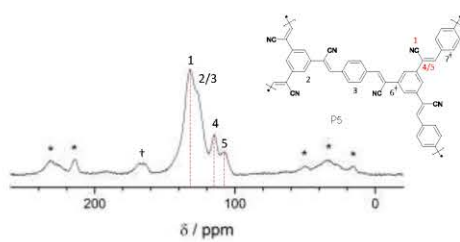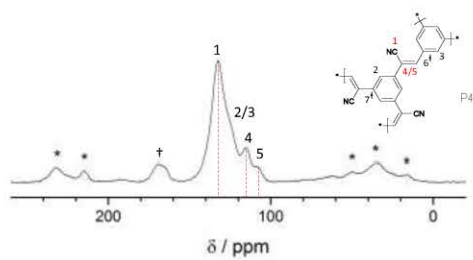
WILEY-VCH

S5: Stack plot comparing the FT-IR spectroscopy of the networks. P2 (red), P3 (green), P4 (blue), P5 (pink), P6 (yellow) and the reference P1 (black)

Spectra were obtained as KBr pellets using a Varian 640-IR spectrometer. The band at 2220 cm^{-1} (between the dashed lines) is assigned to the –CN stretching mode which is absent in the reference network P1.
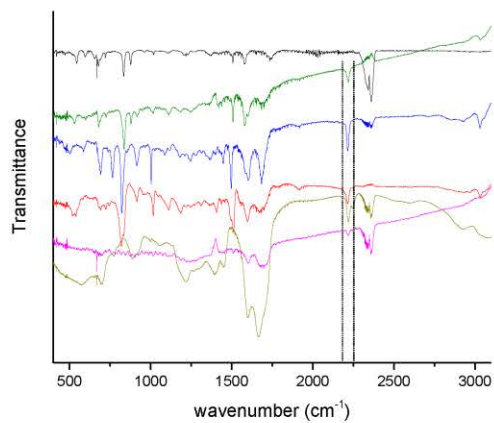
S6: Elemental Analysis data Average of two measurements

Network	Theoretical			Calculated		
	N%	C%	(N/C)%	N%	C%	(N/C)%
P1	0.00	96.53	0	0.83	89.35	0.92
P2	5.40	90.71	5.95	5.18	85.19	6.08
P3	6.96	89.53	7.77	5.69	79.09	7.19
P4	9.20	86.82	10.59	7.35	77.46	9.50
P5	12.27	84.19	14.57	9.78	70.61	13.85
P6	15.15	82.30	18.40	10.52	67.49	15.60

8

Nitrogen sorption isotherms were measured at 77.3 K using a Quantachrome Autosorb iQ2 volumetric analyzer. Prior to measurement the samples were degassed at 80 °C for 10 h (10^{-3} mbar). The nitrogen apparent surface area (SBET) was calculated from the Brunauer-Emmett-Teller (BET) model by selecting adsorption points satisfying the consistency criteria for application of the BET theory.

S7: N$_2$ sorption isotherm measured at 77 K for the networks (left) and their pore size distribution profile calculated after fitting DFT to N$_2$ adsorption data (right)

9
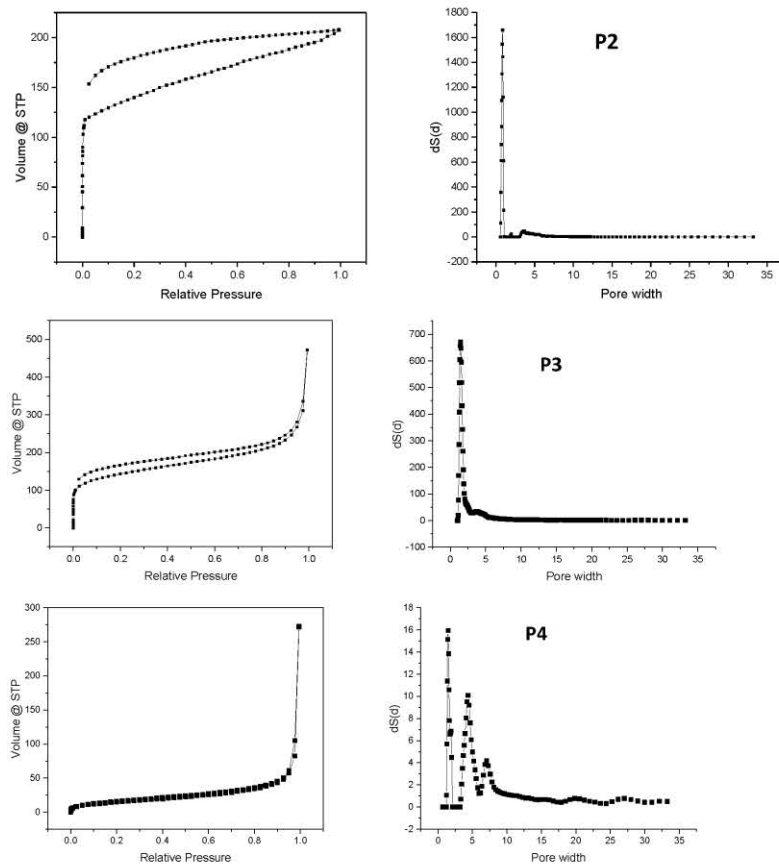
WILEY-VCH
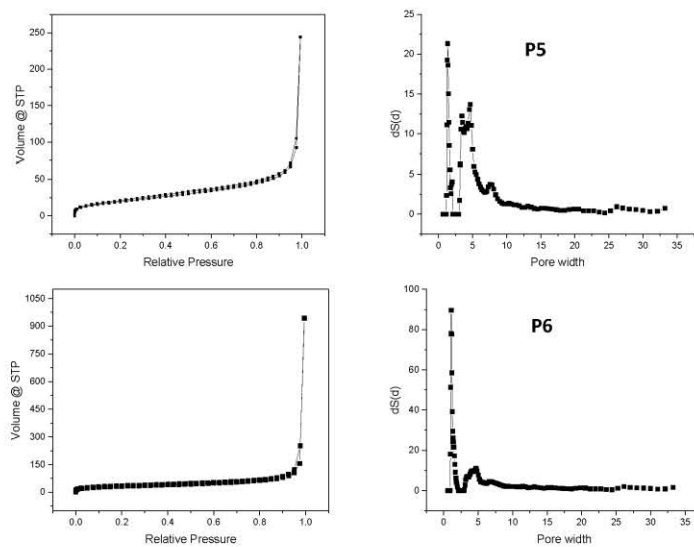
S8: <u>CO$_2$ sorption isotherm measured at 273 and 298 K for the networks in addition to N$_2$ sorption isotherm at 273 K for selectivity calculations.</u> Uptakes given in cm^3 at STP

10
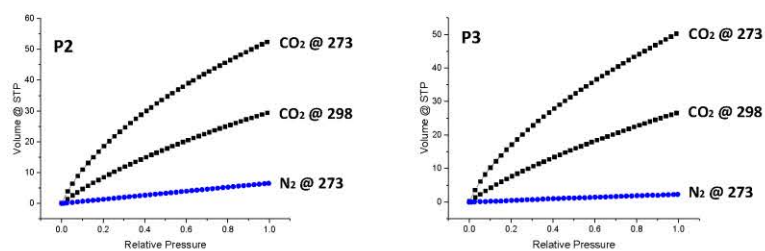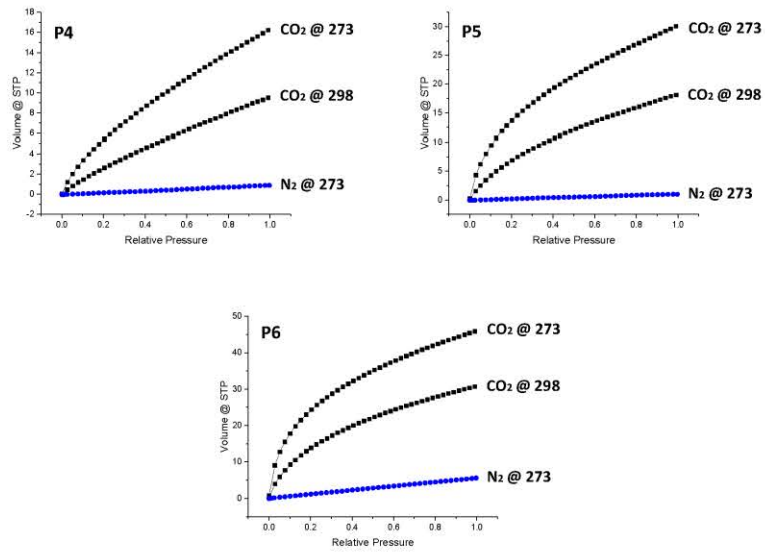
WILEY-VCH

S9: <u>Isosteric heats of adsorptions finely tuned via engineering the cyanovinylene content</u>

The relation holds true for polymers generated under different reaction conditions.

11
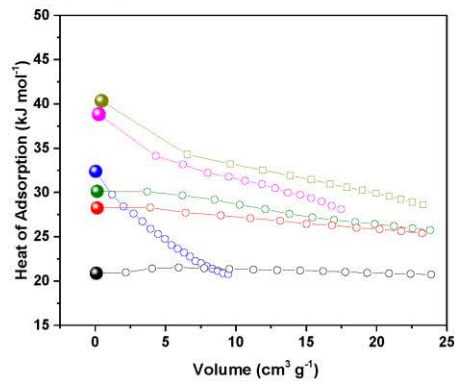
WILEY-VCH
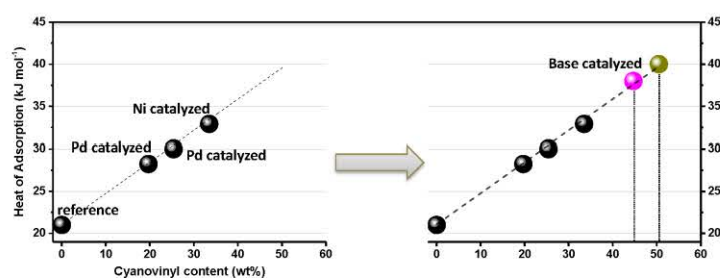
S10: <u>IAST calculated adsorption selectivity</u>

Measured experimental data on pure component isotherms for CO_2 and N_2 were fitted with either a single-site Langmuir model or a dual-site Langmuir model. For N_2 adsorption there are no discernible isotherm inflections and therefore the single-site Langmuir model $q = \frac{q_{sat}+bp}{1+bp}$ was used for fitting of the 273 K isotherms for the six polymers. For adsorption of CO_2 there are subtle isotherm inflections and for fitting the experimental data we used the dual-site Langmuir model $q = q1 + q2 = \frac{q(1)_{sat}+b(1)p}{1+b(1)p} + \frac{q(2)_{sat}+b(2)p}{1+b(2)p}$ where we have two distinct adsorption sites (1) and (2):

b   the parameter in the pure component Langmuir adsorption isotherm, Pa^{-1}
p   the bulk gas phase pressure, Pa
q the molar loading of adsorbate, $cm^3\ g^{-1}$
q_{sat} the saturation loading, $cm^3\ g^{-1}$
(1)   referring to site 1
(2)   referring to site 2
sat referring to saturation conditions

Network	CO_2 loading at 15 kPa ($cm^3\ g^{-1}$)	N_2 loading at 85 kPa ($cm^3\ g^{-1}$)	Selectivity[a] S=(q1/q2) / (p1/p2)
P2	14.82	5.59	15
P3	13.73	7.00	11
P4	3.89	0.74	29
P5	11.71	0.90	74
P6	17.64	1.04	96

[a]at 273 K.

12

WILEY-VCH

S11: Unit cell for the single crystal X-Ray structure of monomer **1**, front and side views
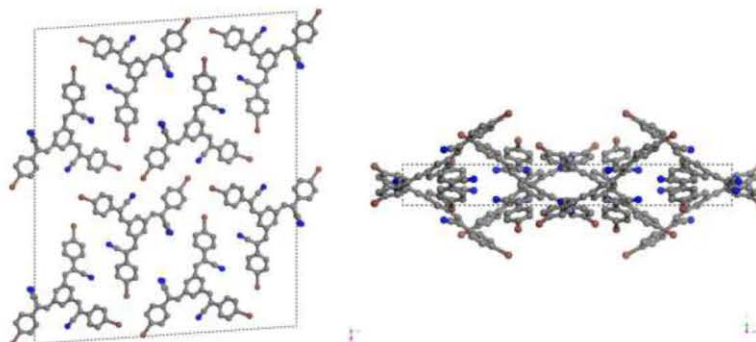
S12: AMBUILD CODE

The HOOMD-blue(*1-3*) GPU-based code is used as the MD and optimization engine throughout, enabling long simulation times and easy integration to the Python code for the reasonably large simulation cells size required. Each MD loop is an NVT MD simulation consisting of 100000 steps with a timestep of 0.5 fs. The Fast Inertial Relaxation Engine (FIRE) rigid-body minimiser is used for optimization of the geometry. Bond and angle parameters and intermolecular forces are taken from the PCFF force field. A harmonic bond potential is used to describe the bonds and dihedrals. Intermolecular forces are described by a Lennard-Jones potential with a cut-off distance of 10 Å. Charges are calculated using the Gasteiger method.[6]

We start with a simulation cell seeded with the stoichiometric quantities of building units. The seeding step works by selecting a random point in the cell, and adding the centroid of the building unit to the cell. A test is then made to determine if any of the atoms in the building unit are close enough to clash with other atoms within the cell. A clash is considered to happen when two atoms are closer than their respective covalent atomic radii, plus a user-specified margin (currently 0.5 Å by default). If a clash occurs, the building unit is removed from the cell, and another position is trailed. Currently 500 attempts are made to seed a building unit in the cell before Ambuild will consider that the seed attempt has failed.

A stepwise approach to the *Seed* procedure is taken with a number of NVT MD simulation followed by optimization of the geometry at each step. Once fully seeded, an MD simulation is undertaken to equilibrate the system.

Each end group atom may also have a dihedral atom specified. This is an atom bonded directly to the end group that is used to define a dihedral angle between two building units. The dihedral angle, and a margin may be specified when running a *Zip* step. If two atoms are close enough to bond by the above criteria, both end group atoms have a designated dihedral atom and a dihedral angle has been specified, then the dihedral angle formed by:endGroup1DihedralAtom - endGroup1Atom - endGroup2Atom - endGroup2DihedralAtom is calculated. If this is within the specified dihedral angle, plus or minus the margin, then the bond is considered permissible within the rules. Section S2 shows the end group and cap atoms for each building unit.

13

WILEY-VCH

Ambuild use cell lists to determine which atoms are close enough to interact. For each *Zip* step a cell list is calculated for all of the end group atoms, based on the maximum permissible bond length for the atoms in the cell, plus the *Zip* step bond length margin. Ambuild then loops through all the available end group atoms within the cell, and determines if any other end groups in that cell, or any of the directly adjacent cells, is able to bond under the length and angle criteria specified above, together with any chemical bonding rules that were given.

Any end group atom pair that is within a set distance criteria is tested to ensure that their bond vectors are within a set angle criteria. If a potential bond is found that fits the bonding criteria then a bond is formed, a water molecule is *Seeded* to the simulation cell and the system is optimized before the structure is subjected to additional MD simulation loops.

S13: Building Block Structures

Building blocks were optimized using DFT in Gaussian 09[7] with the B3LYP functional and the 6-31G* basis set. For the MD simulations we made use of the AMBER force field,[8] Antechamber,[9] and Chemshell[10] to generate the input file for Ambuild and DL_POLY simulations

S14: Polymer Networks Models

Lattice a=b=c = 100 Å^3

Polymer	Building block 1	Building block 2	Ratio	Solvent
P1	C1	D1	3:2	DMF
P2	C2	D2	4:3	DMF
P3	C2	D1	1:1	DMF
P4	C2	-	-	DMF
P5	C3	C1	2:3	THF/BuOH (1:1)
P6	C3	D3	1:1	THF/BuOH (1:1)

Table S1. Building block ratio for the respective polymer model systems.

Polymer	Seed		Grow		Grow/Zip			Total MD steps
	number	ratio	number	ratio	number	ratio	Zip parameters	
P1	10	6:4	10	12:8	170	12:8	5 Å and 60°	180, 00000
P2	10	8:6	10	8:6	40	8:6	5 Å and 60°	50,00000
P3	10	5:5	15	5:5	100	5:5	5 Å and 60°	110,00000
P4	10	20	15	20	35	10	5 Å and 60°	45,00000
P5	10	4:6	10	8:12	200	8:12	5 Å and 60°	210,00000
P6	20	5:5	20	5:5	160	5:5	5 Å and 60°	180,00000

Table S2. AMBUILD network generation procedure for each respective polymer.

14

WILEY-VCH

Polymer	Density (g cm^{-3})	Elemental Models (wt%)					Elemental Experimental (wt%)				
		C	H	O	N	I	C	H	O	N	I
P1	0.81	81.1	3.1	-	0	15.8	89.4	-	-	0.8	-
P2	0.76	82.0	3.7	-	4.3	10.0	85.2	-	-	5.2	-
P3	0.77	84.4	3.4	-	5.8	6.5	79.1	-	-	5.7	-
P4	0.76	72.1	3.4	-	7.9	14.7	77.5	-	-	7,4	-
P5	1.02	82.4	3.6	1.8	12.0	0.2	70.6	-	-	9.8	-
P6	1.04	80.4	3.2	3.3	13.0	0.1	67.5	-	-	10.5	-

Table S3. Structural parameters for the model system of each respective polymer.
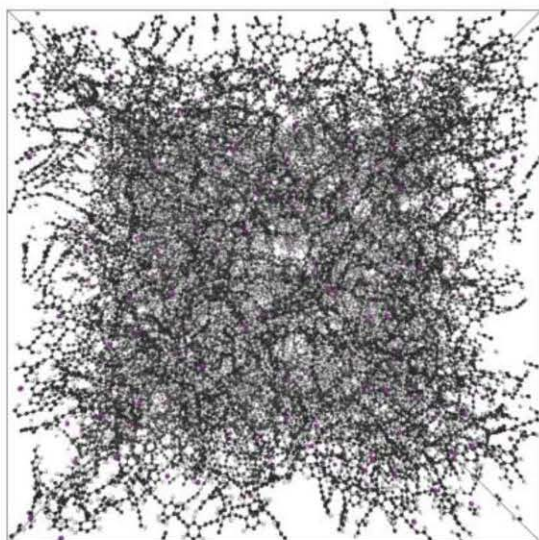
Figure S1. P1 polymer model system.

15
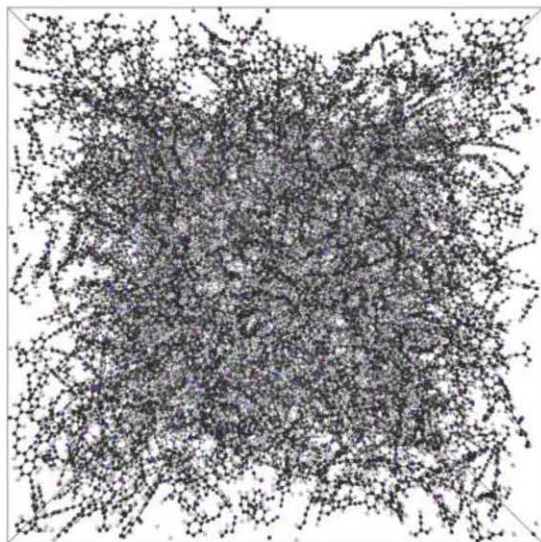
Figure S2. P2 polymer model system.
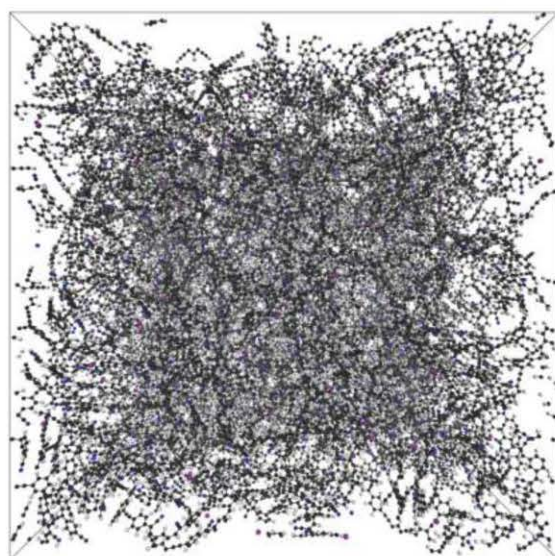
Figure S3. P3 polymer model system.

16
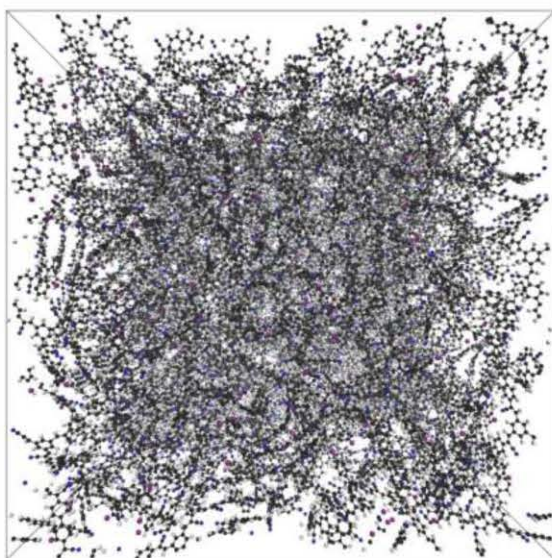
WILEY-VCH

Figure S4. P4 polymer model system.
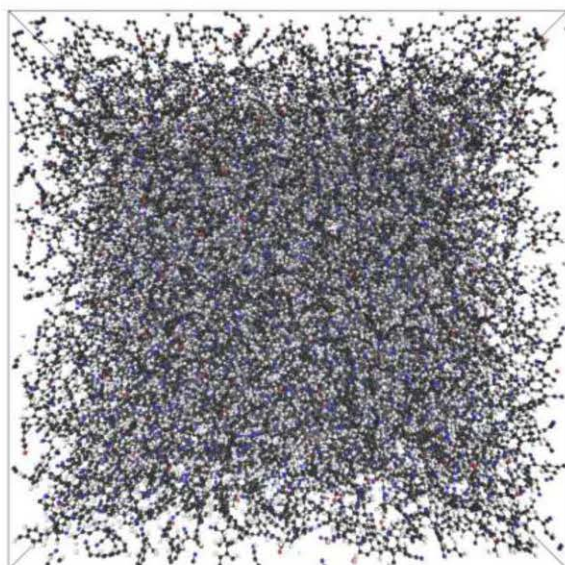
Figure S5. P5 polymer model system.

17

WILEY-VCH
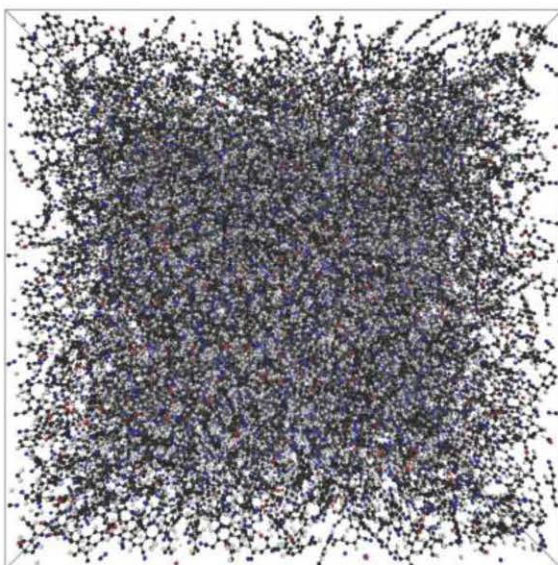
Figure S6. P6 polymer model system.

S15: Porosity computational characterization

Polymer	Connolly Surface area (m² g⁻¹)	Solvent Surface area (m² g⁻¹)	Solvent Accessible Surface area (m² g⁻¹)	Experimental Surface area (m² g⁻¹)
P1	2570	1332	1284	1700
P2	3257	1497	1416	520
P3	2872	1349	1288	510
P4	3265	1668	1605	60
P5	1726	167	37	80
P6	1798	156	26	112

Table S4. Geometric surface area calculated using a probe radius of 1.82 Å, the kinetic radius of N_2.

18

WILEY-VCH

Computationally Determined Pore Size Distribution:
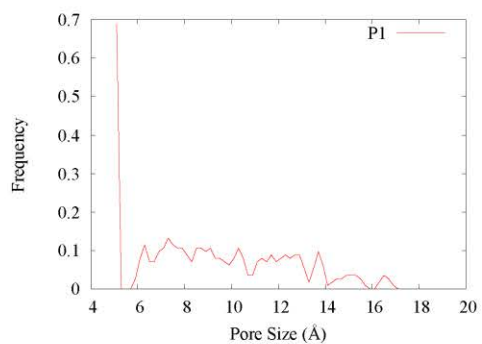
Figure S7. P1 pore size distribution.
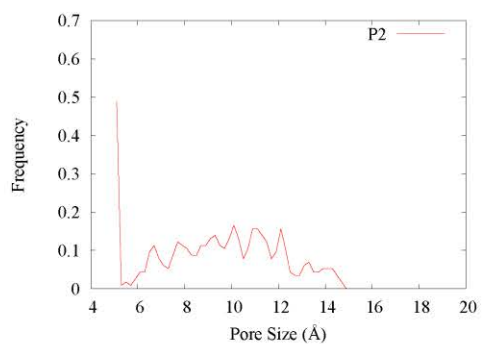
Figure S8. P2 pore size distribution.
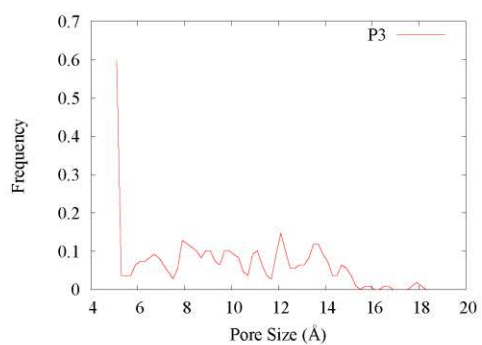
Figure S9. P3 pore size distribution.

19

WILEY-VCH
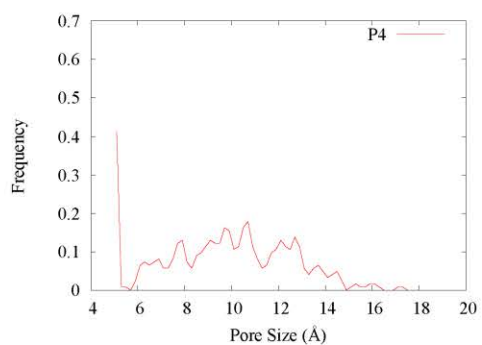
Figure S10. P4 pore size distribution.
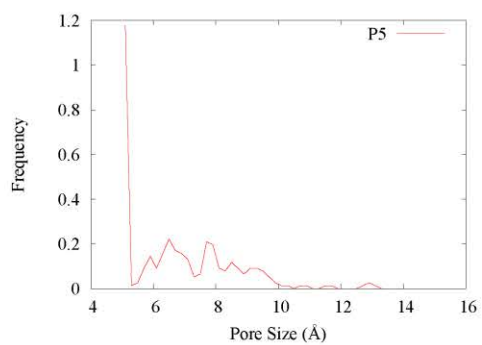
Figure S11. P5 pore size distribution.
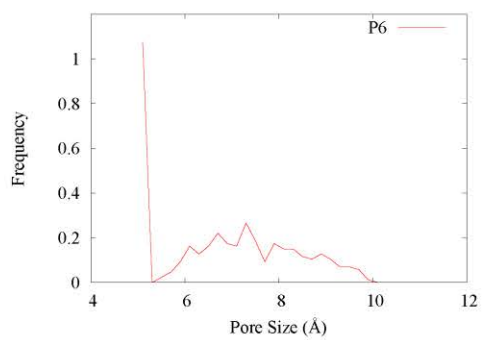
Figure S12. P6 pore size distribution.

20

WILEY-VCH
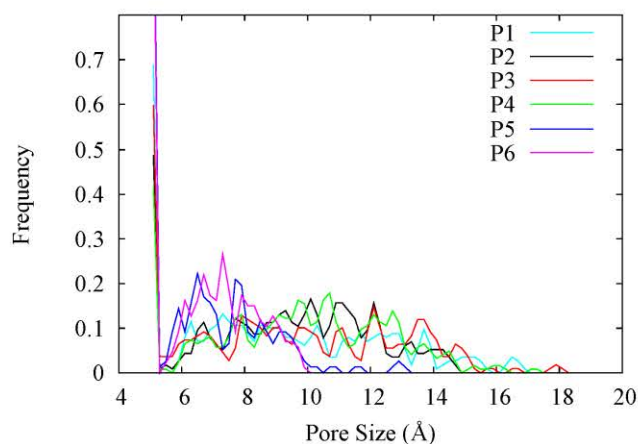
Figure S13. Comparison of the pore size distribution for P1, P2, P3, P4, P5 and P6.

S16: Binding Energy of CO_2

The binding energies were calculated using Gaussian09(5) with the B3LYP functional and the 6-31G** basis set using the empirical dispersion D3 version of the Grimme's dispersion with the original D3 damping function.

Position	Description	Energy kJ mol^{-1}
1	Ph	18.28
2	CN	15.44
3	CN/Ph	13.93
4	CN/Ph	13.93
5	Ph/C=C/CN	21.13
6	CN	13.60
7	CN	13.60
8	Ph	18.28
9	Ph	17.49
10	Ph	16.70
11	Ph/C=C,CN	21.09

Table S5. Calculated binding energy for CO_2 to a fragment of P6 in different positions.

21

WILEY-VCH

Position	Description	Energy kJ mol^{-1}
12	Ph/Ph/CN	23.35
13	Ph/CN	20.33

Table S6. Calculated binding energy for CO_2 to a fragment of P5 in different positions.

Position	Description	Energy kJ mol^{-1}
14	2 x Ph	35.44
15	2 x CN	29.50
16	2 x CN/Ph	29.07
17	2 x CN/Ph	32.43

Table S7. Calculated binding energy for CO_2 to two fragments of P6 in different positions.

Position	Description	Energy kJ mol^{-1}
18	2 x Ph	28.49
19	2 x CN	38.24
20	2 x CN/Ph	25.94
21	2 x CN/Ph	25.73
22	2 x Ph/Ph/CN	34.14

Table S8. Calculated binding energy for CO_2 to two fragments of P5 in different positions.

Position	Description	Energy kJ mol^{-1}
23	3 x Ph	42.97
24	3 x CN	32.76

Table S9. Calculated binding energy for CO_2 to three fragments of P6 in different positions.

Position	Description	Energy kJ mol^{-1}
25	3 x Ph	45.86
26	3 x CN	37.45
27	3 x CN/Ph	36.78

Table S10. Calculated binding energy for CO_2 to three fragments of P5 in different positions.

22
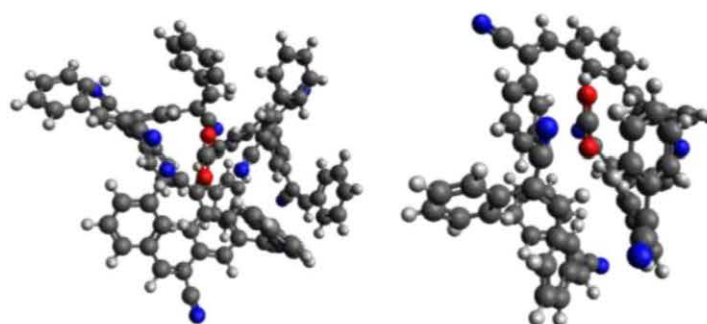
(a)   (b)

Figure S14. Carbon dioxide, CO_2, binding to three fragments of (a) P5 and (b) P6 with binding energies of 45.86 kJ mol^{-1} and 42.97 kJ mol^{-1} respectively.

S17: Radial Distribution Function of N in Network
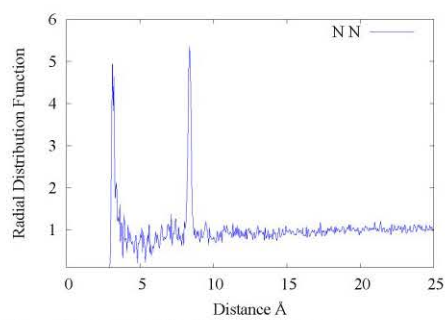
Figure S15. Radial distribution of N in P2.

23

WILEY-VCH
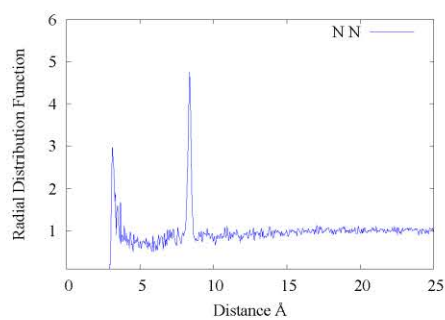
Figure S16. Radial distribution of N in P3.
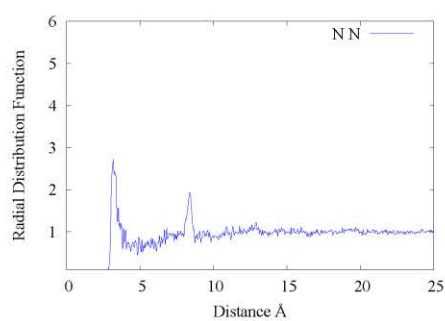
Figure S17. Radial distribution of N in P4.
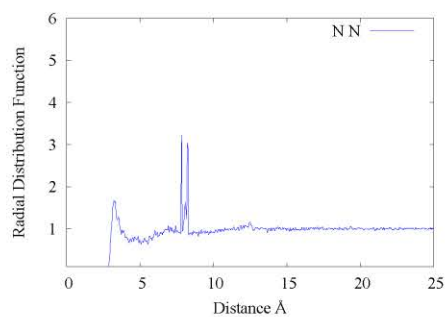
Figure S18. Radial distribution of N in P5.

24
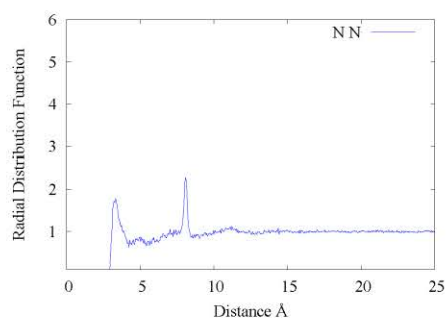
WILEY-VCH

Figure S19. Radial distribution of N in P6.

Comparison:
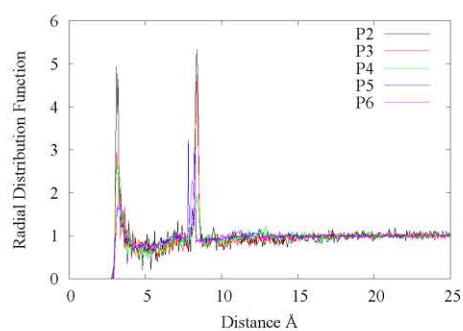
Figure S20. Comparison of the radial distribution of N in polymer systems.
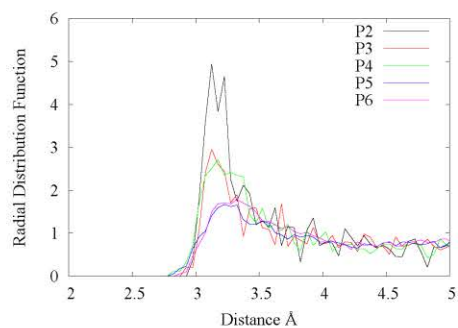
Figure S21. Comparison of the radial distribution of N in polymer systems.

25

WILEY-VCH
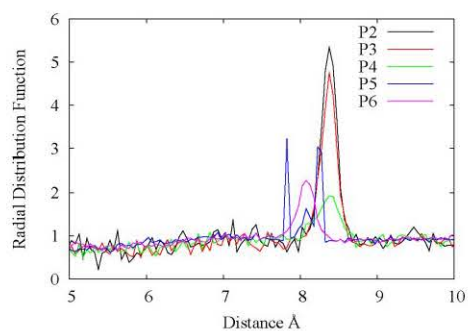
Figure S22. Comparison of the radial distribution of N in polymer systems

S18: Radial Distribution Function of CO_2 in Network
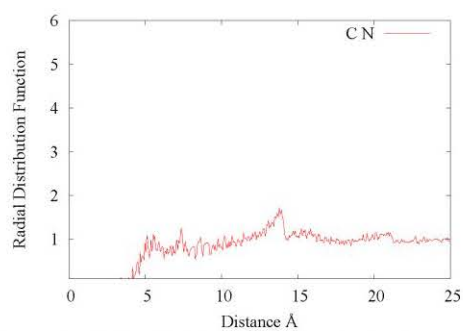
Figure S23. Radial distribution of C of the CO_2 molecule to the N of the polymer P2.
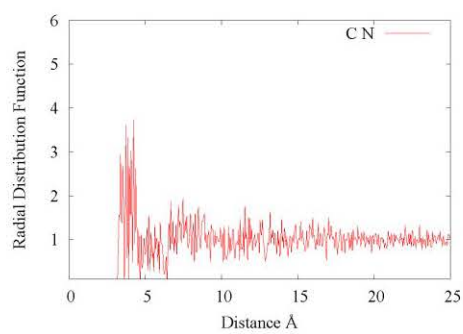
Figure S24. Radial distribution of C of the CO_2 molecule to the N of the polymer P3.

26
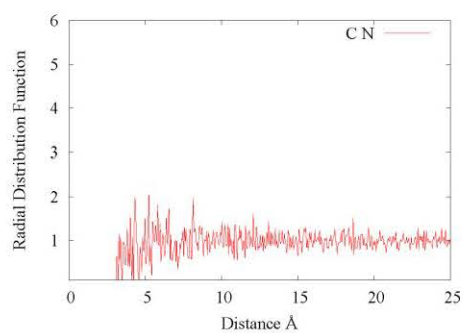
Figure S25. Radial distribution of C of the CO_2 molecule to the N of the polymer P4.
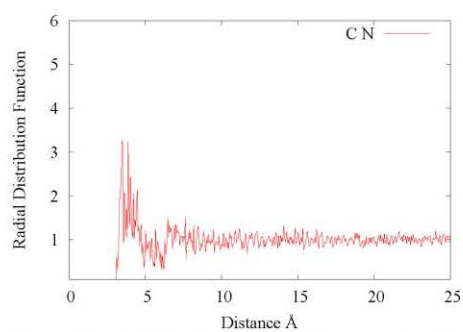
Figure S26. Radial distribution of C of the CO_2 molecule to the N of the polymer P5.
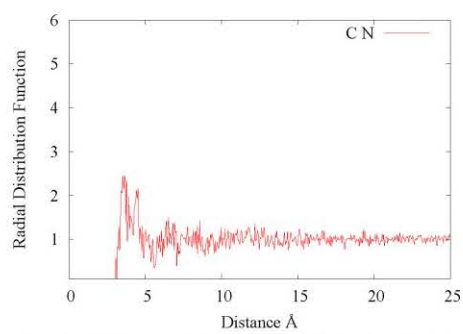
Figure S27. Radial distribution of C of the CO_2 molecule to the N of the polymer P6.

27

WILEY-VCH
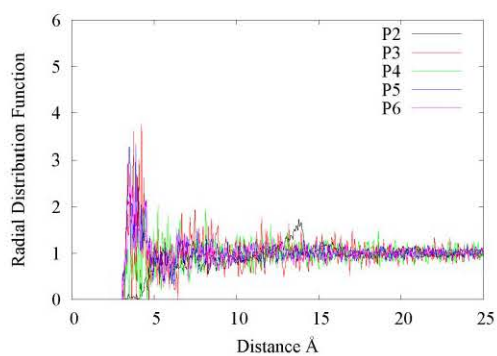
Figure S28. Comparison of radial distribution of C of the CO_2 molecule to the N of the polymer.
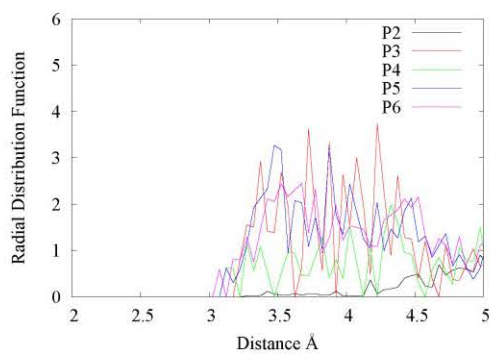
Figure S29. Comparison of radial distribution of C of the CO_2 molecule to the N of the polymer.

28

WILEY-VCH

S19: <u>Diffusion of CO_2 in Network</u>
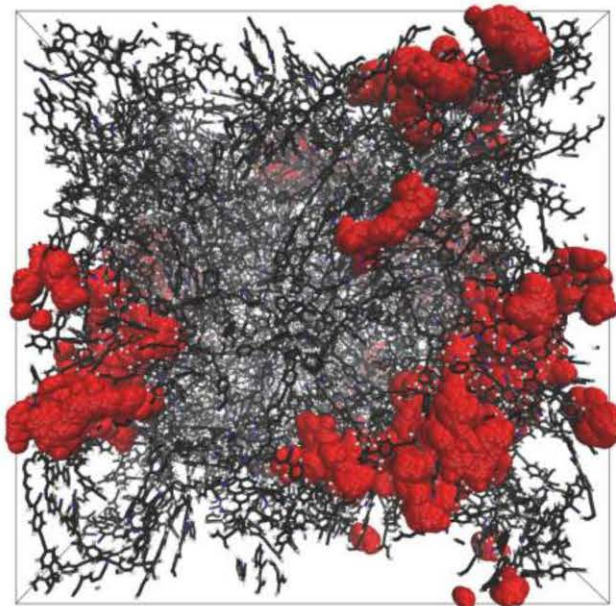
Figure S30. Overlay of CO_2 diffusion in P2.

29

WILEY-VCH
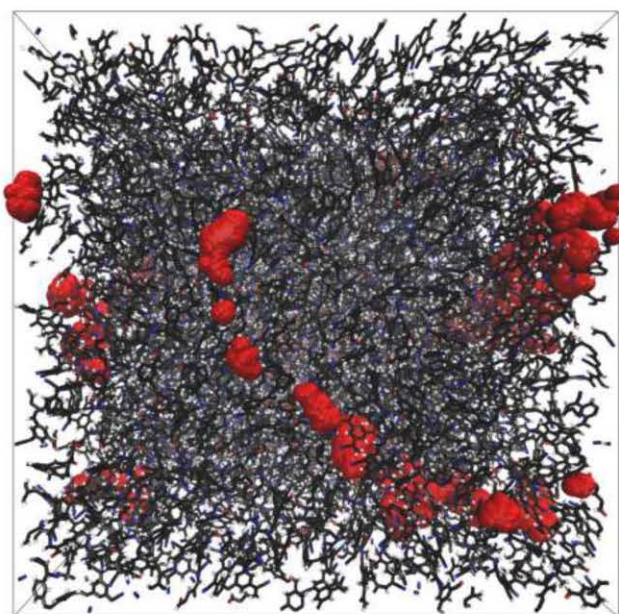
Figure S31. Overlay of CO_2 diffusion in P6
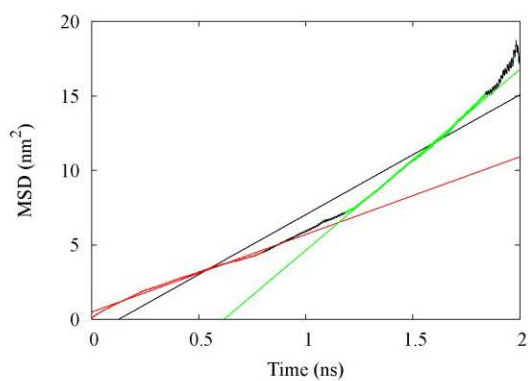
Figure S32. MSD plot for CO_2 diffusion in P2

30

WILEY-VCH
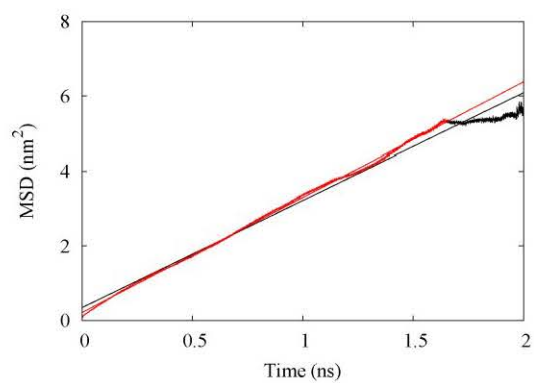
Figure S33. MSD plot for CO_2 diffusion in P6.
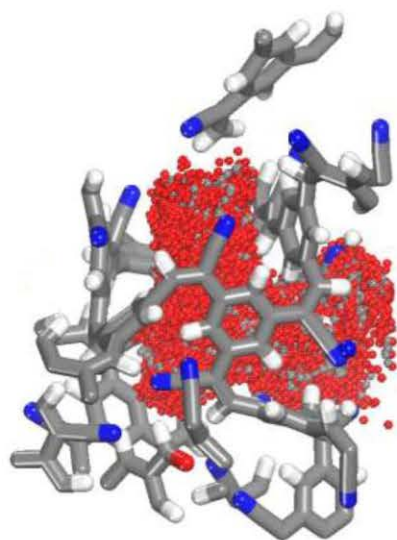
Figure S34. A fragment of the P6 polymer system (rods) with overlay of CO_2 molecule diffusion trajectory (spheres) during a molecular dynamic simulation.

31

WILEY-VCH

References

1. Lim, Y.; Choi, I.; Lee, H.; Kim, I.W.; Chang, J.Y. *J. Mater. Chem. C*, **2014**, 2, 5963

2. Aakeroy, C.; Smith, M.; Desper, J. *CrystEngComm*, **2012**, 14, 71.

3. Rouquerol, J., Rouquerol, F., Llewellyn, P., Maurin, G. & Sing, K. S. W. Adsorption by Powders and Porous Solids (Second Edition). (Academic Press, Oxford, 2014))

4. http://codeblue.umich.edu/hoomd-blue

5. J. A. Anderson, C. D. Lorenz, A. Travesset, General purpose molecular dynamics simulations fully implemented on graphics processing units. *Journal of Computational Physics* **2008**, 227, 5342.

6. T. D. Nguyen, C. L. Phillips, J. A. Anderson, S. C. Glotzer, Rigid body constraints realized in massively-parallel molecular dynamics on graphics processing units. *Computer Physics Communications*, **2011**, 182, 2307.

7. J. Gasteiger, M. Marsill, *Tetrahedron*, **1990**, 36, 3219.

8. M. J. Frisch, G. W. Trucks, H. B. Schlegel, G. E. Scuseria, M. A. Robb, J. R. Cheeseman, J. A. Montgomery, T. Vreven, K. N. Kudin, J. C. Burant, J. M. Millam, S. S. Iyengar, J. Tomasi, V. Barone, B. Mennucci, M. Cossi, G. Scalmani, N. Rega, G. A. Petersson, H. Nakatsuji, M. Hada, M. Ehara, K. Toyota, R. Fukuda, J. Hasegawa, M. Ishida, T. Nakajima, Y. Honda, O. Kitao, H. Nakai, M. Klene, X. Li, J. E. Knox, H. P. Hratchian, J. B. Cross, V. Bakken, C. Adamo, J. Jaramillo, R. Gomperts, R. E. Stratmann, O. Yazyev, A. J. Austin, R. Cammi, C. Pomelli, J. W. Ochterski, P. Y. Ayala, K. Morokuma, G. A. Voth, P. Salvador, J. J. Dannenberg, V. G. Zakrzewski, S. Dapprich, A. D. Daniels, M. C. Strain, O. Farkas, D. K. Malick, A. D. Rabuck, K. Raghavachari, J. B. Foresman, J. V. Ortiz, Q. Cui, A. G. Baboul, S. Clifford, J. Cioslowski, B. B. Stefanov, G. Liu, A. Liashenko, P. Piskorz, I. Komaromi, R. L. Martin, D. J. Fox, T. Keith, A. Laham, C. Y. Peng, A. Nanayakkara, M. Challacombe, P. M. W. Gill, B. Johnson, W. Chen, M. W. Wong, C. Gonzalez, J. A. Pople, Gaussian 03, Revision C.02. citeulike-article-id:3740703).

9. J. Wang, R. M. Wolf, J. W. Caldwell, P. A. Kollman, D. A. Case, Development and testing of a general amber force field. *Journal of computational chemistry*, **2004**, 25, 1157.

10. J. Wang, W. Wang, P. A. Kollman, D. A. Case, Automatic atom type and bond type perception in molecular mechanical calculations. *Journal of Molecular Graphics and Modelling*, **2006**, 25, 247.

11. P. Sherwood, A. de Vries. (1999).

32

Article III

"Room-Temperature Activation of Hydrogen by Semi-immobilized Frustrated Lewis Pairs in Microporous Polymer Networks"

J|A|C|S
JOURNAL OF THE AMERICAN CHEMICAL SOCIETY

Room-Temperature Activation of Hydrogen by Semi-immobilized Frustrated Lewis Pairs in Microporous Polymer Networks

Matthias Trunk,[†] Johannes F. Teichert,[‡][iD] and Arne Thomas[*][,†][iD]

[†]Department of Chemistry, Functional Materials, Technische Universität Berlin, Hardenbergstraße 40, 10623 Berlin, Germany

[‡]Department of Chemistry, Organic Chemistry/Sustainable Synthetic Methods, Technische Universität Berlin, Straße des 17. Juni 115, 10623 Berlin, Germany

Ⓢ *Supporting Information*

ABSTRACT: Porous polymer networks based on sterically encumbered triphenylphosphine motifs, mimicking the basic sites employed in frustrated Lewis pair (FLP) chemistry, were synthesized via Yamamoto polymerization and their interactions with the strong Lewis acid $B(C_6F_5)_3$ probed. The combinations yield semi-immobilized FLPs, which are able to cleave dihydrogen heterolytically at ambient temperature and low hydrogen pressure.

Over the past decade, microporous polymer networks have garnered attention as materials for a wide variety of applications.[1,2] Emanating from rigid organic building blocks, materials with very small pores between 0.5 and 2 nm and accessible surface areas of up to 6400 m^2 g^{-1}, as well as high thermal and chemical stability,[3] have been synthesized by a number of polymerization methods, such as metal-mediated homocoupling reactions, metal-catalyzed cross-coupling reactions, condensation reactions, and many others.[2,4] In contrast to metal−organic frameworks and covalent organic frameworks, these materials do not exhibit crystallinity; emerging from C−C bond-forming reactions, they can forego the use of heteroatoms entirely, allowing for a pure hydrocarbon skeleton. This feature is especially advantageous when designing catalysts with highly sensitive active sites, as it enables the exclusion of nonorthogonal functional groups.

Such types of functional groups can be found as catalytic sites in frustrated Lewis pairs (FLPs).[7] The members of this emerging class of molecular catalysts are solely based on main-group elements and in most cases consist of a boron-based Lewis acid (LA) and a Lewis base (LB), usually comprising phosphorus or nitrogen as basic sites.[8] Both active sites are sterically encumbered by bulky moieties in order to prevent them from forming a strong covalent bond and consequently quenching their opposing reactivities. Small molecules (H$_2$, CO$_2$, etc.) fitting in between these bulky groups can be activated through double polarization by the acidic and basic sites, leading to (zwitter)ionic products (see Scheme 1).[6,7,9] For this activation to take place, the steric hindrance must not be sufficient to prohibit any interaction; in solution, a weak but reversible coordination must be possible, lest the polarization be precluded entirely.[10] Subsequently, the activated intermediate(s) can be used for reactions with a number of substrates.

The most intensely researched application for this type of catalyst is the heterolytic splitting of dihydrogen and its

Scheme 1. (Top) Equilibrium State of a Generic Frustrated Lewis Pair (LA = Lewis Acid, LB = Lewis Base) and Activation of Carbon Dioxide and Hydrogen; (Bottom) (Non)reversible Activation of Hydrogen by Reported FLPs[5,6]
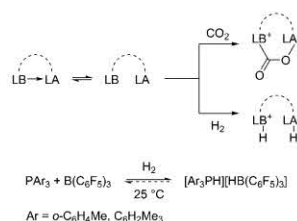
subsequent use in the reduction of C=C,[11] C=N,[12] and C=O[13] double bonds as well as cleavage of silylenol ethers,[14] among others. LA and LB can be part of the same molecule; i.e., both intra- and intermolecular FLPs are capable of activating small molecules.[9] In many cases, though, the mechanistic properties of an activation process are deceptively simple. Even in cases of both active sites within the same molecule, theoretical studies rather suggest intermolecular activation via a two-fold head-to-tail interaction between two intramolecular FLP molecules.[15]

Whereas a great number of Lewis basic polymers has been published, since these are easy to obtain and often display interesting CO$_2$ adsorption properties, only a handful of Lewis acidic moieties in porous polymers have been reported,[16,17] none of which are used for catalytic applications. Due to the use of very strong LAs such as tris(pentafluorophenyl)borane (commonly abbreviated to BCF) or related compounds, these catalysts are often highly sensitive to external factors such as humidity or oxygen, which makes their handling challenging. To overcome this issue, extensive studies toward electronic fine-tuning have produced robust LAs which can be handled without the use of inert gas techniques.[18] Recent advances have furthermore afforded so-called "inverse" FLPs based on a weak and more robust LA but which are used in conjunction with a very strong and sensitive LB on the other hand.[19]

Journal of the American Chemical Society

In order to be able to enhance stability and recyclability and to further increase the appeal of FLPs, the incorporation of FLPs into solid materials, e.g., a microporous polymer network, seems an advantageous endeavor. In this work we focused on the generation of FLPs emerging from porous polymers comprising sterically encumbered phosphine moieties, which are impregnated with a readily available strong LA. We demonstrate the ability of these semi-immobilized FLP systems to activate dihydrogen at ambient temperature and low hydrogen pressure.

The syntheses of the phosphine polymers were carried out according to the synthesis procedure for porous polymer networks via Yamamoto polymerization[20] starting from tris(p-bromophenyl)phosphine derivatives (see Scheme 2) with

Scheme 2. Syntheses of Triarylphosphine Polymers[a]
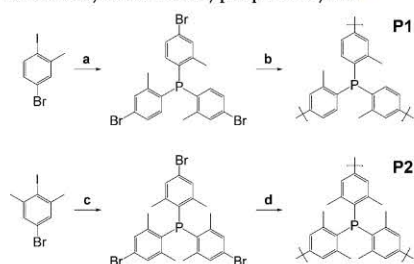
[a]Reagents and conditions: (a) i-PrMgCl, THF, 0 °C, 1 h, then PCl₃, THF, −78 °C to rt, 12 h; (b) Ni(COD)₂, DMF/THF, rt, 15 h; (c) n-BuLi, Et₂O, −78 °C, 2 h, then PCl₃, Et₂O, −78 °C to rt, 12 h; (d) Ni(COD)₂, DMF/THF, rt, 22 h.

increasing steric demand around the phosphorus atoms. The structure of unmethylated triphenylphosphine polymer has been described previously.[21,22] Due to the use of the less reactive aryl chloride starting material, harsher synthesis conditions were required, whereas in this work a milder synthesis protocol[23] was applied due to the exclusive use of the more reactive brominated species.

Purification via Soxhlet extraction with methanol and drying in vacuo at 80 °C yields the product networks (Figure S1). Tris(2-methylphenyl)phosphine polymer **P1** was collected as white and light solid, whereas tris(2,6-dimethylphenyl)-phosphine polymer **P2** has an intense yellow color and fluffy texture. **P1** and **P2** feature surface areas of 1045 and 947 m² g⁻¹, respectively, with **P2** featuring a remarkable hysteresis (see Figure 1). These results are in line with the reported surface area of unmethylated triphenylphosphine polymer of 1284 m² g⁻¹.[21] The decrease in surface area can thus be interpreted as a result of the increased monomer weight and pore blocking by increasing amounts of methyl groups.

Organic solvents such as toluene, bromobenzene, dichloromethane, and THF are readily absorbed by the polymers, which exhibit strong swelling properties and form gel-like mixtures with these solvents. To probe the properties of the synthesized materials as LBs, their behavior toward LAs such as commercially available BCF has to be examined. When a substance is pre-dissolved in the absorbed solvent, it can be introduced into the pores of the polymer. Choosing a volatile
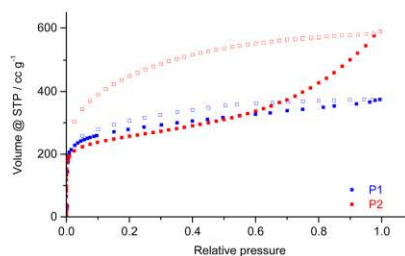
Figure 1. Nitrogen sorption isotherms of **P1** (blue) and **P2** (red).

solvent facilitates drying of the obtained material. BCF is well soluble in aromatic and chlorinated solvents. To gain information on the interaction between BCF as a LA and the bulky LB, no other Lewis acidic or basic functions may be present. Therefore, inside the glovebox, BCF and porous phosphine polymer were suspended in DCM, which is volatile, non-coordinating, and neither acidic nor basic, readily dissolves BCF, and leads to rapid swelling of the polymer. When impregnated with BCF solutions in non-coordinating solvents, e.g., DCM, the LA is readily absorbed into the polymer. The impregnation of the yellow polymer network **P2** was accompanied by darkening of the color, while colorless **P1** remained colorless. Washing with coordinating solvents such as diethyl ether or THF restores the original network. Even weakly coordinating solvents such as methanol or acetone are coordinated preferentially over the bulky phosphine moieties.

Both polymers (see Figure 2) as well as their composites with BCF exhibit strong fluorescence under UV irradiation (bottom row) at 254 (weak) and 366 nm (strong). BCF is readily absorbed by the polymer and quenches the fluorescence (see Supporting Information), especially for polymer **P1**,
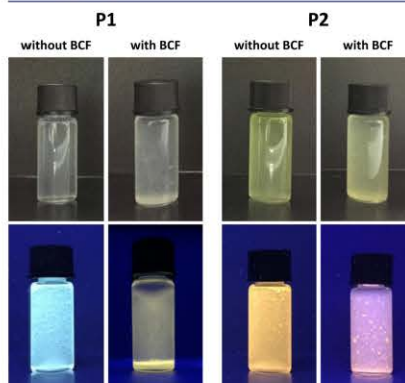
Figure 2. **P1** (left block) and **P2** (right block) in DCM suspension before and after addition of BCF. Top row, UV lamp off; bottom row, under irradiation of UV light (366 nm).

pointing to a stronger interaction with the LA (Figure S1). Furthermore, after addition of BCF, the finely dispersed polymer particles contract and sediment within a matter of minutes, whereas the empty polymer particles tend to collect at the surface of DCM.

Solid-state magic angle spinning NMR spectroscopy of the dried solids confirms the assumed structures (see Figure 3 and
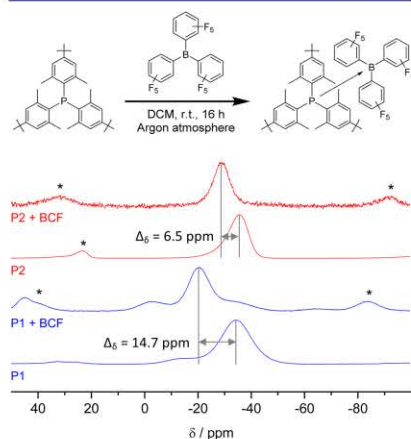
Figure 3. Impregnation procedure of triphenylphosphine derivative polymers (exemplified for **P2**) followed by ^{31}P NMR spectroscopy: **P1** (blue) and **P2** (red) before (upper spectra) and after (lower spectra) impregnation with BCF. Asterisks denote spinning sidebands.

Figure S2). The ^{31}P NMR spectra each exhibit one main peak in the region of −34 and −36 ppm alongside a small impurity at approximately +32 ppm, indicative of small amounts of phosphine oxide present in each network. These traces of phosphine oxide have been reported previously[21] and seem to be the result of a side reaction of the Yamamoto polymerization, since the polymers were synthesized under rigorously inert conditions. Additionally, **P1** and **P2** are prone to phosphine oxide formation in air at elevated temperatures over elongated periods of time and should therefore be stored under inert gas.

Upon impregnation of the polymers with BCF and subsequent solvent removal, the ^{31}P solid-state NMR signals are shifted to lower field, as expected when coordinating to an acidic species. It is noteworthy that nearly the entire signal of the phosphine within the polymers is shifted downfield, showing that almost all phosphine groups in the polymer networks **P1** and **P2** are accessible to the molecular LA. Notably, the extent of the shift strongly correlates with the degree of methylation of the triphenylphosphine derivative. For **P1** a shift of 14.7 ppm is observed, whereas for **P2** a shift of only 6.5 ppm is observed (see Figure 3). This shift difference indicates that the bond strength decreases with increasing steric hindrance around the central phosphorus atom, which means that the higher the degree of frustration is, the weaker the

emerging bond is rendered. This observation is quite remarkable.

According to Heine et al.,[10] the formation of a FLP is usually not observed at ambient temperature in solution; i.e., the solution NMR spectra of the individual components do not differ from the spectra of stoichiometric mixtures. Due to the only weakly coordinating nature of the FLP, the favorable interactions gained from association of LA and LB are dominated by the entropic contribution of the dissociation process. In the solid state, on the other hand, after solvent removal, LA and LB are forced into and kept in a "not-so-frustrated" state, so that the interaction can actually be observed, and its strength is determined by the difference in the chemical shifts, Δ_δ.

To verify this hypothesis, we compared the chemical shifts of the solid-state NMR spectrum of a "dry" FLP, consisting of the molecular counterpart of **P2**, tris(2,6-dimethylphenyl)-phosphine, and BCF to the solid-state NMR spectrum of the phosphine molecule on its own. As expected, in the "dry" FLP, the phosphorus signal is shifted downfield by ca. 10 ppm compared to the phosphine (see Figure S3).

According to the molecular compounds,[5,6] the combinations **P1**/BCF and **P2**/BCF should form FLPs and be active toward the cleavage of dihydrogen. When used in combination with BCF, the molecular equivalent of **P1**, tris(o-tolyl)phosphine, has been reported to activate hydrogen reversibly at ambient conditions to form $[(o\text{-}C_6H_4Me)_3PH][HB(C_6F_5)_3]$, whereas the molecular counterpart of **P2**, trimesitylphosphine, forms the hydrogen adduct $[(1,3,5\text{-}C_6H_2Me_3)_3PH][HB(C_6F_5)_3]$, which remains stable even when exposed to temperatures of up to 150 °C. To prove the hydrogen activation capability of our polymeric materials, we performed H/D isotope scrambling experiments typically employed to demonstrate FLP behavior in a new material[24] for composites of BCF with **P1**, **P2**, and the molecular counterpart of **P1**, tris(o-tolyl)phosphine. To that end, inside a glovebox, a Young-type NMR tube was charged with a stoichiometric mixture of **P1**/BCF or **P2**/BCF and cyclohexane-d_{12}, and the suspension was subjected to ultra-sonication for 15 min to ensure sufficient intermixing of the poorly soluble BCF and the polymer. Subsequently, the tube was pressurized with an H_2/D_2 mixture (ca. 1:1 v/v) to 6 bar and analyzed via ^{1}H NMR spectroscopy beginning several hours after pressurization of the tube. In both cases, an emerging triplet can be observed at 4.54 ppm shortly after pressurization, indicating the formation of HD (see Figure 4).

The control reaction comprising only porous phosphine polymer **P2** and solvent under H_2/D_2 pressure did not result in any conversion to HD. Although the control reaction with BCF as the sole reactant gave the scrambling product, albeit at much lower rate than the BCF/**P2** composite, it must be pointed out that it has been proven theoretically[25] and experimentally under low hydrogen pressure[5] that BCF alone is not active in the heterolytic cleavage of H_2. In our case, residues of protic solvents attached to BCF or trace water on the glass surface might be responsible for providing a proton shuttle in the activation of hydrogen. Furthermore, if a composite of BCF and another highly microporous polymer network devoid of any functional groups (PPN-6, 4172 m^2 g^{-1}, also prepared by Yamamoto polymerization) is used, no hydrogen activation product can be detected. It seems, therefore, that the impregnation procedure of a polymer has a negating effect on the activity of BCF itself. This could be caused by the highly hydrophobic and nonpolarizable surface of the networks. It can

Communication
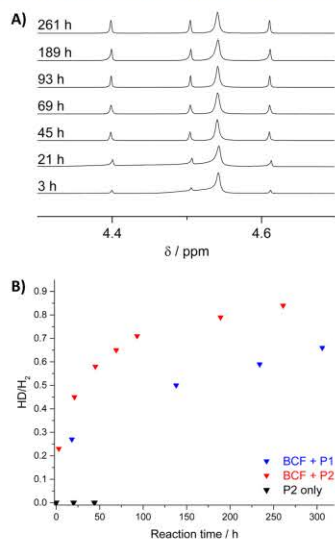
Figure 4. (A) Kinetic measurement of H/D exchange catalyzed be **P2**/BCF determined via ^{1}H NMR. (B) Integral ratio of HD/H$_2$ plotted as a function of time.

therefore be assumed that the observed reactivity of the composites is not only independent of but inherently much higher than the activity of "pure" BCF. The composite tris(*o*-tolyl)phosphine/BCF gives the expected statistical H$_2$/HD ratio after merely a few hours. This shows that the incorporation of the active sites into the polymer imposes a strong kinetic restriction on the H/D exchange process.

In summary, we hereby report the first synthesis of two semi-immobilized frustrated Lewis pairs with the basic components embedded into the backbones of microporous polymer networks. Addition of the commercially available Lewis acid, tris(pentafluorophenyl)borane, to polymers structurally akin to trimesitylphosphine yielded two functional heterogeneous hydrogen activation catalysts. Their ability to cleave dihydrogen at ambient temperature and low pressure was demonstrated via isotope scrambling experiments.

Further combinations of Lewis acidic and basic species need to be created to obtain heterogeneous catalyst systems capable of splitting dihydrogen at low pressures and to enable catalytic hydrogenation. Furthermore, full heterogenization of FLPs could even further enhance the reactivity and applicability of such systems.

■ ASSOCIATED CONTENT

ⓢ Supporting Information

The Supporting Information is available free of charge on the ACS Publications website at DOI: 10.1021/jacs.6b13147.

Experimental details on synthesis of monomers and polymers and hydrogen activation; ^{13}C NMR of polymers and molecular model compounds; fluorescence

spectra and TGA of the polymers, including Figures S1–S4 (PDF)

■ AUTHOR INFORMATION

Corresponding Author

*arne.thomas@tu-berlin.de

ORCID ●

Johannes F. Teichert: 0000-0003-1043-8092

Arne Thomas: 0000-0002-2130-4930

Notes

The authors declare no competing financial interest.

■ REFERENCES

(1) Thomas, A. *Angew. Chem., Int. Ed.* **2010**, *49*, 8328.

(2) Dawson, R.; Cooper, A. I.; Adams, D. J. *Prog. Polym. Sci.* **2012**, *37*, 530.

(3) Yuan, D.; Lu, W.; Zhao, D.; Zhou, H.-C. *Adv. Mater.* **2011**, *23*, 3723.

(4) Rose, M. *ChemCatChem* **2014**, *6*, 1166.

(5) Welch, G. C.; Stephan, D. W. *J. Am. Chem. Soc.* **2007**, *129*, 1880.

(6) Ullrich, M.; Lough, A. J.; Stephan, D. W. *J. Am. Chem. Soc.* **2009**, *131*, 52.

(7) Welch, G. C.; Juan, R. R. S.; Masuda, J. D.; Stephan, D. W. *Science* **2006**, *314*, 1124.

(8) Stephan, D. W. *J. Am. Chem. Soc.* **2015**, *137*, 10018.

(9) Spies, P.; Erker, G.; Kehr, G.; Bergander, K.; Fröhlich, R.; Grimme, S.; Stephan, D. W. *Chem. Commun.* **2007**, *2*, 5072.

(10) Zeonjuk, L. L.; Vankova, N.; Mavrandonakis, A.; Heine, T.; Röschenthaler, G.-V.; Eicher, J. *Chem. - Eur. J.* **2013**, *19*, 17413.

(11) Greb, L.; Oña-Burgos, P.; Schirmer, B.; Grimme, S.; Stephan, D. W.; Paradies, J. *Angew. Chem., Int. Ed.* **2012**, *51*, 10164.

(12) Spies, P.; Schwendemann, S.; Lange, S.; Kehr, G.; Fröhlich, R.; Erker, G. *Angew. Chem., Int. Ed.* **2008**, *47*, 7543.

(13) Lindqvist, M.; Sarnela, N.; Sumerin, V.; Chernichenko, K.; Leskelä, M.; Repo, T. *Dalton Trans.* **2012**, *41*, 4310.

(14) Wang, H.; Fröhlich, R.; Kehr, G.; Erker, G. *Chem. Commun.* **2008**, *45*, 5966.

(15) Liu Zeonjuk, L.; St. Petkov, P.; Heine, T.; Röschenthaler, G.-V.; Eicher, J.; Vankova, N. *Phys. Chem. Chem. Phys.* **2015**, *17*, 10687.

(16) Suresh, V. M.; Bandyopadhyay, A.; Roy, S.; Pati, S. K.; Maji, T. K. *Chem. - Eur. J.* **2015**, *21*, 10799.

(17) Li, Z.; Li, H.; Xia, H.; Ding, X.; Luo, X.; Liu, X.; Mu, Y. *Chem. - Eur. J.* **2015**, *21*, 17355.

(18) Scott, D. J.; Fuchter, M. J.; Ashley, A. E. *Angew. Chem., Int. Ed.* **2014**, *53*, 10218.

(19) Mummadi, S.; Unruh, D. K.; Zhao, J.; Li, S.; Krempner, C. *J. Am. Chem. Soc.* **2016**, *138*, 3286.

(20) Schmidt, J.; Werner, M.; Thomas, A. *Macromolecules* **2009**, *42*, 4426.

(21) Zhang, Q.; Yang, Y.; Zhang, S. *Chem. - Eur. J.* **2013**, *19*, 10024.

(22) Pei, C.; Ben, T.; Guo, H.; Xu, J.; Deng, F.; Xiang, Z.; Cao, D.; Qiu, S. *Philos. Trans. R. Soc., A* **2013**, *371*, 20120312.

(23) Lu, W.; Yuan, D.; Sculley, J. P.; Zhao, D.; Krishna, R.; Zhou, H.-C. *J. Am. Chem. Soc.* **2011**, *133*, 18126.

(24) vom Stein, T.; Peréz, M.; Dobrovetsky, R.; Winkelhaus, D.; Caputo, C. B.; Stephan, D. W. *Angew. Chem., Int. Ed.* **2015**, *54*, 10178.

(25) Nikonov, G. I.; Vyboishchikov, S. F.; Shirobokov, O. G. *J. Am. Chem. Soc.* **2012**, *134*, 5488.

140

Supporting Information for

Room-Temperature Activation of Hydrogen by Semi-Immobilized Frustrated Lewis Pairs in Microporous Polymer Networks

Matthias Trunk,[1] Johannes F. Teichert,[2] Arne Thomas[1,*]

[1]Technische Universität Berlin, Department of Chemistry, Functional Materials, Hardenbergstr. 40, 10623 Berlin

[2]Technische Universität Berlin, Department of Chemistry, Organic Chemistry / Sustainable Synthetic Methods, Straße des 17. Juni 115, 10623 Berlin

1. **General Remarks**
2. **Synthesis of Monomers M1, M2, Tetrakis(4-bromophenyl)methane and Control Phosphine**
3. **Synthesis of Polymers P1, P2 and PPN-6**
4. **Hydrogen Activation Experiments**
5. **Fluorescence Experiments**
6. **Analytic**
    a. Solid State Nuclear Magnetic Resonance
    b. Thermogravimetric Analysis

1. General Remarks

Inert reactions were carried out in an MBraun glovebox type MB 120 BG. All glassware and stir bars were flame-dried before being channelled into the glovebox.

^{1}H NMR, ^{13}C NMR, and ^{31}P NMR were recorded on a Bruker Avance II 200 and Bruker Avance 400 MHz spectrometer in the given solvent. Nitrogen sorption analyses were conducted at 77 K using an Autosorb-iQ-MP from Quantachrome. The pore size distributions were calculated from the adsorption isotherms by quenched solid density functional theory (QSDFT) using the slit/cylindrical pore model for carbon adsorbents. Before analysis, samples were degassed at 80 °C for 12 h. BET surface areas were determined over a 0.05-0.1 p/p$_0$ range.

^{13}C{^{1}H} CP/MAS and ^{31}P MAS measurements were carried out using a Bruker Avance 400 MHz Solid State spectrometer operating at 100.6 MHz for ^{13}C, 168 MHz for ^{31}P and a Bruker 4 mm double resonance probe-head operating at a spinning rate of 7, 9, or 10 kHz. TGA measurements were carried out under air and nitrogen on a Mettler Toledo TGA 1 Star^e thermal instrument with a heating rate of 10 K min^{-1}.

All chemicals were used as received unless otherwise noted. Anhydrous dimethylformamide (99.8 %), 5-bromo-2-iodotoluene (98 %), 2-bromo-1,3-dimethylbenzene (98 %), anhydrous diethyl ether (≥99 %), anhydrous tetrahydrofuran (≥99.9 %), n-butyllithium (2.5 M in hexanes), phosphorus trichloride (99.999 %), 1,5-cyclooctadiene (99 %), and 2,2'-bipyridine (≥99 %) were purchased from Sigma-Aldrich. Tetraphenylmethane (96 %) was purchased from Manchester Organics as was 5-bromo-2-iodo-m-xylene (97 %), which was sublimed prior to use. Bromine (99.8 %) was purchased from Alfa Aesar. Bis(1,5-cyclooctadiene)nickel(0) (98 %) was purchased from ABCR. Tris(pentafluorophenyl)borane (97 %) was purchased from Alfa Aesar and doubly sublimed before use. Tris(o-tolyl)phosphine (97 %) was purchased from TCI and used as received.

2. Synthesis of Monomers

Synthesis of Tris(4-bromo-2-methylphenyl)phosphine M1

In a flame-dried Schlenk flask, 5-bromo-2-iodotoluene (3.39 mL, 7.13 g, 24.00 mmol, 1.00 eq) was dissolved in THF (100 mL) and cooled to 0 °C. *Iso*-propylmagnesium solution (2.0 M in THF, 12.00 mL, 24.00 mmol, 1.00 eq) was added dropwise over a period of 30 minutes, upon which the light yellow solution turned a bright yellow on the first drop of Grignard reagent. The mixture was stirred at 0 °C for 30 minutes and then slowly allowed to warm to ambient temperature upon which the solution turned hazy. The yellow suspension was cooled to -78 °C and phosphorous trichloride was added dropwise over a period of 15 minutes. The solution turned yellow at the end of the addition and was allowed to warm to ambient temperature slowly overnight. Water (100 mL) was added and the mixture stirred vigorously. The organic phase was extracted with diethyl ether (3 x 100 mL), the combined organic phases dried over sodium sulfate, and the crude product purified *via* column chromatography from hexane. The product was obtained as a colorless, crystalline powder. Yield: 2.89 g (5.34 mmol, 75 %).

^{1}H NMR (200 MHz, CDCl$_3$): δ = 7.40 (dd, J_1 = 1.8 Hz, J_2 = 4.0 Hz, 3 H), 7.23 (dd, J_1 = 1.8 Hz, J_2 = 8.2 Hz, 3 H), 6.53 (dd, J_1 = 4.0 Hz, J_2 = 8.2 Hz, 3 H), 2.33 (s, 9 H) ppm

^{13}C{^{1}H} NMR (50 MHz, CDCl$_3$): δ = 144.7 (d, $J_{C–P}$ = 27.7 Hz), 134.4 (s) , 133.2 (d, $J_{C–P}$ = 4.7 Hz), 132.5 (d, $J_{C–P}$ = 11.7 Hz), 129.5 (s), 123.8 (s), 20.9 (d, $J_{C–P}$ = 21.4 Hz) ppm

^{31}P{^{1}H} NMR (81 MHz, CDCl$_3$): δ = -32.0 (s) ppm

*Synthesis of Tris(4-bromo-2,6-dimethylphenyl)phosphine **M2***

In a flame-dried Schlenk flask, 1-bromo-3,5-dimethyl-4-iodobenzene (11.80 g, 38.00 mmol, 1.03 eq) was dissolved in diethyl ether (200 mL) and cooled to -78 °C. To the resulting suspension, *n*-butyllithium (23.00 mL, 36.80 mmol, 1.00 eq) was added dropwise over a period of 60 minutes and the resulting colorless suspension stirred at -78 °C for 2 hours. Phosphorus trichloride (1.00 mL, 11.46 mL, 0.31 eq) was dissolved in THF (10 mL) and added to the prepared lithium reagent solution at -78 °C over a period of 5 minutes, the colorless suspension kept at -78 °C for 15 minutes, then the cooling was removed and the reaction allowed to warm to ambient temperature overnight upon which an off-white precipitate formed. To this were added saturated aqueous NaHCO$_3$ solution (50 mL), and THF until the solid dissolved (ca. 200 mL). The phases were separated and the aqueous phase extracted with THF (2 x 100 mL). The combined organic phases were dried over sodium sulfate, and the solvent removed to yield an orange slurry. This slurry was suspended in THF and purified *via* column chromatography from hexane. The pure product fractions were combined and reduced to dryness to yield a colorless solid. Yield, 2.36 g (4.05 mmol, 35 %).

^{1}H NMR (400 MHz, CDCl$_3$): δ = 7.16 (d, J = 2.9 Hz, 6 H), 2.07 (s, 18 H) ppm

^{13}C{^{1}H} NMR (100 MHz, CDCl$_3$): δ = 144.7 (d, J_{C-P} = 25.0 Hz), 131.9 (s) , 123.2 (s), 22.7 (d, J_{C-P} = 15.9 Hz) ppm

^{31}P{^{1}H} NMR (161 MHz, CDCl$_3$): δ = -35.4 (s) ppm

Synthesis of Tetrakis(4-bromophenyl)methane

A 100 mL Schlenk flask was charged with tetraphenylmethane (2.94 g, 9.19 mmol, 1.00 eq) to which bromine (17.62 g, 110.25 mmol, 12.00 eq) was added dropwise. The mixture was stirred for 20 minutes after which ethanol (40 mL) was added slowly. The resulting orange suspension was stirred for 2 hours after which aqueous sodium thiosulfate solution was added until the solvent turned colourless, the solvent removed *via* filtration, and the off-white residue washed with copious amounts of water and ethanol. The filter cake was recrystallized from a strongly refluxing dichloromethane/ethanol mixture (10:1 v/v, *ca.* 180 mL) to obtain a colourless, analytically pure solid. Yield, 3.57 g (5.61 mmol, 61 %). Recrystallization from toluene/THF (1:1 v/v) afforded colourless crystals.

^{1}H NMR (400 MHz, CDCl$_3$): δ = 7.39 (d, J = 8.7 Hz, 8 H), 7.01 (d, J = 8.7 Hz, 8 H) ppm

Synthesis of Tris(2,6-dimethylphenyl)phosphine

A two-necked 100 mL Schlenk flask equipped with a reflux condenser was flame-dried and flushed with nitrogen gas. Magnesium (1.02 g, 42.00 mmol, 1.00 eq) was suspended in THF (40 mL) and 2-bromo-*m*-xylene (8.33 g, 45.00 mmol, 1.07 eq) added dropwise. The reaction started spontaneously during addition and the solution turned green. The turbid solution was stirred overnight at ambient temperature. The solution was cooled to -78 °C, PCl$_3$ (1.10 mL, 1.73 g, 12.61 mmol, 0.30 eq) added dropwise to the stirred Grignard solution at -78 °C, and the resulting solution kept at this temperature for 30 minutes. The cooling bath was removed and the mixture stirred overnight. Brine was added and the two-phase mixture stirred vigorously for 30 minutes. The phases were separated, the aqueous phase extracted with THF (2 x 100 mL), and the combined organic phases dried over sodium sulfate. The crude

product was adsorbed onto silica gel purified *via* column chromatography from hexane. Yield, 2.43 g (7.01 mmol, 56 %).

^{1}H NMR (200 MHz, CDCl$_3$): δ = 7.09 (m, 3 H), 6.9 (m, 6 H), 2.07 (s, 18 H) ppm

^{13}C{^{1}H} NMR (50 MHz, CDCl$_3$): δ = 142.8 (d, $J_{C–P}$ = 17.4 Hz), 134.6 (d, $J_{C–P}$ = 17.4 Hz) , 128.9 (d, $J_{C–P}$ = 3.6 Hz), 128.2 (s), 22.9 (d, $J_{C–P}$ = 16.6 Hz) ppm

^{31}P{^{1}H} NMR (81 MHz, CDCl$_3$): δ = -34.4 (s) ppm

3. Synthesis of Polymers

Synthesis of Tris(2-methylphenyl)phosphine Homopolymer *P1*

Inside the glovebox, bis(1,5-cyclooctadiene)nickel(0) (531 mg, 1.93 mmol, 3.51 eq), 2,2'-bipyridine (300 mg 1.92 mmol, 3.49 eq), and 1,5-cyclooctadiene (0.23 mL, 1.88 mmol, 3.42 eq) were dissolved in DMF/THF (50 mL each) and stirred for 5 minutes. Tris(4-bromo-2-methylphenyl)phosphine **M1** (300 mg, 0.55 mmol, 1.00 eq) was added and the purple mixture stirred at ambient temperature for 15 hours. The mixture was cooled to 0 °C, aqueous hydrogen chloride solution (20 %, 50 mL) was added slowly, the mixture allowed to warm to ambient temperature, and stirred for 1 hour upon which it turned light blue with a bright precipitate. The mixture was filtered off and the colorless precipitate washed with copious amounts of methanol and water. The product was purified *via* Soxhlet extraction with methanol overnight and dried at 80 °C *in vacuo* overnight to yield pale yellow, glassy particles. Yield, 163 mg (0.51 mmol functional units, 93 %).

^{13}C{^{1}H} CPMAS NMR (100 MHz): δ = 140, 131, 125 ppm

^{31}P{^{1}H} CPMAS NMR (168 MHz): δ = -14, -34 ppm

Synthesis of Tris(2,6-dimethylphenyl)phosphine Homopolymer *P2*

Inside the glovebox, bis(1,5-cyclooctadiene)nickel(0) (949 mg, 3.45 mmol, 3.45 eq), 2,2'-bipyridine (539 mg, 3.45 mmol, 3.45 eq), and 1,5-cyclooctadiene (0.42 mL, 3.42 mmol, 3.42 eq) were dissolved in DMF/THF (90 mL each) and stirred for 5 minutes. Tris(4-bromo-2,6-dimethylphenyl)phosphine **M2** (583 mg, 1.00 mmol, 1.00 eq) was added and the purple mixture stirred at ambient temperature for 22 hours inside the glovebox. The mixture was cooled to 0 °C, aqueous hydrogen chloride solution (20 %, 50 mL) was added slowly, the mixture stirred for 1 hour at 0 °C, then allowed to warm to ambient temperature, and stirred for 1 hour upon which it turned light blue with a bright precipitate. The mixture was filtered off and the bright yellow precipitate washed with copious amounts of methanol and water. The product was purified *via* Soxhlet extraction with methanol overnight and dried *in vacuo* at 80 °C for 5 hours to yield intensely yellow, glassy particles. Yield, 331 mg (0.96 mmol functional units, 96 %).

^{13}C{^{1}H} CPMAS NMR (100 MHz): δ = 140, 131, 125 ppm

^{31}P{^{1}H} CPMAS NMR (168 MHz): δ = -36 ppm

Synthesis of PPN-6

Inside the glovebox, bis(1,5-cyclooctadiene)nickel(0) (1.00 g, 3.64 mmol, 4.49 eq), 2,2'-bipyridine (575 mg, 3.68 mmol, 4.54 eq), and 1,5-cyclooctadiene (0.45 mL, 3.67 mmol, 4.53 eq) were dissolved in DMF/THF (75 mL each) and stirred for 5 minutes. Tetrakis(4-bromophenyl)methane (513 mg, 0.81 mmol, 1.00 eq) was added and the purple mixture

stirred at ambient temperature for 14 hours inside the glovebox. Aqueous hydrogen chloride solution (20 %, 50 mL) was added in small portions and the mixture stirred at ambient temperature for 3 hours. A white solid was filtered off, washed with water and methanol, purified *via* Soxhlet extraction with THF overnight, and dried *in vacuo* at 80 °C for 5 hours. Yield, 225 mg (0.70 mmol functional units, 88 %).

$^{13}C\{^{1}H\}$ CPMAS NMR (100 MHz): δ = 143, 136, 128, 122, 61 ppm

4. Hydrogen Activation Experiments

To obtain rigorously air- and donor molecule-free samples, subsequent to their regular workup **P1** and **P2** were purified *via* Soxhlet extraction from cyclohexane overnight and dried in a Schlenk tube at 80 °C *in vacuo* at the Schlenk line overnight, and the tube backfilled with argon gas. The tube was then channeled into and stored in the glovebox. Subsequently, **P1** and **P2** (5 μmol functional units, 1.0 eq) and tris(pentafluorophenyl)borane (2.5 mg, 5 μmol, 1.0 eq) were suspended in cyclohexane-d_{12} in a pressure-resistant Young-type NMR tube with gas inlet, the tube sealed, removed from the glovebox, and treated in an ultrasonic bath for 30 minutes to effect sufficient mixture of the poorly soluble Lewis acid and the basic network. A steel autoclave was pressurized to 10 bar with D_2 gas and the pressure raised to 20 bar using H_2. This autoclave was then used as a reservoir to pressurize the NMR tube to 6 bar. The progress of H/D exchange was monitored *via* ^{1}H NMR spectroscopy. The control experiment with tris(o-tolyl)phosphine was performed following the same procedure and molecular amounts.

5. Fluorescence Experiments

Inside the glovebox a 2.5 mL vial was charged with **P1/P2** (5 μmol) and optionally with tris(pentafluorophenyl)borane (5 μmol) and dichloromethane (2.5 mL) added. The vial was illuminated with a UV lamp set to 366 nm. Before addition of Lewis acid, the polymer was finely dispersed for several minutes before floating to the top of the solvent. After addition of the Lewis acid, the fluorescence of the polymer particles was quenched (see Figure 2 in main text and Fig. S below). Furthermore, the particles contracted and sedimented within a matter of minutes, presumably due to absorption of the Lewis acid into the pores and the resulting increased density. The shift to higher wavelengths of **P2** is a consequence of the increased steric bulk around the phosphine center, which is more planarized than the phosphorus atom in **P1**.

6. Analytical Data
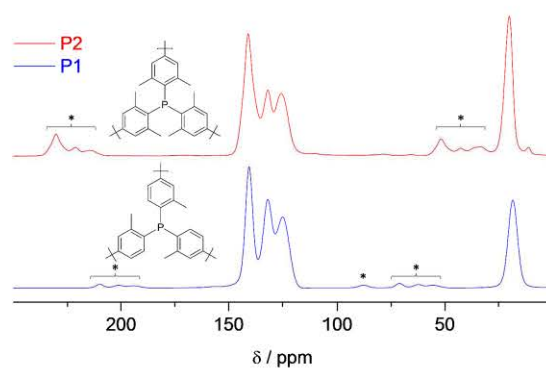
Fig. S 1: ^{13}C CP/MAS spectra of P1 and P2, recorded at 7 and 9 kHz, respectively. Asterisks (*) denote spinning sidebands.
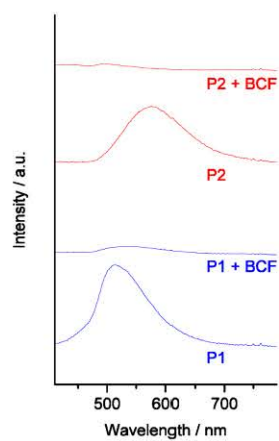
Fig. S 2: Fluorescence spectra before and after addition of BCF under irradiation of UV light (366 nm)

S6

146
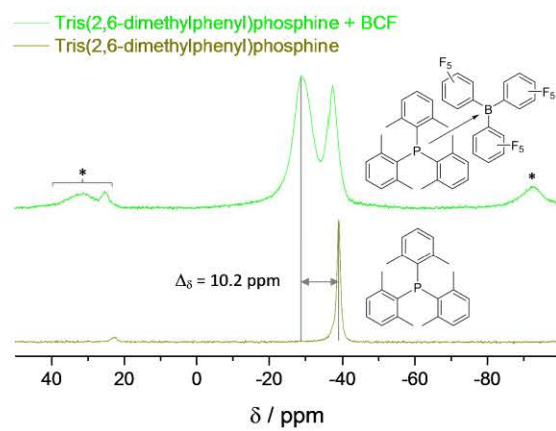
Fig. S 3: ^{31}P solid state NMR spectra of tris(2,6-dimethylphenyl)phosphine and its "dry" FLP with tris(pentafluorophenyl)borane. Asterisks (*) denote spinning sidebands.

S7

a. Thermogravimetric Analysis

The thermal stability of the polymers in air as well as under nitrogen atmosphere decreases with increasing degrees of methylation. In air, oxidation sets in around 250 °C as evidenced by a slight weight increase. In nitrogen atmosphere, decomposition of **P1** and **P2** sets in around 420 and 330 °C, respectively.
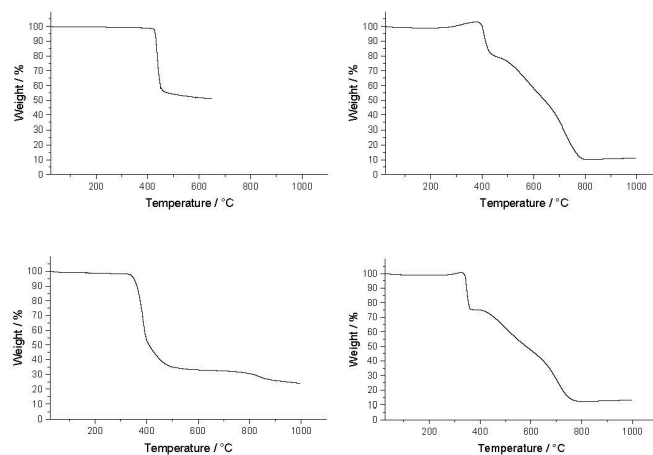
Fig. S 4: Thermogravimetric analyses of P1 (top) and P2 (bottom) in N$_2$ (left) and air (right)

S8